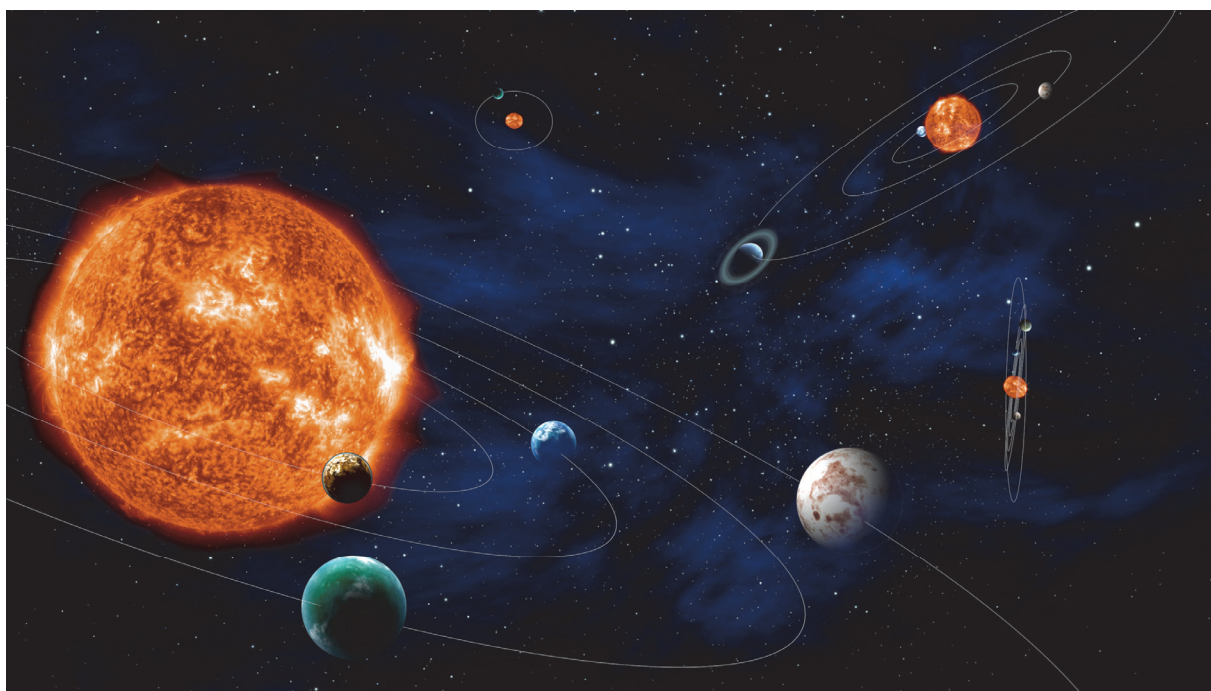


PLATO

**Revealing habitable worlds
around solar-like stars**



Definition Study Report

The front page shows an artist's impression reflecting the diversity of planetary systems and small planets expected to be discovered and characterised by PLATO (©ESA/C. Carreau).

PLATO Definition Study – Mission Summary	
Key scientific goals	<p>Detection of terrestrial exoplanets up to the habitable zone of solar-type stars and characterisation of their bulk properties needed to determine their habitability.</p> <p>Characterisation of hundreds of rocky (including Earth twins), icy or giant planets, including the architecture of their planetary system, to fundamentally enhance our understanding of the formation and the evolution of planetary systems.</p> <p>These goals will be achieved through: 1) planet detection and radius determination (3% precision) from photometric transits; 2) determination of planet masses (better than 10% precision) from ground-based radial velocity follow-up, 3) determination of accurate stellar masses, radii, and ages (10% precision) from asteroseismology, and 4) identification of bright targets for atmospheric spectroscopy.</p>
Observational concept	Ultra-high precision, long (at least two years), uninterrupted photometric monitoring in the visible band of very large samples of bright ($V \leq 11-13$) stars.
Primary data products	<ul style="list-style-type: none"> • High cadence optical light curves of large numbers of bright stars. • Catalogue of confirmed planetary systems fully characterised by combining information from the planetary transits, the seismology of the planet-host stars, and the ground-based follow-up observations.
Payload	
Payload concept	<ul style="list-style-type: none"> • Set of 24 normal cameras organised in 4 groups resulting in many wide-field co-aligned telescopes, each telescope with its own CCD-based focal plane array; • Set of 2 fast cameras for bright stars, colour requirements, and fine guidance and navigation.
Optical system	6 lenses per telescope (1 aspheric)
Focal planes	104 CCDs (4 CCDs per camera) with 4510×4510 18 μ m pixels
Instantaneous field of view	~ 2232 deg ² , with 4 groups of cameras respectively looking on 301 deg ² , 247 deg ² , 735 deg ² , and 949 deg ² .
Overall mission profile	
Operations reference scenario	Nominal in-orbit science operations with a Long duration observation phase including two single fields monitored for two years each. Optionally a split into 3 years long duration pointing and 1 year “step-and-stare” phase.
Lifetime	Satellite built and verified for an in-orbit lifetime of 6.5 years and to accommodate consumables for 8 years.
Duty cycle	$\geq 93\%$ per target in a year
Launcher	Launch by Soyuz-Fregat2-1b from Kourou in 2025
Orbit	Transfer to L2, then large amplitude libration orbit around L2
Description of Spacecraft	
Stabilisation	3-axis
Telemetry band	X and K-band
Average downlink capacity	~ 435 Gb per day
Pointing stability	0.2 arcsec (Hz) ^{-1/2} over time scales of 25 s to 14 hours
Pointing strategy	A 90° rotation around the line of sight every 3 months

... for had we never seen the stars, and the sun, and the heaven, none of the words which we have spoken about the universe would ever have been uttered. But now the sight of day and night, and the months and the revolutions of the years, have created number, and have given us a conception of time, and the power of enquiring about the nature of the universe...

Plato, in Timaeus

Foreword

The PLATO mission was firstly proposed in 2007 as a medium class candidate in response to the call for missions of the Cosmic Vision 2015-2025 program for a launch in 2017–2018. The proposal was submitted by Dr. Claude Catala (Observatoire de Paris) on behalf of a large consortium of scientists from laboratories all across Europe. Following favourable reviews by ESA’s scientific Advisory structure, PLATO was selected in 2007 as one of the missions for which an ESA assessment study was carried out in 2008 and 2009. The PLATO mission was subsequently selected for a definition study, starting in February 2010 (ESA/SRE(2011)13).



Plato in "The School of Athens", by Raphael

Following the non-selection of PLATO in October 2011 for the M1 or M2 launch opportunities, the ESA Science Programme Committee (SPC) endorsed the solicitation of a proposal to the PLATO Mission Consortium to be a candidate for the M3 launch opportunity in 2022–2024. The PLATO Mission Consortium responded with a proposal for the provision of the payload and science ground segment components formulated in the M3 mission framework, which was accepted by ESA. A major change was the transfer of the leading role from France to Germany, with Prof. Heike Rauer (DLR) as new PLATO PI. The submitted science case and mission design are summarised in the Assessment study report (ESA/SRE(2013)5). In February 2014, the SPC selected PLATO as the M3 mission of the Cosmic Vision 2015-2025 program.

The mission Definition study started subsequently, involving three concurrent industrial contracts with Airbus DS, OHB and Thales Alenia Space, for the definition of the mission profile, the satellite, and parts of the payload module. In addition, ESA performed the study of its science ground segment contribution and, together with e2v, of the CCDs procurement. The PLATO Mission Consortium carried out the study of the payload and of their contributions to the science ground segment. The Definition phase concluded with the successful Payload, Science Ground-segment and Science Performance System Requirement Review (PSRR) and Mission Adoption Review (MAR) finalised in May 2016. In June 2016, the SPC approved the PLATO Science Management Plan.

As a result of the MAR recommendations and the mission adoption cost assessment, the mission baseline configuration was redefined to include a payload with 24 normal and 2 fast cameras and four years of nominal science operations, with the requirement that the satellite be built and verified for an in-orbit lifetime of 6.5 years accommodating consumables for 8 years.

This report provides a high-level summary of the large number of scientific and technical documents produced as outcome of the PLATO Definition study. Chapter 1 contains the executive summary, and Chapter 2 the description of the scientific objectives. Chapter 3 addresses the scientific requirements, and Chapters 4, 5, 6, 7, 8, and 9 cover the definition of the mission, (payload, satellite, scientific preparatory work, ground-based observations, scientific performance, ground segment, and management). To finish, Chapter 10 provides highlights for the implementation of the communication and outreach policy.

The PLATO Science Advisory Team

Authorship, acknowledgements

This report was prepared by:

<i>Name (alphabetical order)</i>	<i>Affiliation</i>	<i>City, Country</i>
ESA PLATO Science Advisory Team		
Conny Aerts	Instituut voor Sterrenkunde	Leuven, Belgium
Magali Deleuil	Laboratoire d'Astrophysique de Marseille	Marseille, France
Laurent Gizon	MPI for Solar System Research	Göttingen, Germany
Marie-Jo Goupil	Observatoire de Paris-Meudon	Paris, France
J. Miguel Mas-Hesse	Centro de Astrobiología (CSIC/INTA)	Madrid, Spain
Giampaolo Piotto	Università di Padova	Padova, Italy
Don Pollacco	University of Warwick	Coventry, UK
Roberto Ragazzoni	Osservatorio Astronomico di Padova	Padova, Italy
Heike Rauer	Inst. of Planetary Research, DLR	Berlin, Germany
Stéphane Udry	Université de Genève	Genève, Switzerland
ESA Study Scientist		
Ana M. Heras	ESA	Noordwijk, The Netherlands
ESA Study Team		
David Agnolon	ESA System Engineer	Noordwijk, The Netherlands
Philippe Gondoin	ESA Study Manager	Noordwijk, The Netherlands
Laurence O'Rourke	ESA SOC Study Manager	Madrid, Spain
Anamarija Stankov	ESA Payload Manager	Noordwijk, The Netherlands
ESA Coordinators		
Luigi Colangeli	ESA	Noordwijk, The Netherlands
Arvind Parmar	ESA	Noordwijk, The Netherlands

In addition, the following PLATO Mission Consortium (PMC) members have contributed to this report: Thierry Appourchaux (IAS, FR), Kevin Belkacem (LESIA/CNRS, FR), Othman Benomar (New York U. Abu Dhabi, AE), Anko Börner (DLR, DE), David Brown (U. Warwick, UK), Allan-Sacha Brun (CEA/DSM/CNRS, FR), Juan Cabrera (DLR, DE), William J. Chaplin (U. Birmingham, UK), Jorgen Christensen-Dalsgaard (Aarhus U., DK), Orlagh L. Creevey (U. de Nice Sophia-Antipolis, FR), Szilard Csizmadia (DLR, DE), Margarida Cunha (U. do Porto, PT), Johanna dall'Amico (OHB, DE), Sebastien Deheuvels (U. Toulouse, FR), Anders Erikson (DLR, DE), Antonio García Muñoz (TUB, DE), Mareike Godolt (DLR, DE), Maximilian Klebor (OHB, DE), Yveline Lebreton (LESIA/CNRS, FR), Joao Pedro Marques (IAS/CNRS, FR), Stéphane Mathis (CEA/DSM/CNRS, FR), Andrea Miglio (U. of Birmingham, UK), Josepha Montalban (U. degli Studi di Padova, IT), Thierry Morel (Ins. d'Astrophys. et de Géophys. BE), Benoît Mosser (LESIA/CNRS, FR), Valerio Nascimbeni (U. degli Studi di Padova, IT), Réza Samadi (LESIA/CNRS, FR), Mario Schweitzer (OHB, DE), Matthias Wieser (OHB, DE).

The PMC consists of more than 350 scientists and engineers in virtually all ESA Member States, as well as a few members from the US and Brazil. The contributors to the Definition study activities are acknowledged in the Annex.

Table of contents

1	EXECUTIVE SUMMARY.....	9
2	SCIENTIFIC OBJECTIVES.....	13
2.1	Science Objectives I: Planetary science.....	13
2.1.1	Planet detection and characterisation of bulk parameters.....	13
2.1.2	Habitability of planets around solar-like stars.....	16
2.1.3	Constraints on planet formation from statistics.....	18
2.1.4	Multiple planet systems.....	20
2.1.5	Terrestrial planets.....	21
2.1.6	Gas giants and icy planets.....	22
2.1.7	Planets orbiting intermediate mass stars.....	25
2.1.8	Planets around giant stars.....	25
2.1.9	Planets around post-RGB stars.....	26
2.1.10	Circumbinary planets.....	27
2.1.11	Evolution of planetary systems.....	27
2.1.12	Planetary atmospheres.....	29
2.1.13	Characterising stellar-exoplanet environments.....	31
2.1.14	Detection of rings, moons, Trojans and comets.....	32
2.1.15	Planetary science conclusions.....	34
2.2	Science Objectives II: Probing stellar structure and evolution by asteroseismology.....	35
2.2.1	Stellar parameters as key to exoplanet parameter accuracy.....	35
2.2.2	Stellar models and evolution.....	42
2.2.3	Stellar magnetohydrodynamics.....	46
2.3	Science Objectives III: Complementary science.....	48
2.3.1	Stellar structure and evolution.....	48
2.3.2	Asteroseismology of globular and young open clusters.....	51
2.3.3	Probing the structure and evolution of the Milky Way.....	51
2.3.4	Accretion physics near compact objects.....	53
2.3.5	Classical pulsators.....	54
2.3.6	Classical eclipsing binaries, beaming binaries and low-mass stellar and sub-stellar companions.....	55
2.3.7	Additional complimentary science themes.....	56
2.4	PLATO's long-term legacy.....	56
3	SCIENTIFIC REQUIREMENTS.....	57
3.1	PLATO measurement concept.....	57
3.1.1	The transit method.....	57
3.1.2	Asteroseismology.....	58
3.1.3	The radial velocity method.....	59
3.2	Measurement plans and expected results.....	59
3.3	Top scientific requirements.....	60
3.3.1	Planet detection and characterisation.....	60
3.3.2	Stellar science.....	62
3.4	Derived scientific requirements.....	62
3.4.1	Fields.....	62
3.4.2	Stellar samples.....	63
3.4.3	Wavelength and colour information.....	66
3.4.4	Observation gaps.....	66
3.5	The need to go to space.....	67
4	PAYLOAD 69	
4.1	Basic instrument overview.....	69
4.2	Cameras.....	72
4.2.1	Telescope Optical Unit (TOU).....	73
4.2.2	Focal Plane Assembly (FPA).....	73
4.2.3	Front End Electronics (FEE).....	75
4.2.4	Ancillary Electrical Units (AEU).....	76

4.3	On-board Data Processing subsystem (DPS).....	76
4.3.1	Main Electronics Unit (MEU) and Data Processing Units (N-DPU).....	76
4.3.2	Fast Electronics Unit (FEU) and Data Processing Units (F-DPU).....	78
4.3.3	Instrument Control Unit (ICU).....	79
4.3.4	Telemetry data budget.....	80
5	MISSION DESIGN.....	81
5.1	Mission operations.....	81
5.1.1	Mission profile.....	81
5.1.2	Launch scenario and transfer.....	81
5.1.3	Operations at the Lagrange point 2 (L2).....	82
5.2	Mission implementation.....	85
5.3	Key design challenges.....	85
5.3.1	Payload accommodation and spacecraft interfaces.....	86
5.3.2	Science duty cycle.....	86
5.3.3	Payload environment.....	86
5.3.4	Cameras static co-alignment.....	87
5.3.5	Spacecraft and cameras' pointing stability.....	87
5.4	Spacecraft design.....	88
5.4.1	Airbus – Spacecraft design – Prismatic configuration.....	88
5.4.2	OHB – Spacecraft design – PLM and SVM separation.....	90
5.5	Technology readiness.....	91
6	PREPARATORY WORK AND GROUND-BASED OBSERVATIONS.....	93
6.1	PLATO target and field selection.....	93
6.1.1	Statistical analysis of available stellar catalogues.....	93
6.1.2	Reddening analysis.....	94
6.1.3	Field selection and field content.....	95
6.1.4	Target selection and characterisation from <i>Gaia</i> catalogue.....	95
6.1.5	PIC target characterisation.....	97
6.2	PLATO ground-based follow-up observations.....	97
6.2.1	Filtering observations: the elimination of astrophysical mimics.....	98
6.2.2	Optimisation of the radial velocity follow-up.....	100
6.2.3	Organisation of the ground-based follow-up.....	101
7	MISSION PERFORMANCE.....	105
7.1	Instrument performance.....	105
7.2	Science performance.....	106
7.2.1	Stellar parameters.....	107
7.2.2	Planet parameters.....	108
7.2.3	Planet yield.....	109
8	GROUND SEGMENT.....	113
8.1	PLATO data products.....	113
8.2	Ground Segment overview.....	114
8.3	Mission operations.....	115
8.4	Science operations.....	115
8.4.1	Overall concept.....	115
8.4.2	Calibration activities.....	116
8.4.3	Science Operations Centre.....	116
8.4.4	PLATO Data Centre.....	117
8.4.5	PLATO Mission Consortium Science Management.....	118
8.4.6	PMC Calibration/Operation Team.....	119
8.4.7	Ground based Observations Programme (GOP) Team.....	120
8.4.8	Level 2 and Level 3 data processing.....	120
9	MANAGEMENT.....	123
9.1	Project management.....	123
9.2	PLATO Mission Consortium (PMC) structure.....	123
9.3	Procurement philosophy.....	125

9.3.1	Procurement of spacecraft, industrial contractors and organisation	125
9.3.2	Payload procurement	125
9.4	Schedule	125
9.5	Science management	125
9.5.1	PLATO Science Working Team	125
9.5.2	Guest Observers programme	126
9.5.3	Data policy	126
10	COMMUNICATION AND OUTREACH	127
10.1	Education and public outreach strategy	127
10.2	EPO team and credentials	128
10.3	Wider context	128
11	REFERENCES	129
12	LIST OF ACRONYMS	134
	ANNEX: DEFINITION STUDY CONTRIBUTORS	137

1 Executive summary

The PLATO space mission (PLAnetary Transits and Oscillation of stars) will detect terrestrial exoplanets at orbits up to the habitable zone of solar-type stars and characterise their bulk properties. PLATO will provide key information (planetary radii, mean densities, ages, stellar irradiation, and architecture of planetary systems) needed to determine the habitability of these unexpectedly diverse new worlds. PLATO capitalises on tremendous developments in high-precision photometry from space and ultra-stable ground-based spectroscopy techniques that have largely been led by Europe over the last 20 years.

PLATO will answer the scientific questions:

- How do planets and planetary systems form and evolve?
- Is our solar system special or are there other systems like ours?
- Are there potentially habitable planets?

PLATO is the only mission either approved or in advanced planning that will be able to address these questions. For this purpose, it focuses on the small planets orbiting in the habitable zone of stars, including stars like our Sun. Furthermore, PLATO provides a huge database for all kinds of planets and planetary systems with well determined parameters. This database will complement the Gaia mission and provide a unique data set on planetary systems and stars for generations of scientists to come.

Science objectives

PLATO will explore the diversity of planetary system by accurately determining their bulk properties, by constraining planet formation models, and by better understanding the temporal evolution of planets and planetary systems. While the structure and mass distributions of bodies in our solar system are well known, we only have indirect and partial knowledge of its formation and evolution processes. To place our system into context, we must look at other systems and study their architectures and compositions at different stages of their evolution. Current observations have established that the bulk compositions of exoplanets and the architectures of exoplanet systems can differ substantially from the solar system, and this must be indicative of the complexity and diversity of formation process and evolutionary paths. PLATO will provide ground-breaking insight into these fundamental questions, by constraining with unprecedented accuracy radius, masses, and ages of a large number of planetary systems.

PLATO will provide unprecedented accurate planetary parameters to constraint the interior composition of terrestrial and gas planets. Many confirmed exoplanets fall into new classes unknown from our solar system, for example “hot Jupiters”, “mini-Neptunes” (planets with masses comparable with the terrestrial planets in our solar system, but with much smaller bulk densities), or “super-Earths” (rocky planets with masses below $10 M_E$). It came as a surprise that gaseous planets can be as small (or light) as a few Earth radii (or masses). As a result, many of the smallest (or lightest) exoplanets known today cannot be classified precisely as either rocky (required for habitability) or gaseous, because their mean densities remain unknown for lack of mass or radius measurements. PLATO will help us overcoming these limitations and for the first time, we will be able to determine accurate ages of a large number of stars that can be investigated by asteroseismology. Planetary (system) properties can then be correlated with temporal evolution processes once a sufficiently large database of planet and stellar properties is available from PLATO.

PLATO will characterise for the first time terrestrial planets in the habitable zone of solar like stars. Habitability is defined as the potential of an environment to sustain life of any kind. In this context, the existence of liquid water for long periods of time on the surface of a terrestrial planets is one of the requisites for life. The detection of small planets, similar to Earth, around stars like our Sun, orbiting at distances such that liquid water can exist for long periods of time, and potentially sustain life on the planetary surface, is challenging. The detection of these planets, which is the driver for the design of the PLATO mission, will be a breakthrough for our understanding of the conditions that led to the emergence of life on Earth. The investigation of these small planets with long period orbits will be complemented with planets of all sizes, in all kinds of systems, on all kind of orbits, e.g. binary (or multiple) stars with planets, planets around intermediate-mass and giant stars, post RGB-stars, planets on co-planar or inclined orbits, exomoons, planets

with rings, disintegrating planets, and many more, exploring the diversity of planetary systems in the Galaxy. Since the planets well characterised by PLATO orbit bright stars ($V < 11$ mag), they will also be Rosetta-stone candidates for follow-up transit spectroscopy investigating their atmospheres, e.g. via JWST or E-ELT.

PLATO photometry is designed to allow the detection of planets via photometric transits. But planets will also be detected by timing variations of transits (TTV) and via the reflected stellar light on the planet. The latter, together with the orbital planet movement, cause periodic variations in the light curves, or phase curves, which provide a means to investigate planet atmospheres and planetary albedos. PLATO's long pointings and high photometric precision are unique for enabling the observation of thousands of photometric planet phase curves.

PLATO will determine stellar properties with asteroseismology and complement information available from ESA's Gaia mission. Asteroseismology of a large number of different types of stars at different stages of their evolution will provide a unique, revolutionary, understanding of stellar interior and evolution models. PLATO will be the first mission to make systematic use of asteroseismology to characterise planet host stars allowing us to link planetary and stellar evolution. The core program focuses on stars showing oscillations similar to those of the Sun, which are intrinsically stable and excited stochastically by the near-surface convection, providing strict requirements for the photometric performance of the payload.

The PLATO legacy database will provide a unique resource that will be crucial to test our models of planetary and stellar evolution. The large number of PLATO light curves possible as complementary science allows for a wide science program reaching far beyond the exoplanet science community. This program will include topics like, e.g., structure and evolution of Red Giant stars, hot OB sub-dwarf stars, massive stars, asymptotic giant branch stars and supergiants, white dwarfs, pre-main sequence stars, variable stars like eclipsing binaries or classical pulsators, as well as stellar clusters of various ages and metallicity. PLATO data in combination with Gaia results will help significantly to better understand processes in our Milky Way. The PLATO catalogue of thousands of characterised planets and between 300,000 and $\sim 1,000,000$ high precision stellar light curves (depending on the final observing strategy) will provide the basis of a huge legacy for stellar and (extra)galactic science, which will be explored by the community in the years to come during and after the PLATO mission.

Mission design

The measurement principle of PLATO is to carry out high precision, long (months to years), uninterrupted photometric monitoring in the visible band of very large samples of bright ($V \leq 11-13$) stars. The resulting light curves will be used for the detection of planetary transits, from which the planetary radii will be determined, and for the asteroseismology analysis to derive accurate stellar parameters and ages. Thanks to the brightness of the PLATO targets, the masses of the detected planets will be determined from radial velocity observations at ground-based observatories.

PLATO comprises the spacecraft, provided by ESA, and the payload, provided by the PLATO Mission Consortium. The payload consists of 24 "normal" telescopes with CCD (ESA provided) based focal planes, operating in white light and providing a very wide field of view (FoV). They are read out with a cadence of 25 s and will monitor stars with $V > 8$. Two additional "fast" cameras with high read-out cadence (2.5 s) will be used for stars with $V \sim 4-8$ and as fine guidance sensor. The paucity of bright stars necessitates a wide FoV, while the science drivers dictate the required sensitivity (numbers of cameras). Hence, the multi-telescope design allows for a large photometric dynamic range of $4 \leq V \leq 16$ ($4 \leq V \leq 11$ for the core sample) and an extremely wide field ($\sim 2232 \text{ deg}^2$). The ensemble of instruments is mounted on an optical bench. The cameras are based on a fully dioptric design with 6 lenses. Each camera has an 1100 deg^2 FoV and a pupil diameter of 120 mm and is equipped with a focal plane array of 4 CCDs each with 4510^2 pixels of $18 \mu\text{m}$ size, working in full frame mode for the "normal" camera and in frame transfer mode for the "fast" cameras.

The satellite will be built and verified for an in-orbit lifetime of 6.5 years and to accommodate consumables for 8 years. The duration of the nominal science operations phase is 4 years. The current baseline strategy is to carry out a long duration observation phase including two single sky fields monitored for two years each. An alternative scenario is a split into 3 years long duration pointing and 1 year "step-and-stare" phase with several pointings. The final observing scenario will be decided two years before launch. PLATO will be launched by Soyuz-Fregat2-1b from Kourou in 2025, into a large amplitude libration orbit around L2.

PLATO performance

The analysis of the PLATO performance has shown compliance with the science requirements related to the accuracy of the planetary parameters. In particular, for the reference star (G0V, $V=10$), PLATO will allow for the determination of the radius of a planet of the same size as the Earth with an accuracy of 3%, and of the stellar age with an accuracy of 10%. The main PLATO targets will also be bright enough ($V < 11$) such that the planetary mass can be derived through radial velocity measurements with $< 10\%$ uncertainty at existing or in development ground-based facilities.

Considering the current observing baseline, the estimated planet yield for all planet sizes and orbital periods ($V < 13$) is $\sim 4,600$. In bright sources ($V < 11$), the planet yield for small planets ($R < 2R_E$) in all orbital periods is 770 and, in the habitable zone of solar like stars, the estimated value lies between 6 and 280, depending on the planet occurrence rate assumed, which is strongly debated in the literature.

The mass determination with radial velocities observations can be carried out for a significant number of the detected small planets using resources comparable to those available through a large ESO programme (55 nights per year at 8m class telescopes, 65 nights per year at 4m class telescopes). In particular, with these resources it will be possible to measure the mass of 100 super Earths (9 of them with semi-major axis about 1 au), 22 Earth-sized planets (7 of them with semi-major axis comparable to 1 au) and some tens of Neptunes. Using facilities in La Palma (32 nights per year) additional 52 super-Earths (including 5 with semi-major axis about 1 au) could be followed up.

PLATO data products

The baseline telemetry budget yields a daily data volume of 435 Gb. This will enable downloading the imagerettes of all high precision PLATO targets for an enhanced processing on the ground. The remaining targets will be processed on-board. The prime PLATO data product (Level-1) is a large sample of high precision calibrated stellar light curves and centroids for all bright targets. The Level-2 product consists of the list of planetary transit candidates and their parameters, the results of the asteroseismic analysis, the stellar rotation periods and stellar activity properties, the seismically-determined stellar masses, radii and ages of stars, and the list of planetary systems confirmed through the detection of Transit Time Variations (TTVs). The Level-3 product consists of the list of confirmed planetary systems, which will be fully characterised by combining information from the planetary transits, the seismology of the planet-hosting stars, and the results of ground-based observations. The public release of L0, L1 and L2 products for each three-month observing period will be made within one year after the L1 product has been validated.

PLATO ground segment

The PLATO Ground Segment consists of six main elements: i) an ESA provided Mission Operations Centre (MOC), in charge of satellite operations; ii) an ESA provided Science Operations Centre (SOC), in charge of the scientific mission planning and the generation and archival of data products; iii) a PLATO Data Centre (PDC), provided by the PLATO Mission Consortium (PMC), which will provide the pipeline algorithms and modules and generate the high level scientific data products; iv) a PMC Science Management team (PSM), which will carry out scientific preparatory and operational activities, as well as support ESA in public relations and outreach activities; v) a PMC Calibration/Operation Team (PCOT); and vi) a Ground-based Observations Programme Team, that will carry out the ground-based observation of the core sample targets.

Guest observer programme

Members of the scientific community may participate in the PLATO mission by becoming Guest Observers (GOs) selected by ESA through calls for proposals. The calls will ask for complementary science programmes targeting objects within the PLATO sky fields that have been defined for the core science, therefore not requiring dedicated repointing of the spacecraft.

The search for planets similar to our Earth, potentially suitable for the development of life, is one of the greatest scientific, technological, and philosophical undertakings of our time, which is captivating public interest. The PLATO results will have a profound influence on our understanding of the Universe and our place in the *Cosmos*. PLATO will accurately measure the radii, masses, and ages of Earth-like planets in the habitable zones of stars similar to our own. This is unique to PLATO and will lay the foundations for exoplanetary research in the following decades.

Page intentionally left blank

2 Scientific objectives

PLATO is a transit survey mission with the goal of detecting and providing bulk characterisation for new planets and planetary systems around bright stars, including planet parameter ranges that will otherwise not be explored in the next decade. PLATO's design is optimised to:

- *Determine the bulk properties (mass, radius, mean density) of planets in a wide range of systems, including terrestrial planets in the habitable zone of solar-like stars.*
- *Study how planets and planet systems evolve.*
- *Study the typical architectures of planetary systems.*
- *Analyse the correlation of planet properties and their frequencies with stellar parameters (e.g. stellar metallicity, stellar type).*
- *Analyse the dependence of the frequency of terrestrial planets on the environment in which they formed.*
- *Study the internal structure of stars and how it evolves with age.*
- *Identify good targets for spectroscopic follow-up measurements to investigate planet atmospheres.*

Addressing these science objectives requires the detection and determination of accurate bulk properties for a large number of planets. PLATO will detect hundreds of small and/or low-mass planets, for which accurate and precise radii, masses, bulk densities, and ages can be derived. These will include planets in the habitable zones (HZs) of bright, Sun-like stars. Owing to their brightness, PLATO targets are more amenable to radial velocity (RV) follow-up than *Kepler* targets. Furthermore, they will provide prime targets for spectroscopic follow-up observations to investigate their atmospheres.

2.1 Science Objectives I: Planetary science

2.1.1 Planet detection and characterisation of bulk parameters

Since the discovery of the first extrasolar planet orbiting a solar type star in 1995 (Mayor & Queloz 1995), just over 3000¹ extrasolar planets have been detected and confirmed as planets (see Figure 2.1). For many of these planets only one of their fundamental parameters (radius or mass) has been determined directly. In those cases where planets have been observed with both the transit and RV methods, their mass and radius, and thus bulk density, have been measured. This has led to exciting discoveries, including new classes of intermediate planets called “super-Earths” ($R_{\text{planet}} \leq 2R_{\text{E}}$) and “mini-Neptunes” ($2R_{\text{E}} \leq R_{\text{planet}} \leq 4R_{\text{E}}$).

CoRoT (Baglin et al. 2006), *Kepler* (Koch et al. 2010; Borucki et al. 2009), and K2 (Howell et al. 2014) have provided approximately 120 planets with known radii and masses from RV measurements, including a few hot super-Earths. Transit timing variations, induced by gravitational interactions between planets, measured from space are an alternative and powerful method to confirm the planetary nature of transiting candidates, but typical mass uncertainties are in the range of few tens of percent (see the paradigmatic case of Kepler-11, Lissauer et al. 2013). Few tens of percent uncertainty in the mass is enough to confirm a planet, but not to constrain its composition. In the giants domain, ground based surveys have found about 260 hot giant planets with accurately measured bulk parameters in short period orbits.

For the cool terrestrial planets, however, *Kepler* and K2 do not provide precise planet parameters due to the faintness of its target stars (K2 suffers additionally from the limitation of the observation baseline of 90 days). This caveat also applies to transiting planets that will be detected in photometry from *Gaia* (Dzigan & Zucker 2012; Sozzetti et al 2014), which will mostly be orbiting stars fainter than $V=11$. Figure 2.2 shows that many transiting planet hosts, including the majority of CoRoT, *Kepler* and K2 discoveries, are too faint

¹ <http://exoplanet.eu> accessed 07.09.2016

to permit full characterisation of the transiting planet. PLATO’s main detection range is however $V \leq 11$, and it will thus provide large numbers of targets that are suitable for follow-up spectral characterisation.

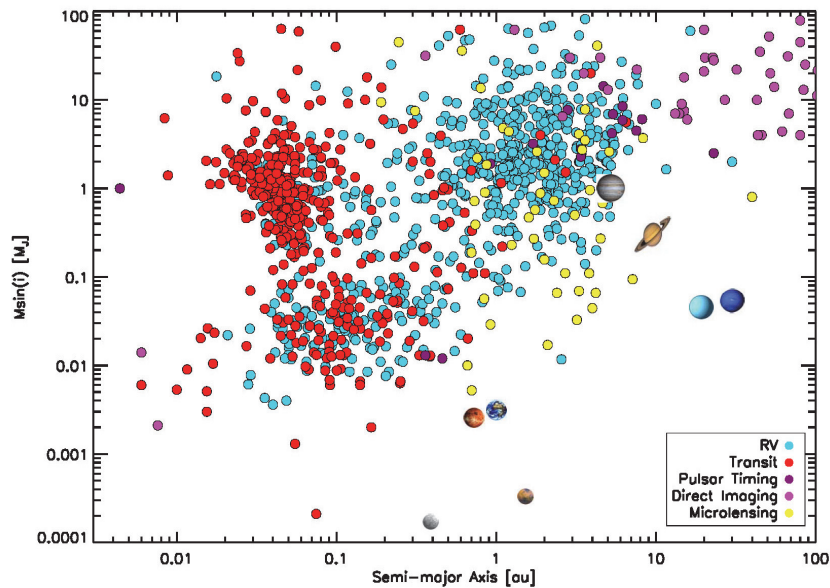


Figure 2.1: Current status of planet detections. Blue dots indicate RV detections with $m \sin i$ limits. Red dots are transit detections (update from Rauer et al. 2014).

While future RV searches for small planets in the habitable zone of Sun-like stars (e.g. the ESPRESSO project; Pepe et al. 2014) will help to unveil the presence of Earth-like planets, on Earth-like orbits around Sun-like stars, the numbers of such planets will be small. Furthermore, since their geometric transit probability is $\sim 0.5\%$, the chance of finding subsequent transits will be rather low, leaving their radius and thus their exact nature unknown. Fortunately, a large scale, wide-angle, space-based transit survey like PLATO can be optimised by observing a very large number of stars simultaneously, and by adopting an appropriate observing strategy.

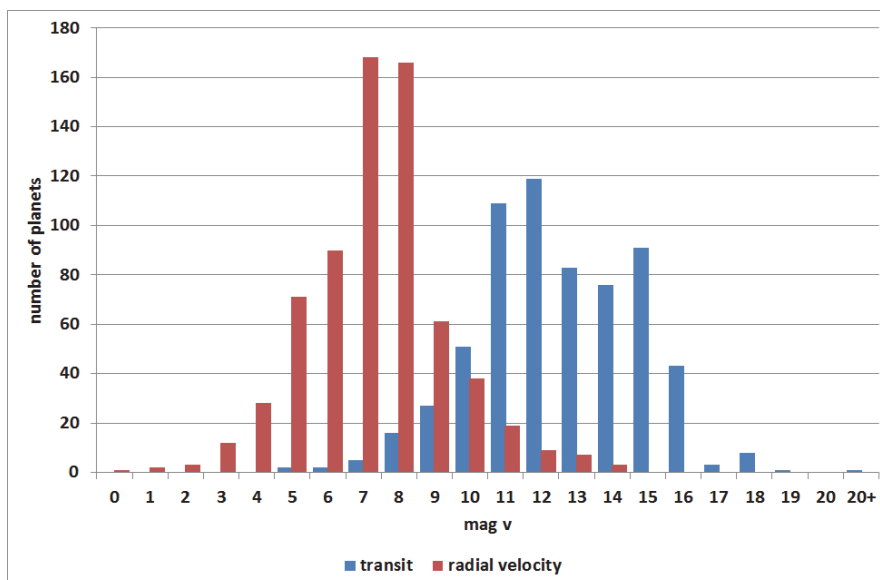


Figure 2.2: Histogram of the visual magnitude of stars hosting exoplanets known to date. The left distribution (bright red end) corresponds to planets discovered by radial velocity and the right distribution (faint blue end) to planets discovered by the transit method. There is little overlap between both samples. The PLATO core sample will provide discoveries around stars brighter than magnitude 11, within reach of ground-based radial velocity facilities.

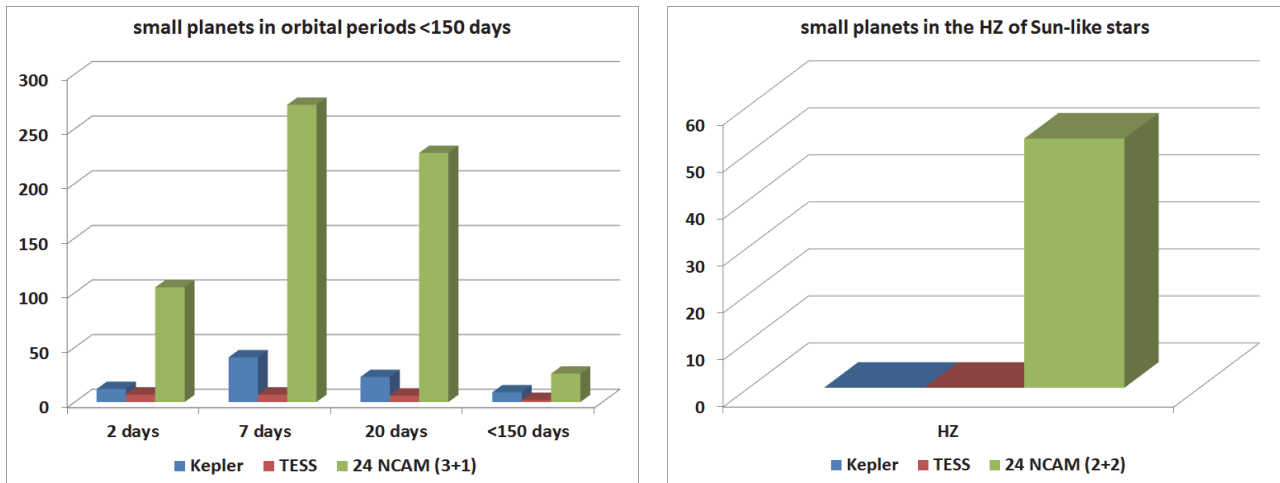


Figure 2.3: Expected yield of planets with highest characterisation accuracy (from P1 sample) in comparison to Kepler and TESS missions for two observing scenarios. Left, expected detection yield of small planets ($R < 2 R_E$) around dwarf and sub-giant stars suitable for asteroseismology studies for Kepler (Lundkvist et al. 2016), TESS (Campante et al. 2016) and the PLATO core sample for an observing sequence of 3 years long pointing plus 1 year step-and-stare phase. We show orbital periods shorter than 150 days. Right, expected detection yield of small planets ($R < 2 R_E$) in the habitable zone of solar-like stars for a scenario of 2 long pointings (baseline). For more details about how these values were derived, see Section 7.2.3.

In the near future, ESA’s CHEOPS (Broeg et al. 2013) will be the first significant step towards improved characterisation of exoplanets, since it will provide bulk properties for a small number of previously detected planets around bright stars at short orbital periods. NASA’s TESS (Ricker et al. 2015), in contrast, will search over large parts of the sky for short-period planets around bright stars. It is expected to detect about 600 small planets ($R_{\text{planet}} < 2R_E$) among their pre-selected target stars, most of them orbiting M dwarfs (Sullivan et al. 2015). In contrast to PLATO, TESS will focus mainly on planets in short period orbits (up to approximately 20 days) because of its pointing strategy. Its yield of small, long-period planets is expected to be low, since only the ecliptic poles ($\sim 2\%$ of the sky) will be covered for a whole year. In the next decade, PLATO is the only mission able to discover and characterise small planets in long period orbits around solar-like stars.

PLATO was designed to maximise the yield of detected small planets around bright stars that could be characterised with asteroseismology and followed-up with RV from the ground. The left part of Figure 2.3 shows the comparison of the performance of Kepler, TESS, and PLATO for this scientific goal. The Kepler data are taken from Lundkvist et al. (2016), which builds on the work by Huber et al. (2013) and Silva Aguirre et al. (2015). For the list of planetary systems from Lundkvist et al. (2016), we take planetary parameters from the NASA Exoplanet Archive (status August 2016) for all planets smaller than $2 R_E$, which add up to 86 planets. For TESS we follow the approach of Campante et al. (2016), who has studied the capability of TESS for obtaining asteroseismic information for dwarf and subgiant stars. We take the detection limits from Campante et al. (2016), and we extract from the planetary catalogue by Sullivan et al. (2015) the expected yield of small planets orbiting dwarf and sub-giant stars characterised with asteroseismology, which add up to 22 planets. For PLATO we follow the procedure described in Section 7.2.3. There are no planets from Kepler or TESS with orbital periods beyond 150 days, that is, no small planets in the habitable zone of dwarf and sub-giant stars characterised with asteroseismology with Kepler or TESS (unless by single transit detections). PLATO outnumbers the performance of Kepler and TESS for planets with bright host stars for asteroseismology.

While TESS will have a sizeable impact on the detection of small planets around stars close to our solar system, it will not address the science case of characterising rocky planets at intermediate distances ($a > 0.3$ au) around Sun-like stars. This goal remains unique to PLATO. Whether our solar system is typical or special will thus remain unclear until we can reliably detect and characterise Earth-like planets, in Earth-like orbits, around all kinds of bright host stars. Detecting these planets, and accurately and precisely determining their radii, masses, bulk densities, and ages, is the primary objective of PLATO.

2.1.2 Habitability of planets around solar-like stars

Habitability is defined as the potential of an environment to sustain life of any kind (e.g. Steele et al. 2006). Life as we know it has the following requirements: liquid water, availability of nutrients, an energy source, the possibility for complex carbon chemistry, as well as protection from hazardous radiation.

From the pre-requisite of liquid water comes the concept of the habitable zone (HZ), i.e., the region around a star where liquid water on the surface of an Earth-like planet is in principle possible. The classical HZ as calculated by Kasting et al. (1993), and updated by e.g. Kopparapu et al. (2013), assumes an Earth-sized planet with an Earth-like water reservoir and a cloud-free atmosphere consisting of molecular nitrogen, carbon dioxide and water vapour. An Earth-sized water reservoir allows for the assumption that the water vapour in the atmosphere is in phase equilibrium with the surface (though the assumption of a saturated atmosphere overestimates the amount of water vapour in the atmosphere as shown by Leconte et al. 2013).

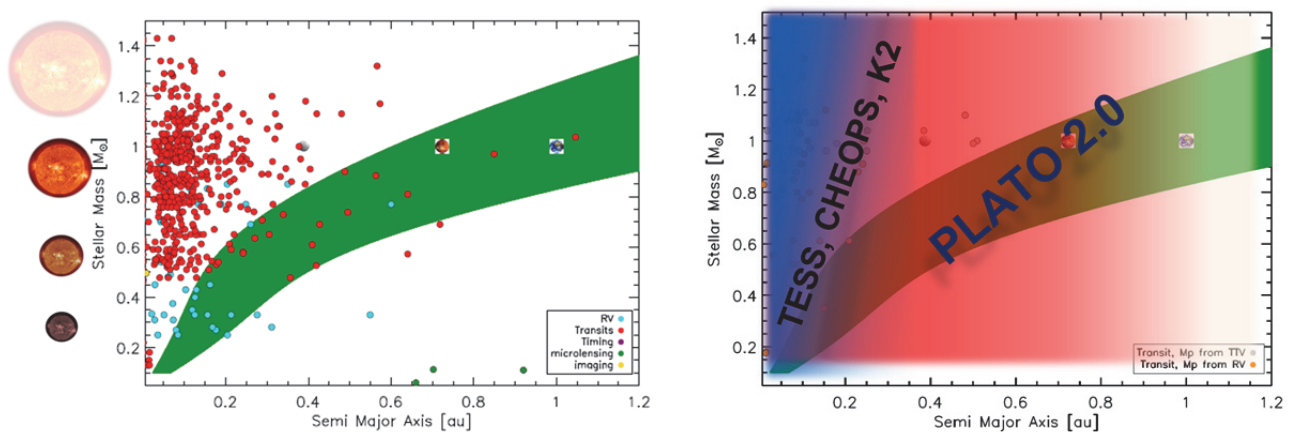


Figure 2.4: Super-Earth exoplanets ($1 < M_{planet} \leq 10 M_E$ or $R_{planet} \leq 2 R_E$) for different host star masses in comparison with the position of the habitable zone (green). Left: as September 2016, there are several planets orbiting in the HZ, but we only know either their radius or their mass. Right: TESS, K2, and CHEOPS will detect and characterise small planets up to the HZ of M dwarfs ($P < 80$ days), but the HZ of solar-like stars is only accessible for PLATO.

Furthermore, such a liquid water reservoir is small enough to avoid the formation of high pressure ice at the bottom of the ocean, which is expected for ocean planets (see e.g. Léger et al. 2004), suspected to prevent the functioning of the carbonate-silicate cycle. While the inner edge of the HZ is dominated by the greenhouse effect of water vapour evaporated from the ocean due to the increased surface temperatures, the outer edge is determined by the greenhouse effect of carbon dioxide, which is assumed to be maximised via the carbonate silicate-cycle. Hence, the width of the classical HZ includes assumptions about the carbonate-silicate cycle, which may not hold for larger planetary water reservoirs leading to a smaller extent of the HZ (see e.g. Kitzmann et al. 2015). Several studies have shown that a smaller liquid water reservoir may allow for habitable surface temperatures closer to the host star than for planets with an Earth-like water reservoir as the greenhouse effect of water vapour is much smaller, see e.g. Abe et al. (2011), Zsom et al. (2013), and Leconte et al. (2013). On such dry planets habitable regions with liquid water on the surface may then exist e.g. at the poles.

The need for an energy source, e.g. in the form of star light or chemical energy, as well as complex carbon chemistry, which is also operating in the interstellar medium, do not seem to put strong constraints on habitability. On the contrary, two crucial, limiting factors may be the availability of nutrients and the protection from hazardous radiation. Planetary wide habitability requires a larger nutrient reservoir, which in turn might need the renewal of nutrients via plate tectonics. It is furthermore discussed that the liquid water should be in contact with rocky material, hence not separated e.g. via high-pressure ice, to allow the nutrient to be dissolved in the water. Protection from hazardous radiation and particle fluxes may be provided by a planetary magnetic field, a suitable atmosphere, or via living in the subsurface or within the ocean; however life in the subsurface may be hard to detect.

Figure 2.4 shows the status of Super-Earth planet detections in comparison with the position of the classical HZ, defined as the region around a star where liquid water can exist on a planetary surface (scaling based on

Kasting et al. 1993). Most super-Earths have been found at orbital distances to the star closer than the HZ. Detections in the HZ have been made by RV or transit measurements (red and blue dots). However, only a small number of super-Earths have both mass and radius determinations (purple dots), and these do not lie in the HZ.²

PLATO will provide terrestrial planets in the HZ of Solar-like stars (up to about 1 au) with accurately and precisely determined bulk parameters, which necessitates direct transit and RV measurements, hence planets orbiting bright host stars. In addition, PLATO's bright target stars allow for asteroseismology studies, increasing not only the accuracy of stellar, and thus planet parameters, but also providing the age of the systems detected.

For M and K dwarfs, PLATO will be able to detect planets beyond the snow lines (the distance to the snow line roughly scales as $2.7*(M/M_{\odot})^2$), providing targets that could be further studied (e.g. by the JWST) for atmospheric signatures. This gives PLATO the unique possibility to build a sequence of planets in largely different temperature and irradiation conditions, and test the fraction of volatiles incorporated in planets from beyond the snow line to very short stellar distances.

Small planets in the habitable zone around M dwarf stars have been found with current instrumentation, e.g. Trappist-1d (Gillon et al. 2016), K2-3d (Crossfield et al. 2015), Proxima Centauri b (Anglada-Escudé et al. 2016). But in all these cases we either do not know the planetary mass or the radius, therefore preventing us from concluding on their true composition and their potential habitability, except in theoretical studies (e.g. Meadows et al. 2016; Barnes et al. 2016; Turbet et al. 2016; Ribas et al. 2016, Bolmont et al. 2017). However, with the contribution of TESS, it is likely that planets orbiting in the HZ of M-dwarfs with known mass and radius will be found in the next decade, even those whose atmosphere can be characterised (de Wit et al. 2016).

Considerable effort has been invested in investigating the potential habitability of planets around M dwarfs in general, see e.g. Scalo et al. (2007) for a review. One main problem may be the ability to retain a suitable water reservoir over a sufficiently long time, as these planets may either form too dry or too wet, see e.g. Lissauer (2007). Since the HZ around M-dwarf stars is much closer in, tidal interactions between the planet and the stars may lead to tidal locking (e.g. Kasting et al. 1993). It was proposed that an atmosphere may collapse onto the night side of a rocky planet, which is in synchronous rotation. It was shown that atmospheric dynamics may prevent an atmospheric collapse, if the atmosphere is sufficiently thick (e.g. Joshi et al. 1997) and habitable surface temperatures may be reached for Earth-like planets if the heat is efficiently transported from the day to the night side. However, such an efficient heat transport on tidally locked planets would impose a very different atmospheric circulation with super-rotation aloft (e.g. Showman & Polvani 2011) and mean wind speeds at the surface which are higher than on Earth, with unclear consequences for the potential of life on the planetary surface (e.g. Edson et al. 2011). The slow rotation of such planet may however also lead to a negative cloud feedback for Earth-like atmospheres, which may allow for liquid water on the planetary surface at even smaller distances to the host stars as determined via the classical HZ calculations (Yang et al. 2014; Kopparapu et al. 2014). If large temperature differences between day and night side occur due to the tidal locking of the planet, the carbonate silicate cycle may work differently than on Earth (e.g. Edson et al. 2012). The generation of a magnetic field on a tidally locked planet may be more difficult than on an Earth-like planet, keeping in mind that also Venus has no magnetic field. Hence there would be less protection from ionising particle radiation, which should be much stronger in the HZ around an M dwarf as the planet needs to be closer in and M stars tend to be more active. This may be a limiting factor for the habitability of such planets. Due to the different spectral energy distributions of M dwarf stars, the atmospheric feedbacks may operate differently on such planets from the ice albedo and water vapour feedback (e.g. Joshi & Haberle 2012; Godolt et al. 2015). Furthermore, atmospheric climate-chemistry calculations show that ozone may build-up differently than on Earth, and spectral signatures of Earth-like planets may be dampened due to changes in the vertical temperature structure depending on the UV radiation of the star (e.g. Rauer et al. 2011; Grenfell et al. 2014). Abiotic production of ozone via water and carbon dioxide photolysis seems to be efficient for M-dwarf stellar irradiation, which will pose problems in the interpretation of spectral signatures of future follow up spectral characterisation of these planets. On Earth,

² An example is the system around Kepler-62 with two planets orbiting in the HZ; no masses could be derived for these planets owing to the faintness of the host star (Borucki et al. 2013).

the invention of photosynthesis caused a large increase in biodiversity and regional extent of life. For a spectral energy distribution as supplied by M-dwarf stars, inventing an operating photosystem is much more challenging, as shown by Kiang et al. (2007). Hence, despite that exploring rocky planets which lie in the HZ of M dwarf stars is a very interesting field in exoplanet research – both today and in the near future, for which we expect a lot of exciting results – the suspected differences in planetary environments could mean that life, if it has evolved on such worlds, will also be very different (less Earth-like) than what could be expected for an Earth-like planet around a Sun-like star.

2.1.3 Constraints on planet formation from statistics

A prime goal of PLATO will be to detect a large number of planets, down to the terrestrial regime in size, and with well-determined masses and radii, and hence bulk densities, with unprecedented precision. Bulk density is a testable quantity to probe the input physics, constrain planet formation models, and evaluate simulated planet population distributions. However, a better understanding of the relevant input physics into these models will require a large statistical sample covering a wide parameter space.

Figure 2.5 shows the bulk density of confirmed planets versus planetary mass (left: for all planets; right: planets with $P > 80$ days). In the figure, we note again that there are very few exoplanets similar to, or less massive than, Earth and Venus that have measured densities and masses. The mass range below $0.1 M_J$ is sparsely populated, and the highest priority detection space for PLATO.

The dashed lines in Figure 2.5 indicate modelled densities for planets with different bulk compositions (following Wagner et al. 2012; see also Zeng et al. 2016 and references therein). The right branch in each figure contains gas giant planets that roughly follow the green dashed line that corresponds to a Jupiter-like, H-He dominated bulk composition. The left branch of the roughly V-shaped density-mass distribution in Figure 2.5 is composed of planets with bulk compositions of silicates or ices, some of which have extended atmospheres that reduce their bulk density.

Several hundreds of small planets ($R < 2 R_E$) will be discovered with well-determined radii (3% precision), orbiting stars bright enough ($V \leq 11$) to be characterised with asteroseismology and amenable to spectroscopic follow up from ground, which can provide planetary masses down to 10% uncertainty, filling the left branch of Figure 2.5 with a high number of planets. Precise determination of planetary and stellar parameters is mandatory to understand some of the processes of planetary evolution, such as the photoevaporation of the atmospheres (Lammer et al. 2016, and references therein), especially those of highly irradiated super-Earths (Lundkvist et al. 2016), or the alignment between the planetary orbital axis and the stellar rotation axis (Campante et al. 2016).

During its nominal observations, PLATO will find several thousand planets of all sizes at all orbital periods (see Section 7 how these values were derived). These planets will orbit relatively bright stars ($V < 13$) compared to *Kepler* and their parameters will be obtained with classical methods in the same way as it has been done for previous missions. Although the parameter's precision will be smaller than for the brighter stars observed with PLATO, their much larger number will enable further constraining of the physical processes governing planet formation and evolution.

The formation of planets is presently believed to result from two different scenarios, which may or may not be mutually exclusive. In the core-accretion scenario, a planetary core is formed by the collision of solid planetesimals. As the planet grows it exists in a state of quasi-static equilibrium, whereby the energy loss at the surface of the planetary core is compensated for by the energy resulting from the accretion of planetesimals. When the mass of the core reaches a so-called critical mass, however, this compensation is no longer possible; the planet envelope starts to contract, the contraction energy being radiated away at the surface. This contraction triggers a very rapid accretion of gas, which is rapidly limited by the amount of gas that can be delivered by the protoplanetary disk surrounding the forming planet. This scenario has been studied by many authors, accounting for different physical effects, such as protoplanet migration (Alibert et al. 2004, 2005), opacity reduction in the planetary envelope (e.g. Hubickyj et al. 2005), excitation of accreted planetesimals by forming planets (e.g. Fortier et al. 2007, 2013), competition between different planets (e.g. Guilera et al. 2011), etc.

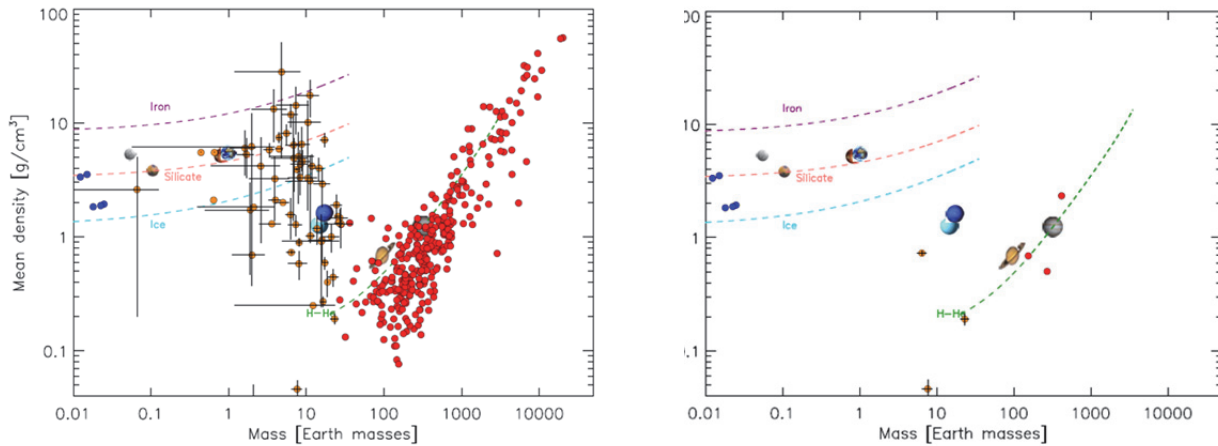


Figure 2.5: Mean planet density versus mass with density lines for different bulk compositions. Left: All currently known planets with measured radius and mass (hence bulk density). Right: only planets with $P > 80$ days.

In the disk instability model, the formation of a giant planet results from the presence of a gravitational instability in a cold, massive protoplanetary disk (e.g. Boss 1997; Mayer et al. 2005; Boley et al. 2010). After its formation, a giant planet clump is believed to cool and contract, eventually accreting planetesimals to form a planetary core (e.g. Helled & Bodenheimer 2011; Vazan and Helled 2012).

In the framework of the core-accretion model, one of the central issues is how to build a core larger than the critical mass. The critical mass, in turn, depends on a number of poorly known quantities: core luminosity (which results mainly from the accretion of planetesimals), decreasing for low luminosity (e.g. Ikoma et al. 2000); the opacity inside the planet envelope (low opacity envelopes lead to a reduced critical mass, and a larger envelope mass for a given core mass), and the mean molecular weight inside the planetary envelope, which again depends on the planetesimals' characteristics (size, strength, composition, see e.g. Hori and Ikoma 2011). Observationally determining the critical core mass as a function of distance to the star, stellar metallicity, and other parameters would therefore place constraints on the characteristics of planetesimals (e.g. mass function, excitation state, internal strength). It would also determine the maximum mass of planet that might potentially be habitable, since the presence of a massive H_2 -He envelope in a super-critical planet probably prevents any habitability.

The core accretion model scenario can be tested by increasing the sample of high density, low-mass rocky exoplanets, since those planets define the mass limit beyond which efficient gas accretion starts. This likely explains why almost no planets appear at high densities in the density-mass distribution in Figure 2.5. For example, following the silicate composition line with increasing mass in Figure 2.5, we find few planets with $M_{\text{planet}} > 0.03 M_J$ (about 6-9 M_E). This is consistent with the core accretion scenario, whereby higher-mass silicate planets would quickly accrete significant H-He envelopes and end up as high mass, lower density planets in Figure 2.5, i.e. in the ice planet regime or even growing to gas giant planets. See the interesting debate on the composition of planets like Kepler-10c (Dumusque et al. 2014; Weiss et al. 2016) and BD+2059b (Espinoza et al. 2016).

We emphasise that PLATO will not only discover such planets, but will also deliver accurate and precise measurements of their radii, masses, hence their bulk densities, allowing us to better understand their real nature. This is only possible because PLATO asteroseismic measurements will obtain accurate and precise stellar parameters, and because the targets are bright and thus amenable to RV measurements. Multi-planet, co-planar systems can be supplemented by TTV measurements.

We note that the low-mass planets in Figure 2.5 show a wide range of densities that span more than an order-of-magnitude. Planets with low masses and densities below that of pure ice (blue line) are indicative of a large H-dominated envelope. By filling the parameter space in Figure 2.5, PLATO will identify a large sample of low-mass planets that are likely to have H-dominated envelopes, around different types of stars with different ages. Planet population synthesis models (e.g. Mordasini et al. 2012b) predict a large number of low-mass planets (super-Earths and below) with large hydrogen envelopes. Such predictions can be validated by PLATO observations, testing our planet formation theories.

The situation becomes even more complex if one also considers atmospheric loss processes (see Section 2.1.13) that can remove a primordial H-envelope over time. These processes are stronger closer to the host star, and reduce the planetary envelope with time. It will be interesting to observationally study these effects by correlating planetary mass and bulk density of low-mass objects with other parameters, for example orbital distance and system age. We also expect the lowest-mass planets to lose their H-envelopes completely (like Earth, Venus, and Mars). PLATO will determine for which planets primordial atmospheres are unlikely to exist after a certain lifetime of their system, and will determine which planets have likely developed a secondary atmosphere (resulting in smaller scale heights, hence apparent radii and higher mean densities).

The right-hand panel of Figure 2.5 shows the current sample of planets with orbital periods >80 days that have been bulk characterised. The sample is small, with only two transiting exoplanets with measured RV masses (orange dots), and an additional five (red dots) with TTV mass determinations. Only a few additional planets from K2, TESS, and CHEOPS are expected to fill this diagram. Thus, while we will be able to compare planet population synthesis models with observational data for planets at small orbital distances, the picture will remain very limited for planets on longer orbits (i.e. orbits undisturbed by their host star and with potentially temperate surface conditions) until PLATO provides the capability to probe these large orbital distances.

PLATO will be the first mission to cover the parameter range of small, characterised (mass, radius, bulk density, age) planets with sufficiently large detection statistics to provide direct observational constraints on formation models and their predictions, as well as the dynamical evolution of young planetary systems.

PLATO will answer fundamental questions about planetary formation such as:

- What is the bulk density distribution of low-mass, terrestrial planets?
- What is the observed critical core mass for giant planet formation?
- Can super-massive rocky planets exist and how are they formed?
- When and where do planets stop accreting gas?
- Which planets likely have extended, primordial H-envelopes?
- How do these parameters depend on orbital distances, stellar type, metallicity, chemical composition or age?

These questions have to be studied as a function of planet orbital separations, stellar metallicities, and spectral type. They can only be addressed with a sufficiently large sample of planets of all sizes, from rocky to giant, with well determined masses, radii and bulk densities, around stars of different types and ages.

2.1.4 Multiple planet systems

One of the major findings of *Kepler* is the catalogue of multiple-planet transiting systems (see Lissauer et al. 2014). Multiple systems provide information about the relative inclinations of the orbits, a fundamental parameter to understand planet formation and evolution, and, thanks to their mutual gravitational interactions, provide information about their masses via the analysis of the transit timing variations and photodynamical effects (i.e. see Lissauer et al. 2013, and references therein). Photodynamical analysis can, in some cases, provide values of the planetary densities with excellent accuracy (in the few percent range, see Almenara et al. 2015). It is estimated that about 10% of the planetary systems discovered by *Kepler* show significant transit timing variations (Ford et al. 2011) providing meaningful constraints on their masses, in the range of few percent (Kepler-36, Carter et al. 2012) to few tens of percent (Kepler-11, Lissauer et al. 2013).

Multiple systems tend to be aligned (Figueira et al. 2012; Fabrycky et al. 2014; Ballard & Johnson 2016, and references therein), but there are several systems where this is not the case (McArthur et al. 2010; Dawson et al. 2014; Mills & Fabrycky 2017). The mutual alignment of the orbits, the distribution of eccentricities (Shabram et al. 2016), of orbital periods (Steffen & Hwang 2015), of sizes (Ciardi et al. 2013), and the distribution of densities, let it be homogeneous (e.g. Lissauer et al. 2013; Millis et al. 2016) or

inhomogeneous (e.g. Cabrera et al. 2014; Becker et al. 2015; MacDonald et al. 2016), provide fundamental information about formation and evolution processes (see also Ford 2014; Winn & Fabrycky 2014, and references therein).

There are about 700 multiple planet systems published by *Kepler*. Most of them orbit faint stars (their median magnitude is 14.5) and, with the notable exceptions of Kepler-10, 20, 25, 48, 56, 424, 432, 454 systems, at best only TTV masses are known. Typical uncertainties on the masses are of few tens of percent and little is known about their eccentricities. K2 is in the same situation as *Kepler*, only that it is discovering shorter period planets, and TESS will observe bright stars, but in the vast majority of the cases only in very short period orbits.

PLATO will discover several thousand transiting planets of all sizes and periods (see Section 7.2.3 on how this number was obtained) around stars brighter than $V=13$, reaching orbital periods beyond the range observed by K2 and TESS. Multiple systems discovered by PLATO will be characterised by TTVs with larger precision than *Kepler*, thanks to the higher observation time and sampling rate, providing meaningful constraints to the processes of planetary formation and evolution, especially in regions of the parameter space beyond reach for any other mission in the next decade.

2.1.5 Terrestrial planets

This section discusses in more detail what can be learned from accurate radii and masses of terrestrial exoplanets, in spite of the limitations in observables compared to our solar system.

After many years of effort from the thousands of *Kepler* and CoRoT planet candidates with $R < 2R_E$ we now have a handful of objects with masses believed accurate to $\pm 30\%$ (Figure 2.6) and this is starting to reveal tantalising correlations in the mass v's radius relationship for small planets (Dressing et al 2015; Buchhave et al. 2016). In all apart from one case, the masses have been determined from radial velocity instruments (the exception is Kepler-36b with a mass derived from a transit timing variation model, Carter et al. 2012). According to Dressing et al. (2015), there are other planets with less accurate masses that are not consistent with this correlation suggesting that other bulk compositions are likely. However, in general *Kepler* and CoRoT candidates are too faint to permit an accurate mass determination via RV observations. In many cases, even a rocky or icy nature cannot be distinguished owing to the size of the uncertainties. TESS will make little impact on the detection and precise characterisation of these small planets except for those around the coolest stars.

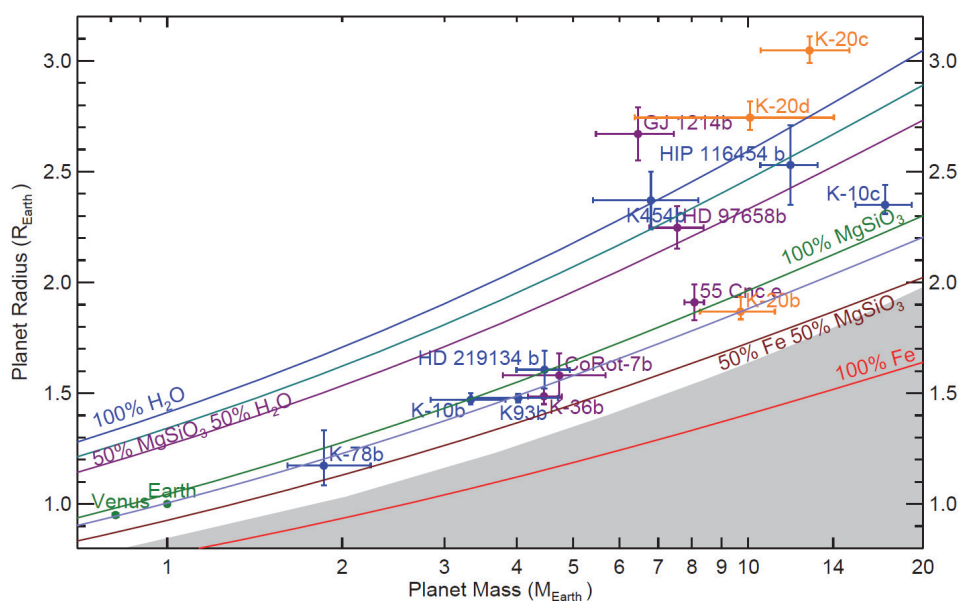


Figure 2.6: The mass v's radius relationship for small planets with the best determined masses (30%) from Buchhave et al. (2016). Planets with less well determined masses suggest other compositions are likely. The grey region to the lower right indicates the region where planets would have an iron content exceeding the maximum value predicted from models of collisional stripping.

Our knowledge of bulk planet density (and therefore composition) is, first and foremost, dependent on the quality of the stellar mass and radius determinations that feed into the determinations of planetary mass and radius. One of the main goals of PLATO is therefore to provide highly precise and accurate measurements of the planet host stars' characteristics, in particular their radii, masses and ages. Typical current uncertainties for radius and mass determinations of small planets are around $\pm 6\%$ and $\pm 20\%$, respectively, leading to uncertainties of 30 to 50% in bulk density. The observational precision envisaged for PLATO will reduce the uncertainty in planetary bulk density to about 10%.

Current detection limits have prevented the discovery of more than a few rocky exoplanets, although low-mass planets around other stars are most likely abundant. PLATO will provide masses and radii of a large number of terrestrial planets from close-in orbits up to 1 au distant from their host stars. Studying temperate planets at large orbital separations allows us to address the architecture of planetary systems and its connection to proto-planetary disk properties, and also to study the relationship between planet interiors and atmospheres in planets up to the HZ. These will be complemented by the detection of giant planets at larger orbital separations expected from the *Gaia* mission, expanding our characterisation of these systems. Constraining the mean composition and bulk interior structure of small planets, PLATO will enable us to answer the following questions:

- Are there other planetary systems that include a terrestrial planet like Earth?
- What is the typical bulk density distribution (and mass function) in planetary systems?
- How is the planet bulk density distribution correlated with stellar parameters (e.g. metallicity, mass, age, etc.)?

2.1.6 Gas giants and icy planets

Giant planets are planetary bodies primarily consisting of hydrogen and helium, with a small fraction of heavy elements (i.e. rocks and ices). The solar system gas giants, Jupiter and Saturn, orbit the Sun at distances of 5.2 and 9.6 au, respectively. The composition of a giant planet, and its depth dependence, are calculated by interior models, which are constrained by the observational properties of the planet, such as its mass, radius, rotation rate, and gravitational field coefficients. For Jupiter and Saturn these physical parameters are well known from space missions.

There is still uncertainty in the bulk composition of Jupiter and Saturn, in particular in the amount of high atomic number ($Z > 2$) material and the presence (or absence) of a central core. The uncertainties in giant planet interior models reflect the uncertainty in the equations of state (EOS) and model parameters, as well as in assumptions such as the number of layers, the distribution of the heavy elements within the planet, and the rotation profile/state. An additional uncertainty arises from the fact that the planets are assumed to be adiabatic, and therefore fully convective. However, if the planets have non-adiabatic structures, which is an outcome of double diffusive convection (Leconte & Chabrier 2012, 2013), the heavy element mass can be significantly higher owing to higher internal temperatures. In this case, constraining the bulk composition of the planets becomes even more challenging.

Internal models of Jupiter and Saturn using EOSs of hydrogen, helium, and heavier elements suggest that Jupiter's core mass lies between 0 and $10 M_E$, and that the mass of high- Z material in the envelope is approximately $30 M_E$ (e.g. Saumon & Guillot 2004; Nettelmann et al. 2008). Militzer et al. (2008) suggested that Jupiter's interior consists of a core of about 14 to $18 M_E$ surrounded by a homogenous envelope composed mainly of hydrogen and helium. Determinations of Saturn's total enrichment in heavy elements typically range from ~ 10 to $\sim 30 M_E$, with a core mass between ~ 0 – $15 M_E$ (e.g. Saumon & Guillot 2004; Fortney & Nettelmann 2010; Helled & Guillot 2013).

Standard interior models of the solar system ice giants, Uranus and Neptune, suggest that they consist of three main layers: an inner rocky core; a water-rich envelope, and a thin atmosphere composed mostly of hydrogen and helium with some heavier elements (e.g. Podolak et al. 1995; Marley et al. 1995; Fortney & Nettelmann 2010). However, it should be noted that, owing to measurement uncertainties, it is still unclear whether Uranus and Neptune are truly 'ice giants', or whether they are planetary bodies which primarily

consist of silicates, with hydrogen and helium envelopes (e.g. Helled et al. 2011). In addition, calculations of Uranus' cooling history imply that the planet contracts “too slowly”; simulations find that Uranus cannot cool to its measured intrinsic luminosity by the age of the solar system, assuming an adiabatic interior. This suggests that Uranus' interior may not be fully convective, and/or that it contains an additional energy source (e.g. compositional gradients) besides its gravitational contraction (e.g. Fortney & Nettelmann 2010). Neptune too, likely has a significant internal energy source.

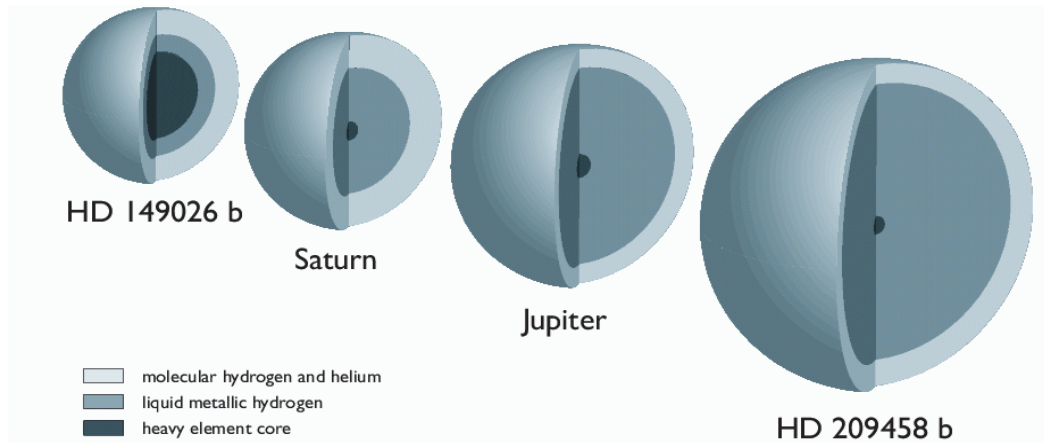


Figure 2.7: Illustration of the interior structure of HD149026b and HD209458b in comparison to Jupiter and Saturn (from Charbonneau et al. 2007).

Another important open question regarding these planets is their formation process. It is still unclear what conditions and physical mechanisms lead to the formation of these moderately low-mass objects, especially at the large orbital distances at which we find them in the solar system today (e.g. Dodson-Robinson & Bodenheimer 2010). It was suggested by the so-called ‘Nice model’ that the architecture of the solar system has changed over time thanks to dynamical interactions of the giant planets with the dense planetesimal disk. Due to momentum exchanges the giant planets all (with the exception of Jupiter) migrated outwards, and thus their current distances from the Sun do not have to reflect the distances where they formed. By capturing various planetary systems at different evolutionary states, PLATO may provide some verification of the planetary migration hypothesis.

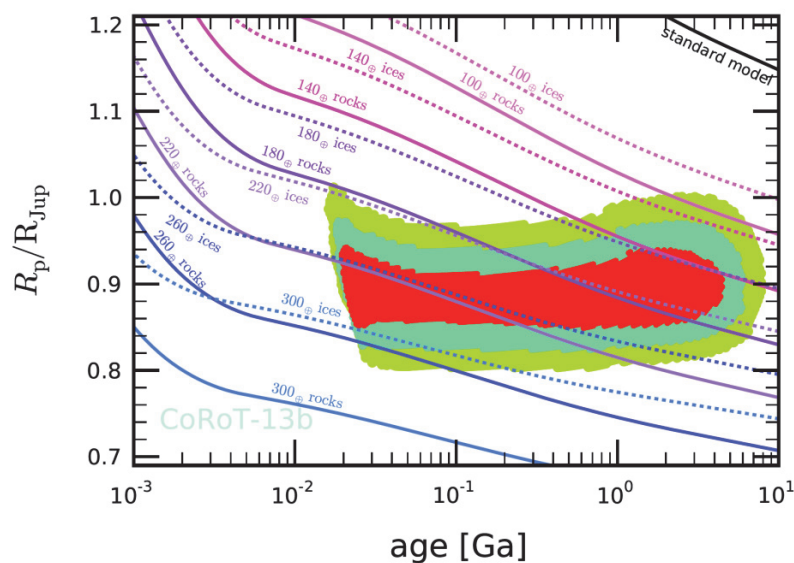


Figure 2.8: The development of CoRoT-13b’s radius with time (Cabrera et al. 2010 and references therein). The coloured areas provide the uncertainty in planet radius and in stellar age derived from stellar evolution models matching the stellar density and effective temperature (within 1 (red) to 3 (green) sigma uncertainty). The curves show evolution tracks for CoRoT-13b (assuming $M=1.308 M_J$, $T_{eq}=1700$ K) for different amounts of heavy elements concentrated in a central core, surrounded by a solar-composition envelope.

The compositions and internal structures of extrasolar giant and Neptune-sized planets are less constrained than those of the planets in the solar system, but they offer the opportunity to study giant planets as a class. The diversity of gas giant and ‘icy’ exoplanets is much larger than expected from our solar system, thus expanding the parameter range that can be studied. Many gas and ice planets are already known, and more are expected from ground-based surveys (e.g. NGTS) in the near future. The CHEOPS mission will provide significantly improved constraints on the radii of transiting planets discovered from the ground. The first steps towards a deeper understanding of gas and ice planet interiors will thus be made in this decade. The main role of PLATO, following these activities, is to dramatically increase the mas-radius parameter space for exoplanet detection and add the time dimension we are still missing, and to further extend it towards intermediate orbital separations. Again, we note that the PLATO observations will be complemented at large orbital separations (where the transit probability is low) by detections from the *Gaia* mission.

Although the majority of transiting giant planets are composed mostly of hydrogen and helium (e.g. Guillot et al. 2006; Miller & Fortney 2011), their internal constitution is not necessarily similar to that of the gas giants in our solar system. In fact, exoplanets show a large diversity of masses and radii that has yet to be explained. Extrasolar giant planets can differ significantly from Jupiter and Saturn (e.g. Figure 2.7) since they formed in different environments. In addition, giant planets close to their parent stars are exposed to intense stellar radiation that prevents their atmospheres from cooling, and therefore affects the contraction of their interiors. Although our understanding of hot Jupiters is still incomplete, substantial progress in studying these objects has been made. Interior models that include the effects of irradiation have been computed (e.g. Guillot et al. 1996; Bodenheimer et al. 2003, Batygin et al. 2011), and detailed models of the giant planets’ atmospheres are now available, although the mechanisms that can inflate the radii of irradiated giant planets are still unclear (Laughlin et al. 2011). With its precise determinations of planet radii, PLATO will significantly contribute to understanding the mechanisms responsible for the inflation of gas giants. Indeed, it has been shown by Schneider et al. (2011; their Fig. 9) and confirmed by Demory et al. (2011a) that inflation decreases with the planet illumination by the parent star. PLATO will provide broad statistics of this correlation, and of the influence of the stellar wind.

Detailed studies of the interior structure of extrasolar giant planets suggest that these objects typically consist of cores of at least $10M_E$ (Guillot et al. 2006; Miller & Fortney 2011). The heavy element mass is proportional to stellar metallicity (often proxied by $[Fe/H]$), while planetary enrichment is inversely proportional to the planet’s mass (Miller & Fortney 2011). Recently, a class of planets has emerged that possesses a large fraction of rocky material in their cores, with CoRoT-13b (Cabrera et al. 2010) as an example (Figure 2.8).

PLATO will improve our understanding of the composition and evolution of gas giant and Neptune-sized planets in major ways:

- The planets discovered by PLATO around bright stars will have 3 times more precise radius determinations and 5 times more precise mass determinations than current results. This will allow us to classify detected planets as rocky or icy small planets, or as ice or gas giants, with high accuracy. High precision measurements of planetary radii and masses will allow us to constrain core masses from interior modelling. These can be compared to the largest observed core sizes that failed to undergo gas accretion, and help to constrain planet formation.
- PLATO will provide the masses and radii of giant planets of various ages. This will allow us to address the contraction history of ice and gas giant planets.
- PLATO will allow us to address the possibility of compositional change with time, and the connection between age, inflation, and atmospheric loss rate.

The compositions of gas giant planets can reveal important information on giant planet formation. As previously discussed (see Section 2.1.3), there are two leading theories for giant planet formation: core accretion (the standard model), and disk instability. While both formation scenarios can lead to a large range of compositions and internal structures, the core accretion model typically predicts a non-Solar composition for giant planets, while giant planets formed by gravitational disk instability can have different compositions that depend on stellar metallicity, planet mass, the efficiency of planetesimal accretion, etc. (Helled &

Schubert 2008). Clearly, a more accurate and precise determination of the bulk composition of giant extrasolar planets that are not strongly irradiated, as will be obtained by PLATO, can provide valuable constraints on giant planet formation and evolutionary models. For close-in gaseous and icy giant planets, the knowledge of their interior structures will furthermore allow us to better understand tidal dissipation processes in these planets (Ogilvie 2013; Remus et al. 2012).

In summary, PLATO will address the following questions regarding gas and ice planets:

- Up to which orbital distance do we find inflated gas giant planets?
- How does this correlate with stellar parameters (e.g. stellar abundances, type, activity, age)?
- Are gas giants with massive cores frequent and how does their distribution depend on orbital distance and stellar type?
- How do gas giants with massive cores form?
- How do planetary parameters depend on orbital distances, stellar type, metallicity, chemical composition or age?

2.1.7 Planets orbiting intermediate mass stars

It is now well established that planets form within a few million years from the dusty, circumstellar disk of young stars. It is thus expected that the properties of the planets must be closely related to the structure, lifetime, mass, and chemical composition of the disk, but how they relate to each other is not known. Finding such correlations would give us key information on how planets form. In order to find out how the properties of the planets relate to the properties of the disk, we have to take a statistical approach. Theoretical studies have shown that more massive stars should also have more massive planets, because they had more massive disks (Kennedy & Kenyon 2008). This prediction is in fact confirmed observationally; intermediate-mass stars (1.3–2.1 M_{\odot}) have twice as many massive planets as Solar-like stars, and they can also have planets that are much more massive than Sun-like stars (Johnson et al. 2010a, 2010b; Vigan et al. 2012). PLATO is the first mission to allow the study of how the planet population changes with the mass of the host star over a wide range of masses, for a large number of targets. Since we now know, thanks to Spitzer and Herschel observations, how the average properties of disk change with the mass of the host star, we will for the first time be able to statistically relate properties of the disks with the properties of the planets. A key question to be addressed is: how do the properties of planets change with the mass of the host stars?

2.1.8 Planets around giant stars

Several ground-based Doppler planet searches target sub-giant and giant stars instead of main-sequence stars. The number of planets known to orbit giant stars (~60; Niedzielski et al. 2015) is still small compared to those known to orbit main-sequence stars, but their number has dramatically increased in recent years and is expected to do so in the near future thanks to TESS (Campante et al. 2016), CHEOPS, and *Gaia*. The discovery and characterisation of planets orbiting sub-giant and giant stars is of particular importance for the following reasons:

- Confirmation of a planet orbiting a giant star is, in many cases, almost impossible based on RVs alone, since the RV signal of an orbiting planet is hard to disentangle from the signature of radial and non-radial pulsations, unless their timescales are very different. Thus, independent confirmation of planets orbiting giant stars is most useful.
- Sub-giants and giant stars are more massive than Sun-like main-sequence stars, so by finding more planets around giant stars we can disentangle the influence of the host star's mass and its disk on the forming planets and their properties.
- Sub-giants and giant stars have undergone significant stellar evolution, which will have affected planetary orbits (close-in giant planets risk to be engulfed, see Lillo-Box et al. 2016, and references therein). Studying the planet population around sub-giant and giant stars offers the opportunity to investigate the influence of stellar evolution on the properties of the planetary population.

- It is still not clear if evolved giant planet hosts are mostly metal-rich (Pasquini et al. 2007; Mortier et al. 2013). This could be checked using the PLATO planet sample in combination with its well-characterised host stars.

Kepler has detected a small number of planets around giant stars (e.g. Steffen et al. 2012; Huber et al. 2013; Lillo-Box et al. 2016). Owing to the much larger stellar disk of a giant star compared to the stellar disk of a main-sequence star, the transit probability is much higher for a planet orbiting a giant star than for a planet orbiting a main-sequence star. On the other hand, the transit depth is much smaller for the same reason (a much smaller percentage of the stellar disk is blocked by the planet), so that the planet is harder to detect; indeed, the false-alarm rate of *Kepler* planet candidates (KOIs) around giant stars in *Kepler* data was recently found to be higher than previously thought (Santerne et al. 2015).

PLATO is in a better position to find planets around these stars. The depth of a transit of a Jupiter-sized planet in front of a giant star with a radius of 10 solar units is 100 ppm, which is within the mission's detection capabilities. Detection will still be challenging, however, owing to the photometric activity of giant stars, which will have to be well characterised. The planets found by RV surveys around this type of star have typically periods of several hundreds of days. For example, at 400 day orbital periods, the transit probability is 3% and the transit duration almost 4 days.

2.1.9 Planets around post-RGB stars

To date not a single bona fide planet has been identified orbiting an isolated white dwarf (e.g. Hogan et al. 2009), though the discovery of transiting objects around WD 1145+017 (EPIC201563164, Vanderburg et al. 2015) shows that they should exist. We therefore remain ignorant about the final evolutionary configuration of >95% of planetary systems. Theoretical models (e.g. Nordhaus & Spiegel 2013) predict a gap in the final distribution of orbital periods, due to the opposite effects of stellar mass loss (planets pushed outwards) and tidal interactions (planets pushed inwards) during the red giant branch (RGB) and asymptotic giant branch (AGB) phases. If a planet enters the envelope of the expanding giant star, its survival depends a number of poorly constrained parameters, particularly its mass. Currently, the lowest mass brown dwarf companion known to have survived such “common envelope” evolution to the WD stage has a mass of 25–30 M_J (Casewell et al. 2012), but theoretical models suggest much lower mass gas giants may survive.

Over its five-year primary mission, *Gaia* is expected to astrometrically detect tens or hundreds of WD planets ($M_{\text{planet}} > 1 M_J$) in long period orbits (Sozzetti et al. 2014), but the likelihood of planets surviving in close orbits around WDs will likely remain an open question for some time. Recently, more than 15 planets around post-RGB stars were detected, orbiting extreme horizontal branch subdwarf-B (sdB) stars, or cataclysmic variables. Most of them were on long-period orbits, and discovered from eclipse or pulsation timing (e.g. Silvotti et al. 2007), while two sdB planetary systems with very short orbital periods of a few hours were detected by *Kepler* through illumination effects (Charpinet et al. 2011; Silvotti et al. 2014). The *Kepler* discoveries suggest that ~10% of sdB stars could have close planets (or planetary remnants) and ~2.25% of sdB stars could show a transit. PLATO will collect large-number statistics for these objects, detecting sdB planets not only from illumination effects, but also from transits, giving the first estimates of their radii.

Even more importantly, PLATO has the capability to detect the first WD planet transits, which requires large statistics (Faedi et al. 2011). PLATO can easily detect gas giants eclipsing WDs, placing limits on the masses of planets that can survive “common envelope” evolution. In addition, since WDs are similar in radius to Earth, PLATO can detect transiting bodies down to sub-lunar sizes. Such objects may exist in close orbits to WDs, possibly through perturbations with other planets in a complex and unstable post-main sequence system. Indeed, at periods of ~10–30 hours, these rocky bodies would exist in the WDs' HZs (Agol 2011), and their atmospheres would be detectable with JWST (Loeb & Maoz 2013).

Discovery and characterisation of post-RGB planets is essential to study planetary system evolution and planet-star interaction during the most critical phases of stellar evolution: RGB and AGB expansion; thermal pulses; planetary nebula ejection, etc. We note that sdB/WD asteroseismology allows a very good characterisation of these stars and their planets.

2.1.10 Circumbinary planets

Planets that orbit around both components of a stellar binary were suggested as favourable targets for transit surveys (Borucki 1984) due to the expected alignment between the planetary and the stellar orbital planes, which strongly increases detection probabilities on eclipsing binaries with near edge-on orbits. Some early surveys (e.g. Deeg et al. 1998) subsequently focused on such systems, but it was not until the *Kepler* mission that the first transiting circumbinary planets (CBPs) were found (Doyle et al. 2011). The discovery of 11 transiting CBPs in 9 systems has been announced to date³. Their orbital periods are of the order of several months and planet-masses are relatively low, the most massive being Kepler-16b with $M_{\text{planet}} \sim 0.33 M_{\text{J}}$. All CBP orbits have an inner limit to their stability (e.g. Dvorak et al. 1989; Chambers et al. 2002), and most of the transiting CBPs orbit close to that limit (Welsh et al. 2012). It is also notable that all planet-hosting binaries have orbital periods on the order of 10 days or longer and have an occurrence frequency probably similar to that in single stars (Armstrong et al 2014).

An additional photometric method to detect CBPs, based on the detection of the binaries' eclipses in the planet's reflected light, was suggested by Deeg & Doyle (2011). In *Kepler* data this method can potentially detect CBPs that are close to the inner stability limit around short-periodic binaries, with a large range of orbital inclinations. No discoveries have been reported yet, however.

Formation and evolution models predict the formation of circumbinary protoplanets to occur in relatively distant disks, with subsequent migration to the planets' observed positions being accompanied by the further accretion of matter. In particular, the accumulation of CBPs near the inner stability limit has been foreseen by Pierens & Nelson (2007), who predicted that the inward drift of a protoplanet can be stopped near the edge of the disk cavity formed by the binary stars. In more general terms however, any generic theory on planet system formation and evolution needs to be compatible with planets found around binary stars, making this population of planets an interesting test-bed for many theoretical advances.

The number of CBP detections that was found to date in *Kepler* data is likely limited by the number of light curves sampled and not by photometric precision, i.e. all known CBP transits can be identified "by eye" in the light curves. One difficulty comes from the precession of the orbit which results in appearance and disappearance of transits.

With the sample size and observing duration of PLATO, we can expect that the sample of transiting circumbinary planets (CBPs) of the types that are currently known will multiply several-fold. We can also expect a subsequent detailed analysis of the planet(s) thanks to their host star brightness, and investigating whether the planets that form in such systems are different from those around single stars.

For PLATO, this presents the following objectives:

- What are the properties of the circumbinary planetary systems? What are their masses, orbital periods, and the types and ages of host stars? Can their special features be explained by existing planet formation theories, and/or do they need modifications?
- Do other classes of CBPs besides currently known ones exist? In particular, no CBPs on short-period binaries have been found to date, although these binaries are by far the most common and there are no special obstacles to the detection of their planets.

2.1.11 Evolution of planetary systems

The ability to derive the age of planetary systems is one of the key assets of PLATO. The age of stars is traditionally poorly constrained, to within (at best) only a few Gyr for stars on the main-sequence. Furthermore, young planets, that are the most important when trying to decipher the conditions under which planetary systems are formed, orbit around young, active stars; the determination of their parameters has thus far remained elusive (e.g. Gillon et al. 2010; Czelsa et al. 2009; Guillot & Havel 2011).

³ As of September 2016.

With relative ages of a large sample of main-sequence stars known to 10% precision, PLATO will essentially remove the age ambiguity in planet evolution. A large sample of planetary systems with well-determined ages will allow us to search for archetypes of planet and planetary system evolution, and identify correlations with host star parameters, planet interior composition, and planetary structure.

Planets and planetary systems evolve with age in several different ways:

- Gas giant planets progressively cool and contract, a process that lasts up to several Gyr (see Section 2.1.6). An accurate knowledge of age is therefore crucial for the interpretation of measured radii and a determination of interior structure.
- Planet formation theories predict rocky planets with primordial hydrogen atmospheres, but terrestrial planets evolve with time, as exemplified by the planets in our solar system (see also Section 2.1.5). The atmospheres of the terrestrial planets in our solar system are secondary atmospheres produced by impacts and outgassing from the interior, both processes having been more intense in the young solar system. In the case of Mars, a possibly denser young atmosphere has since been lost to space. In the case of the Earth the atmosphere has been further modified by the development of oxygen-producing life (tertiary atmosphere) since the planet was about 2.5 Gyr old.
- Host stars evolve with time and expose young planets to much higher UV and high-energy radiation levels than found on Earth today (see Section 2.1.13). This affects processes such as atmospheric losses, and also increases radiation levels at the surface of terrestrial planets, affecting the prospects for life. Therefore, good characterisation and dating of planet host stars is crucial if we are to obtain an understanding of the evolution of planetary atmospheres, and of habitable conditions. The significance of atmospheric loss processes is also crucial for understanding whether small planets are able to retain their extended, hydrogen-dominated, primary atmospheres over a significant part of the lifetime of a planetary system (see Section 2.1.12). An observational constraint on the presence of primary atmospheres for planets with different ages will allow us to test planet synthesis models (e.g. Mordasini et al. 2009, 2012b; Section 2.1.2). Crucial here are planets at intermediate orbital distances, which are less affected by loss processes caused by strong stellar radiation.
- The architecture of planetary systems is shaped through planet formation and subsequent dynamical processes that cover a wide range of timescales, up to billions of years. The comparison of planetary system populations with different ages will allow us to investigate whether typical evolution scenarios exist. In the case of hot Jupiters, precise ages of different systems will allow us to assess their evolution (disk or Kozai migration) and their fate. For small size planets, *Kepler* has discovered several compact multiple systems which show significant dynamical interactions, and are very interesting for the understanding of planetary formation: Kepler-90 with 7 planets (Cabrera et al. 2014); Kepler-11 with 6 planets (Lissauer et al. 2011), and Kepler-154 with 6 planets (Ofir & Dreizler 2013; Rowe et al. 2014).

The distinct evolution of the terrestrial planets in our solar system is far from being fully understood. Exoplanets can complement our investigations of terrestrial planet evolution by contributing information not accessible in the solar system, namely a large number of planets covering a wide range of bulk parameters, with different ages. This will allow us to search for systems to be used as case studies. Such a sample will also allow investigation of possible correlations of planetary evolution processes with stellar and planetary system parameters, which will provide a breakthrough in our understanding of the evolution of atmospheric composition and habitability. PLATO will provide key steps towards this ultimate goal.

Terrestrial planets at intermediate orbital distances play a crucial role; PLATO will measure their bulk densities and masses, necessary to estimate outgassing efficiencies and atmospheric scale heights, and will determine accurate and precise ages. Since PLATO target stars are bright, they will be ideal targets for future large missions that will spectroscopically characterise the atmospheres of nearby Earth-like planets for signatures of life.

PLATO will be able to provide accurate and precise masses for complex planetary systems. Furthermore, TTV observations over long time periods, e.g. by combining PLATO with already available *Kepler* observations, would allow measurement of the Q-factor describing internal tidal energy dissipation of planets, a factor crucial to understand the tidal evolution of close-in planets.

The accurate and precise determination of planetary system ages for thousands of systems is one of the key features of the PLATO mission. This crucial goal will not be achieved by any other current or planned transit mission. Key science questions PLATO can answer include:

- What are the ages of planetary systems?
- How do planet parameters (e.g. mean densities, radii of gas giants, planet star distance distributions, and, if combined with spectroscopic follow-up, atmosphere properties) correlate with age?
- How many super-Earths retain their primary atmosphere? Is there a correlation of small planet primary atmospheres with system age? What are the main parameters governing the presence of primary atmospheres (e.g. formation mechanism, stellar type, orbital distance, age, metallicity)?
- What is the planetary evolution timescale compared to the lifetime of the system?
- How does the structure/architecture of planetary systems vary and evolve with age?

2.1.12 Planetary atmospheres

Numerous studies have been published on the use of wavelength-dependent primary transits and secondary eclipses to characterise the atmospheres of exoplanets including GJ 1214b (e.g. Charbonneau et al. 2009; Bean et al. 2010; Berta et al. 2012; de Mooij et al. 2012) and 55 Cancri e (e.g. Crossfield et al. 2012; Demory et al. 2012; Ehrenreich et al. 2012). Highlights of these studies include claimed detections of molecular features in the infrared (e.g. Knutson et al. 2011; Sing et al. 2016), the inferred presence of clouds/hazes in the visible in the atmospheres of hot Jupiters (e.g. Pont et al. 2013), and the detection of exoplanet's exospheres that contain atoms of hydrogen, carbon, and oxygen (Vidal-Madjar et al. 2003; Lecavelier des Etangs et al. 2012; Ben-Jaffel & Ballester 2013). More recent discoveries of transiting exoplanets in suitable orbital and nearby configurations for atmospheric characterisation such as GJ 1132 b (Berta-Thompson et al. 2015) and the TRAPPIST-1 b, c, d planets (Gillon et al. 2016; de Wit et al. 2016) bear the promise of new transmission studies for these Earth-sized planets.

Visible data are particularly useful for determining the planet's albedo (e.g. Evans et al. 2013), the identity of the major spectroscopically inert molecules, and the relative abundance of clouds/hazes of the atmosphere.

Clouds have long been an obstacle to our understanding of the atmospheres of Earth, other solar system planets, and brown dwarfs. Now they are rapidly emerging as a major theme in the study of hot Jupiters, super-Earths, and directly imaged exoplanets (e.g. Gibson et al. 2013; Barstow et al. 2014; Nikolov et al. 2015; Sing et al. 2015; Parmentier et al. 2016; Sing et al. 2016; Skemer et al. 2016; Apai et al. 2016). For small exoplanets, visible data help to determine if a thick, gaseous atmosphere is present, and thus can identify the exoplanet as a prime candidate for follow-up, atmospheric spectroscopy with JWST, E-ELT, and future L-class missions. Potentially, the pre- and post-transit halo caused by visible-wavelength starlight refracted in the planet atmosphere may reveal whether the atmosphere is cloudy/hazy or not (García Muñoz et al. 2012).

The albedo measures the fraction of starlight reflected by an atmosphere, and therefore participates in its energy budget. The geometric albedo is a measure of the reflectivity of the planet when viewed fully illuminated, whereas the spherical albedo is phase-averaged measure of the reflectivity and therefore more relevant for energy balance considerations and for the determination of the atmospheric thermal structure. Measuring the secondary eclipse (occultation depth) in the visible directly yields the geometric albedo (e.g. Demory et al. 2011b, 2014; Esteves et al. 2013, 2015; Angerhausen et al. 2015). By detecting reflected light over the full planet orbit, the spherical albedo can also be derived (García Muñoz & Isaak 2015). For the hottest objects (~2000 to 3000 K), thermal emission from the exoplanet may contaminate the broadband visible data, thus confusing the measurement of reflected light versus thermal emission. In these situations, the two broad-bands of the fast cameras of PLATO will be useful in decontaminating the occultation depth measurements for the brightest stars. Indeed, simultaneous measurements with the two filters of the fast cameras will provide insight into the reflected starlight-vs.-thermal emission contributions from the exoplanet atmosphere, and into the cloud properties of the object. In reflected starlight for planets around the brightest targets, the shorter-wavelength photons are expected to penetrate less than the longer-wavelength ones, which entails that different atmospheric depths are being probed.

The spectroscopically active molecules of an atmosphere typically contribute spectral features in the infrared, but these molecules are often minor constituents (by mass) of an atmosphere. Of central importance in interpreting an exoplanetary atmosphere is the knowledge of the pressure scale height, which is set by the mean molecular weight. This is determined by the dominant (by mass) inert molecule, and the gravity and temperature of the planet. On Earth, the dominant inert molecule is nitrogen; in gas giants like Jupiter, it is believed to be molecular hydrogen. Analyses of the spectra of hot Jupiters often assume the atmosphere to be hydrogen dominated (Madhusudhan & Seager 2009), but for rocky or terrestrial exoplanets with secondary atmospheres, the mean molecular weight cannot be assumed. First indications of the mean molecular weight can be obtained by measuring the primary transits at two visible wavelengths (Benneke & Seager 2012), which can be accomplished using the two broad-bands of the fast cameras of PLATO. The method is complicated by the presence of clouds, but still provides first hints (strong/weak Rayleigh slope) as to the nature of the atmosphere, which can be followed up with spectroscopic observations. If only one broad-band measurement is made, then one may be able to distinguish between hypothesized atmospheres (e.g. hydrogen-dominated versus water-dominated models; de Mooij et al. 2012). Alternative methods include the detailed analysis of the line shape of a certain molecular species, or the relative strength of its features at different wavelengths (Benneke & Seager 2012), but such an approach requires a robust line opacity list, which is not always the case. Visible data thus provide an important check on the analysis of infrared data of exoplanetary atmospheres. Identifying the dominant, inert molecule in an atmosphere has significant implications for inferring its thermal structure and spectrum, as the inert component often exerts an indirect influence on the spectroscopically active molecules via processes such as pressure broadening and collision-induced absorption.

Phase curves show the exoplanet's flux as a function of orbital phase, which may be deconvolved to obtain the flux versus longitude, known as a "brightness map" (Cowan & Agol 2008; Demory et al. 2016). Infrared phase curves contain information about the efficiency of heat redistribution from the dayside to the night side of an exoplanet (Showman & Guillot 2002; Cooper & Showman 2005; Showman et al. 2009; Cowan & Agol 2011; Heng et al. 2011), as previously demonstrated for hot Jupiters (e.g. Knutson et al. 2007, 2009). To a lesser extent, infrared phase curves also constrain the atmospheric albedo and drag mechanisms (shocks, magnetic drag). In contrast, visible phase curves encode the reflectivity of the atmosphere versus longitude (e.g. García Muñoz & Isaak 2015; Shporer & Hu 2015), which in turn constrains the relative abundance of clouds or hazes if they are present (e.g. Webber et al. 2015). The cloud/haze abundance depends on the size and mass density of the particles, as well as on the local velocity, density, pressure and temperature of atmospheric flow, implying that a robust prediction of cloud properties requires one to understand atmospheric chemistry and dynamics in tandem. The physics relevant to the phenomena of reflected starlight and planet thermal emission, which dominate the phase curve measurements at visible and infrared wavelengths respectively, is complementary. In the optical, the scattering properties of condensates depend more strongly on the particles' refractive index (and therefore composition) and sizes. This consideration is useful in the inverse step of trying to pin down potential condensates in exoplanet clouds.

Examples of exoplanets where clouds are likely present include Kepler-7b, which has a high albedo (~ 0.3 , comparable to the solar system giant planets) and a phase curve containing a surprising amount of structure (Demory et al. 2011a; García Muñoz & Isaak 2015), as well as numerous hot Jupiters detected from the ground. The feasibility of obtaining visible phase curves has already been demonstrated for the CoRoT (Alonso et al. 2009a,b; Snellen et al. 2009, 2010) and *Kepler* (Borucki et al. 2009; Batalha et al. 2011) missions, and it has been demonstrated they that can be used for planet confirmation (Quintana et al. 2013) and bulk parameter determination (Barclay et al. 2012). A few comprehensive studies of phase curves and secondary eclipses with *Kepler* data have recently been published. They investigated both giant planets (Angerhausen et al. 2015; Esteves et al. 2015) as well as super-Earths (Demory 2014) and suggest that, on a statistical basis, super-Earths are comparatively more reflective than hot Jupiters. This information is key towards validating theoretical models of exoplanet clouds and towards the preparation of both transmission and phase curve observations at infrared wavelengths.

Information from the phase curve of the exoplanet can also be used to constrain the temporal evolution of the temperature distribution of its upper atmosphere (e.g. Stevenson et al. 2014), and to set constraints on the dynamics and clouds coverage (see Parmentier et al. 2016) of its atmosphere (e.g. Knutson et al. 2009). An interesting goal would be to establish the frequency of planets showing super-rotation on their atmospheres, a phenomenon which involves displacement of the hottest atmospheric spot of a tidally locked planet by an equatorial super-rotating jet stream (see Faigler et al. 2013, and references therein). Optical data from *Kepler*

have indeed enabled a first investigation of atmospheric super-rotation. It is now known that the hottest giant planets tend to exhibit their brightness peak east of the sub-stellar point, possibly as a result of a thermal hot spot shifted by atmospheric dynamics (Esteves et al. 2015; Hu et al. 2015; Shporer & Hu 2015). In contrast, the cooler objects tend to exhibit their brightness peak westwards of the sub-stellar point, a configuration that is likely explained by clouds formed on the planet night side and reaching onto the planet's western dayside hemisphere. The optical phase curves of some of these exoplanets have also revealed higher-order harmonics whose physical origin remains uncertain (e.g. Esteves et al. 2015). PLATO's long temporal coverage and its high photometric precision are the best mean to detect and accurately model phase curves for a large number of targets. Neither CHEOPS nor TESS will match these capabilities.

PLATO will provide targets to carry out the investigations described above. Furthermore, among PLATO's detections will be nearby giant planets on wide orbits, for which both transit spectroscopy and direct imaging spectroscopy will be possible. The comparison of these two approaches will then allow us to study the vertical structure of exoplanet atmospheres. PLATO's fast cameras, equipped with two colour filters, will also provide unique insight into the dusty envelope of disintegrating planets (e.g. KIC 12557548b, KIC 8639908, K2-22b; DeVore et al. 2016) and planetesimals orbiting white dwarfs (e.g. WD 1145+017; Vanderburg et al. 2015). Simultaneous measurements at two colours will impose key constraints on the optical properties and particles sizes of the dusty envelopes for these systems and for new similar systems to be discovered.

As the scientific community prepares for the launch of the JWST (which will be in its extended operations phase when PLATO is launched), as well as ground-based telescopes such as E-ELT (first light planned for 2024), it is vital that we correctly identify the best targets for follow-up, atmospheric spectroscopy of small exoplanets. Earth-like exoplanets with sizes $\sim 2 R_E$ are believed to be either composed predominantly of rock, or to be scaled-down versions of Neptune with thick gaseous envelopes. If the bulk composition of an exoplanet cannot be made from a material lighter than water, then one can calculate the thickness of the atmosphere, relative to the measured radius, by utilising the mass-radius relation of pure water (Kipping et al. 2013). It was shown that such a simple approach can be used to imply a mostly rocky composition (e.g. Earth, Kepler-36b; Kipping et al. 2013). By quantifying this metric for the entire PLATO catalogue of small exoplanets, one could construct a valuable database of optimal follow-up targets. Knowledge of the fraction of small exoplanets with and without thick atmospheres, as a function of their other properties, will provides new constraints on planet formation theories (see Section 2.1.3).

In summary, the key science questions that PLATO can answer about the atmospheres of exoplanets are:

- What is the diversity of albedos present in exoplanetary atmospheres? How does the albedo correlate with other properties of the exoplanet (incident flux, metallicity, etc.)? Are these albedos associated with the presence of clouds or hazes?
- What are the dominant, inert molecules present in exoplanetary atmospheres? What are the mean molecular weights?
- When are clouds present in exoplanetary atmospheres? What is the diversity of the cloud properties (particle size, reflectivity, etc.)? This information will be key for the validation of theoretical models and in the interpretation of infrared observations.
- For small exoplanets ($\sim 2 R_E$ in size), what are the best targets for follow-up, atmospheric spectroscopy? Here, small planets at intermediate orbital separations are of particular interest.

2.1.13 Characterising stellar-exoplanet environments

Transit observations of exoplanets around bright host stars, together with advanced numerical modelling techniques and known astrophysical parameters (such as the host-star age and radiation environment), offer a unique tool for understanding the interaction of exoplanet upper atmosphere with the magnetospheres of their host stars. Hubble Space Telescope (HST) UV transmission spectroscopy and Spitzer secondary eclipse measurements of known, bright exoplanetary systems have been used to study a number of issues related to the upper atmospheres of exoplanets, including: space weather events (e.g. Lammer et al. 2011a; Lecavelier des Etangs et al. 2012); thermospheric structure (e.g. Koskinen et al. 2012); the exosphere-magnetosphere-stellar plasma environment (Holmström et al. 2008; Ekenbäck et al. 2010; Llama et al. 2011); outflow of

planetary gas including atomic hydrogen (Vidal-Madjar et al. 2003; Ben-Jaffel 2007; Ben-Jaffel & Hosseini 2010; Ehrenreich et al. 2012), and heavy species such as carbon, oxygen and metals (Vidal-Madjar et al. 2004; Linsky et al. 2010; Fosatti et al. 2010).

Moreover, transiting Earth-like or super-Earth exoplanets orbiting bright M-stars detected by PLATO can be used as a proxy for the early history of solar system planets such as Venus, Earth, and Mars. When young, these planets faced a much harsher UV radiation environment than today, closer to that produced by active M-dwarf stars (Lammer et al. 2011b; Lammer et al. 2012). PLATO detections of such terrestrial planets will allow for the study of EUV heated and extended upper atmospheres around Earth-type exoplanets follow up observations, as has already been demonstrated for other classes of exoplanets (e.g. Ehrenreich et al. 2015). The expected results of such observations are essential for testing early terrestrial atmosphere evolution hypotheses (Erkaev et al. 2013; Kislyakova et al. 2013).

To really examine the complex physics involved in the interaction of close-in exoplanets with their host stars, PLATO's contribution of bright nearby systems will be essential. UV transmission spectroscopy, particularly examining Lyman alpha, is key for studying mass loss from hot Jupiters. Owing to the present lack of bright target stars, only four exoplanets (HD 209458b, WASP-12b, HD 189733b, and 55 Cancri b) are able to be studied in detail. WASP-12b is a particularly interesting and extreme hot Jupiter, but is too distant to be studied at Lyman alpha with the HST. By using the near-UV where the host star is much brighter, mass loss from WASP-12b was able to be detected (Fosatti et al. 2010; Haswell et al. 2012), but without Lyman alpha data the quantitative comparison of the mass loss rate with models is uncertain. PLATO is expected to find hundreds of exoplanets orbiting nearby, bright stars, and follow-up of these discoveries will produce a step-change in our ability to probe the processes governing the catastrophic end-point of hot Jupiter evolution. Such observations will fundamentally improve our knowledge of the exoplanet-upper atmosphere-magnetosphere environments, and future space observatories such as the World Space Observatory-UV (WSO-UV) (Shustov et al. 2009, 2011; Gómez de Castro et al. 2011) will be able to take advantage of this legacy.

PLATO will also detect small planets (mini-Neptunes, $R_{\text{planet}} \sim 2-4 R_{\text{E}}$) around A-stars. However, it might be that mini Neptunes do not exist at small distances for these stars, if the XUV-radiation is strong enough to erode the gaseous envelope. The minimum distance at which mini Neptunes are detected around A-stars therefore constrains the erosion of planetary atmospheres for stars with extreme environments.

Among the surprising findings from *Kepler* is the existence of a number of extremely close-in rocky bodies orbiting their host stars at periods of less than a day. Kepler-78b is an Earth-sized planet in an 8.5h orbit (Sanchis-Ojeda et al. 2013), Kepler-42c is a sub-Earth sized planet in an 11h orbit (Muirhead et al. 2012), and KIC 12557548b appears to be a disintegrating, Mercury-like object in a 16h orbit (Rappaport et al. 2012). These objects are fascinating from an evolutionary point of view, and may be remnant cores of hot Jupiter analogues to WASP-12b that are losing mass. Alternatively, they may have been rocky bodies throughout their evolution. In either case these objects, in particular KIC 12557548b with its prodigious mass loss, give an unprecedented opportunity to study the composition of exo-rocks through transmission spectroscopy. Unfortunately, the *Kepler* discoveries are distant, and hence the signal-to-noise of any follow-up observations will limit the scope of the inferences we can draw from them. PLATO will find many similar systems around nearby, bright targets.

2.1.14 Detection of rings, moons, Trojans and comets

The combination of high-precision photometry, large number of planets, and well-characterised host stars that will be provided by PLATO will significantly increase our chances of detecting planetary rings, moons, Trojan planets, and exo-comets.

Aside from the detection of exoplanets, searching for modulations in transit light curves also allows for the detection of planetary rings (Barnes & Fortney 2004; Ohta et al. 2009) and large moons (Sartoretti & Schneider 1999). One of the main drivers for the search of moons is that they might share the orbits of Jupiter-sized planets in the habitable zone (Heller & Barnes 2012), and thus be interesting targets for atmospheric characterisation. There are well-developed projects searching for moons around transiting

extrasolar planets in the *Kepler* mission (Kipping et al. 2012, 2013a, 2013b, 2014, 2015; Simon et al. 2012, 2015; Hippke 2015), but so far they remain elusive.

Moons produce two types of observable effects: photometric transits superimposed on planetary transits, and perturbations in the timing and length of the host planet’s transits. Unfortunately, for typical solar system satellites such as Ganymede around Jupiter, the amplitude of the timing perturbations is extremely small, on the order of several seconds. This is well below current detection limits. Furthermore, the photometric transit of a moon, when superimposed onto planetary transits, can very well be confused with the patterns produced by spot crossings (Silva-Valio & Lanza 2011; Sanchis-Ojeda et al. 2012) or instrumental systematics. On the other hand, planets that orbit closer than 0.1 au to their host star are not thought to be able to host stable moons (Namouni 2010). This means that we can focus on finding moons around planets with large orbital separations, which reduces the number of possible transit events for a given duration of observations. The scarcity of the observations, and the fact that the orbital phase of the moon is sampled at the orbital period of the planet (below the Nyquist frequency of the moon’s orbit), make the characterisation of these systems extremely challenging.

An efficient method to find evidence for satellites around a transiting planet is in the search for an extra signal due to moons in the phase-folded transit light curve of the planet. After about a dozen transits, a moon on a circular orbit around its planet will create a symmetric extra dip in the wings of the planetary transit light curve (see Figure 2.9) because the moon’s positions relative to the planet will behave more and more like a ring the more transits are being folded. In fact, the moon’s orbit is statistically sampled after many transits, which is why this transit effect has been termed the Orbital Sampling Effect, or OSE for short (Heller 2014). The OSE could be detectable with *Kepler* for moons as small as Ganymede around photometrically quiet M dwarf stars (Heller 2014).

We have carried out additional simulations for PLATO assuming the most favourable scenario of a bright ($V=8$) white-noise dominated G dwarf star that is transited by a Jupiter-sized planet with a $0.7R_E$ -sized moon. We found that PLATO would detect the OSE of such a moon with $< 10\%$ error in the retrieved moon radius and orbital semi-major axis after about 8 transits or a little less than a year of continuous observations, assuming the planet is in a ~ 45 d orbit around the star (see Figure 2.10). Taking into account red noise effects and the fact that the star might be slightly dimmer than 8th magnitude, we estimate that PLATO could detect large moons (if they exist) after about 2 years of continuous observations. An extension to 3 years would certainly increase the odds significantly.

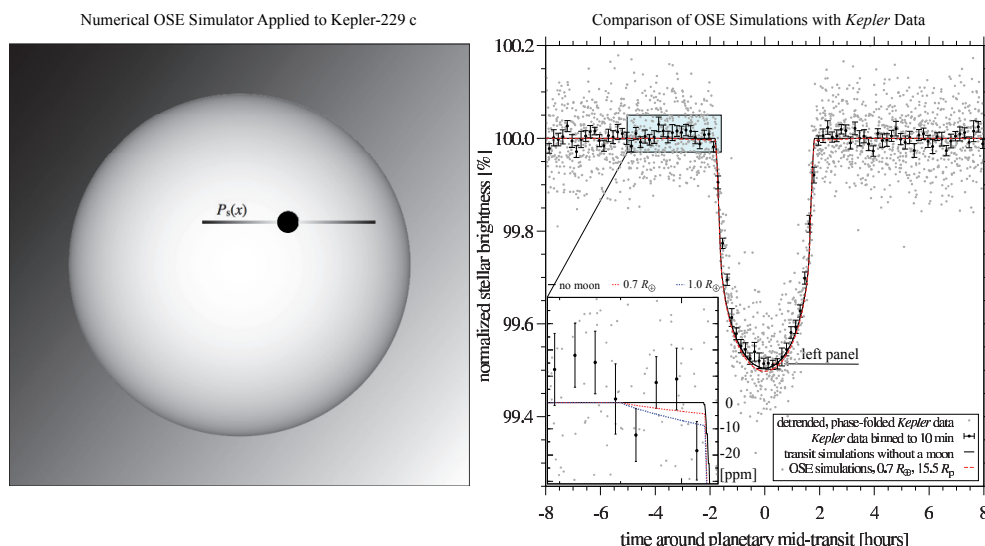


Figure 2.9: Illustration of the orbital sampling effect (OSE) of an extrasolar moon. This example shows the transit of Kepler-229 c, a $4.8R_E$ planet around a $0.7R_\odot$ star every 17 days with a transit impact parameter of $b = 0.25$. Left: The planet (black circle) and the moon’s probability function (shaded horizontal strip) of a hypothetical $0.7R_E$ super-Ganymede moon with an orbital semi-major axis of eight planetary radii transit the limb-darkened star (large bright circle). Right: The red cross on the transit light curve at 0.5 hours refers to the moment shown in the left panel. The inset zooms into the wings of the transit ingress. Three OSE models are shown: no moon (black solid), a $0.7R_E$ moon (red dashed), and a $1R_E$ moon (blue dotted). Figure from Heller et al. (2016).

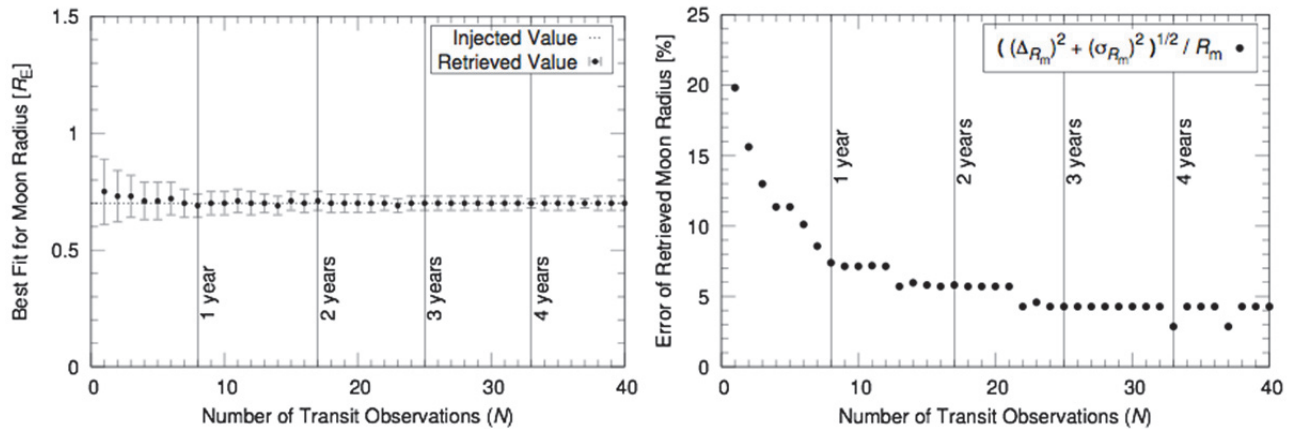


Figure 2.10: Best fit for an OSE signal of an injected moon of $0.7 R_E$ in size. The error in the retrieved radius falls below 10% after about 8 transits.

Trojan orbits close to the Lagrange points L4 and L5, and in 1:1 mean-motion resonance with planets, are thought to be very stable configurations for planets up to and including super-Earth sized bodies. In our solar system there are multiple examples of bodies in such orbits, albeit with sizes comparable with asteroids, so planetary objects in Trojan orbits would be a new class of system. To date, none have been detected (see Cabrera 2008; Ford & Holman 2007, and references therein), but PLATO will have the precision to detect Trojan-planets as small as the Earth.

Finally, exo-cometary tails lead to transit light curves that can be as deep as those produced by Earth-sized planets, albeit with a different shape (Lecavelier des Etangs 1999), and exo-cometary tails detected around nearby stars might be observable with future direct imaging experiments (Jura 2005). Giant planets can also develop comet-like tails (Schneider et al. 1998), and indications for such tails have already been found in *Kepler* data (Budaj et al. 2013). Exo-comets are of interest, as they might provide a route for redistribution of organic material, both within and between planetary systems.

The tantalising discoveries of the peculiar light curves of KIC 8462852 (Boyajian et al. 2016) and EPIC 204278916 (Scaringi et al. 2016) by *Kepler* and K2 have intrigued researchers about possible families of comets (Bodman & Quillen 2016) or dust disks (Thompson et al. 2016) which could explain the evolution of the stellar brightness observed (Montet & Simon 2016; Hippke et al. 2016). Such rare systems might be found around brighter, closer-by stars by PLATO, continuing further their characterisation with ground based instruments.

2.1.15 Planetary science conclusions

PLATO will detect thousands of new planetary systems of all kinds, including hundreds of small planets suitable for precise characterisation (RV and asteroseismology). Depending on the actual occurrence rate, which is still debated in the literature, PLATO will detect and characterise tens of small/low-mass planets in the HZ of bright, Sun-like stars for which accurate radii, masses, mean densities, and ages can be derived. This goal is unique to PLATO. In addition, PLATO will be able to detect exomoons, planetary ring systems, Trojan-planets, exo-comets, etc., thereby expanding our knowledge about the diversity of planetary systems.

The mission aims not only at a statistical approach to studying the frequency of terrestrial planet occurrences, but also asks about the nature of these planets, their bulk properties, atmospheres, and ultimately whether they could harbour life. Answering these questions require a new approach and impose new requirements on planet detection surveys, because they need detailed follow-up observations at high SNR. To address these science questions, PLATO will:

- Detect planets around bright stars ($V \leq 11$) to determine accurate and precise bulk densities and ages, and allow for follow-up spectroscopy of planetary atmospheres;
- Detect and characterise terrestrial planets at intermediate orbital distances up to the habitable zone around Solar-like stars to place our solar system in context;

- Detect and characterise planets in statistically significant numbers for a broad range of planet and planetary system classes to constrain planet formation scenarios.

These requirements are at the core of the design of PLATO, and define its main target range and observational strategy.

2.2 Science Objectives II: Probing stellar structure and evolution by asteroseismology

Asteroseismology is the study of the global oscillations of stars (see Aerts et al. 2010, Chaplin & Miglio 2013). These oscillations are due either to trapped acoustic waves (p-modes) or to internal gravity waves (g-modes), or to a mixture of the two. Their frequencies depend on the radially varying density and internal sound speed of the star. Thus, measurements of oscillation frequencies can be used to infer both the internal structure of stars and their bulk properties. The precision of stellar bulk parameters determines the precision of related parameters for its orbiting planets. Asteroseismology of planet host stars is therefore of key importance for derivation of accurate and precise planet parameters (Gizon et al. 2013; Van Eylen et al. 2014). For instance in an early study on the CoRoT target HD46375 hosting a Saturn-like planet, the seismic mass determination of the host star improved the mass estimate of the planet by a factor of 2 (Gaulme et al. 2010). Furthermore, asteroseismology is the only method that provides accurate and precise ages for planetary systems (Lebreton & Goupil 2014; Silva Aguirre et al. 2015; Huber 2015).

Asteroseismology is therefore part of the core science of PLATO, which, thanks to its bright target sample, will be the first mission to make systematic use of asteroseismology to characterise planet host stars. The core program focuses on stars showing oscillations similar to those of the Sun, which are intrinsically stable and excited stochastically by the near-surface convection. Extremely small amplitudes generally characterise solar-like oscillations, which makes their detection difficult. Nonetheless, data acquired by the CoRoT (Baglin et al. 2013, Baglin and the CoRoT team 2016) and *Kepler* (Borucki et al. 2010; Gilliland et al. 2010; Borucki 2016) missions have clearly demonstrated the power of this technique. While asteroseismic analyses are currently carried out for tens to hundreds of Sun-like oscillating dwarf and subgiant stars, PLATO will enable the technique to be applied to tens of thousands of stars (Section 2.2.1). Moreover, PLATO will focus on bright stars and will therefore fully benefit from the strong synergies with the *Gaia* mission as well as ground-based high-resolution spectroscopy. Asteroseismology of cool dwarf stars with PLATO will thus drastically improve our understanding of stellar evolution beyond what has been achieved with previous missions, and significantly enhance the quality of current stellar evolution models (Section 2.2.2).

PLATO will measure the oscillation frequencies of at least 15,000 dwarf and subgiant stars with $V \leq 11$. In total, more than 300,000 stellar photometric light curves will be obtained for stars with $V \leq 13$. It will thus be a powerful new tool for the characterisation and study of the evolution of star-planet systems.

2.2.1 Stellar parameters as key to exoplanet parameter accuracy

The main focus of the asteroseismology programme of PLATO will be to support exoplanet science by providing:

- stellar masses with a precision better than 10%,
- stellar radii to 1–2% precision,
- and stellar ages to 10% precision

for a reference star similar to the Sun at $V = 10$.

Starting with the Sun decades ago, it has long been demonstrated that seismology is the most efficient method to provide precise stellar parameters for solar-like oscillating stars (Chaplin & Miglio 2013; Lebreton et al. 2014a, b; Silva Aguirre et al. 2015). The precision and accuracy on the stellar mass, radius and age determination depend on the type, precision and number of seismic and non-seismic observational constraints. The quality of the seismic determinations also depends on the choice and on the efficiency of the

procedure used to derive the parameters; the choice of a procedure in turn depends on the quality of the available data. In addition, the age determination relies on the use of stellar models. Significant improvements will come with the results of the *Gaia* mission and PLATO.

2.2.1.1 Seismic radius

Gaia will provide the distances to the stars via direct, geometric measurements, allowing the absolute luminosity of the star to be derived with high precision (www.cosmos.esa.int/web/gaia/science-performance). Combining the luminosity with the effective surface temperature of the star obtained from (ground-based) high-resolution spectroscopy, we will obtain the radii of target stars at a precision of 1–2%. Note that *Gaia* will be complete down to $V \sim 20$, while PLATO will observe stars at $4 < V < 16$, so all PLATO targets will also be observed by *Gaia*. The first *Gaia* data release was successfully presented in September 2016. It should be noted that measurements of T_{eff} to within 1% will be achievable through dedicated high-resolution, high signal-to-noise spectroscopic observations obtained as part of PLATO's ground-based follow-up program (see Section 6.2). Determination of chemical abundances and T_{eff} will be based on state-of-the-art spectral analysis techniques and model atmospheres, taking 3D and non-LTE effects into account (Bergemann et al. 2012; Magic et al. 2013, 2015a,b; Martins et al. 2014). Taken together with the luminosities expected from *Gaia*, the effective temperature will lead to stellar radii with a relative precision within 1–2% for un-reddened stars.

For the brightest stars, combining *Gaia* distances and interferometric measurement of angular radius will provide model-independent measurement of the stellar radius. This has already been achieved for a small set of host stars (Huber 2016). This provides an additional and independent constraint on stellar interiors. Such independent information can be used together with seismic constraints to provide further constraints on stellar interiors.

2.2.1.2 Seismic mass from scaling relations or inversion technique

Asteroseismology can provide the bulk density of the star via scaling relations even with data of relatively low signal-to-noise ratio (SNR), or via inversion techniques from data of high SNR.

Scaling relations based on solar values have already been tested and validated using *Kepler* targets by comparing the asteroseismic radii and distances with interferometric observations and *Hipparcos* parallaxes (Huber et al. 2012; Silva Aguirre et al. 2012; White et al. 2015). Fits to global averages of seismic quantities (assuming the effective temperature is known) provide a determination of stellar radius and mass. The fitting can be done in a model-independent way (e.g. Chaplin et al. 2011a) but typically is further constrained by the inclusion of a grid of models. An extensive analysis of this nature for 500 *Kepler* dwarfs and subgiants observed in short cadence for one month was carried out by Chaplin et al. (2014). Due to their importance, scaling relations are the subject of many studies to investigate their precision and possible biases (e.g. Huber et al. 2013; Coehlo et al. 2015; Pinheiro et al. 2014; Mosser et al. 2013). Such studies require precise photometric data and will largely benefit from PLATO. A full understanding of the domains of validity and biases to be corrected will in turn make the seismic scaling relations efficient tools for deriving precise and accurate stellar mass and radius, even when the data are not at their optimum precision or for step-and-stare observations. Subsequently, with the help of stellar models and calibrated scaling relations, PLATO will allow to perform ensemble seismology on a very large number of stars by providing information far beyond the only bulk density.

Inversions of mode frequencies have been used extensively in helioseismology to infer solar internal properties, and are presently being adapted to asteroseismology (Reese et al. 2012; Buldgen et al. 2015a, b). One advantage of inversion techniques is that the solutions are not restricted to those of a space of standard stellar models. In particular, they allow for the determination of a model-independent mass, if the stellar radius is known independently from the seismic data. These techniques require the highest quality data and are therefore applicable for the brightest stars and longest observing runs.

Hence, by combining the very precise bulk density values of PLATO's asteroseismic analysis with stellar radii from *Gaia*, we will obtain precise stellar masses for a large set of stars.

2.2.1.3 Seismic mass, radius and age inferences from stellar modelling

Stellar age determination by asteroseismology is more complex, and requires invoking models of stellar evolution. Age will be estimated by comparing grids of stellar models computed for different initial parameters (mass, metallicities, helium abundances, convection parameters) to the combined non-asteroseismic and asteroseismic observational constraints. Given data with high SNR, it is indeed possible to determine individual oscillation frequencies. This is illustrated in Figure 2.11 and Figure 2.12 showing the observed power spectra of the Sun, a CoRoT star and a bright *Kepler* target, 16 Cygni A. The parameters of the stars and their internal structure are inferred by fitting model oscillation frequencies to the observed oscillation frequencies. This procedure is now routinely applied by the scientific community to retrieve stellar radii, masses, and ages from space-based asteroseismic data. The fit may either use grids of stellar models and oscillation frequencies, or more sophisticated search techniques requiring repeated stellar model calculations.

Kepler has carried out asteroseismic observations for several transiting planets. Examples of such planetary systems containing rocky/icy planets are Kepler-36b (Carter et al. 2012), Kepler-68 (Gilliland et al. 2013), and the smallest planet detected so far, Kepler-37b (Barclay et al. 2013). Characterisation of the terrestrial and/or rocky planets via the seismic characterisation of their host stars has been successfully performed (Huber 2015), for instance, for Kepler-93b (Ballard et al. 2014; Dressing et al. 2015) and Kepler-10b (Fogtman-Schulz et al. 2014).

Based on the asteroseismic analysis of 66 *Kepler* planet host stars, Huber et al. (2013) claim typical uncertainties of 3% and 7% in radius and mass, respectively, from the analysis of global asteroseismic parameters.

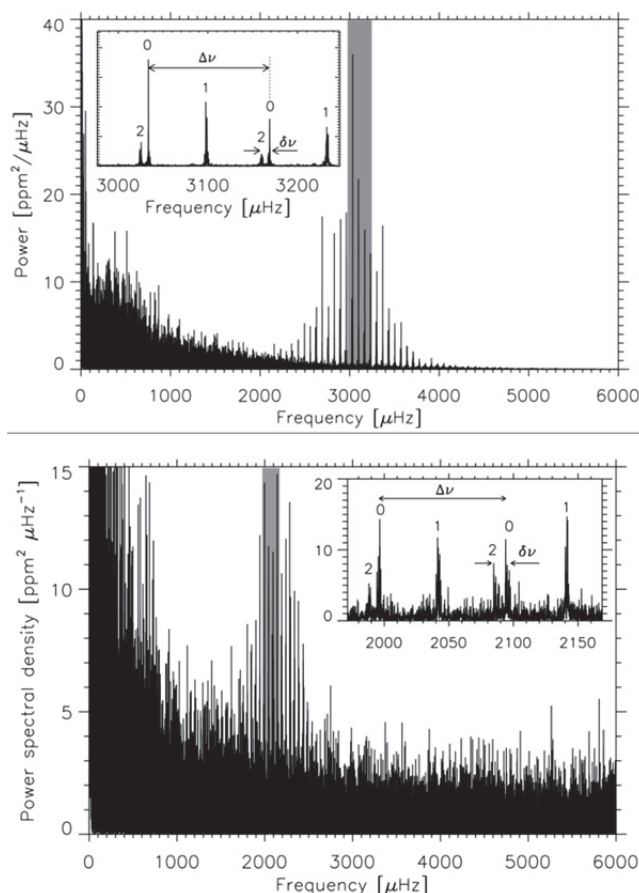


Figure 2.11: Top - Solar power spectrum from 2 years of SOHO/VIRGO photometric data. Bottom - Power spectrum of HD52265 from 117 days of observation with CoRoT (Gizon et al. 2013). The insert figures zoom in on the sections of the power spectra highlighted in grey.

Metcalfe et al. (2014) provided a uniform seismic modelling of 42 solar-type *Kepler* targets observed for 9 months and analysed by Appourchaux et al. (2012). The authors found that using the individual frequencies in the search for an optimal stellar model typically doubles the precision of the resulting seismic radius, mass, and age compared to grid-based modelling of the global oscillation properties, and improves the precision of the radius and mass by about a factor of three over empirical scaling relation. Lebreton & Goupil (2014) derived the stellar parameters for the star HD 52265 observed by CoRoT for four months. This star has an effective temperature around 6100 K and was inferred to have a mass and radius around $1.2 M_{\odot}$ and $1.3 R_{\odot}$, respectively, with the central hydrogen abundance reduced to roughly half the original value. Lebreton & Goupil (2014) and Lebreton et al. (2014a, b) studied the impact of different choices of seismic diagnostics and of different assumptions for the input physics. Figure 2.13 shows the results of the analyses for the age, for different choices of seismic diagnostics, observational (seismic and non-seismic) constraints, assumptions on the chemical composition, and physics input. A drastic decrease of the dispersion of the results occurs for the cases c, d, e, i.e. when some diagnostic(s) appropriate for the age is/are included. The final errors are found around 1.5, 7 and 13% in radius, mass and age, respectively. The analysis demonstrated the striking improvement in precision that results from including seismic data.

Silva Aguirre et al. (2015) analysed data on individual frequencies for 33 stars observed by *Kepler* to be (potential) planet hosts. The baseline of the observations is long enough that the uncertainties of individual frequencies are about $0.3 \mu\text{Hz}$ for frequencies close to ν_{max} (and down to $0.1 \mu\text{Hz}$ in the best cases). The stars broadly sample the region of the HR diagram where asteroseismic inferences can be expected. The main analysis was based on ratios of frequency separations, which are insensitive to surface effects, but additional analyses were carried out with different techniques to test for the consistency of the results and the sensitivity to differences in model physics and numerical techniques. Figure 2.14 shows the distribution of errors in the sample, in radius, mass, mean density, and age. The median errors in radius, mass, and age were 1.1, 3.3 and 14%, respectively. These uncertainties account for systematic effects of the use of different modelling or fitting techniques. As a specific example, let us consider the star KIC 4141376 observed by *Kepler*. It has a mass and evolutionary state very similar to the Sun, although a somewhat lower metallicity. Frequencies were obtained with typical errors around $0.5 \mu\text{Hz}$, while the error in T_{eff} was assumed to be 91 K and the error in metallicity [Fe/H] was 0.1 dex. For this star, Silva Aguirre et al. (2015) determined mass and radius with precisions of 2.5% and 1%, while the precision of the age was around 20%.

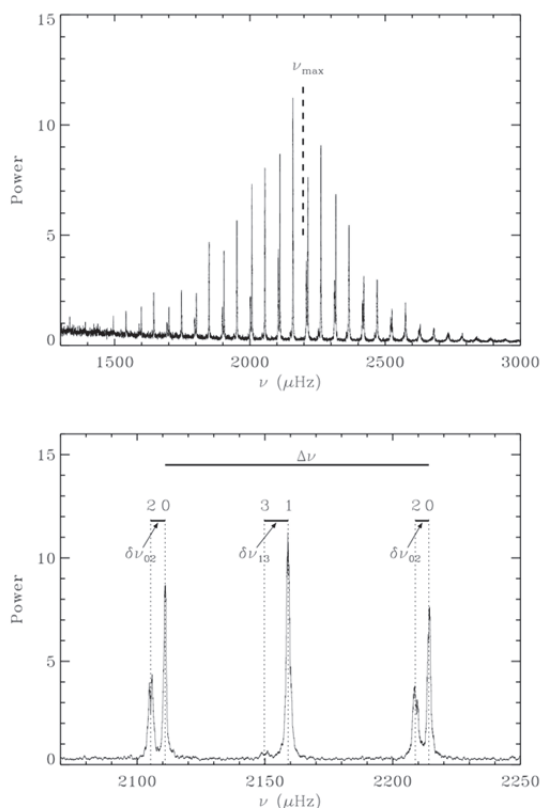


Figure 2.12: Top - power spectrum of 16 Cyg A from 35 months of *Kepler* photometric data. Bottom - zoom over three groups of modes clearly showing individual $l=0$, $l=1$ and $l=2$ mode frequencies (Christensen-Dalsgaard 2016).

Besides the precisions of seismic stellar mass, radius, and age, the accuracy can also be estimated with theoretical investigations. It is usually measured as the differences between the estimated value of a given quantity and its exact counterpart using *hare and hound* exercises. Reese et al. (2016) performed such exercises by generating solar like-oscillations of several artificial main-sequence stars, for which random noise were added, in the mass range $[0.78\text{--}1.33] M_{\odot}$. These frequency sets were provided to modellers who derived the properties of the stars with their own means. Results indicate that the accuracy is of the order of 4% for the mass, 1.5% for the radius, and 22% for the age. For the Sun-like cases in that sample the PLATO performance requirements are easily satisfied (Reese et al, 2016). These figures are consistent with the estimates obtained with hare and hound exercises carried out with simulated PLATO light curves. Again here, these uncertainty estimates take into account systematic effects of the use of different modelling or fitting techniques.

Depending on the assumptions on stellar modelling, the age accuracy for the PLATO simulated data was obtained at the level of 10% for a bright ($V=9\text{--}10$) young Sun (with the proper physical description used in the modelling) and 15% for a slightly more massive star with a chemical composition different from that of the Sun. The fitting procedures are indeed intrinsically model-dependent, but the understanding of the biases introduced by considering particular model physics and/or the exploitation of a particular parameter space allows one to assess the most important systematics that may be present in the results. For instance, Valle et al. (2015a, b) used the global seismic parameters and a grid of models to study the impact of several uncertainties of some physical input and chemical composition. The result is similar to other studies in the same conditions: the precision is dependent on the mass and the evolutionary stage. The authors estimated uncertainties of 2–10% in mass, 1–3% in radius for seven *Kepler* stars observed over one month.

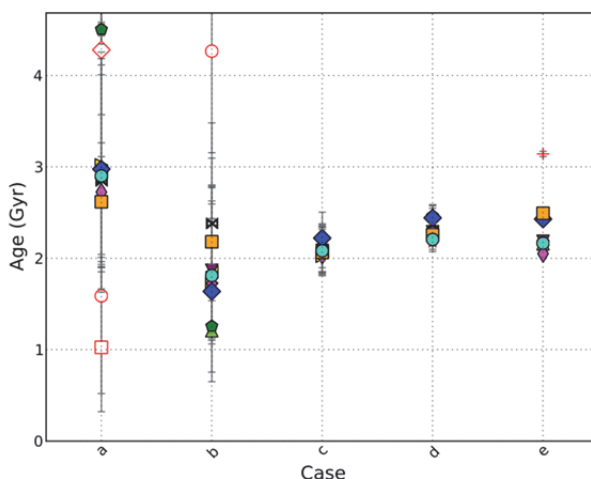


Figure 2.13: Ranges of ages derived from stellar model optimisation for HD 52265. In abscissae are listed the case numbers. For all cases (in abscissae), the non-seismic constraints T_{eff} , L , $[Fe/H]$ are included. Case a: no seismic constraints. Case b: only $\langle \Delta\nu_{n,l} \rangle$. Case c: $\langle \Delta\nu_{n,l} \rangle$ and the averaged small separation. Case d: individual ratios of frequency combinations. Case e: individual frequencies corrected for surface effect. Symbols and colours refer to different assumptions about the input physics and the chemical composition. For instance, in case a, square and diamond are for a conv values changed by ± 0.20 dex with respect to solar. In case e, the red cross is a model without corrections from surface effects. From Lebreton et al. (2014b).

These examples show that precisions requested for the stellar mass and radius will be easily achieved for bright stars of the core program P1 sample (see Section 3.4.2). The tools already exist which can provide age uncertainty at the level of 10% for a Sun-like star, again with PLATO expected high-quality data and *given the proper physical description of the stellar models*. Indeed, it has been demonstrated that the largest contributions to the uncertainties on the age come from imperfections in the physical description of the stellar models. However, the stellar models will themselves be also improved using the asteroseismology of PLATO observations (Section 2.2.2) so will be the age uncertainties.

Focusing on a much larger number of bright stars for several years of highly precise photometry, PLATO will then provide substantially better performance than *Kepler*, K2 and TESS, and, crucially, for thousands of planet hosting stars.

2.2.1.4 Constraints on the convective envelope structure and surface helium abundance

The interior of a star shows rapid structural variations such as those associated with the regions of element ionisation and with the edges of convectively unstable regions. Procedures (glitch inferences) have been developed in order to detect and characterise these variations. They can then be used to estimate the helium content of the stellar envelope and the size of the mixed regions (e.g. the depth of a convective envelope), which, in turn, may serve as additional constraints for the stellar mass and age inferences. The signature of these structural variations on the oscillation frequencies is rather small so that highly precise frequencies are required for a successful helium content measurement or location of the base of the convective envelope. For instance, the location of the base of the convective zone was established for 19 main-sequence *Kepler* stars (Mazumdar et al. 2014). The helium content of the stellar envelope was also determined for the bright *Kepler* eclipsing binary 16 Cyg (Verma et al. 2014a, b). Such measurements will be achieved for a large sample of bright PLATO targets.

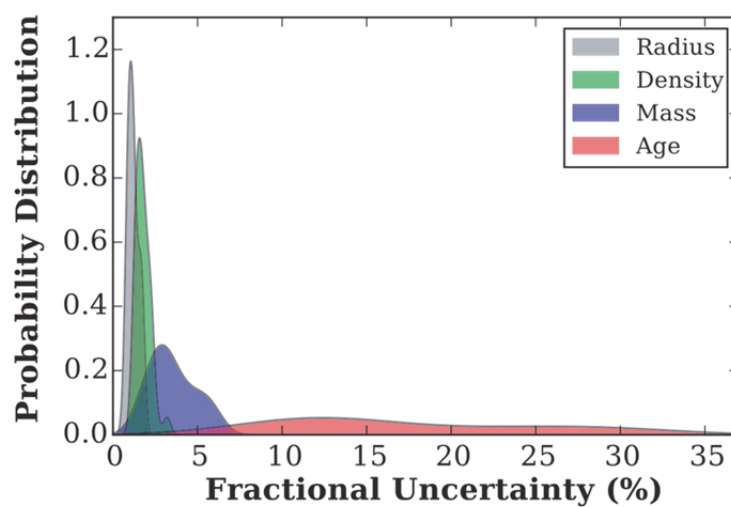


Figure 2.14: Fractional uncertainties for the mass, radius and ages obtained with seismic modelling of 33 *Kepler* stars. From Silva Aguirre et al. (2015).

2.2.1.5 Seismic rotation

The oscillation frequencies can also provide information about stellar interior rotation (e.g. Beck et al. 2012a, b; Deheuvels et al. 2012; Gizon et al. 2013). This requires a high SNR and frequency resolution because one must resolve and extract signatures of rotation (rotational frequency splittings) in the power spectra of non-radial modes of oscillation (e.g. Gizon & Solanki 2003; Ballot et al. 2006, 2008; Benomar et al. 2009; Campante et al. 2011). Seismic rotation periods were recently determined for 22 main-sequence CoRoT and *Kepler* targets with masses in the range $1.0\text{--}1.6M_{\odot}$ (Benomar et al 2015). Nielsen et al. (2014, 2015) showed that seismic constraints can be placed on the internal differential rotation of Sun-like stars. For the bright star 16 Cygni A ($V \sim 6$), the precise seismic measurements of the rotation period (Davies et al. 2015) and age (Metcalf et al. 2015) after 928 days of *Kepler* short cadence observations can be used to calibrate gyrochronology relations (Davies et al. 2015). Such seismically validated calibrations will serve to derive ages for stars without seismic characterisation. This will be very valuable to the research fields that rely on accurate stellar ages, such as galactic evolution studies. Of course, several benchmark stars like 16 Cygni A must be used to establish and calibrate gyrochronology relations with a broad range of validity. PLATO will do so.

2.2.1.6 Spin-orbit angle

The angle between the stellar spin and the planetary orbital axes of the exoplanetary systems (also called spin-orbit angle or obliquity) is a unique observational indicator of the origin and evolution of planetary systems. For example, the existence of Jupiter-size planets orbiting in less than a week indicate that inward migration could be required to explain their formation and evolution. While a planet-disk interaction predicts

orbital planes parallel to the stellar spin axis, a planet-planet scattering scenario or the Kozai mechanism predicts oblique orbits. Thus, a precise determination of the spin-orbit angle and its statistical distribution would give tight constraints on the contribution of different migration scenarios (Queloz et al. 2000; Winn et al. 2005). The measure of the spin-orbit angle is however not easy because its determination usually requires the knowledge of three angles:

- The orbital inclination, which is determined with a precision of only a few per cents from the transit light curve.
- The projected spin-orbit angle onto the sky plane. This is commonly measured using the Rossiter-McLaughlin effect (Rossiter 1924; McLaughlin 1924; Queloz et al. 2000; Winn 2011) and is determined with a precision of 1–10%.
- The stellar inclination, which can be directly determined by asteroseismology (e.g. Gizon et al. 2013; Benomar et al. 2014, 2015) or indirectly by combining the spectroscopic $v \sin i$ and the surface rotation measured using stellar activity signatures (surface spots) on the light curve (Hirano et al. 2014).

To date, most statistical studies rely on the projected spin-orbit angle onto the plane of the sky (Albrecht et al. 2013; Xue et al. 2014). While this is an indicator of the planetary systems obliquity, the projection effect makes its interpretation difficult. In order to obtain tight and reliable constraints on the formation and evolution of exoplanetary systems, it is therefore important to measure the true obliquity, free of projection effects. Asteroseismology can contribute in achieving this goal, as shown by Chaplin et al. (2013), Benomar et al. (2014), and Campante et al. (2016). In addition to the rotation, measurements of the relative amplitudes of the split components of the modes also reveal the stellar inclination, i.e., inclination of the rotation axis relative to the line of sight (Gizon & Solanki 2003; Gizon et al. 2013; Chaplin et al. 2013). This is because geometric cancellation effects, which depend on the stellar inclination, affect these visibilities. The necessary high SNR and the frequency resolution implies that one must observe bright enough targets for a long enough time. In that respect, the initial phase of the *Kepler* mission was remarkable for its four continuous years of observations of a specific region of the sky, which allows us to measure the stellar inclination of Sun-like stars with a precision of $\sim 10\%$. However, the stellar inclination is only available for ~ 30 stars with known planets of the *Kepler* field (Campante et al. 2016) and one for the CoRoT field (HD52265). This represents approximately 10% of main-sequence stars with detected Sun-like pulsations, but corresponds to less than 1% of the total number of planet candidates. The example of the planet host *Kepler* 25 is shown in Figure 2.15. Another example is HAT 7 (Campante et al. 2016; Lund et al 2014; Benomar et al 2014).

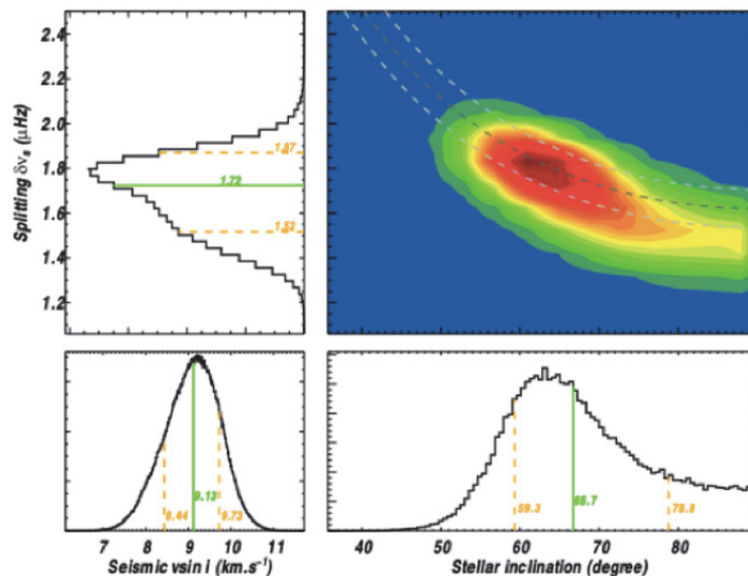


Figure 2.15: Seismic measurement of the inclination angle of the *Kepler* star, *Kepler* 25. The plot shows the probability distribution function for the stellar inclination with the median (green). Blue represents region of lowest probability. Red areas are of highest probability. From Benomar et al. 2014.

The main reason for this low number is that most of the claimed detections of exoplanets are made around stars with apparent magnitude higher than 12, while high precision seismology often requires brighter stars. This is also due to the fact that the initial *Kepler* field corresponds to a very limited region of the sky.

By performing a high precision photometry of the bright stars ($V < 12$) for long observation durations, and a global sky survey, PLATO circumvents these issues. Thus, one might expect the space mission to provide the first large-scale statistical study for the orbit configurations of exoplanets around Sun-like stars. This will enable us to discriminate clearly the scenario of formation and evolution of planets.

One must stress that the K2 mission observes several regions of the sky. However, its degraded observation mode (compared to the *Kepler* initial phase) limits the seismic observation to very bright stars during only ~ 75 days. This prevents us from measuring accurately the stellar inclination for a large ensemble of stars. In addition, none of the fields observed by K2 contains planetary systems with a known Rossiter-McLaughlin effect, so that the true obliquity cannot be measured. Furthermore, for most of the targets it will observe, TESS is not expected to surpass K2 in terms of what will be possible from asteroseismology, because of 1) its small aperture, which will limit asteroseismology of solar-type stars to targets brighter than about $V = 7$ (e.g. see Campante et al. 2016); and 2) the fact that most stars will be observed for only 27 days.

2.2.2 Stellar models and evolution

With sufficiently good data, the asteroseismic determination of mass and radius can be essentially independent of stellar models. For other quantities, particularly the age, the inferences involve fitting models to observables, and their accuracy and precision depends on our ability to model stellar evolution. Thus, the asteroseismic investigation of stellar structure and evolution is an essential part of the characterisation of planet hosts, and is necessary if we are to put planetary systems into an evolutionary context. Asteroseismic investigation of a large number of stars, with a range of masses and ages, is a necessary tool for constraining models of stellar interiors, identifying missing physics, and improving our understanding of stellar evolution.

2.2.2.1 Surface convective transport and granulation

A longstanding problem in stellar modelling is the description of *convective transport and energy flux*. Prescriptions for such transport in 1D stellar model computation require knowledge of quantities that cannot be derived easily from first principles. One therefore needs information from numerical simulations and, most importantly, from observations of stars in various evolutionary stages and with differing chemical compositions. One example is the filling factor of downdraft plumes carrying energy from the top of a convection zone to the bottom. These types of observational constraints can only be obtained with highly precise seismic measurements (frequencies, amplitudes, mode lifetimes), and only for bright enough stars. Furthermore, the necessary seismic precision demands these stars to be observed over long runs.

Stellar parameters are derived by comparing observed oscillation frequencies with the theoretical frequencies. As well known in the solar case, the differences between observed and theoretical frequencies increase with the frequency. The higher the frequency of a mode, the closer its eigenfunctions peaks to the surface. The increasing difference between observed and theoretical frequencies therefore mainly reflects the imperfection with which the standard models treat the turbulent convective superficial layers but also how non-adiabatic pulsations are modelled and how the acoustic wave propagates across an heterogeneous, turbulent medium. These phenomena, referred to as *near-surface effect*, affect the accuracy of seismic measurements, which ultimately limits the power of seismic diagnosis. In order to correct for this effect, several authors have proposed empirical or semi-empirical corrections based on the assumption of adiabatic pulsations (e.g. Kjeldsen et al. 2008; Ball & Gizon 2014; Sonoi et al. 2015). Most of these corrections involved one or several free parameters. For instance, in Sonoi et al (2015), surface effects were modelled assuming adiabatic pulsation and using a coarse grid of 3D surface models. The predicted surface effects were next fitted with a Lorentzian function involving two free parameters. The authors have shown that these parameters vary in the HR diagram as a function of the surface parameters of the star, such as the effective temperature and the surface gravity. Another approach by Ball & Gizon (2014) based on a formula given by Gough (1990) consists in correcting the theoretical frequencies by a term proportional to v^3/I where v and I are the frequency and inertia of the mode. The departure from adiabatic pulsations is also expected to contribute to the surface effects (Houdek 2010; Grigahcène et al. 2012). However, the current non-adiabatic treatments of pulsations still rely on a crude description of the complex coupling between pulsation and

convection (for reviews see Belkacem & Samadi, 2013; Houdek & Dupret 2015). All these models, however, involve free parameters. They must be confronted with the observations. This can be done with bright objects with seismic data of very high quality and detailed spectroscopic characterisation (T_{eff} , metallicity). Available CoRoT and *Kepler* data sets allow us to test the current theoretical modelling but only for a small set of bright objects. This is insufficient to cover properly the free parameter space. On the other hand, PLATO will observe a high number of bright main-sequence and subgiant stars with various surface abundance and with different evolutionary status.

The *granulation* is a manifestation of convection at the surface of the stars. Measuring the properties of surface granulation is an important step for a better understanding of the physics of surface convection and to provide constraints on its modelling. Using *Kepler* data, scaling relations linking the granulation characteristics to the stellar parameters and seismic properties have been established (Kallinger et al. 2014; Mathur et al. 2011) and a theoretical basis to these scaling relations exists (Mathur et al. 2011; Samadi et al. 2013). It is theoretically expected that the turbulent Mach number controls the granulation properties to second order. The *Kepler* observations unfortunately cannot confirm this trend. A confirmation requires observing a statistically larger number of dwarfs cooler than the Kepler stars. For hotter (F) stars, the comparison between theoretical models and observations indicates significant departures (Ludwig et al. 2009; Samadi et al. 2013), which are not yet explained. A possible explanation could be the partial inhibition of the convection by a magnetic field (cf. Ludwig et al 2009; Samadi et al 2013; Cranmer et al 2014). Another issue is the theoretically predicted dependence of granulation on the surface metal abundances (Ludwig et al. 2009; Tremblay et al 2013). Testing all these theoretical developments requires high quality observations – high signal-to-noise ratio and high frequency resolution – for a sample of different types of stars larger than available with *Kepler*. The PLATO mission, on the other hand, is perfectly suited for such a purpose.

2.2.2.2 Constraints on internal stratifications

Glitch observational constraints as mentioned in Section 2.2.1.4 are powerful tools for placing constraints on the stratification inside solar-type stars (Monteiro et al. 2002; Mazumdar 2005). With the availability of precise frequency sets for a large number of stars, the variation of the locations of acoustic glitches in a large ensemble of solar-type stars populating the main-sequence and subgiant branches can be followed (Mazumdar et al. 2014). This will provide very strong constraints on the various transport processes (diffusion, turbulent chemical mixing) taking place at the base of the convection zone (Christensen-Dalsgaard et al. 2011; Lebreton & Goupil, 2012; Zhang C. G. et al 2012, 2013; Zhang Q. S. & Li 2012a, b). This will lead to necessary improvements in the physics in order to ensure that all observables including the location of the base of the convection zone are well fitted. We must stress that the initial helium content is an essential input to computations of stellar models but cannot be directly observed for F to K dwarfs. Systematic studies about the helium content in a given environment will then require its seismic measurement for a large sample of bright stars as proposed by the PLATO mission. However, one must keep in mind that the seismic measurements determine the helium abundance *of the envelope* and that its relation with the initial helium content (input to stellar models) depends on the processes taking place at the bottom of the convective envelope, which therefore must be constrained as well.

2.2.2.3 Constraints on the core structure

Targets for the PLATO main program will have a spectral type from F5 to K7, which corresponds, for solar metallicity and MS-phase, to the mass interval $0.6\text{--}1.4 M_{\odot}$. One of the most important issues in dating main-sequence (MS) stars with masses larger than the solar one is the inability for estimating from first principles the extension of chemically mixed regions. The main contributors to the uncertainty of the extension of chemically mixed regions are the transport processes of chemicals such as those related to convection and rotation. Before the development of asteroseismology of solar like oscillators from space, the current way to estimate the extension of central mixed regions was the comparison of theoretical isochrones with the HR diagram of open clusters of different turn-off mass (or age), and the study of eclipsing binaries. These studies have made clear that:

- the extension of the central mixed region is underestimated by the models using the classical local MLT theory to describe convection and the Schwarzschild (or Ledoux) criterion for defining the boundaries of stable regions against convection. To reach a good fit of observations, an amount of

extra-mixing above the classic boundaries is usually introduced in the models by using an opposite parameter, called overshooting parameter (for a review see Chiosi 2007).

- the efficiency of this extra-mixing increases with the stellar mass significantly in the mass interval corresponding to the onset and development of a convective core ($\sim 1.0\text{--}1.5 M_{\odot}$). The variation of the efficiency with mass is expected to depend also on stellar metallicity (Bressan et al. 2012). Such a dependence on mass of the extra-mixing efficiency has been found for some targets in the *Kepler* field (Deheuvels et al. 2016).

Main-sequence stars more massive than about $1.1\text{--}1.2 M_{\odot}$ (depending on the chemical composition) develop a convective core on the main-sequence. A more or less efficient extra mixing then takes place at the boundary of convective cores. This directly influences the age of the star: in presence of extra mixing, the star is older at a given stage (central hydrogen content) along the main-sequence. The process of extra mixing is a 3D non-local process that cannot be fully modelled in 1D stellar evolutionary codes. The extension of the associated mixed (i.e. chemically homogeneous) region therefore is a free parameter in a 1D stellar model computation. A range of values for this parameter can be obtained by fitting clusters or eclipsing binaries, but when applied to individual stars, this generates large uncertainties on their ages. Besides, for small convective cores as for stars of interest in the PLATO P1 sample, the parameter seems to vary with mass of the star. One therefore needs to implement a modelling from 3D simulations, to provide calibrations that will have to be tested with a set of seismically well-characterised stars. It is indeed well known that the edge of this core produces an acoustic glitch (rapid local variation in the sound speed profile), to which the acoustic modes are sensitive (e.g. Cunha & Metcalfe 2007). This glitch induces an oscillation of the mode frequencies as a function of the radial order. The period of this oscillation is directly related to the location of the glitch, and thus to the size of the mixed core. It has thus been possible to measure seismically the extent of the mixed core and to obtain estimates of the efficiency of the extra mixing that takes place at the boundary of convective cores owing to various physical processes, such as core overshooting or rotational mixing. This has been achieved for several individual targets (Deheuvels et al. 2010; Goupil et al. 2011; Silva Aguirre et al. 2013) and more recently for a sample of eight *Kepler* targets (Deheuvels et al. 2016). These studies all showed the need for an extension of the mixed core beyond the Schwarzschild limit. Deheuvels et al. (2016) hinted that the extension of the mixed core increases with stellar mass for low-mass targets, and they suggested that this quantity could therefore be calibrated. This would help obtain more precise stellar ages, especially toward the end of the main-sequence, because the size of the mixed core determines the duration of the main-sequence.

So far, a seismic measurement of the size of the mixed core has been possible for only about ten stars. However, the PLATO mission will provide much more numerous targets for which such a method can be applied, thus making it possible to perform a calibration of the extension of convective cores. This will help produce more reliable ages for stellar models, and potentially reach a better understanding of the processes that are responsible for extending convective cores.

For the hottest main-sequence stars of the P1 sample such as F stars, the translation of seismic observations into constraints upon the central properties of the star may be difficult. However, we can have access to the information on the sizes of mixed regions during the MS phase (and hence main-sequence lifetime), from studying populations of stars during the post-MS evolution, that-is during H-shell burning phase (subgiant and low-luminosity red giant (RGB) stars) and during the central-He burning phase (Red Clump stars).

Subgiants, whose progenitors are massive enough to have had a convective core during the main-sequence, could provide precious constraints on the extent of convective cores. After the main-sequence turnoff, the rapid increase in the central density induces an increase in the Brunt-Vaisala frequency near the core. As a result, non-radial modes become mixed: they behave both as p-modes in the envelope and as g-modes in the core. This phenomenon occurs due to the coupling between the p-mode and g-mode cavities, which arises through the evanescent region that separates these cavities. It has been shown that the strength of this coupling depends crucially on the gradient of the mean molecular weight at the edge of the evanescent region (Deheuvels & Michel 2011). This gradient is in fact the result of the withdrawal of the convective core at the end of the main-sequence. Its location is therefore directly related to the size of the convective core during the main-sequence. For this reason, measuring the strength of the coupling using the observed frequencies of mixed modes can bring information about the extent of the mixed core during the main-sequence. The feasibility of such an approach has been demonstrated by Deheuvels & Michel (2011) using CoRoT data for the subgiant HD49385. This diagnostic can only be applied to early subgiants (shortly after the turnoff)

because after this, the H-burning shell washes out the gradient of chemical composition that was left by the convective core during the main-sequence. The *Kepler* satellite has also observed such early subgiants. However, only the stars observed in the "short cadence" mode could provide detections of mixed modes for these stars. The PLATO mission will greatly increase the number of such targets, making it possible to measure the extent of the end-of-main-sequence convective core for stars of various masses and chemical composition. This will be a valuable addition to the measurement of the size of convective cores during the main-sequence by exploiting acoustic glitches.

Red giants: Transport processes leave in the stellar structure features that not always have a distinct signature on the classical or asteroseismic properties when the star evolves on the main-sequence. However, the effect of these features can be clearly seen in post-main sequence evolution phases. Moreover, some stars will be barely detected as solar-like oscillators during their MS (intermediate stellar masses) or during the sub-giant phase because of the rapid crossing of the HR diagram before starting to burn He. Therefore, the goal of improving stellar evolution models to reach the highest accuracy in the characterisation of planetary systems requires seismic information about stellar structure where it is available, hence in main-sequence as well as post-main sequence stars (sub-giants, RGB and He-burning phases).

Low-mass red giant stars all have a similar He-core mass ($\sim 0.48 M_{\odot}$) and populate the so-called Red Clump. Red giants with higher masses populate the secondary Red Clump. In young stellar clusters populated enough, such as clusters in the Magellanic Clouds, these two groups are clearly identified from their luminosity. For red giants in the field, seismic indexes for red giants such as the dipole period spacing ($\Delta\Pi_1$) can be used to classify red giant stars as RGB, He-burning phases (RC1 and RC2). $\Delta\Pi_1$ is closely linked to the mass of the He-core, with two different linear laws for RGB and He-burning phases. The chemical composition and/or MS extra-mixing process determine the stellar mass distribution in the RC2 population (Montalbán et al. 2013). From comparison with stellar models, the seismic indexes ($\Delta\nu$, v_{\max} and $\Delta\Pi_1$) will determine the efficiency of chemical mixing processes acting during the MS phase, essential for stellar dating. Therefore, seismic and spectroscopic studies of RC2 populations are a key tool to characterise the efficiency of extra-mixing processes for MS stars in the galactic field.

2.2.2.4 Constraints on angular momentum transport

Another main source of uncertainty affecting age determination is the presence and efficiency of transport mechanisms in radiative zones (Zahn 1992; Maeder 2009). While these mechanisms can have a significant impact on the main-sequence lifetime, they are still poorly understood and crudely modelled. The rotationally induced chemical mixing is believed to be directly linked to the evolution of angular momentum inside the stars (Zahn 1992; Maeder & Zahn 1998). Indeed, angular momentum and chemical elements can be both transported in the radiative zones of rotating stars through meridional circulation and hydrodynamical instabilities. This results in a change of the global and asteroseismic properties of stars when rotational effects are taken into account, and in particular to an increase of the main-sequence lifetime due to the transport of fresh hydrogen fuel in the stellar core (e.g. Eggenberger et al. 2010). These changes depend on the poorly known efficiency of rotational mixing, which can be constrained by obtaining information about the internal rotation profiles in stellar radiative zones. Radial differential rotation can be inferred by asteroseismology for stars that have mixed modes (e.g. Suárez et al. 2006). These modes have a g-mode character in the core and a p-mode character in the envelope. They are therefore sensitive to the core, while having amplitudes large enough to be detected at the surface. Mixed modes are present in subgiant and red giant stars (e.g. Beck et al. 2011), and depth variation of internal rotation has already been measured using *Kepler* data (e.g. Beck et al. 2012; Deheuvels et al. 2012, 2014). This brings valuable constraints on the transport processes during and, perhaps more importantly, prior to the post-main sequence stage.

The interpretation of *Kepler* data (Figure 2.16) has shown that the core of red giants is spinning down, in spite of its contraction (Mosser et al. 2012b). This has brought clear evidence that an efficient transport of angular momentum takes place in these stars while its origin remains unknown. On the contrary, the contracting core spins up during the subgiant phase (Deheuvels et al. 2012, 2014), which thus corresponds to a period of relative decoupling between the core and the envelope. Late subgiants and early red giants correspond to the intermediate phase between these two regimes, and probing the internal rotation profile of these stars can provide estimates of the timescale over which angular momentum is redistributed. Moreover, inversions of internal rotation profiles using *Kepler* data have hinted at the existence of a sharp rotation gradient near the H-burning shell in early red giants (Deheuvels et al. 2014). If it is confirmed, this will bring strong constraints on the mechanism that transports angular momentum in these stars. Late subgiants and

early red giants are ideal targets to test this further. However, only the longest observing runs provided sufficient precision to derive the information on the core rotation of these evolved stars, and on the evolution of core rotation with time. The sample of available *Kepler* sub-giant stars is too small to allow for an unbiased statistical study. To proceed further, we will need a larger sample of bright post-main sequence stars. The necessary high quality needed to study these stars and this for a large number of such stars will only be available with the PLATO mission.

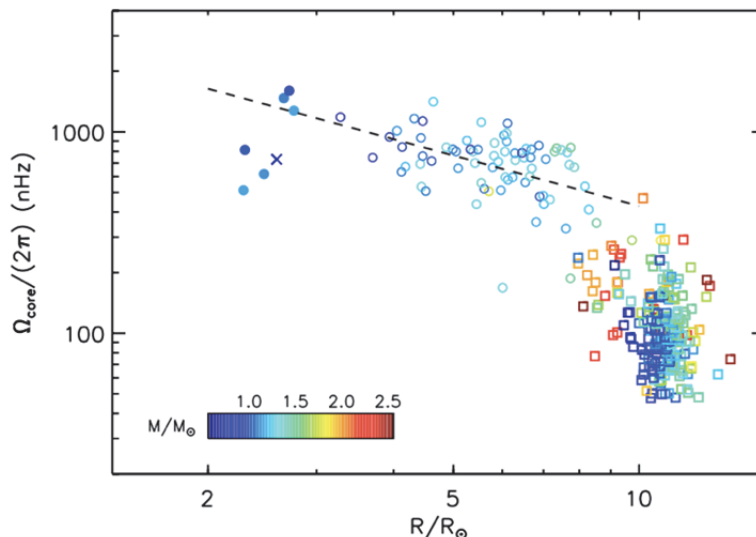


Figure 2.16: Core rotation rate as a function of the stellar radius. The open symbols correspond to the stars studied by Mosser et al. (2012b, circles: RGB stars, squares: clump stars). The filled symbols indicate the stars that were studied in Deheuvels et al. (2014), and the cross corresponds to the young giant KIC 7341231 studied by Deheuvels et al. (2012). Figure from Deheuvels et al. (2014).

2.2.3 Stellar magnetohydrodynamics

All stars rotate and many exhibit complex surface magnetic fields and activity. Coupled with the presence of turbulent convective envelopes or convective cores and stably stratified radiative zones, a large spectrum of nonlinear physical mechanisms and instabilities are at play in stars that deeply impact their evolution (Brun et al. 2015; Mathis 2013). It is essential to better characterise their relative amplitude and influence as a function of global parameters such as mass, age, rotation, and metallicity.

2.2.3.1 Understanding stellar magnetism with PLATO

The conditions to achieve cyclic magnetic activity or grand minima states (Auguston et al. 2015), stable inner magnetic field configurations (Duez & Mathis 2010), eruptive events such as flares or CME's and various internal and surface rotation profiles are still poorly understood.

Confrontation between seismic data and surveys covering ranges of stellar masses and ages has shown that there is substantial variation in the nature of magnetic output (Petit et al. 2008; Marsden et al. 2014). This already provided constraints on theories of stellar convection and magnetism and results from numerical simulations (Alfvén et al. 2015). A more detailed picture of magnetohydrodynamics of solar-like stars starts to emerge. Nevertheless, current multi-D simulations and theoretical modelling of stellar magnetohydrodynamics will benefit greatly from accurate constraints on convective powers and the extent of convective envelope or core, states of internal and surface rotation, properties of magnetic field, starspot coverage and period of cyclic activity, occurrence of flares and intense magnetic events. The asteroseismic techniques when applied to high quality data are able to assess how several key stellar parameters such as mass, age, rotation, metallicity and various stellar dynamical states are correlated and to improve our overall understanding of stars and their evolution. A larger survey than currently available is needed in order to constrain further multi-D numerical magnetohydrodynamics simulations of stars of various types. PLATO will provide such high quality survey. This will lead to a new generation of dynamical stellar evolution models, making more realistic their seismic modelling.

CoRoT provided evidence of a magnetic activity cycle (García et al. 2010), and initial constraints on stellar dynamo models under conditions different from those of the Sun (e.g. Mathur et al. 2013, 2014). This study was extended in terms of both the number of stars and measurement precision by Chaplin et al. (2011b) who used *Kepler* observations of a sample of Solar-type pulsators, and found a strong correlation between the strength of the activity and the level of inhibition of stochastically excited solar-like oscillations. Magnetic cycle has also an impact on the oscillation frequencies, whose values differ significantly depending on which phase of the cycle one observes. This bias must be taken into account when deriving the seismic properties of the host stars.

PLATO's long time series will allow the study of magnetic activity cycles and spot decay time for various types of stars. The observation of starspot evolution, frequency, activity cycles, and surface distributions will allow us to better understand the physics behind activity phenomena, and to derive constraints for dynamo theories.

2.2.3.2 *Surface rotation period and gyrochronology calibrated by seismology*

For stars in the core programme that are too faint for detection of their oscillation frequency, the age will be determined by other means. One such technique is gyrochronology (e.g. Barnes et al. 2007, 2011) that provides the age as a function of the surface period rotation of the star. Several such relations have been established empirically by fitting observational data for different sets of stars. Today, the precision on the age derived from such relations is clearly insufficient with respect to the PLATO specification (Lebreton & Goupil, 2014). Actually the relations between the rotation period and the age are not unique, they also depend on the effective temperature and the mass of the star. Theoretical investigations are necessary to understand better the physics behind these relations, and calibration with well seismically characterised stars will define the validity domain of these relations and how they can be used properly. Such studies have started with *Kepler* data (Angus et al. 2015; Van Saders et al. 2016) but will be fully developed with PLATO. Indeed, for a large set of bright stars – therefore well spectroscopically characterised – PLATO will provide precise surface rotation *and* seismic age periods from the analysis of light curves. This will allow reliable statistical studies on the biases that keep gyrochronology today to provide precise and accurate stellar ages. Identifying these biases and understanding their physical origin will lead to improve the domain of validity of gyrochronology and its dating precision. These studies are very demanding in terms of the quality of observational data. This will be only possible with PLATO that will provide the appropriate large sample of fully well characterised stars.

2.2.3.3 *Synergy star-planet*

In direct link with the main goal of PLATO, that is to find earth-like planets around solar-like stars, a better knowledge of stellar nonlinear dynamics will improve our ability to understand their impact on the surrounding planets. Indeed, through either their magnetic activity, wind of particles and tidal effects, stars have a direct influence on planets and on their habitability (Strugarek et al. 2015; Mathis 2015). There is a complex feedback loop between rotation, magnetic field, and mass and angular momentum loss through stellar wind and tidal dissipation in stars, that needs to be constrained. This will allow us to understand the orbital evolution of star-planet systems and the rotational evolution of their components on secular time scales, and to improve the realism of numerical simulations of such systems (Réville et al. 2015; Auclair-Desrotour et al. 2014). Stellar dynamical processes coupled with tidal dissipation in planets and MHD interactions with their magnetospheres will lead to a large diversity of configurations of star-planet systems that can be modelled. By providing constraints on the host star, surrounding planets and orbital architecture PLATO will improve greatly the study of star-planet interactions and the characterisation of key physical properties of stars, planets and planetary systems as a whole.

An important part of the stellar property characterisation for the exoplanet studies is therefore a precise knowledge of the surface activity of the host stars. One of the manifestations of stellar activity is spots at the surface of the star rotating with the star that generate temporal variability of the light curve. The high quality PLATO data will enable to measure micro variability and thereby provide highly valuable observational information on the surface rotation of the stars, on their magnetic activity on short and longer time scales (solar-like cycles) for a large set of stars. The information power of this type of investigation has been demonstrated with *Kepler* data (Bonomo & Lanza 2012; Lanza 2016; Moutou et al. 2016).

The occultation of starspots by transiting planets produces anomalies in the transit light curves that may lead to inaccurate estimates of transit duration, depth, and timing (Czesla et al. 2009; Oshagh et al. 2013). These inaccuracies can affect the precise derivation of the planet radius, and consequently affect estimates of the planet's density. Thus, having an estimate of the size and position of starspots would help to overcome this issue. Furthermore, repeated starspot occultations can reveal the stellar rotation period (Silva-Valio 2008) and even differential rotation (Silva-Valio & Lanza 2011).

Thorough investigation of stellar evolution requires a large number of bright stars sampling all relevant stellar parameters (mass, age, rotation, chemical composition, environment). The PLATO mission will, for the first time, provide such necessary data in order to:

- Improve understanding of internal stellar structure, including the identification of missing physics.
- Better understand the pulsation content and its interaction with the physics of the star, in particular with respect to rotation and magnetism.
- Improve our understanding of stellar evolution.

2.3 Science Objectives III: Complementary science

In addition to its focus on relatively bright stars, one major advantage of PLATO over the CoRoT and *Kepler* space missions is its ability to observe in many directions on the sky. This will enable us to sample a much wider variety of time-variable phenomena in various populations of the Galaxy than was hitherto possible. Moreover, PLATO's asteroseismic characterisation of stellar ensembles, binaries, clusters and populations will be a significant addition to the *Gaia* data. This capability will obviously give rise to a very rich legacy for stellar and galactic physics, promising major breakthroughs in a variety of subjects.

2.3.1 Stellar structure and evolution

2.3.1.1 Low- and intermediate-mass red giants

Red giants are cool and luminous stars, which, by virtue of covering a wide domain in mass, age, chemical composition, and evolutionary state, are an important source of information for testing chemo-dynamical stellar models. An important legacy from the CoRoT and *Kepler* missions has been the discovery of solar-like oscillations in thousands of G-K red giants (De Ridder et al. 2009; Bedding et al. 2010; Hekker et al. 2011). The occurrence of non-radial modes was only unambiguously proven from CoRoT observations (De Ridder et al. 2009). This opened up the field of asteroseismology of low-mass evolved stars.

Thanks to the discovery of gravity-dominated mixed modes in more than 300 days of continuous *Kepler* monitoring of red giants (Beck et al. 2011, Bedding et al. 2011), the promise of asteroseismology being able to discriminate between different nuclear burning phases was finally delivered. Indeed, with PLATO we will be able to use the oscillation period spacing of dipole mixed modes to probe the properties of the core structure of red giants. This will reveal whether they are already in the helium core burning stage, or are still climbing up the red giant branch while shell-burning hydrogen (Bedding et al. 2011; Mosser et al. 2012a). PLATO will be able to distinguish between stars in these two fusion modes, because they occupy different locations in frequency spacing-diagrams and PLATO's frequency resolution is good enough. Additionally, the capability to perform seismology analyses on red giants will constrain mixing processes in main-sequence stars. Red giants at the transition between low and intermediate mass (2–2.5 M_{\odot}) will provide information on the extent of central mixing during their main-sequence phase, allowing the study of transport processes in mass ranges and evolution phases where Solar-like oscillations are not expected. On the other hand, the seismology of low-mass red giants will constrain the extent of the central mixed region during the central He-burning phase (Montalbán et al. 2013). The description of transport processes as well as the size of the mixed region are a matter of strong debate, and have important consequences for stellar population studies (e.g. Straniero et al. 2003).

PLATO will also improve the period-luminosity relationships of these types of objects, which will aid with their use as galactic, or even extragalactic, distance-indicators, providing higher precision than is currently

the case. PLATO will increase our understanding of the internal structure of red-giant stars by providing accurate and precise oscillation frequencies for an unprecedented number of targets in different areas of the galaxy.

2.3.1.2 Hot OB sub-dwarf stars

Hot OB sub-dwarf (sdB hereafter) stars are core He-burning stars with an extremely thin H-rich envelope (Heber 2009). They exhibit pulsation instabilities driving both acoustic modes of a few minutes and gravity modes with 1–4 hour periods. While the asteroseismic exploitation of p-mode pulsators started a decade ago (Brassard et al. 2001), it is only recently, with CoRoT and *Kepler*, that data of sufficiently high quality could be obtained for g-mode sdB pulsators (Charpinet et al. 2010; Østensen et al. 2010), though the time resolution is sub-optimal owing to oscillation timescales on the order of minutes. Asteroseismic modelling provides measurements of their global parameters (e.g. mass and radius) with a precision of typically 1% (Van Grootel et al. 2013). The mass distribution of sdB stars (Fontaine et al. 2012) is consistent with the idea that they are post-RGB stars that went through the He-flash, and that have lost most of their envelope through binary interaction.

While more than half of sdB stars reside in binaries with either a white dwarf or low-mass stellar companion, the recent discoveries of planets around single sdB stars (Charpinet et al. 2011; see Section 2.1.6) support the idea that planets could influence the evolution of their host star by triggering the mass loss necessary for sdB star formation.

Thanks to the combination of its rapid observing cadence and bright targets, PLATO will be the only space-based facility able to develop the science of deep seismic probing of sdB stars. It will provide high-quality data on g-mode pulsations in these stars that cannot be obtained from the ground. Thereby, PLATO will increase the number of sdB stars that can be modelled by asteroseismology. It will also discover new planets around these objects, enabling us to disentangle the question of the origin of such stars and explore star-planet interactions in the advanced stages of stellar evolution.

2.3.1.3 Massive stars

Despite their scarcity compared to low-mass stars, stars massive enough to end their lives in core-collapse supernovae dominate the chemical enrichment of galaxies, and of the Universe as a whole. Most of the heavy elements (by mass fraction) are created by stars with birth masses above $\sim 9 M_{\odot}$. For such stars, the effects of internal rotational mixing remain largely uncertain, despite being crucial for predictions of their future evolution as blue super-giants. Interestingly, g-mode oscillations have been discovered in evolved massive supergiants (e.g. Saio et al. 2006; Lefever et al. 2007), and hold similar potential for probing the stellar core as the gravity-dominated mixed modes found in red giants (Moravveji et al. 2012a). PLATO can provide a homogeneous sample of blue supergiants, studied by asteroseismology, with a broad range of pulsation periods.

From five months of CoRoT data, Degroote et al. (2010a) measured a periodic deviation of amplitude superimposed on a constant period spacing for the high-order g-modes of a star of $\sim 8 M_{\odot}$. This allowed for the deduction that this star has experienced 60% of its core hydrogen-burning lifetime, and also allowed for the determination of the detailed shape of the near-core chemical composition gradient. The only barrier to the application of similar diagnostics to blue supergiant pulsators is the complete lack of suitable high-precision, uninterrupted light curves. These will be provided by PLATO, allowing identification of the highest amplitude modes.

2.3.1.4 White Dwarfs (WDs)

White dwarfs are the evolutionary endpoint for the vast majority ($\sim 95\%$) of stars in the Universe. They no longer undergo fusion reactions but gradually evolve along the cooling sequence, where several classes of g-mode pulsations allow asteroseismic probing of this final stage of stellar evolution (Fontaine & Brassard 2008).

WDs can be used to constrain the ages of the various populations of stars in the Galaxy during their later, evolved stages (cosmochronology: Fontaine et al. 2001; Liebert et al. 2013). The cooling tracks are very sensitive to the exact core composition and envelope layering, two parameters that are inaccessible from direct observations and poorly constrained from theory, but that can be determined from asteroseismology (Giammichele et al. 2012). WD cosmochronology complements the *Gaia* mission, adding accurate age

estimates to 3D mapping of the Galaxy. Internal dynamics can also be probed by asteroseismology, allowing study of the rotation and angular momentum evolution in the WD stage (Charpinet et al. 2009). Finally, “exotic” physics that is due to the extreme, compact nature of white dwarfs can be calibrated (neutrino production rates, conductive opacities, interior liquid/solid equations of state, crystallisation at the end of cooling, etc.) WDs are also becoming interesting targets for planet search campaigns (Agol 2011).

PLATO will be the very first mission to bring WD seismology into the space era, allowing for significant asteroseismic probing of the final stages of stellar evolution. Simulations show that, assuming $V \leq 16$, approximately 10 WDs should be observable with sufficient quality in the long-monitoring fields, and ~ 50 pulsating WDs in the step-and-stare fields. These numbers are in good agreement with the three WD pulsators discovered in the *Kepler* field; none were observed by CoRoT.

2.3.1.5 Probing angular momentum transport using gravity modes

An important missing input for stellar models is a measurement of the internal rotation as a function of evolutionary stage. Such a measurement is needed to estimate the amount of rotational mixing and angular momentum transport, which are crucial aspects for the outcome of stellar evolution, but which remain essentially unconstrained by experiment so far. It required two years of continuous *Kepler* data to make the first steps towards measuring the internal rotation of evolved low-mass stars (Beck et al. 2012; Deheuvels et al. 2012; Mosser et al. 2012a). Those first results imply that current models neglect an important angular momentum coupling between the core and envelope of evolved stars (Ceillier et al. 2013; Eggenberger et al. 2012; Marques et al. 2013). An unknown physical process which transports angular momentum much more efficiently than hitherto assumed is clearly needed. Very recently, internal gravity waves (IGW) were proposed to leave observable surface light fluctuations at a level of hundreds of micromagnitudes by Shiode et al. (2013) and Rogers et al. (2013). Rogers et al. show that IGWs are very efficient in transporting angular momentum in stars and, in particular, can be responsible for spinning up and/or slowing down their outer layers. They also suggest that IGW angular momentum transport may explain many observational mysteries, such as:

- The misalignment of hot Jupiters around hot stars, or stars with weak tidal forces
- The Be class of stars
- Nitrogen enrichment anomalies in massive stars
- Non-synchronous orbits of interacting binaries.

Thanks to its high-precision photometric data and long time-base, PLATO can observationally explore the theory of excited IGWs. PLATO has the potential to characterise this major missing ingredient in stellar evolution theory, by deriving internal rotational profiles from inversion of rotationally split oscillation frequencies for a carefully selected sample of target stars covering entire evolutionary paths.

2.3.1.6 Early stellar evolution – the pre-main sequence

During stars’ early evolution from their births in molecular clouds to the onset of hydrogen core-burning, complex physical processes are acting which challenge current theory and observing techniques. This transition takes place in several steps, starting with planet formation in the protoplanetary disc surrounding the pre-main sequence (PMS) star, and which is directly connected to the stellar photosphere; it is the conservation of angular momentum within the contracting molecular core that gives rise to the formation of protoplanetary disks and planetary systems.

The different stages in the star formation process have been distinguished based on the spectral energy distribution of young stellar objects (YSO). Protoplanetary disks are composed of a mixture of gas and dust, where the gas represents the dominant component in mass but the dust provides the best diagnostic value for the study of the structure and mass of the disk.

Studies of the star formation process are focused on low to intermediate-mass stars because high-mass stars evolve so fast that they do not reveal a PMS phase. The end product of star formation is an object with a disc that has lost most of its gas; the newborn star is left with a dusty debris disk, potentially with a planetary system. In order to understand planet formation, detailed studies of the structure and evolution of protoplanetary discs are necessary; in the last decade, our understanding of has drastically improved thanks

to enhanced observational capability. Spatially resolved, infrared images have shown that debris discs may be maintained by replenishment of small grains, and revealed that they may contain gaps where planets could have formed. Various morphologies of discs have been found for PMS stars, but what is lacking is a relative aging tool so that their classification can be placed into an evolutionary sequence.

Coordinated, multi-wavelength, time-resolved, high-precision, high-cadence, long-duration studies of young open clusters seem the best approach for building up a solid picture of star and planetary system formation. So far, the most extensive study has been done for the young cluster NGC 2264 (Cody et al. 2014), but the time base of one month was too short to perform relative aging of its PMS stars. X-ray data revealed the levels of activity of the member stars; it was found that optical and infra-red light curves are weakly correlated, and that flux variation are correlation with H α variability and effective temperature, while the morphology classes at various wavelength regimes are not necessarily the same for one object. Multiple sources of young star variability were identified, including circumstellar obscuration events, hot spots on the star and/or in the disc, accretion bursts, and rapid structural changes in the inner disc. Interestingly, asteroseismic aging of eight of the cluster's PMS pulsators was achieved, pointing to multi-epoch star formation (Zwintz et al. 2014).

All of these phenomena make young stars interesting objects that allow us to investigate, among other things, how our Sun formed and evolved to its present state, and to study how stellar evolution depends on initial conditions. Sadly, the *Kepler* field-of-view contained no PMS pulsators, and only a handful are planned to be observed by K2. Furthermore, the time base of most TESS fields is too short for a detailed study of PMS stars.

PLATO variability studies of PMS stars, accompanied by multi-wavelength data, would therefore provide a major step forward in our understanding of star and planetary system formation, allowing us to study their different types of variability, and revealing ground-breaking insights into early stellar evolution.

2.3.2 Asteroseismology of globular and young open clusters

Testing stellar evolution theory using asteroseismology will be most successful if applied to the extremes of stellar evolution. This should include both young open clusters with (pre-) main-sequence and pre-supernova supergiant pulsators on the one hand, and old globular clusters of various metallicities that contain main-sequence, horizontal branch, and WD stars, on the other hand.

Current asteroseismic studies involve, for example, the study of solar-like oscillations of the red giant members (Stello et al. 2011; Hekker et al. 2012), and have led to the first seismic cluster constraints on age, metallicity, and mass-loss rates on the red giant branch (Basu et al. 2011; Miglio et al. 2012a; Corsaro et al. 2012). Unfortunately, only clusters in a relatively narrow range of ages, from 0.4 Gyr for the youngest to \sim 8 Gyr for the oldest, have been studied.

Owing to pointing restrictions, no young clusters (i.e. with ages younger than a few tens of million years) could be observed by *Kepler*, and only one young cluster, NGC 2264, could be observed in two short runs by CoRoT. Recent asteroseismic results from these observations include the discovery of the first two PMS Υ Doradus pulsators (Zwintz et al. 2013), and a homogeneous study of the relation between pulsations and stellar evolution from the early stages to the main-sequence phase (Zwintz et al. 2014).

PLATO's sky coverage during a step-and-stare phase would lead to major breakthroughs in this area. No other experiment with the capability for full cluster asteroseismology is currently on the horizon.

2.3.3 Probing the structure and evolution of the Milky Way

Studying the chemical enrichment of the Universe is one of the main thrusts of modern astrophysics, and the Milky Way (MW) can be seen as the key to understanding this evolution. The origin and evolution of the MW is encoded in the motion and chemical composition of stars of different ages. In particular, the MW halo contains the oldest and most metal-poor stars observable, which were born at times, or equivalently redshifts, still out of reach for the deepest surveys of primordial galaxies. These stars retain the memory of the unique nucleosynthesis that took place in the first stars, as revealed by the striking abundance patterns observed at very low metallicities (Chiappini et al. 2006). A serious obstacle to being able to discriminate between different scenarios of formation and evolution of galactic components (halo, thin and thick disk, and bulge) is the difficulty of measuring distances, and more importantly ages, for individual field stars. Crucial

ingredients for the study of evolutionary processes in the disk are, for example, the age-metallicity and age-velocity dispersion relations for different directions, and at different galactic radii and heights from the plane.

PLATO’s red giant asteroseismology will be crucial to improve stellar models of exoplanet host candidates, but it will also serve galactic structure studies by providing far better ages than are currently available for various populations in the Milky Way.

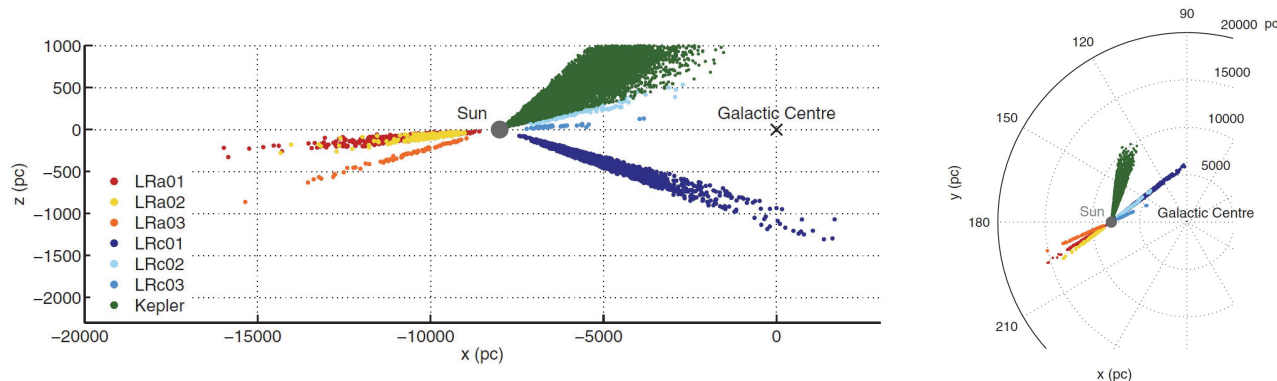


Figure 2.17: Distribution on the galactic plane of the red giants with asteroseismic characterisation from the light curves obtained in the CoRoT exofield for six long runs: LRA01 (red), LRA02 (yellow), LRA03 (orange), LRC01 (blue), LRC02 (green), LRC03 (cyan). From Miglio et al. (2012b).

Even if not completely free from stellar modelling, the mass of a red giant star, given its evolution rate, is a good proxy for its age. In addition, oscillation spectra of red giants allow us to deduce their masses, radii, and ages from scaling relations, which have seen major upgrades thanks to *Kepler*, including the capacity to distinguish the phases of hydrogen-shell burning on the red giant branch and helium core burning on the horizontal branch (Bedding et al. 2011; Mosser et al. 2011). Once the chemical composition is known, asteroseismology can provide stellar ages with 10% uncertainty, while classical methods such as isochrones are typically uncertain by a factor two. Using seismic data from CoRoT and *Kepler*, Miglio et al. (2012b, 2013) showed that pulsating red giants can be used to efficiently map and date the Galactic disk in the regions probed by observations (Figure 2.17).

Given the high intrinsic luminosity of red giants compared to dwarfs, they allow us to see quite far through the Galaxy, up to about 10 kpc, whereas *Hipparcos*’ precise parallaxes are only available up to 100 pc. This is illustrated by the CoRoT sample of 606 red giants followed-up spectroscopically with APOGEE and modelled seismically by Anders et al. (2017). Figure 2.18 shows the seismic age of these red giants as a function of their seismically derived distance. The latter will be over-ruled in accuracy by the *Gaia* distance measurement, which will lead to decreased error bars in both quantities shown in Figure 2.18 for thousands of red giants to be observed with PLATO. The capability of seismic data to derive individual stellar ages indicates a clear vertical gradient in the ages of disc red giants. These results show the enormous potential of red giant seismology with PLATO, which will not be limited to pencil-beam surveys as is the case for CoRoT and *Kepler*, but will rather deliver high-precision age estimation for thousands of red giants across the entire Milky Way reaching distances of tens of kpc.

Gaia will create a 3D map of stars throughout our Galaxy, hence providing an observational test bench for theoretical predictions about the origin, structure and evolutionary history of the Milky Way. Additional, crucial information on both velocities and chemical abundances will come even earlier from several on-going/planned spectroscopic surveys such as SEGUE-2, APOGEE and the *Gaia*-ESO surveys. By the time PLATO launches, a far better understanding of the different scenarios for the formation and evolution of our Galaxy’s main components will be available. The missing ingredient for galactic archeology studies will be the age component, hence age-metallicity and age-velocity relations for different positions and populations in the Milky Way will still be subject to large uncertainty. Observing red giants with the combination *Gaia* & PLATO will thus allow to map and date the galactic regions probed by these two missions, with high precision, for distances up to tens of kpc.

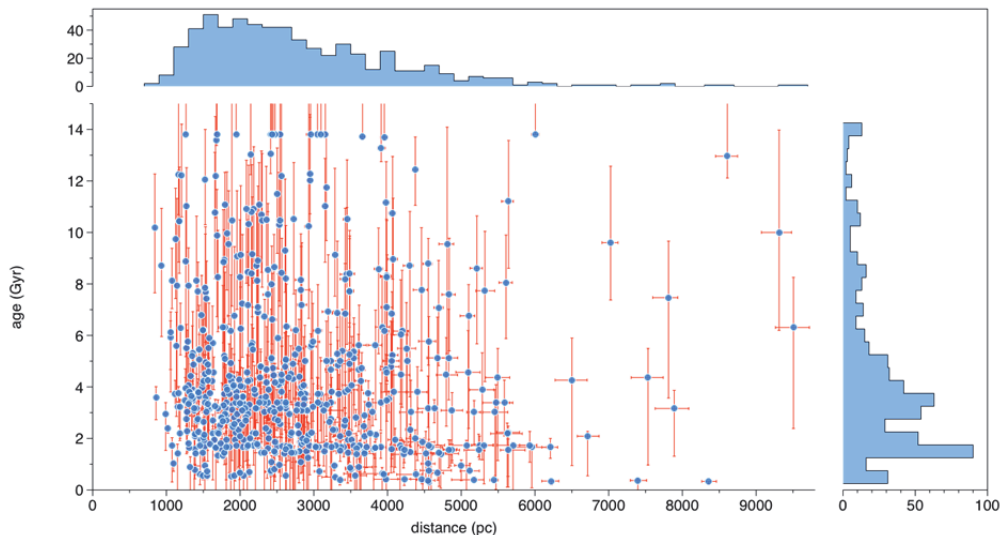


Figure 2.18: Seismically modelled ages versus seismic distances for 606 red giants observed with CoRoT and APOGEE as computed by Anders et al. (2017) from scaling relations of the detected solar-like oscillations. Future independent Gaia distance estimates from astrometry will imply even smaller errors for the seismic ages for thousands of red giants to be observed with PLATO. Figure courtesy of Joris De Ridder.

The combination of chemical compositions from spectroscopic surveys with distances from *Gaia* and ages from seismic data, as provided by PLATO for large samples of stars, will allow us to comprehensively study chemical gradients and their time evolution in different directions of the galaxy. It will provide information on the metallicity distribution of thick and thin disk stars at different positions in the galaxy, and their time evolution. In addition, the evolution of the stellar velocity dispersions in the disk can be studied. All of these crucial constraints will allow us to quantify the importance of stellar radial migration in the formation of the Milky Way, which is otherwise difficult to quantify from first principles. This will represent invaluable information not only for the formation of the Milky Way, but also spiral galaxies in general.

2.3.4 Accretion physics near compact objects

While the *Kepler* mission produced an extensive legacy in the area of eclipsing binaries (e.g. Prsa et al. 2011; Slawson et al. 2011; Matijevic et al. 2012), including the detection and characterisation of circumbinary planets (Doyle et al. 2011; Winn et al. 2011; Welsh et al. 2012), ultra-short periodic phenomena in binaries are hard to observe owing to the sampling cadence and single pointing of the telescope. Accretion phenomena in compact binaries, such as cataclysmic variables or X-ray binaries (XRBs), display variability on a range of timescales, involving both the orbital and spin periods of the components. In such systems, the secondary transfers material to the primary, which is either a white dwarf, a neutron star or a black hole. XRBs show variability due to accretion at timescales ranging from milliseconds to hours, while the time scales for cataclysmic variables (CVs) are in the range from minutes to days. To date, *Kepler* has provided only some 5 CVs with high enough quality data to perform detailed studies of their aperiodic variability properties, with R magnitudes ranging from 12.8 up to ~ 19 . Although a solid starting point, this is by no means sufficient to understand how accretion-driven variability differs between CV subsets (dwarf nova, nova-like, magnetic systems).

PLATO's all-sky accessibility, optical photometry, and cadence of 25 and 2.5 seconds for normal and fast telescopes, respectively, is well suited to shed new light on the physical processes involved in disc accretion of compact objects, by studying a sample of carefully selected CVs and XRBs. Phase-lags of a few percent, and time-lags of 2–15s, have recently been discovered in fast multi-colour optical photometry with ULTRACAM for the two CVs MV Lyr and LU Cam (Scaringi et al. 2013). Similar lags have also been observed for X-rays compared with optical measurements for XRBs and in Active Galactic Nuclei (AGN). PLATO's fast telescopes hold the potential to unravel the physical origin of these lags by studying a carefully chosen, modest sample of bright CVs in two colours.

Accreting systems exist at all mass and length scales: from proto-stars and YSOs to super-massive black holes. The brightness variations observed across various types of accreting systems provide a perspective that is complementary to spectroscopic observations, and possibly the best probe to understand how material is transferred through accretion discs. Understanding the detailed physics of accretion-induced variability and mass transfer variations will allow us to unravel questions relating to the mass growth of the central objects, and accretion-related outflows and their impact on their surrounding medium.

From only a handful of *Kepler* systems we now know that the aperiodic variability shares important characteristics across all accreting systems. This provides the starting point of a universal physical model for accretion. Testing such a unifying model will require observations of a large sample of objects of different sub-classes, allowing us to characterise similarities and isolate differences. In this respect PLATO has revolutionary potential. Its exquisite accuracy and continuous observations will also allow the study of the relationships and physical mechanisms linking accretion to ejection.

PLATO observations will be complemented by continuous radio observation using LOFAR/AMI and/or SKA, allowing the coverage of transient sources in radio as well as optical. Correlations between radio and optical light curves will allow us to assess the importance of jets in a way that has, to date, only been possible for GRS1915+105 and V404 Cyg. Continuous optical monitoring by PLATO of bright optical flares associated with the tidal disruption of stars by a super-massive black holes would allow the study of (transient) accretion in such systems, informing studies of the influence of the feeding mechanism on the properties and physics of the accretion flow

2.3.5 Classical pulsators

PLATO will obtain high-precision photometric light curves for classical pulsators, such as β Cep stars, slowly pulsating B stars (SPBs), δ Sct stars, γ Dor stars, as well as distance indicators such as RR Lyrae stars, high-amplitude δ Sct stars, and Cepheids (e.g. Chapter 2 of Aerts et al. 2010). The mean densities of those stars can now be determined with a precision of about 6% for stars observed by CoRoT (e.g. García Hernández et al. 2009; Suárez et al. 2014).

CoRoT and *Kepler* have revolutionised our knowledge of such classical pulsators through several discoveries:

- Observed regularities in the frequency spectra (Breger et al. 2011; Zwintz et al. 2013) and the existence of relationships between low and high frequencies in δ Sct stars (Breger et al. 2012)
- The high fraction (23%) of δ Sct stars - γ Dor hybrid pulsators among the A and F-type stars (Tkachenko et al. 2013; Uytterhoeven et al. 2011)
- The dense frequency spectra of δ Sct stars below 5 μ Hz (Mantegazza et al. 2012; Poretti et al. 2009),
- SPB type g-mode period spacings and p-mode frequency spacings in OB type pulsators (Degroote et al. 2010b, 2012). Moreover, B type stars were shown to exhibit a much larger diversity in their variability than expected before from ground-based observations.
- Stars with spotted (or at least inhomogeneous) surface configurations (e.g. Degroote et al. 2011; Pápics et al. 2012) pointing towards the presence of a magnetic field.
- Pulsating stars outside (and constant stars inside) the theoretical instability strips calculated with current stellar evolution models and oscillation codes (e.g. Pápics et al. 2011)
- Stars exhibiting gravito-inertial modes (Pápics et al. 2012; Thoul et al. 2013)
- Pulsations driven by rare excitation mechanisms, such as tidal excitation and non-linear resonant excitation (Pápics et al. 2013) in addition to the ε -mechanism in blue supergiants (Moravveji et al. 2012b).

PLATO is expected to expand on these discoveries, revealing more features of classical pulsators that will lead to a better understanding of the underlying physical processes, and their influences on stellar evolution.

The precision of PLATO data, and the expected number of β Cep stars, may be key to understanding their pulsational properties through analysis of splitting asymmetries, as well as internal rotation profiles. For these stars the convective core was found to rotate faster than the surface (Aerts et al. 2003; Dziembowski &

Pamyatnykh 2008; Suárez et al. 2009), but the number of stars studied is, at present, too limited to draw general conclusions that would improve stellar evolution theory.

The study of Cepheids and RR Lyrae stars will greatly benefit from the large number of PLATO targets. A rough estimate gives 550 (730) Cepheids (of both classical and Type II) down to 13th (15th) magnitude compared to about a half dozen observed with CoRoT, and only one well documented case in the *Kepler* field (Szabó et al. 2011). The improvement is similarly large for RR Lyrae stars; the current design and observing strategy of PLATO promises the observation of at least 800 (3600) of such stars down to the 13th (15th) magnitude limit, as opposed to ~ 30 and ~ 50 found in CoRoT and *Kepler* fields respectively. These calculations used the GCVS catalogue (Samus et al. 2012) and neglected the results of recent all-sky surveys, and therefore these numbers should be regarded as lower limits.

The large number of observable Cepheid and RR Lyrae stars will facilitate the investigation of the Blazhko effect (Kolenberg et al. 2011), to test current theories (e.g. Gillet 2013) of its occurrence rate and phenomenology (Le Borgne et al. 2012), the excitation of non-radial modes (Poretti et al. 2010) and other light curve variations, the stability of pulsation periods (Derekas et al. 2012), stellar evolutionary effects and non-linear dynamics (e.g. Szabó et al. 2010; Kollath et al. 2011; Molnár et al. 2012), as well as the Blazhko effect's appearance in the light curves of high amplitude δ Sct stars (Poretti et al. 2011). The availability of accurate asteroseismological measurements and radial mode pulsational period estimates, combined with a detailed evolutionary framework, could be pivotal when investigating the well-known discrepancy between theory and observations of pulsational period change rates. Observed rates are an order of magnitude larger than those predicted by Horizontal Branch models (Kunder et al. 2011, and references therein).

2.3.6 Classical eclipsing binaries, beaming binaries and low-mass stellar and sub-stellar companions

PLATO will provide the opportunity to significantly increase the samples of binaries and sub-stellar companions studied in the following areas:

- Classical eclipsing binaries (EBs) allow us to measure the masses of the components via *Kepler's* third law in a model-independent way, when high quality photometry and a radial velocity curve of the two-lined binaries are available. The addition of effective temperature measurements for both stars allows luminosity, and thus absolute magnitude, to be calculated, providing high quality distance estimates. However, at present good quality mass, radius, and luminosity data are available for only 185 such systems (DEBCat⁴; Southworth 2015).
- There exists a persistent mismatch between the properties of low-mass stars in EBs and the predictions of theoretical models, with stars typically being 10% larger and 5% cooler than expected. The mass range affected ($< 1.1 M_{\odot}$) is exactly that of most interest for transiting exoplanet studies, and the lack of understanding of the host stars limits our understanding of the planets. A related issue is the lack of metal abundance determinations for EB components, which would make it much easier to find a set of theoretical predictions matching the observations.
- Low-mass stellar companions can be detected via the so-called beaming effect. This relativistic effect causes a small light curve modulation with the period of the orbital period of the companion, and allows us to determine the companion mass without radial velocity measurements (e.g. Zucker et al. 2007; Mazeh et al. 2010; Faigler et al. 2013).
- The gravity darkening effect can be used to probe the internal heat-distribution of stars via radial and meridional circulations (Rafert & Twigg 1980).
- Observations of contact binaries will permit the study of formation processes, internal structure, activity, and especially the final evolutionary stage of binary systems (Csizmadia et al. 2004; Eggleton 2012; Tran et al. 2013). The rapid observing cadence of PLATO makes it ideal for studying these very short period objects.

⁴ <http://www.astro.keele.ac.uk/jkt/debcats/> accessed at 14:34 on Thursday 24th March 2016

2.3.7 Additional complimentary science themes

Apart from the above themes in stellar and galactic physics that PLATO will address, various additional subjects are within reach, including common-envelope and Roche-Lobe overflow evolution of close binaries, tidal asteroseismology, and the mass-loss and structure of stars rotating at critical velocity. In some favourable cases, PLATO might observe the microlensing amplification of massive objects eclipsing bright companions (Maeder 1973; Muirhead et al. 2013), super-novae, GRBs, and even microlensing of black holes (Cieplak & Griest 2013), as well as Kuiper-belt and Oort clouds objects in our solar system. PLATO will also make high precision measurements of a small, well-selected sample of compact objects, both galactic and extragalactic, where the fast cadence and precision will benefit the interpretation of poorly understood phenomena.

2.4 PLATO's long-term legacy

The PLATO's catalogue of thousands of characterised planets and between 300,000 and ~1,000,000 high precision stellar light curves (depending on the final observing strategy) will provide the basis of a huge legacy for stellar and galactic science, which will be explored by the community in the years to come after the PLATO mission. PLATO will provide a large catalogue of very well characterised stars. No other missions (actual or planned) will provide such a sample with the same accurate long-term photometric characterisation. Planets around bright stars, detected and characterised by PLATO, will be ideal targets for spectroscopic studies to investigate their atmospheres and link them with the planetary bulk properties. Observing further transits of large planets around suitably bright objects from the ground over long periods, well beyond the mission's lifetime, will enable searches for planets or exomoons by TTVs and Transit Duration Variations (TDVs) over a very long time base. During the mission RV follow-up to determine planet masses will focus on the most scientifically interesting targets; candidates detected by PLATO, but not confirmed by RV within the mission lifetime, will provide a wealth of targets for future mass determinations by the science community, resulting in thousands of further characterised planets.

3 Scientific requirements

3.1 PLATO measurement concept

PLATO will achieve its science objectives by performing: 1) planet detection and radius determination from photometric transits; 2) determination of planet masses from ground-based radial velocity follow-up; 3) determination of accurate stellar masses, radii, and ages from asteroseismology, and 4) identification of bright exoplanet hosts that will be targets for atmospheric spectroscopy.

3.1.1 The transit method

PLATO will detect and characterise exoplanets with the transit method. It will perform long uninterrupted high precision photometric monitoring of large samples of stars to detect the dimming of stellar flux by an orbiting planet passing through the line-of-sight to Earth. When the planet is in front of the star, it obscures an area on the stellar surface proportional to the ratio of its size compared to that of the star. The dimming of stellar flux is therefore proportional to the square of the radius of the planet, R_{planet} , relative to the radius of the star, R_{Star} : $\Delta F \propto (R_{\text{planet}}/R_{\text{Star}})^2$. Figure 3.1 shows as an example the transit light curve of Kepler-10b, the smallest known exoplanet with the most accurate radius and mass measurement so far ($R_{\text{planet}} = 1.416 \pm 0.03 R_{\text{E}}$, $M_{\text{planet}} = 4.6 \pm 1.2 M_{\text{E}}$, Batalha et al. 2011). The round shape during this central transit is caused by the limb darkening of the host star. The transit method allows us to measure directly a planet's size once the size of the star is known.

The mass of a detected transiting planet has to be determined by other means, for example by spectroscopic radial-velocity follow-up or Transit Time Variations (TTVs) measurements. The combination of radius and true mass provides the mean density of the planet, which, in combination with models of planetary interiors, allows us to constrain the planetary inner structures.

The periodicity of transit events allows us to derive the orbital period and therefore orbital distance according to *Kepler's* 3rd law. If the secondary eclipse can be detected, i.e. if the planet disappears behind its host star, the orbital eccentricity can also be derived. Furthermore, the combination of transits with radial-velocity measurements during the transit allows us to determine the complete orbital parameters, including the eccentricity and alignment of the planetary orbital plane with the projected stellar rotation axis and the sense of orbital revolution of the planet around its star by the Rossiter-McLaughlin (RM) effect (Rossiter 1924; McLaughlin 1924). The RM effect will also be a more efficient way of confirming the planetary nature of a small planet, since their RM signal may be 2-3 times that of the orbital radial velocity signal and could be determined in the best cases from a single night of observations.

In addition, the variation of the light reflected by the planet's surface all along its orbit, that is, its phased light curve, can also be measured. Thanks to space-based observations (Snellen et al. 2009; Borucki et al. 2009), this kind of observation allows us to determine the planet's albedo and provides insights into the atmosphere properties. Complementary observations in the IR of the secondary eclipse could complete the analysis by providing the planet's thermal emission (e.g. Demory et al. 2011). Finally, one can also take advantage of the primary transit to carry out spectroscopic observations of the planet's atmosphere and detect some atomic species (e.g. Charbonneau et al. 2009). The analysis of the transit ingress and egress can be used to map the planetary atmosphere, at least for close-in hot giants (Cowan & Agol 2008).

The sensitivity of PLATO will also allow us to detect, not only planets, but also their rings and moons, trojans (objects that share an orbit with a larger planet), as well as large comets. Moons and trojans can be used to constrain models of planet formation but are also themselves potentially habitable objects. Rings can influence measurements of planetary radii and are thus important to improving the precision of these measurements.

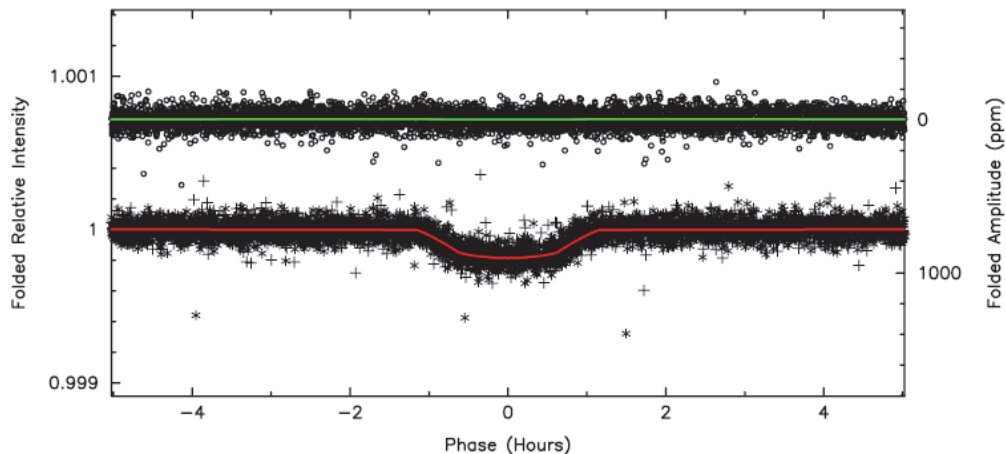


Figure 3.1: Transit light curve of Kepler-10b (Batalha et al. 2011). The planet has an orbital period of about 0.8 days and was observed by Kepler for a period over 8 months for this data set. The V magnitude of the host star is 10.96.

In summary, transiting planets combined with radial velocity measurements allow us to derive the following parameters of a planet:

- Orbit: Period, semi-major axis, orbital inclination, eccentricity, spin-orbit alignment
- Planet parameters:
 - radius, mass, density, constrain inner structure and composition
 - effective temperature, albedo, atmospheric composition (from optical light curves, and from transit spectroscopy with other observatories), surface heat distribution, and reflectivity variations from phase curves for gas giants
 - exomoons, planetary rings, Trojan objects

3.1.2 Asteroseismology

Asteroseismology is the study of the intrinsic oscillations (e.g. normal modes) of stars (Aerts et al. 2010). The oscillations generate small amplitude variations of the light curves which are analysed in Fourier space. Modes of stellar oscillations can be described by spherical harmonics $Y_{\ell,m}(\theta,\varphi)$ as functions of position (θ,φ) on the stellar surface. The eigenfrequencies $\nu_{n,\ell,m}$ are described by the three quantum numbers (n,ℓ,m) , where n is the radial order, ℓ the latitudinal degree, and m the azimuthal order of the spherical harmonic. Unlike for the Sun, the stellar disk cannot be resolved and the signal from modes of higher degree is strongly suppressed by averaging the disk. As in CoRoT and *Kepler*, measurements of modes with ℓ values up to at least 3 are expected for PLATO targets. For a spherical star, there is no dependence on the azimuthal order m ; but this degeneracy is broken by rotation and/or magnetic fields. For slow rotation, the frequencies are $\nu_{n,\ell,m} = \nu_{n,\ell} + m \langle \Omega \rangle$, where m belongs to $\{-\ell, \ell\}$, and $\langle \Omega \rangle$ is a weighted average of the interior rotation depending on the internal structure of the star and the particular eigenmode. This can be used to probe the internal angular velocity of the star (e.g. Beck et al. 2012; Mosser et al. 2012b).

The oscillation frequencies, including the rotational splitting, are found by fitting peaks in the power spectrum of the light curve. Determining frequencies of modes with $\ell = 0, 1, 2, 3$ with the solar data can be achieved, with estimated errors $< 0.1 \mu\text{Hz}$. For the 137 day run on the CoRoT target HD 49385, we extracted frequencies with errors $\sim 0.3 \mu\text{Hz}$. Appourchaux et al. (2012) extracted frequencies of 61 main-sequence and subgiant stars *Kepler* observations. The 1-sigma errors ranged from $0.1 \mu\text{Hz}$ to $0.4 \mu\text{Hz}$ depending on the magnitude and the spectral type of the star. Silva Aguirre et al. (2015) analysed data on individual frequencies for 33 stars observed by *Kepler* to be (potential) planet hosts. The baseline of the observations was long enough that the uncertainties of individual frequencies were about $0.3 \mu\text{Hz}$ for frequencies close to ν_{max} (and down to $0.1 \mu\text{Hz}$ in the best cases). The goal to be performed with PLATO is to achieve precisions of about $0.1 \mu\text{Hz}$ for thousands of stars.

The power spectra show characteristic spacings between the peaks. These are usually described in terms of separations, such as the large separations $\Delta\nu = \nu_{n,\ell} - \nu_{n-1,\ell}$ between modes of the same degree ℓ and adjacent n values and the small separations, e.g. $\delta_{02} = \nu_{n,0} - \nu_{n-1,2}$ between the narrowly separated peaks corresponding to modes $\ell = 0, 2$. Additionally we have the small separations $\delta_{01} = \nu_{n,0} - (\nu_{n-1,1} + \nu_{n,1})/2$. These are particularly valuable when only modes of degree $\ell = 0, 1$ can be reliably determined. The separations provide diagnostic information on the stellar internal structure near the core and hence information on the age of the star. The large separations provide a measurement of the star’s acoustic radius, i.e., the travel time of a sound wave from the stellar centre to the surface, which is related to the stellar mean density $\sim M/R^3$, while the small separations such as δ_{01}, δ_{02} give diagnostics of the interior structure. Periodic modulations in the frequencies or separations give diagnostics of the location of the boundaries of envelopes, of convective cores, and the extension of nucleary processed regions with a direct impact on the ages, as well as properties of the helium ionisation zone and surface helium content (e.g. Verma et al. 2014a; Roxburgh 2009; Miglio et al. 2010; Mazumdar et al. 2014).

3.1.3 The radial velocity method

Ground-based radial velocity measurements of candidate planets detected by PLATO will be carried out to confirm or reject the planet detection and to determine the planet mass and the complete orbital parameters.

As a planet orbits its host, the star moves back and forth along the line-of-sight due to the gravitational influence of the planet, and the Doppler effect will thus alternately blue- and red-shift the spectral signatures of the star. By measuring a large number of spectral absorption lines (typically several thousand per star), it is possible to determine the position of the line centre to a precision of a few parts in a thousand, consequently providing a velocity value that nowadays can be measured with a precision better than 1 m/s. Assuming enough observations have been made, this results in a usable radial velocity curve with the same precision. The presence of an influencing body can be inferred and its $M_p \sin i$ determined (where i is the inclination of the orbital plane). Today, the Radial Velocity method enables the discovery of small planets (a few Earth masses) close to low-mass stars. The detection of an Earth orbiting a true Sun-analogue requires an increase of an order-of-magnitude in precision to be achieved by future instruments. With the ESPRESSO instrument to be installed on the VLT in 2017, we will reach 10 cm/s in 15 min for a $V = 8$ star, or 20 cm/s in 1 hour for a $V = 11$ star. These estimates demonstrate the need for bright stars and large collecting areas when considering the radial velocity follow-up of very low-mass planet candidates detected by PLATO.

3.2 Measurement plans and expected results

The scientific objectives mentioned in the beginning of Section 2 will be achieved during the nominal science operations mission by carrying out the measurements summarised in Table 3.1, where also the expected results are indicated. These are compliant with the current mission performance as shown by the stellar counts estimates given in Table 6.1, including uncertainties, and the derived planetary characterisation accuracies and yields presented in Section 7.

Table 3.1. Measurements and expected results for the PLATO mission

SCIENTIFIC OBJECTIVES	MEASUREMENTS	EXPECTED RESULTS
S1. Determine the bulk properties (mass, radius and mean density) of planets in a wide range of systems, including terrestrial planets in the habitable zones of solar-like stars	Photometry of > 15,000 solar-like stars with $V \leq 11$ and precision of 34 ppm in 1 hour. RV spectroscopy for >100 (goal: 400) planets.	A sample of >100 (goal: 400) exoplanets, characterised for their orbits, radii (accuracy better than 3%) and masses (accuracy $\sim 10\%$) over a wide range of physical sizes and mean densities, including >5 (goal: 30) (super-)Earths in the habitable zone of solar-like stars.
S2. Study how planets and planet systems evolve with age	Asteroseismology for > 5,000 stars with $V \leq 11$ and photometric precision of 34 ppm in 1 hour.	A sample of >100 (goal: 400) bright planetary host stars with accurate ages ($\sim 10\%$) and planets with accurate densities.

S3. Study the typical architectures of planetary systems	Photometry of > 245,000 stars with $V \leq 13$. RV spectroscopy for > 100 (goal: 400) planets, and mass determination from TTVs and upper mass limits.	Planet distribution of orbital parameters for > 4,000 (goal: 7,000) of planetary systems (with less accurate masses); for >100 (goal: 400) planets, with accurate masses (~10%); for a sub-set of planets, with TTV determined masses.
S4. Analyse the correlation of planetary properties and their frequencies with stellar parameters (e.g., stellar metallicity, and stellar type)	Photometry of > 15,000 stars with $V \leq 11$ and precision of 34 ppm in 1 hour; observations of 245,000 stars with $V \leq 13$; Observations of M dwarf stars and stars across the HR diagram. RV spectroscopy for > 100 (goal: 400) planets; mass determination from TTVs and upper mass limits.	Well-known stellar parameters (age accuracy ~10%) for > 5,000 stars, leading to improved stellar models. Characterised host stars of hundreds of planetary systems.
S5. Analyse the dependence of the frequency of terrestrial planets on the environment in which they formed	Photometry of > 245,000 stars with $V \leq 13$.	A sample of > 4,000 (goal: 7,000) detected planetary transits from different regions in the sky.
S6. Study the internal structure of stars and how it evolves with age	Asteroseismology for > 5,000 solar-like stars with $V \leq 11$ and photometric precision of 34 ppm in 1 hour.	A sample of > 5,000 bright stars for which asteroseismic modes can be analysed with high precision to improve stellar models (age accuracy ~10%).
S7. Identify good targets for spectroscopic measurements to investigate planetary atmospheres	Photometry of ~1,000 stars with $V \leq 8$ and precision of 34 ppm in 1 hour Photometry of 5,000 M dwarf stars with $V \leq 16$.	A sample of >10 (goal: 30) planets around bright stars and > 100 planetary transits around M dwarfs from different regions in the sky.

3.3 Top scientific requirements

Here we describe the high-level science requirements that address the science objectives described in sections 2.1 and 2.2, and summarised in Table 3.1, which are the drivers for the mission design. Complementary science goals as those explained in section 2.3 will be achieved by using the scientific capabilities specified here for the core science objectives.

The requirement ids are the same as in the Science Requirements Document, 2016.

3.3.1 Planet detection and characterisation

R-SCI-L0-01 PLATO shall detect and characterise hundreds of planets around dwarf and subgiant stars of spectral types from F5 to K7, orbiting at distances up to the stellar habitable zones.

Characterise means to determine the radius, mass, age and orbital parameters of the planet (see requirements below). Habitable zone is defined as the region around a star where liquid water can exist on a planetary surface. The stars that shall be observed to detect and characterise planets with the precision required in this section and section 3.4 will constitute the PLATO core sample.

- R-SCI-L0-03 PLATO shall provide photometric data for the detection of a planet orbiting a G0V star with an orbital period of one year.
- According to the latest estimates from Kopparapu et al. (2013), the habitable zone around a G0V star for a planet of $1 M_E$ lays between 0.75 and 1.733 au, which corresponds to periods of 0.64 and 2.2 years, respectively. The choice of 1 year is driven by reaching a compromise between the longest periods detectable and the number of stars to be observed during the mission. For later type stars, this is already covered since the orbital period of habitable planets is less than 1 year, down to a few weeks for M dwarf stars.
- R-SCI-L0-05 PLATO shall provide photometric data to determine the radius of a planet of the same size as the Earth and orbiting a G0V star of $V=10$ (goal $V=11$) with an accuracy better than 3%.
- R-SCI-L0-07 PLATO shall provide photometric data to determine the ratio of planetary-to-stellar radius with an accuracy of 2%, for a planet of the same size as the Earth orbiting a G0V star of $V=10$ (goal $V=11$).
- Typical current uncertainties for radius and mass determinations of small planets are around $\pm 6\%$ and $\pm 20\%$, respectively, leading to uncertainties of 30 to 50% in mean density. The observational accuracy envisaged for PLATO will reduce the uncertainty in mean density to about 10%.
- R-SCI-L0-10 PLATO shall provide photometric data to enable the determination of the stellar ages of the core sample planets defined in R-SCI-L0-01.
- R-SCI-L0-12 PLATO shall determine the age of a G0V star of $V=10$ (goal $V=11$) with an accuracy of 10%.
- R-SCI-L0-15 PLATO shall observe stars that are bright enough to allow for a determination through radial velocity measurements of the mass of a terrestrial planet orbiting a G0V star with an accuracy of 10% or better.
- “Terrestrial planet” is defined as having $R < 2 R_E$ and $M < 10 M_E$.
- In requirements R-SCI-L0-05, -07, -12, -55 and -57, accuracies are specified for $V=10$, defining a sample of bright stars for which asteroseismology and the radial velocity follow-up may be carried out comfortably within the current expectations. To improve significantly the science return, however, the goal is set to $V=11$, which increases by a factor of ~ 2 the sample of stars and possible planets whose masses, radii and ages can still be accurately determined, although possibly with lower precision.
- R-SCI-L0-25 PLATO shall detect planets orbiting at distances up to the star habitable zone in a large sample of dwarf and subgiant stars ($> 100,000$) of spectral types from F5 to K7.
- The characterisation of these planets may be possible, but with less accuracy than in the core sample. The aim is to provide enough detections for statistical studies of planetary systems properties.
- R-SCI-L0-35 PLATO shall detect terrestrial planets which orbit M dwarf stars at distances that include the star habitable zone.
- R-SCI-L0-40 PLATO shall be able to observe between 10 and 50% of the sky to allow for statistical studies of planetary formation under various conditions (e.g. clusters).
- The PLATO observing strategy and the amount of sky coverage may be subject to modification pending future developments and scientific priorities in the field.
- R-SCI-L0-45 PLATO shall detect and characterise terrestrial planets in orbit around very bright ($V < 8$) dwarf and subgiant stars of spectral types from F5 to K7 at distances up to the stellar habitable zones. The characterisation requirements are the same as for the core sample (R-SCI-L0-05, -10, -12, -15).

These planets will be the main targets for detailed follow-up and atmospheric spectroscopic characterisation.

3.3.2 Stellar science

R-SCI-L0-55 PLATO shall provide photometric data to determine the radius of a G0V star of $V=10$ (goal $V=11$) with a precision of 1–2%.

This requirement is directly derived from R-SCI-L0-05 and R-SCI-L0-07. In order to meet R-SCI-L0-05, and given R-SCI-L0-07, the radius of the star needs to be determined with the precision specified here.

R-SCI-L0-57 PLATO shall provide photometric data to determine the mass of a G0V star of $V=10$ (goal $V=11$) with a precision of 15%.

Planet mass uncertainty scales as $M_{star}^{2/3}$. Accordingly, the requirement of 10% accuracy for the planet mass imposes 15% accuracy for the mass of the host star.

R-SCI-L0-60 PLATO shall provide photometric data to enable the measurement of frequencies of normal oscillation modes in main-sequence stars with precisions $\sim 0.1 \mu\text{Hz}$ for several mode frequencies below and above the frequency of the mode with the maximum amplitude.

PLATO must be able to measure modes with sufficient precision to allow separating solar-like oscillations.

R-SCI-L0-65 PLATO shall be able to observe between 10 and 50% of the sky to allow for asteroseismology analysis of several thousands of stars at different stages of their evolution and different locations in the sky.

The PLATO observing strategy and the amount of sky coverage may be subject to modification pending future developments and scientific priorities in the field.

R-SCI-L0-67 For asteroseismology measurements, the duration of the observations shall be at least two months.

For the asteroseismic analysis of the target stars, the total monitoring time must be sufficient since it translates directly into a relative precision for the measurement of individual mode frequencies. Based on CoRoT short-runs a duration of ~ 2 months is considered a minimum for good asteroseismology data. For solar-like stars an absolute precision of 0.2 to 0.1 μHz is desirable, which translates into a monitoring time of 5 months for a reasonable SNR of 10 in the power spectrum.

3.4 Derived scientific requirements

These requirements provide the specification of the mission capabilities, and are derived from the high-level science requirements given in section 3.3.

3.4.1 Fields

R-SCI-035 The capability shall be provided to carry out two phases during nominal science operations:

- A Long-Duration Observation Phase of at least two years (LOP)
- A Step-and-stare Observation Phase (SOP)

The Long-Duration Observation Phase is required for the detection of planets with periods long enough to orbit in the habitable zone of solar-type stars. The Step-and-stare Observation Phase is intended to include (i) repointings of the spacecraft to observe more transits of long-period Earth-like planets detected in the Long-Duration Observation Phase; (ii) observations

of large numbers of targets in different areas of the sky to satisfy the Level-0 requirements R-SCI-L0-40, -45 and -65.

R-SCI-037 The in-orbit nominal science operations duration shall be four years.

R-SCI-045 During a Long-Duration Observation Phase it shall be possible to observe one field for up to 4 years.

The minimum duration of the LOP observations is 2 years, so that at least 2 consecutive transits for Sun-Earth analogues can be detected. For the P1 sample (< 34 ppm in 1 hour), the SNR of a single transit for an Earth-Sun analogue is 9 and 13 when integrating 2 transits. It is generally considered that a $\text{SNR} > 10$ guarantees the detectability of 100% of the transit signals (see Fressin et al. 2013, based on studies by Jenkins et al. 1996, 2010). A third transit event is beneficial to confirm the consistency of previous observations.

The requirements are defined in this way to allow for flexibility in the definition of the observation strategy, such that it can be adapted to the scientific priorities in exoplanet science in the next decade.

For the seismic analysis of the target stars, the total monitoring time must be sufficient to yield a relative precision of 10^{-4} for the measurement of individual mode frequencies, which is needed to extract valuable stellar modelling information from the oscillation frequencies. For solar-type stars, this comes down to an absolute precision of 0.2 to 0.1 μHz , which translates into a minimum monitoring time of 5 months for a reasonable SNR of 10 in the power spectrum needed to achieve the envisioned mass, radius, and age precision of the core sample stars.

R-SCI-060 During a Step-and-stare Observation Phase, it shall be possible to observe between 6 and 3 fields for between 2 and 5 months, when feasible due to the position of the Sun.

Experience with CoRoT and *Kepler* has shown that two months is the shortest time base required to perform useful asteroseismology modelling of various types of stars.

3.4.2 Stellar samples

3.4.2.1 Stellar samples specifications

In order to achieve the science requirements, four stellar samples have been defined for the PLATO observations. The definition of each star sample is displayed in Table 3.2. Sample 1 (P1) is the backbone of the PLATO mission and must be considered as the highest priority objective. It consists of dwarfs and subgiants with spectral types from F5 to K7 and magnitudes down to $V=11$, observed with a maximum random noise (or random Noise-to-signal ratio, NSR) of 34 ppm in one hour. Ground-based radial velocity follow-up will be most effective for these stars.

Sample 2 (P2) consist of stars brighter than $V = 8.2$, with the same spectral types and maximum random noise as sample 1, observed over long time periods. Observing very bright stars will provide new significant facts about the physics of a large number of different stellar classes. Furthermore, the detection of a number of short period planets around such bright stars will also be used as input for observatories aimed at characterising exo-planetary atmospheres. In this regards, the E-ELT first light is targeted for 2024. In addition, JWST would be in its extended mission operations, which could continue until ~ 2028 (the JWST mission lifetime after launch will be between 5.5 years and 10 years).

The P4 sample is composed of nearby M dwarfs. These stars are cool enough that their habitable zone is relatively close-in, therefore planets in the habitable zone have orbital periods of just a few weeks.

Finally, the fifth sample (P5) is derived from the requirement to observe an even higher number of stars and obtain statistical information on planet occurrence and system properties.

Table 3.2: Requirements of the PLATO stellar samples

	Sample 1 (P1)	Sample 2 (P2) ⁵	Sample 4 (P4)	Sample 5 (P5)
Stars	≥ 15 000 (goal 20 000)	≥ 1000	≥ 5000	≥ 245 000
Spectral type	Dwarf and subgiants F5-K7	Dwarf and subgiants F5-K7	M dwarfs	Dwarf and subgiants F5-K7
Limit <i>V</i>	11	8.2	16	13
Random noise (ppm in 1 hour)	34	34	800	
Observation phase	LOP	LOP	LOP	LOP
Sampling time (s)				
Initial measurement	-	-	-	≤ 600
Centroid measurements	-	-	-	≤ 50 for 5% of targets
Transit oversampling			-	≤ 50 for 10% of targets
Imagettes	25	2.5	25	25 for > 9000 targets
Wavelength	500–1000 nm	500–1000 nm 300 stars with colour information	500–1000 nm	500–1000 nm

3.4.2.2 Random noise

The random noise in the light curves of P1 and P2 has been specified as less than or equal to 34 ppm in 1 hour, with the constraint that for a star of $V=11$ it shall be dominated by the photonic noise. In addition, the residual error in the light curves related to systematic effects, after all corrections are applied, shall remain below one third of the random noise associated with a star of $V=11$. These requirements ensure that for the stars in samples P1 and P2, the dominating noise contribution is the stellar photonic noise.

The random noise specification is driven by (a) asteroseismology measurements that provide the accurate radius, mass and age of the host star; (b) the accuracy of the radius determination for terrestrial planets. In addition, this value of the random noise practically eliminates the possibility of spurious detections, and enables the detection of Transit Time Variations (TTVs) and Transit Duration Variations (TDVs).

- a) Results from CoRoT and *Kepler* have shown that detecting, measuring and identifying oscillation modes in solar type stars requires a noise level in amplitude Fourier space below about 2.0 ppm per $(\mu\text{Hz})^{1/2}$ (Michel et al. 2008; Deheuvels et al. 2010; García-Hernández et al. 2009; Ballot et al. 2011), which is equivalent to 3.2 ppm in 5 days, or 1.3 ppm in 1 month. This translates into a noise level of approximately $3.4 \cdot 10^{-5}$ in 1 hour.
- b) This requirement on the maximum random noise is also linked to the detection and characterisation of Earth-like planets. The depth of a planetary transit is given by the ratio of the areas of the planet and its transited star, which is $\Delta F_{\text{star}}/F_{\text{star}} \cong (R_{\text{planet}}/R_{\text{star}})^2 \cong 8.4 \cdot 10^{-5}$ in the case of a star with $1 R_{\odot}$ radius and a planet with $1 R_{\text{E}}$ radius. For a planet at a distance of 1 au from the star, the transit duration would be typically of the order of 13 hours. (The duration Δt_{tr} of a transit of a planet with semi-major axis a and orbital period P in front of a star with radius R_{star} is given by $\Delta t_{\text{tr}} = P R_{\text{star}}/(a/\pi)$. For true Earth analogues $\Delta t_{\text{tr}} = 13$ hours.)

⁵ Sample P3 has been removed from the requirements.

In order to detect such transits at around 4σ , a dimensioning requirement, we need to obtain a photometric noise level lower than about $3 \cdot 10^{-5}$ in 13 hours, i.e. about $8 \cdot 10^{-5}$ in one hour. This is the minimum requirement for the detection of an Earth-like planet in front of a solar-like star. But PLATO also aims at accurately characterising these planets. To achieve an accuracy of the planetary-to-stellar radius better than 2% for a $V=10$ solar type star and an Earth size planet (R-SCI-L0-07), simulations have shown that a random noise level of $2.8 \cdot 10^{-5}$ in one hour is required when three transits are observed. This translates into a noise level of $3.4 \cdot 10^{-5}$ for $V \cong 11$ star, assuming the current PLATO configuration. For a larger random noise, the uncertainty in the planetary-to-stellar radius determination of terrestrial planets increases as much as $\sim 9\%$ for a random noise of 80 ppm in one hour.

Additionally, a value of the random noise of 34 ppm in one hour will allow us to reduce the number of spurious detections, such that 100% of the transits of Earth-sized planets can be detected. With an accuracy of 80 ppm in one hour, the detection rate decreases to 50%.

A random noise of 34 ppm in one hour will also enable us to measure the transit depth with sufficient SNR ratio at several points during the transit, particularly during the ingress and egress, even for terrestrial planets. This is essential for the detection of Transit Time Variations (TTV) in multiplanet systems, that indicate the presence of non-transiting planets and from which the planetary masses can be derived. It is also necessary for the measurement of Transit Duration Variation (TDV) produced by exomoons. The fitting of the ingress and egress portions of the light curve dominate the accuracy of the TTV and TDV measurements. The random noise of PLATO combined with the short exposure times, will allow us to determine the mass of planets through TTVs with a 10% accuracy.

3.4.2.3 *Imagettes and sampling time*

For stars in samples P1 and P4, and for a subset of samples P2 and P5, imagettes shall be downloaded for their processing and the generation of light curves and centroids with the ground segment pipeline. For the remaining stars in sample 5, the processing of light curves and centroids shall be done on-board.

The main data products of CoRoT are N2-level light curves (Baudin et al. 2006, Ollivier et al. 2016). These light curves integrated the flux of all pixels within a given mask at every exposure time. The integration process was done on board and the pixel information was not transmitted to ground as a rule. However, for the bright star (sismo) channel and for a limited number of targets in the faint star (exo) channel, CoRoT downloaded time series of flux values for each pixel inside the aperture defined around the target star. This piece of information is called “imagette” (Samadi et al. 2006). The typical size for a CoRoT bright (sismo) imagette is 35×35 pixels and for a faint (exo) imagette 10×15 pixels. A CoRoT “imagette” is the same kind of data product as a *Kepler* “postage stamp”, the difference is only the use of a different terminology.

Obtaining imagettes for all stars in P1 will allow us to derive the PSF at different positions of the detector, increase our capability to sample variations over the focal plane of each telescope and over the full field of PLATO, and therefore improve the accuracy of the PSFs determination and jitter correction. This will enable:

- The verification of the data reduction pipeline performance over a large sample of stars per camera, therefore allowing us to improve the data processing in particular for the detection of the smallest transits.
- To increase the level of confidence in the planetary nature of candidates through a much better quality of the light curve and of the centroid. This robust filtering of candidates will ensure the most efficient use of follow-up observations.
- A continuous improvement of the pipeline in charge of the data processing during and after operations, with the capability to apply the improvements to the data of past and future observations.

Imagettes will also provide accurate spatial information that will allow us to identify false positives due, e.g., to a background eclipsing binary.

Because individual transits have durations longer than 2 hours, a time sampling of about 10 to 15 minutes is in principle sufficient to detect all types of transits, as well as to measure transit durations and periods. However, a higher time resolution is needed to sample sufficiently the ingress and egress of the planet transit. Studies have shown that a high temporal sampling of ingress and egress of the transit light curve is needed to derive accurate planet parameters, in particular for long-period planets. For TTV analysis, the

accurate timing will allow us to detect the presence of an additional planet which cause e.g. offset and to derive the precise shape of the transit which, evaluated against eclipsing binaries signatures, will allow us to solve ambiguities on the nature of the detected transiting body. In practice, a time sampling of about 50 sec will be necessary to analyse in such detail the detected transits.

The needed time sampling for the asteroseismology objectives can be derived directly from the frequency interval we need to explore, which is from 0.02 to 20 mHz. In order to reach 20 mHz, the time sampling must correspond to at least twice this frequency, and therefore the specification has been set to 25 seconds.

3.4.3 Wavelength and colour information

R-SCI-290 The payload shall provide high precision photometric time series in the wavelength band of 500 nm to 1000 nm.

R-SCI-L0-70 PLATO shall provide two colour information for the brightest stars ($V < 8$).

Colour information is useful for planet validation, planetary atmospheres studies, and complementary science. In particular, colour information will allow us to break degeneracies in asteroseismology models of pulsators with a convective core experiencing heat-driven coherent oscillation modes.

Various topics within PLATO Complementary Science benefit greatly from colour information. As an example, having light curves in two instead of one colour not only improves the modeling of eclipsing binaries, but also allows to determine the degree of the dominant pulsation modes of heat-driven O to F-type pulsators across the HR diagramme and thus perform asteroseismic (and if applicable binary) modelling. In addition, having light curves in two colours allows us to distinguish between pulsational and differential rotational variability, because the dependence of the pulsation signal on wavelength is different from the wavelength dependence of differential rotation or spots. This is particularly valuable for stars in their formation process. Other science cases that require two colours are connected with transient phenomena in cataclysmic variables or neutron-star/black-hole compact binaries.

The bandwidth of the filters shall be chosen wide enough to allow for precise white-light photometry of stars too bright to be accurately observed by the normal cameras.

3.4.4 Observation gaps

“Gaps” are defined as time during which science observations are suspended while other spacecraft operations are performed.

R-SCI-400 During nominal science operations, gaps shall represent less than 7% of the total observing time per target during one year.

It is desirable that gaps represent less than 5% of the total observing time per target during one month.

The probability that N successive transits of the same planet are observed is given by $p_N = d_f^N$, where d_f is the fractional duty cycle of the instrument. In order to achieve an 80% probability that all transits of a three transit sequence are observed, a duty cycle of 93% is needed. The requirement for planet-finding is therefore that gaps do not occur over more than 7% of the time in one year, with a loss by gaps as small as 5% in one month being desirable.

R-SCI-410 The amplitude of the first side lobe of the power spectrum response function of the observation time series shall be less than 1% of the main peak. This first side lobe shall be separated by at least 70 μ Hz from that main peak.

Periodic gaps produce aliases (1st order side lobes) around the peaks of interest for asteroseismology analysis.

This requirement is imposed for asteroseismology. Gaps in the data produce side lobes in the power spectrum, which make oscillation mode identification ambiguous. Periodic gaps in the data must be minimised, as they will produce the most severe side lobes in the power spectra.

3.5 The need to go to space

The science goals of PLATO require the detection and characterisation of a very large number of planetary transits, as well as the seismic analysis of their host stars. As explained above, this requires very high precision, very long duration and high duty cycle photometric monitoring, which cannot be done from the ground. The Earth's atmosphere causes indeed strong disturbances that limit the achievable performance to milli-magnitude accuracies, mostly through scintillation noise. The small amplitude of the photometric dips caused by terrestrial planets is therefore beyond the range of ground-based observations.

Alternative techniques can be used from the ground to detect new exoplanets, and this field has seen tremendous progress in recent years. The most efficient of these relies on radial velocity measurements, performed by high resolution spectroscopy. The most severe drawback of the radial velocity technique is that the resulting mass determination suffers from the $\sin i$ ambiguity, except in the rare cases where the inclination angle i can be estimated. Photometric transit techniques are the only ones that can overcome this difficulty. In addition, long, uninterrupted observations, that only space-based instruments can provide, are necessary to optimise the probability of transit detection, as well as to avoid side lobes in stellar oscillation power spectra. Achieving a high duty cycle ($\geq 93\%$) is very difficult from ground, even if a network of multiple telescopes, or a powerful observatory in Antarctica, would be available. Space is therefore necessary to achieve the goals of PLATO, on one hand because of its stability and the absence of photometric disturbances, and on the other hand because it offers the possibility to perform the long, uninterrupted observations that are needed to detect and bulk characterise exoplanets and to perform seismic analysis of their host stars.

Page intentionally left blank

4 Payload

The PLATO Payload comprises the cameras including focal planes and related electronics as well as the on-board data processing system. The PLATO Payload (provided by the PLATO Mission Consortium) plus the optical bench on which the cameras are mounted (provided by ESA), constitute the PLATO *Payload Module*.

During most of the Definition phase, the payload configuration consisted of 28 or 32 normal and 2 fast cameras, which evolved to 24 normal and 2 fast cameras as a result of the Mission Adoption Review recommendations and final mission cost assessment. Because of this development, this chapter still includes some figures of the design with 28+2 cameras.

4.1 Basic instrument overview

The instrument concept is based on a multi-telescope approach, involving a set of 24 “normal” cameras working at a cadence of 25 s and monitoring stars fainter than $V = 8$, plus two “fast” cameras working at a cadence of 2.5 s, and observing stars in the V range from 4 to 8.

A camera includes a Telescope Optical Unit (TOU), a Focal Plane Assembly (FPA), which supports four CCD detectors, the Front End Electronics (FEE) box, the FEE Support Structure (FSS), and related thermal equipment. The TOUs are based on a fully dioptric telescope including 6 lenses.

Each camera is equipped with its own, passively cooled FPA, comprised of 4 CCDs with 4510×4510 pixels each, working in full frame mode for the “normal” cameras, and in frame transfer mode for the “fast” cameras. This results in 1037 deg^2 effective field-of-view for the “normal” cameras and 619 deg^2 field of view for each of the two “fast” cameras.

Besides providing star brightness measurements for bright stars, the “fast” cameras also work as fine guidance sensors for the attitude control system of the Spacecraft. In addition they allow measurements of stars in two spectral bands. For this purpose one of the “fast” cameras is equipped with a blue, the other one with a red bandpass filter.

The 24 “normal” cameras are arranged in 4 groups of 6 cameras (Figure 4.1). All 6 cameras of each group have exactly the same field-of-view. However, the lines of sight of the four groups are offset by an angle of 9.2° from the PLM +Z axis. This particular configuration allows us to survey a total field of about 2232 deg^2 per pointing, with various parts of the field monitored by 24, 18, 12 or 6 cameras. This strategy optimises both the number of targets observed at a given noise level and their brightness. The satellite will be rotated around the mean line of sight by 90° every 3 months, resulting in a continuous survey of exactly the same region of the sky.

At the beginning of each pointing full images will be transferred to ground to serve deriving the PSF at each target position. To reduce the high data volume produced on-board during operation, each assigned target star will be allocated a CCD window around it from which all the pixel values will be gathered, forming a small image called an “imchette”. The size of this window is typically 6×6 pixels (9×9 pixels for the fast cameras), large enough to contain the whole image of the target star. These imchettes will either be sent as raw data to ground or processed on-board to get centroids and light curves to further reduce the telemetry data volume. The raw imchettes are used on ground to derive the PSF at different positions of the detector, a step which is needed to verify the quality of the photometric and centroiding data. For calibration purposes and to define imchette positions after re-pointings, also full frame images will be transmitted to ground.

There is one Data Processing Unit (DPU) per two “normal” cameras performing the basic photometric tasks and delivering a set of light curves, centroid curves and imchettes to a central Instrument Control Unit (ICU), which stacks and compresses the data, then transmits them to the SVM for downlink. Data from all individual cameras are read-out every 25 s and transmitted to the ground, where final instrumental corrections, and e.g. jitter correction, are performed. The DPUs of the fast cameras will also deliver a pointing/attitude error signal to the AOCS, at a cadence of 2.5 s.

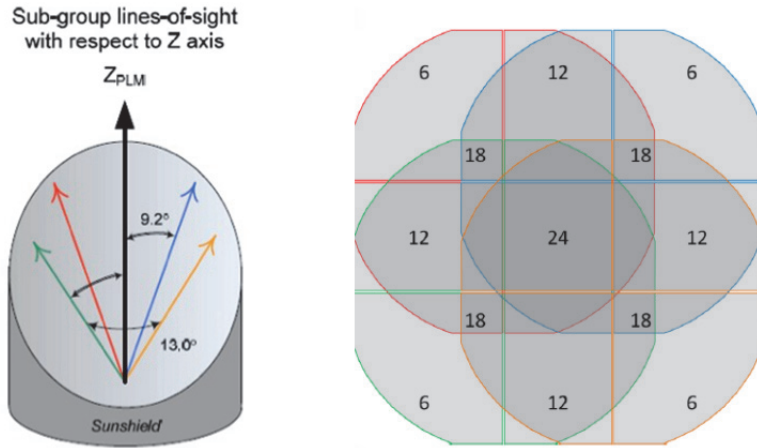


Figure 4.1: The overlapping line-of-sight concept (left) and the resulting field-of-view configuration (right).

Each DPU of the “normal” cameras (N-DPU) is associated with two FEEs. They are grouped together in a Main Electronics Unit (MEU). There are 2 MEUs containing 14 N-DPUs for the 28 normal cameras, each one including its own power supply electronics.

The fast DPUs (F-DPU) are functionally associated to the fast FEE. There are 2 F-DPUs, one per fast FEE, grouped in one box called Fast Electronics Unit (FEU), also including its power supply.

Cameras receive their power from the Ancillary Electronics Units (AEUs), one AEU per fourteen “normal” cameras and one AEU for both “fast” cameras. The AEUs also provide synchronisation signals for data acquisition and cameras thermal control. The payload is controlled by two ICUs used in cold redundancy.

The two ICUs are grouped in a single box with their own power supply. In addition, the instrument includes on-board software, operating on the DPUs and ICUs, which can be modified during the flight. See Figure 4.2 for an overview on the on-board data treatment architecture. Table 4.1 provides an overview of the Payload.

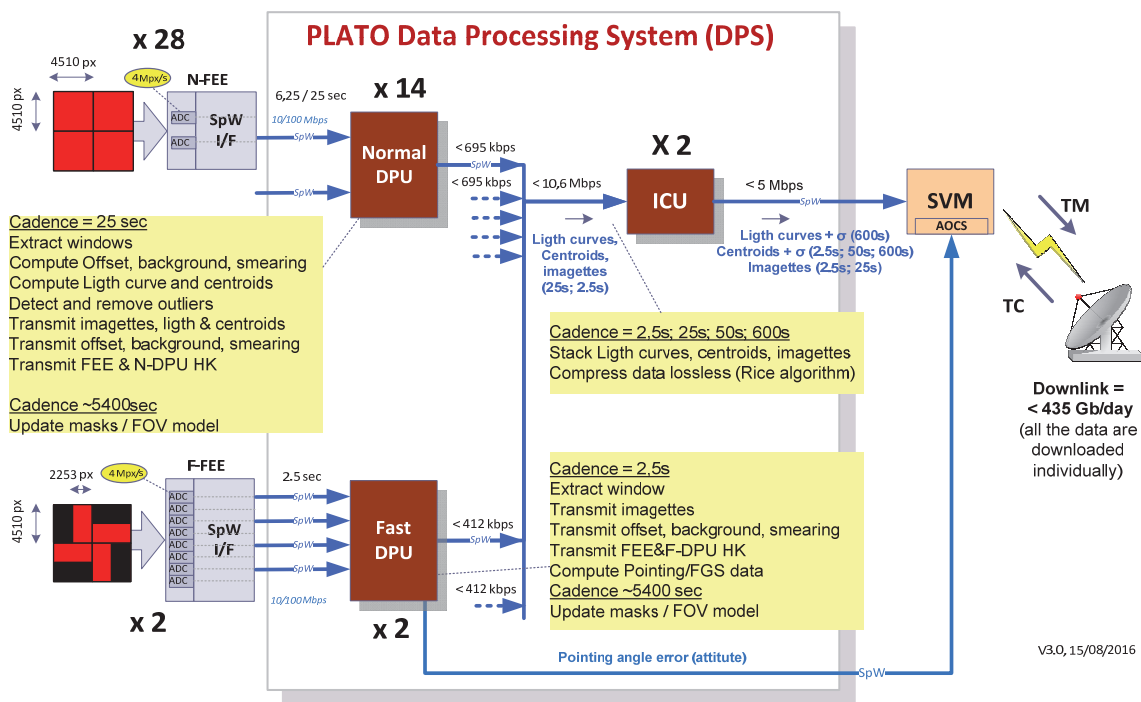


Figure 4.2: The PLATO on-board data treatment architecture.

Table 4.1: Summary of the payload.

Characteristics	Value	Comments
Camera Level		
Optics	Full refractive design with 6 lenses and 1 entrance window	Axisymmetric design
Optics spectral range	500 – 1000 nm	
Pupil diameter	120.0 mm	For one telescope
Camera focal plane layout	4 CCDs in a square	
Normal camera detectors	Full frame CCDs 4510 × 4510 light sensitive, 18 μm square pixels	e2v CCD 270
Fast camera detectors	Frame transfer CCDs 4510 × 2255 18 μm square pixels	e2v CCD 270
Normal camera field of view	~ 1037 deg ² ~ circular, diameter 37.8°	For each telescope
Fast camera field of view	~ 619 deg ²	For each telescope. Only 50% of the focal plane light sensitive due to selection of frame transfer CCDs
Plate scale	15.0 arcsec / px	For both normal and fast telescope
PSF surface	Always included within 9 px	
CCD temperature	< - 65°C	By passive cooling
Read-out frequency	3 Mpx/s	
Normal camera CCD cycle period	25.0 s fixed	
Fast camera CCD cycle period	2.5 s fixed	
Normal camera exposure time	~ 22.0 s fixed	+ a shorter exposure time for on-ground, at room temperature, tests
Fast camera exposure time	~ 2.3 s fixed	
Payload Level		
Number of telescopes	24 Normal + 2 Fast	
Payload field-of-view	Overlapping FoV of 2232 deg ²	24 cameras looking on 301 deg ² 18 cameras looking on 247 deg ² 12 cameras looking on 735 deg ² 6 cameras looking on 949 deg ²
Power needed by payload	~ 820 W	
Mass of the payload	533 kg	

Characteristics	Value	Comments
Electronics	<p><u>N-chain</u> 1 × N-FEE / camera 1 × N-DPU / 2 cameras 2 × MEU with 12 NDPUs+PSU 1 × N-AEU/ 12 N-FEEs</p> <p><u>F-chain</u> 1 × F-FEE / camera 2 × F-DPU / 2 cameras 1 × FEU with 2 × F-DPU/PSU 1 × F-AEU/ 2 fast cameras</p> <p>2 × ICUs in cold redundancy</p>	FEE and CCD activities are fully synchronised

4.2 Cameras

Each of the 24 normal (see Figure 4.3) and 2 fast cameras includes:

- the Telescope comprised of
 - the Telescope Optical Unit (N-TOU and F-TOU)
 - the Focal Plane Assembly (FPA) holding 4 CCD detectors
- the Front End Electronics (N-FEE for N-CAM and F-FEE for F-CAM).

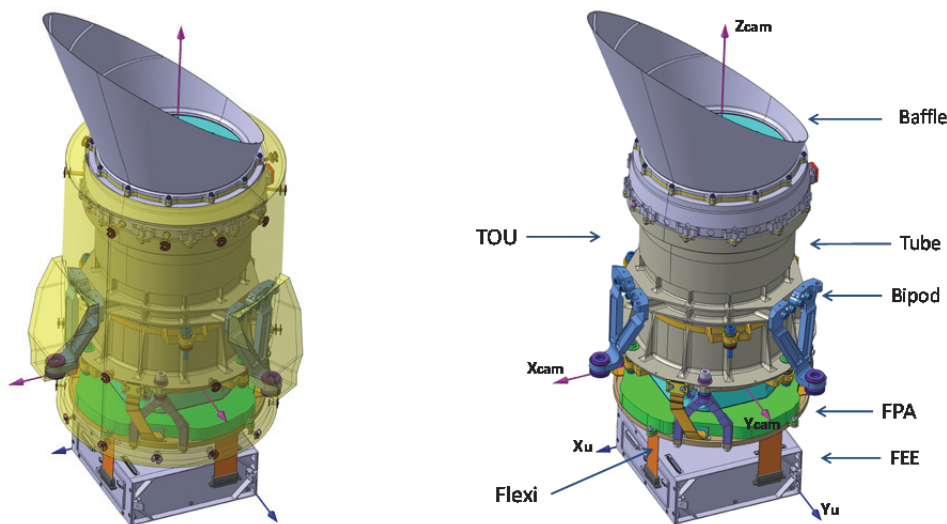


Figure 4.3: Camera views (without FSS). Left: with MLI structure around telescope. Right: without MLI. The heaters (not shown) will be attached to the TOU tube above bipods interfaces. The flexi cables are not connected to FEE in this figure. In reality they are plugged-into connectors on the top of FEE box.

The design of normal and fast cameras is very much the same except for:

- read-out in frame-transfer mode
- design of FEEs

- availability of bandpass interference filters in F-CAM: shorter wavelength bandpass in “blue” camera and longer wavelength bandpass in “red” camera. The filters are needed to allow measurements of stars in two spectral bands.

The following sub-sections provide more details on the individual camera subsystems.

4.2.1 Telescope Optical Unit (TOU)

There is no general difference in the TOU design for normal and fast telescopes, but the latter will include filters in form of special coatings on an optical surface of the optical train. The optical configuration consists of 6 lenses, plus one window, placed at the entrance of the telescope, providing protection against radiation and thermal shocks. The first surface of the first lens contains even aspherical terms (K, a4, a6), while the second surface is flat in order to facilitate the interferometric surface measure during the aspheric manufacturing. All the other lenses are standard spherical surfaces. The first surface of the third lens is the optical system stop and guarantees a real entrance pupil diameter of 120 mm. This configuration provides a corrected field-of-view up to 18.9° accepting slightly degraded image quality, as well as a ~14% vignetting, in this small region at the edge of the field. A layout of the design is shown in Figure 4.4 and the general performance and parameters of the baseline optical configuration are summarised in Table 4.2.

The TOU main structure consists of a machined tube with all the interface planes, threads and holes necessary to mount the other components. The heat dissipated by the CCD needs to be transported through the TOU structure, which therefore must be made of material with high thermal conductivity. In addition, the large temperature difference between integration and operation requires a design able to accommodate the dimensional changes of the assembled components without leading to unacceptable mechanical stresses. The TOU is quasi-static mounted to the Camera Support Structure with three bipods.

Table 4.2: Camera parameters

Spectral range	500 – 1000 nm
Entrance Pupil Diameter	120 mm
Working f/#	2.06 @ 700 nm
Field of View	~ 1037 deg ²
Image quality	90% enclosed energy within 2.5 × 2.5 pixel ² for 95% of nominal camera FoV
Maximum Field Distortion	3.84%
Plate scale	15 arcsec/pixel
Working Temperature	–80°C

The thermal design of the TOUs is such that the mean temperature at TRP1 is –95° with the heater switched off. During science observations the heater is switched on and provides the nominal operation temperature of TRP1 at –80°C. The CCDs, mounted in FPA, are approximately 5° warmer, i.e. are at –65°C. The TOU heaters are used not only for active temperature control but also for camera focusing. A 1° change corresponds to approximately 10µm focus shift. Once focused to the best image plane the camera temperature must remain very stable in order to keep PSF of exactly the same size during long observation period.

Figure 4.4 below shows the TOU optical layout and view of the camera.

4.2.2 Focal Plane Assembly (FPA)

The PLATO detectors are CCDs provided by e2v, model CCD270, specifically developed for this mission. They are built with two separately connected sections to allow full frame (FF) or frame transfer (FT) readout modes. They are back-illuminated, back-thinned devices, non-inverted type, whose characteristics are summarised in Table 4.1. An antireflection coating on its sensitive surface provides for the highest quantum

efficiency over a broad wavelength range. Only one readout register with two outputs is required for both the FF and FT devices. The detectors will work at a temperature lower than -65°C to minimise dark current and radiation damage.

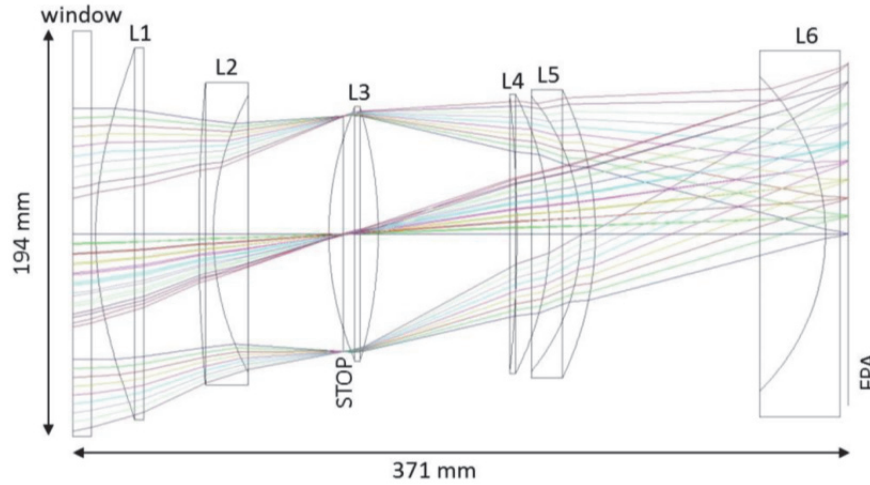


Figure 4.4: The baseline optical layout is shown together with detector position (FPA at the right side).

Each Focal Plane Assembly structure supports 4 CCDs via quasi-static mount on a support plate, ensuring a very good planarity. The support plate is made in Titanium, attached to the telescope structure by 3 bipods, also in Titanium. It has the possibility to be adjusted in position (along the optical axis and around the camera transverse axes) by using 3 shims located at the interface between the FPA bipods and the telescope structure. It is electrically isolated from the telescope, and the thermal power dissipated at FPA level is evacuated to the telescope structure by means of 3 flexible thermal straps thermally connected to the CCD packages.

Figure 4.5 shows the CCD array configuration for both normal and fast cameras, while Figure 4.6 depicts the different elements of the Focal Plane Assembly. Figure 4.7 shows some PLATO CCDs during the successful characterisation and qualification tests performed along 2015 – 2016.

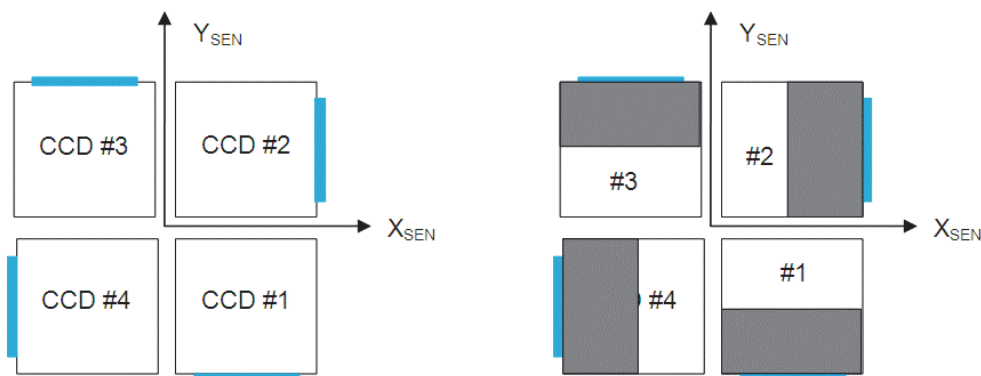


Figure 4.5: The CCD array configuration for normal cameras (left, full frame CCDs) and fast cameras (right, frame transfer devices). Blue rectangles represent the flexi-cables. The shaded area in the fast cameras CCD corresponds to the frame transfer storage area, and is aluminised to be not light sensitive.

The flexi-cables connecting each CCD to the FEE have a free length of ~ 80 mm from the bottom of the FPA to the top of the FEE. The distance between FPA and FEE is limited to a nominal value of 65 mm to get slightly bended flexi-cables allowing small misalignments, displacements or rotations between them during AIT, and launch.

Extensive analysis has been performed to guarantee the PLATO FPA performances in terms of vibration robustness, flatness, CCD temperature, while remaining within mass and power budget. Finally, integration and verification procedures for the FPA have been defined and tested using a mock-up manufactured in Al.



Figure 4.6: The Focal Plane Assembly seen from top (left) and from bottom (right). In blue the array of 4 CCDs and in green the straylight mask. FPA is supported by 3 bipods to the TOU structure. 3 thermal straps evacuate the heat. Each CCD is connected by a flexi to the FEE box.

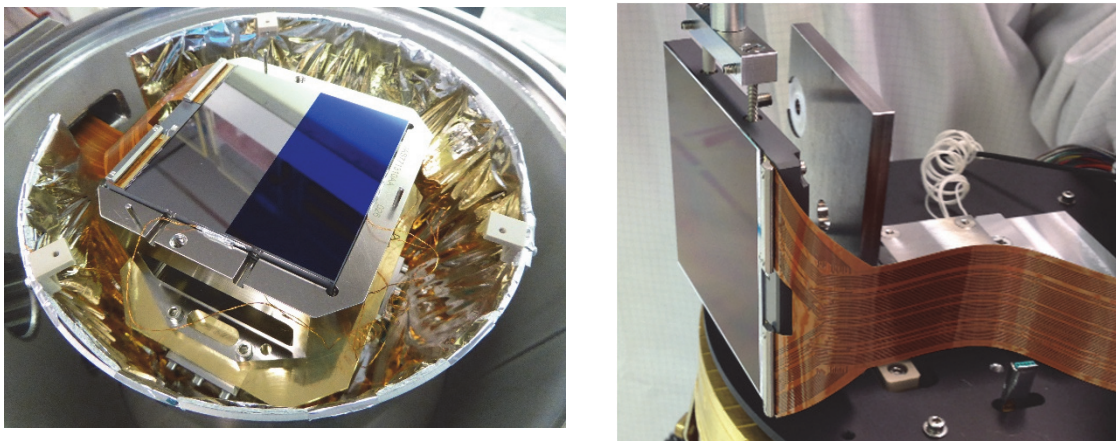


Figure 4.7: PLATO e2v-270 CCDs during characterisation/qualification tests: left, frame transfer device; right, full frame CCD.

4.2.3 Front End Electronics (FEE)

The N-FEE operates the 4 CCDs of a normal camera, digitizes the image data and transfers them to the DPU (see context in Figure 4.2). Each normal CCD has an integration time of 22.5 s and a readout time of ~2.5 s. The readouts are staggered at every 6.25 s, in equal intervals of the 25 s frame time. The readout and data transfer to the DPU are arranged such that the readout of one CCD is finished before the next begins, in order to minimise crosstalk and interference effects.

An FPGA is the core of the N-FEE, and receives command packets from the DPU and timing and synchronisation data from the AEU. It generates all the clocks necessary for driving the 4 CCDs and drives the DACs responsible for providing the bias voltages.

The interface between N-FEE and N-DPU is made by two SpaceWire links. The protocol used is RMAP in all cases, but the command interface is actually simulated RMAP with e.g. control registers, HK data, memory mapped for simple access.

The F-FEEs operate the CCDs of the two fast cameras. It has many aspects in common with the N-FEE: commanding, CCD bias supplies, clock waveforms, and housekeeping. Other aspects are significantly different due to the use of frame-transfer devices and shorter integration times: FPGA and programming, number of SpaceWire interfaces and data rate.

For the fast cameras, the 4 CCDs are read out simultaneously every 2.5 s. Due to less critical noise requirements, the F-FEE uses an integrated analogue front-end (AFE) electronics, instead of the non-integrated 16-bit AFE used by N-FEE. As for the N-FEE, synchronisation of the two cameras is ensured by receiving from the associated F-AEU a high frequency signal (50 MHz) and a signal giving the information of the 2.5 s period beginning, also synchronised with the 25.0 s period of the normal cameras.

4.2.4 Ancillary Electrical Units (AEU)

The AEU's have the following main functions:

- To supply secondary power to the Front End Electronics (FEE) of each camera.
- To synchronise the various sub-systems: Cameras, AEU's internal power converters and camera heating.

The instrument includes two different types of ancillary electrical units. The F-AEU is connected to the two fast cameras and each of the two N-AEU's is connected to 12 normal cameras. They are located in the Service Module of the satellite and are controlled by the Instrument Control Unit (ICU).

The cameras are supplied with secondary power from the AEU's as follows:

- 2 normal-AEU boxes, one for 12 normal cameras. Each N-AEU box will contain 12 independent DC/DC converters to supply the connected N-FEE's.
- One Fast-AEU box which will supply secondary power to the two Fast-FEE's, and includes a Master Synchronization Module (MSM).

The synchronisation signals are generated in two master synchronisation modules (MSM) inside the F-AEU operating in cold redundancy. The synchronisation signals are distributed from there to the Camera FEE's, the AEU's internal power converters and to the camera heater control inside the Service Module.

4.3 On-board Data Processing subsystem (DPS)

4.3.1 Main Electronics Unit (MEU) and Data Processing Units (N-DPU)

Each Main Electronics Unit (MEU) gathers in the same box (see Figure 4.8 for the MEU architecture and Figure 4.2 for a DPS overview):

- 6 N-DPU boards: each N-DPU board is responsible for handling two normal cameras.
- 2 SpaceWire routers: one main and one redundant.
- A redundant Power Supply Unit that converts the primary voltage received from the SVM into the secondary voltages needed for powering the N-DPU boards and the routers.
- A Motherboard for internal connections.

There are two modes of data acquisition from the N-FEE's and data handling by the N-DPU.

- a) A nominal science mode acquiring imagerettes (or CCD windows) from the N-FEE which have already been extracted by the FEE from the full image. The data of all 4 CCDs from each of the two cameras are transferred inside 25 s to one N-DPU. The data products after data processing are sent as TM packets to the ICU.
- b) A test and calibration mode acquiring full CCD images from the N-FEE. These data are not processed and sent as TM packets to the ICU. The data of one N-camera/FEE are sent to the N-DPU within 50 s. Only one camera is read-out at the same time due to the high amount of data and the limited SpW interface bandwidth from the FEE to the DPU and also from the DPU to the ICU. That means two cameras are read-out and the data transferred to the ICU within 100 s.

Each N-DPU board is connected to 2 N-FEE via only 2 SpaceWire links configured to run at 10 Mbps for window mode or 100 Mbps for the full image mode. Each N-DPU board is connected to the nominal router and to the redundant router. Nominally, both MEU routers are working in cold redundancy. However, to

handle certain failure cases, both MEU routers can be switched on simultaneously and can work in hot redundancy.

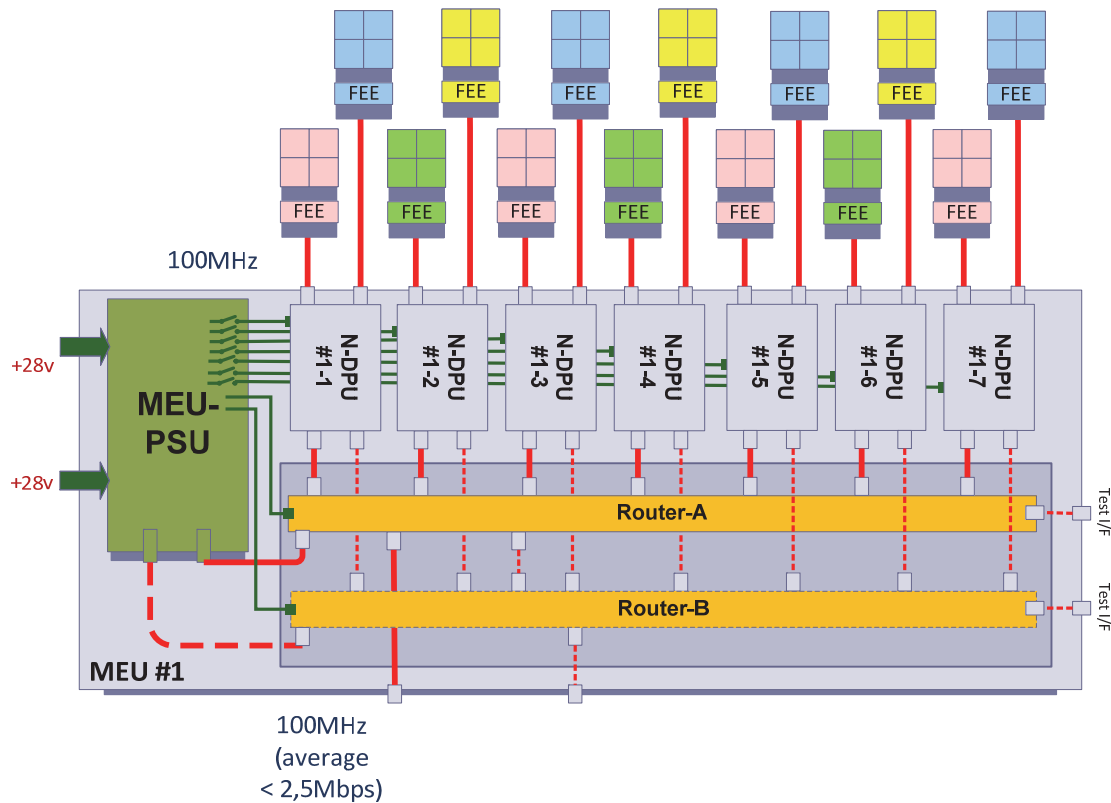


Figure 4.8: MEU box architecture.

In full image mode the instantaneous data rate between 2 N-FEEs and one N-DPU is about 160 Mbps, i.e. the data rate over one link is 80 Mbps, compatible with a SpaceWire link configured to run at a bit rate of 100 Mbps.

In FEE window mode, where the FEE extracts and sends imagerettes to the DPU, the data rate is significantly lower.

The data rate between one N-DPU and the MEU router is in average about 700 kbps. The full data rate between one MEU and the active ICU is 4.9 Mbps from all 6 N-DPUs.

In the nominal science observation mode, the main tasks of the N-DPUs are:

- To acquire and store CCD windows as a stream of pixels extracted and sent by the FEE from one 4510×4510 px image within 6.25 s and all CCDs per normal camera within 25 s. At the FEE level windowing is done to reduce the data volume transferred via SpaceWire.
- To reconstruct the star windows/imagerettes to be able to process them (N-DPUs: 6×6 -px windows, every 6.25 s, nominally for P1, P4 samples).
- To reconstruct and compute offset, background and smearing data (6.25 s)
- To correct pixel data with offset, background and smearing data (6.25 s)
- To detect and remove outliers (nominally for P5 samples) (600 s)
- To compute light curves and centroids and send them to the ICU (for P5 samples) (600 s)
- To estimate the attitude (every about 5400 s)
- To update the photometric masks positions to correct for differential kinematic aberration (every about 5400 s)

- To transmit imagettes, light curves, centroids, offset, background and smearing data to ICU every 25 s or 600 s
- To collect and transmit HK data and send them to the ICU (every 25 s)

The data products and number of extracted windows for 4 CCDs are given in Table 4.3.

Table 4.3: Data products of one N-DPU and two N-cameras sent to the ICU

Data product (cadence)	Number
Imagettes (25 s)	25750 ([P1: 2 cameras × 5970 + P4: 2 × 1675 + P5: 2 × 4730 + Guest observer: 2 × 500] star windows)
Light curves (50 s)	54736 ([P5: 2 cameras × 7868 + Guest observer: 2 cameras × 19500] star windows)
Light curves (600 s)	141630 (P5: 2 cameras × 70815 star windows)
Centroids (50 s)	7868 (P5: 2 cameras × 3934 star windows)
Background values (25 s)	800 (2 cameras × 400 Background windows)
Offset values (25 s)	16 (2 cameras × 2 × 4 CCDs á 2255 pixels) offset windows
Smearing values (600 s)	36080 (2 cameras × 4 CCDs á 4510 overscan rows) smearing rows
Housekeeping	120 values

The application software running on each DPU performs the complete data reduction and photometrical extraction process. It is triggered as soon as a set of windows extracted from a full-frame image is available.

The needed processing power has been estimated by prototyping LEON2@100 MHz processor simulator. The measured CPU occupation rate is about 37% which implies sufficient margin for the development process up to the Flight Model. The conclusion is that the normal N-DPU board can be implemented with at least one LEON AT697F processor working at 100 MHz. The CPU load margin could be used to improve the algorithms, to implement new algorithms, to process more targets, to update with a higher frequency the photometric masks or to reduce the processor frequency. The total memory required per N-DPU board will be 256 Mbytes, assuming +50% margin in the number of stars to be monitored per CCD.

4.3.2 Fast Electronics Unit (FEU) and Data Processing Units (F-DPU)

Data of the two fast telescopes are processed by two Fast DPUs (F-DPU). The data acquisition and handling of each exposure is similar to that of the N-DPU, except that the cadence is 2.5 s instead of 25 s; only imagettes will be processed; FGS algorithms are implemented to provide pointing error measurements with an accuracy better than 0.032 arcsec/ $\sqrt{\text{Hz}}$ and transmitted to the AOCS (Fine Guidance System: FGS).

In the nominal science observation mode, the main tasks of the F-DPUs are:

- To acquire and store CCD windows as a stream of pixels sent by the F-FEE from 4 CCDs with 4510 × 2255 pixels every 2.5 s. At the FEE level windowing is done to reduce the data volume transferred over SpaceWire. Full images are transmitted in calibration and test modes only. The raw data acquired from the ADC are just serialized and sent to the each N-DPU through 4 SpaceWire links.
- To reconstruct the star windows/imagettes (9 × 9 pixel windows / 2.5 s).
- To send imagettes to the ICU (nominally for all stars in the P2 sample)
- To extract and compute offset, background and smearing data
- To send offset, background and smearing data to the ICU
- To calculate/estimate the attitude for the FGS/AOCS every 2.5 s
- To collect HK data and send them to the ICU

The data products provided are given in Table 4.4.

Table 4.4: Data products of one F-DPU (one F-camera) sent to the ICU and to the AOCS.

Data product (cadence)	Number
Imagettes (2.5 s)	636 ([P2: 1 camera × 586 + Guest observer: 1 × 50] star windows)
Lightcurves	No
Centroids	No
Background values (50 s)	100 (1 camera × 100 Background windows)
Offset values (2.5 s)	8 (1 camera × 2 × 4 CCDs á 2255 pixels) offset windows
Smearing values (50 s)	5724 (1 camera, 636 imagettes × 9 pixels on 4 CCDs)
FGS data to S/C and ICU (attitude/pointing error)	Quaternions, Covariance matrices, Status word(s)

The FGS algorithms are based on an extended Kalman filter (EKF) used for recursive nonlinear optimisation. In full image mode with 4 links (one per CCD output) a peak data rate of 80 Mbps is transferred including the SpaceWire overhead. In order to cope with this bit rate with margin, the links are configured at 100 Mbps. In window mode a lower data rate for transferring imagettes windows only a much lower data rate from the F-FEE is required so that the links can be operated at 10Mbps.

The CPU load needed by the data acquisition, correction and reduction process is about 40% with a MDPA LEON2 FT processor running at 80 MHz. In total 512 Mbytes of SDRAM will be needed per F-DPU.

The FEU is an integrated electronics box, which consists of two data processing (F-DPU) boards (each within one module frame) and 2 power converters (PSU) integrated into a single frame.

4.3.3 Instrument Control Unit (ICU)

Both ICUs (main and redundant) are located in a single box and work in cold redundancy. Each ICU shall implement the following common functions (non-exhaustive list):

- Handle communications with spacecraft.
- Receive and process telecommands.
- Format and transmit cyclic and sporadic HK telemetry and scientific payload telemetry packets.
- Manage the SpaceWire network: the ICU is a remote network manager (router configuration, router monitoring, router status reporting...).
- Receive the on-board time (Central Time Reference) from the S/C, handle the time stamping of the data transmitted in HK TM and forward the CTR to the DPUs.
- Receive a SpaceWire time code from the S/C and forward it to the DPUs.
- Produce state and diagnosis information (cyclic status, progress event).
- Schedule the DPU tasks (by the way of commands sent to the DPUs).
- Manage the data flow (especially in configuration mode) and the mode transitions.
- Manage the maintenance of the ICU, N-DPU and F-DPU software and parameters.
- Manage the star catalogue.
- Compress the data using a lossless compression algorithm. A compression factor of at least 2.0 is required.
- Acquire and transmit to the S/C its own voltage and current consumptions.

Every 2.5 s, the active ICU receives the data (e.g. imagerettes, HKs and FGS data) sent by the F-DPUs. The imagerettes are compressed before being transmitted to the SVM.

Every 25 s, the active ICU receives the data (e.g. flux, centroids, imagerettes, HKs) sent by the N-DPUs.

The incoming data are stacked before compression and transmission to the SVM.

In configuration mode, the main functions of ICU are to transmit the star catalogues and all other configuration parameters to the DPUs, to compress full-frame images sent by the DPUs, to pack and transfer to SVM all the data from DPUs necessary for subsequent validation of on-ground operations.

The expected data volume including compression is 435 Gb/day.

4.3.4 Telemetry data budget

The telemetry data budget is given in Table 4.5. The available data volume transmitted by K- and X-band antenna is 435 Gb average per day. The budget is separated in a data volume available for the nominal science and the guest observer program.

Table 4.5: Telemetry data budget.

	Total	Nominal	Guest Obser.
Daily volume for all normal cameras (science data)	393.0 Gb	366.4 Gb	26.7 Gb
Daily volume for all fast cameras (science data)	29.0 Gb	26.7 Gb	2.2 Gb
Daily volume for all cameras (with compression, without header)	422.0 Gb	393.1 Gb	28.9 Gb
CCSDS Packet header overhead	0.6%	0.6%	0.6%
Data auxiliary header overhead	2.5%	2.5%	2.5%
<i>Science data (incl. packaging overhead)</i>	<i>435.0 Gb</i>	<i>405.2 Gb</i>	<i>29.8 Gb</i>
<i>HK data (incl. packaging overhead)</i>	<i>0.4 Gb</i>	<i>0.3 Gb</i>	<i>0.1 Gb</i>
Total daily volume with compression, with header	435.4 Gb	405.5 Gb	29.9 Gb

5 Mission design

This chapter provides an overview of the mission profile, launch scenario, mission orbit and operations as well as an introduction to the common key mission design challenges.

Following the definition phase (B1), two spacecraft competitive concepts, respectively led by Airbus DS Ltd and OHB System AG, are currently proposed and are presented hereafter.

5.1 Mission operations

5.1.1 Mission profile

The overall PLATO mission profile consists of the following phases:

- Pre-launch phase, from launch campaign preparation to launch vehicle lift-off;
- Launch and Early Orbit Phase (LEOP), from lift-off to the completion of the first trajectory correction manoeuvre performed by the spacecraft on day 2 latest after separation from the launcher upper stage;
- Transfer phase, from the end of the LEOP up to the insertion at the operational orbit around the Earth-Sun Lagrangian point 2 (L2) where scientific observations will be conducted;
- Commissioning phase, starting during the transfer phase and running in parallel to it (and after if necessary) until the completion of the check-out and calibration of the spacecraft and its payload maximum 3 months after launch;
- Nominal science operations phase, starting at the end of the commissioning phase, with a duration of 4 years;
- Extended science operations phase, starting at the completion of the nominal science operations phase and lasting up to 4 years;
- Decommissioning phase, starting close to the end of the science operations phase, and consisting of a disposal manoeuvre to comply with the space debris mitigation requirements and the spacecraft passivation.

The figure below depicts the various nominal mission phases and their respective durations, the key events and ground stations foreseen to ensure the communications coverage.

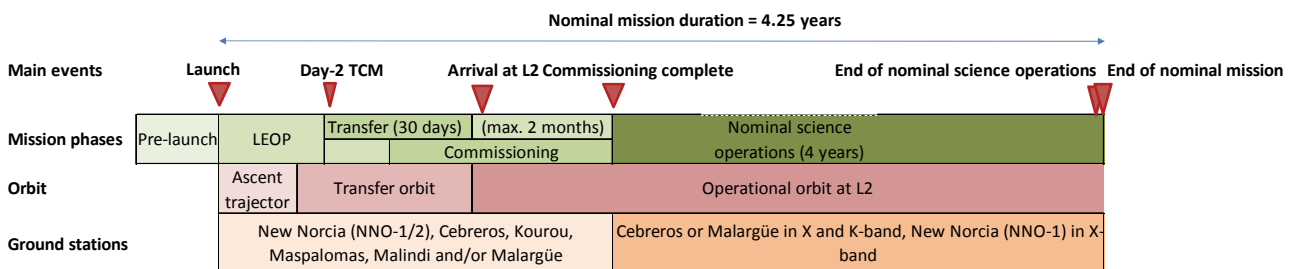


Figure 5.1: PLATO mission phases.

5.1.2 Launch scenario and transfer

PLATO is foreseen to be launched in 2025 from Kourou by a Soyuz 2-1b rocket with Fregat upper stage and injected onto a transfer trajectory to L2. The Fregat stage will inject the spacecraft either directly to L2, similarly to Euclid, or via a low Earth-bounded circular parking orbit, similarly to Gaia.

PLATO features a 40 degree half-cone zone, so-called prohibited zone, around the payload line of sight in which the Sun must never enter to prevent degradations of the telescope optics. If the spacecraft configuration is such that the payload line of sight is up-oriented towards zenith, it cannot be launched directly to L2 due to the required launch around noon local time of the perigee. A later lift-off time must be adopted which then requires an intermediate parking orbit keeping the prohibited zone safe, before the injection to L2 can take place at the next perigee pass.

Both launch strategies are designed so that launch is possible all year round with some exclusion windows to avoid Moon and Earth eclipses during transfer. The daily launch window lasts between 30 minutes up to 2 hours depending on the launch date.

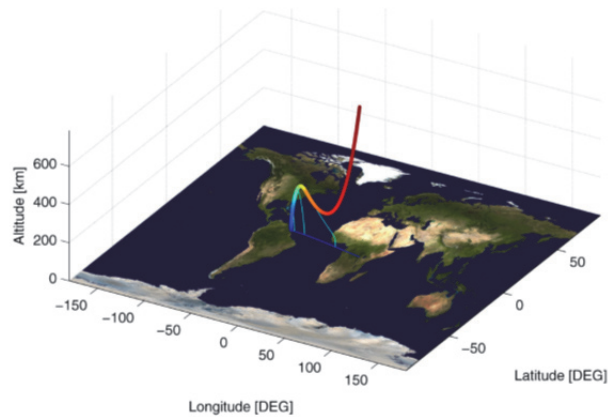


Figure 5.2 – Left: Soyuz launch from Kourou (Credit: ESA); Right: Soyuz ascent trajectory for a direct transfer to L2.

The transfer will last approximately 30 days during which the spacecraft commissioning also takes place. Trajectory correction manoeuvres shall be performed by the spacecraft the latest 2, 5 and 20 days after the separation from Fregat (occurring about 2400 s and 6800 s after lift-off, respectively in the direct ascent and parking orbit scenario) in order to remove the launcher dispersions and correct the perigee velocity. A total delta-V of about 40 m/s is budgeted before margins for the transfer phase.

5.1.3 Operations at the Lagrange point 2 (L2)

5.1.3.1 Operational orbit

PLATO will perform its scientific observations on a free-insertion, large amplitude, eclipse-free libration orbit around L2. This orbit, shown on Figure 5.3, is unstable and shall be maintained by regular station-keeping manoeuvres every 30 days. The angular size of the libration orbit seen from the Earth is approximately 33° in the ecliptic plane and 25° out of this plane.

From the end of the Transfer Phase to the completion of the nominal science operations phase, PLATO will spend in total 4 years around L2. Three additional months in total are currently allocated to launch, transfer, and commissioning.

5.1.3.2 Communications with ground

During science operations, a communication session with the nominal ground station will be used several days per week. The largest part of it (>3.5 hours) is dedicated to file-based science and stored housekeeping data transmission at 36 Mbps in K-band and real-time housekeeping data transmission at 26 kbps in X-band via a dual X/K-band high gain antenna. This enables downloading to ground the required 435 Gbits of science data produced daily by the payload. Within this slot, a small window is used for communication setup and ranging and the 16 kbps uplink is ensured via X-band. Outside these nominal communication periods, a low-rate data link will be ensured via low gain antennas in X-band for minimum and contingent telemetry (2 kbps), telecommand (4 kbps).

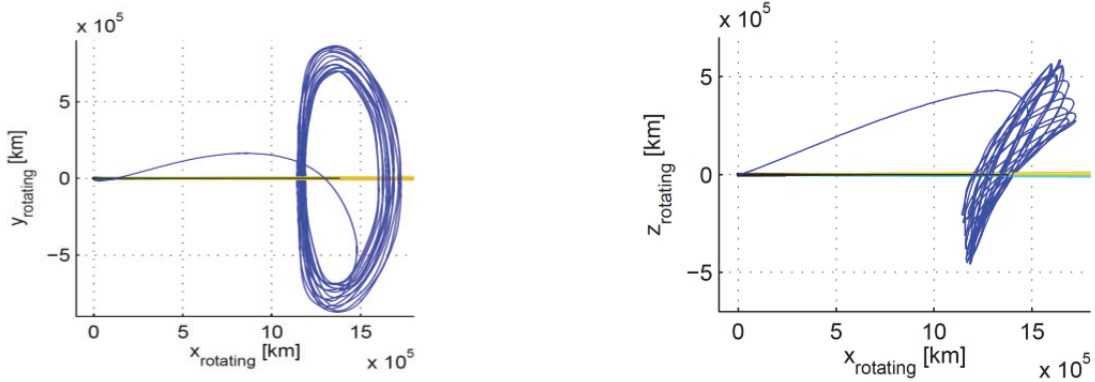


Figure 5.3: Example of a large amplitude libration orbit around L2 for PLATO. The orbit shape and amplitudes depend on the launch date.

5.1.3.3 Mission observation strategy

PLATO has a flexible observing approach. Two observing strategies are reflected in the science requirements, long-duration observation of the same field versus shorter coverage of shorter different fields, or step-and-stare. These strategies complement each other and allow for a wide range of different science cases to be addressed. Long-duration pointings would be devoted to surveys for small planets out to the Habitable Zone of solar-like stars. Short pointings would be devoted to shorter-period planet detections and will address a number of different science cases such as galactic exploration.

In its nominal science operations, PLATO’s current baseline observation scenario assumes a Long-duration Observation Phase (LOP) consisting of continuous observations of two sky fields, lasting 2 years each. An alternative scenario would consist of a LOP of three years and a step-and-stare phase (SOP) of one year. The current mission design constraints impose the centre of the LOP fields to be at least above 63 degrees or below -63 degrees in ecliptic latitude. The LOP fields preliminary selected are shown as blue areas in Figure 5.4.

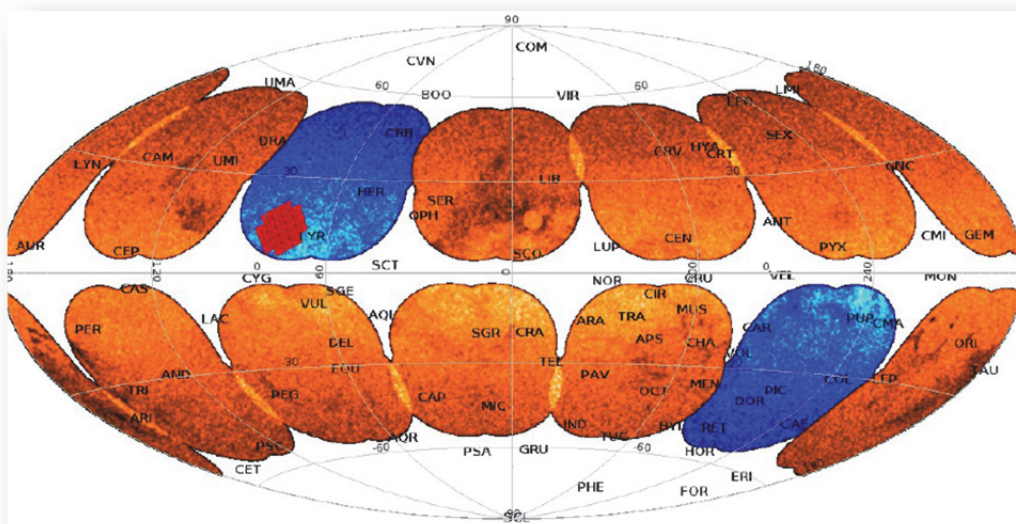


Figure 5.4: Schematic comparison of observing approaches. Red area: the Kepler target field. Large areas: size of the PLATO field. A combination of short (orange) and long (blue) duration pointings is able to cover a very large part of the sky. Note that the final locations of long duration and step-and-stare fields will be defined two years before launch and are drawn here for illustration only.

Although the nominal science operation duration is four years, the satellite will be built and verified for an in-orbit lifetime of 6.5 years, accommodating consumables for 8 years. Consequently, four years of mission

operation extensions are possible conditional upon approval by the SPC, in which LOP sky fields may be re-observed or new LOP sky fields may be added. In addition, step-and-stare pointings may be carried out, lasting 2-5 months each.

In view of the exceptionally fast development of exoplanet science, this reference scenario will be investigated throughout the mission development and adapted to the needs of the community about two years before launch.

5.1.3.4 In-orbit spacecraft and payload events

During long observations, the spacecraft must maintain the same line-of-sight (LoS) towards one field for up to several years. However, the spacecraft must be periodically re-pointed in order to ensure the solar arrays are pointed towards the Sun. This is achieved by rotating the spacecraft around the LoS by 90° roughly every 3 months, as shown in Figure 5.5.

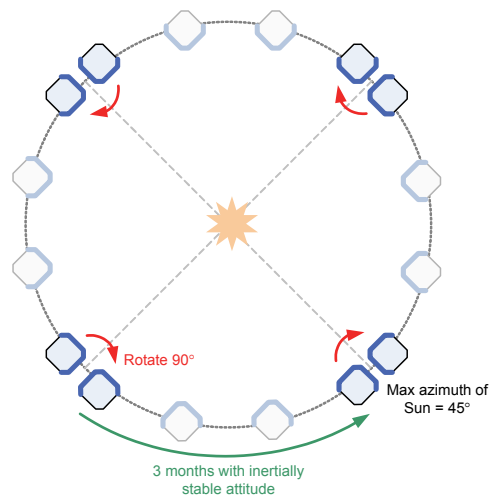


Figure 5.5: Spacecraft rotation around payload LoS during one orbit.

Due to the constant pointing requirements of PLATO and high science measurement duty cycle, and besides the necessary re-pointings between observation fields, only few manoeuvres and interruptions to the scientific measurements are planned. Nevertheless, some are required to maintain the orbit and control capability of the spacecraft as well as for the calibration needs of the payload.

On-station, the spacecraft must maintain its position on the nominal orbit via station keeping manoeuvres which are foreseen to take place every 30 days. Their amplitudes depend on the residual accelerations induced by the spacecraft and therefore depend on its design.

Since the spacecraft fine control is based on reaction wheels, those will need to be de-saturated on a regular basis. These offloading operations can take place for instance once a month or as often as every few days, depending on the wheels' design and the control strategy. The daily communications will also require regular antenna re-pointing, which may impact the nominal pointing of the spacecraft.

Even if safe modes are required to be limited by design, those events might take place and some off-nominal operations must be allocated in that respect.

The payload itself requires some calibration operations. In particular, the payload needs to acquire a very high-resolution Point Spread Function (PSF) characterisation of each star for each telescope used in the ground data processing later on, typically to correct for long-term drifts and high-frequency pointing jitter (see Section 5.3.5). For this purpose, the spacecraft will perform for a few hours a micro-scanning of the field of interest on a regular basis, at least after every field re-pointing and quarterly slew, potentially more often.

Other calibration needs, such as download of full CCD images and telescopes at the beginning after each re-pointing and slew do not require any spacecraft manoeuvres but will interrupt the scientific measurement for a minimum amount of time. Update of the position of the star imagerettes are also foreseen to cope with the

large-scale and long-term movements of the star in the focal plane due to kinematic aberration and thermo-elastic for instance, but essentially do not impede the science data acquisition.

The duration of all events described above as well as the time required to reach the science nominal mode are accounted for as downtime of the scientific measurements and the associated gaps are evaluated against the scientific gap requirements (see Section 5.3.2). Particularly, following any manoeuvre (e.g. orbit maintenance, re-pointing, slew, micro-scanning) the spacecraft will have to retrieve its thermal and structural stability in order to resume its thermal and fine pointing performances.

At the end of mission eventually, a delta-V of 10 m/s is allocated to the disposal manoeuvres in order to place the spacecraft on a heliocentric orbit.

5.2 Mission implementation

The PLATO spacecraft is configured with two main modules that can be individually integrated and tested:

- Payload Module (PLM), the full set of instruments including cameras and associated electronics and data processing units as well as the optical bench, supporting structures and the hardware thermal control.
- Service Module (SVM), the part of the Spacecraft that supports the PLM. It consists of the platform equipment and the main structure including sunshield that protects the payload from the Sun, as well as generates power via body-mounted solar cells.

The top-level product tree of the PLATO spacecraft resulting from this system architecture and from the definition of the reference Payload is provided in Figure 5.6. Within the PLM, the products under the responsibility of the PLATO Mission Consortium (PMC), also known as payload elements, will be delivered to the industrial prime contractor as Customer Furnished Equipment (CFE) by ESA for their integration in the spacecraft. These elements (in pink in the figure below) are described in Chapter 4. This chapter describes the overall spacecraft system design, focusing on the elements designed and procured by the prime contractor, also known as the platform elements (in green in the figure below).

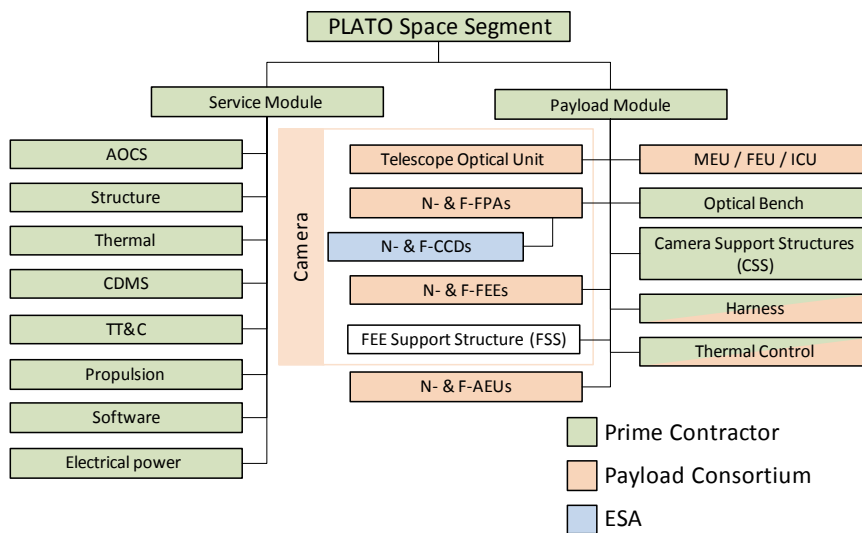


Figure 5.6: PLATO high-level product tree.

5.3 Key design challenges

In order to reach the scientific goals, the PLATO spacecraft and its instrument suite must be extremely stable and produce as little photometric noise as possible to meet the scientific requirements, and for instance reach the required 34 ppm random noise in one hour for stellar sample P1. The payload is designed such as to optimise the observing strategy and to limit the intrinsic instrument-induced photometric noise as described in Chapter 4. This chapter focuses on the generic challenges put onto the platform in order to comply with

the scientific and mission requirements in consistency with the payload interfaces, design and calibration needs.

5.3.1 Payload accommodation and spacecraft interfaces

The accommodation of 24 normal + 2 fast cameras and associated electronic units has a mass allocation of 533 kg, with the specified camera groups' orientation and offset on a spacecraft whose volume and mass are constrained by the Soyuz fairing and launch performance of 2165 kg to L2. The maximum allowed mechanical and thermal loads onto the payload units, especially the cameras, as specified in the interface requirements, drive the platform design.

Among others, this affects in particular the mechanical sizing of the optical bench assembly and the camera support structures, which interface with the optical bench to limit e.g. quasi-static, sine and random loads or shocks onto the cameras. The cameras thermal control, even though powered by the platform, is designed by the PMC and ensured by the payload itself. The telescopes' absolute temperatures are around -70 to -90 °C in order to obtain nominal working temperatures for the CCDs (-65 °C) and required PSF focused point. These are not extremely challenging, but once set to the specified level for a given camera, the thermal control must keep this set point within narrow limits on the telescope body (~ 200 mK over 6 hours). The purpose is to guarantee the stability of the telescopes focusing points and to avoid PSF breathing effects, which could affect photometric performances, especially in the frequency range of interest to asteroseismology. In order to do that, the spacecraft must also provide a very stable conductive and radiative environment towards the cameras, including the front end electronics.

The set of 26 cameras leads to an unusual large amount of harness to fulfil all functions, i.e. power, thermal control, data (via space wire), synchronisation. The main issues are the high mass of the harness and its routing between the SVM equipment and the payload units. In addition, the Ancillary Electronics Units (AEU) are providing secondary power to the Front-End Electronics (FEE) to limit high power dissipations close to the cameras. Due to the large distance between the FEEs located on the cameras and the AEU's located on the SVM, the harness losses must be carefully mitigated.

5.3.2 Science duty cycle

In order to continuously monitor the star fields, so as not to miss any planetary transit, as well as to increase the signal-to-noise ratio for those transits and for asteroseismology mode detections, the science duty cycle of the mission has been set to be above 93%. Among others, this requirement drives:

- the need to perform operations at L2,
- the duration and frequency of spacecraft manoeuvres and off-nominal performances (e.g. reaction wheel offloading, slews, station keeping, post-slew thermal stabilization),
- the duration and frequency of payload calibrations (e.g. micro-scanning).

Furthermore, periodic gaps must be avoided as required by the need to keep disturbing peaks away from the frequencies of interest in the power spectrum of star oscillations. Despite being relatively benign as demonstrated by the studied concepts, this requirement might favour to render operations as aperiodic as possible, e.g. wheel offloading, communications, quarterly slews.

5.3.3 Payload environment

5.3.3.1 Straylight

The low levels of allowed straylight and high duty cycle goal of the mission drive the angular size of the libration orbit seen from the Earth, and thus amplitude, so as to avoid direct Earth and Moon light inside the payload field of view, leading to the orbit described in Section 5.1.3.1. It also imposes as a minimum to align the camera baffles and the sunshield cutting plane and minimise manufacturing and alignment tolerances. Furthermore, mitigation measures may be adopted by the prime contractor to further reduce the diffracted straylight from spacecraft parts e.g. the sunshield onto the entrance windows of the cameras, via for example multiple diffracting blades accommodated on the sunshield edge.

5.3.3.2 Radiations

Both optics and CCDs are sensitive to radiations. Radiation-hardened materials are implemented for the most sensitive optics. PLATO CCD performances are especially sensitive to Charge Transfer Inefficiencies (CTI). Local shielding is currently foreseen for protecting the CCDs most exposed to radiations, which is particularly the case for cameras located on the outer part of the PLM, less shielded by the platform structure and other cameras. 2.5 krad ionising dose and 1.3×10^{10} protons/cm² (10 MeV equivalent) non-ionising dose are the current design specifications for the PLATO CCDs.

5.3.3.3 EMC

The PLATO payload, in particular its video chain (CCD – flexi-cables – FEE), is susceptible to electromagnetic interferences, which would then affect the science data. These could be caused by cross-talks between cameras or any other onboard electromagnetic source, e.g. power and data lines, thermal control, electronics units located on the SVM (e.g. DC/DC converters), RF transmitters and receivers. Therefore PLATO adopts a number of design mitigation measures to limit these effects to the greatest extent such as adequate grounding and bonding, harness shielding, power supply separation, far enough accommodation of sensitive units, etc. In addition, the camera data read-out and thermal control are fully and centrally synchronised at payload-level. The EMC control plan will be carefully defined and implemented and requires a close collaboration between the payload and spacecraft designers. At platform and spacecraft levels, a comprehensive EMC test campaign is foreseen, covering conducted and radiated susceptibility and emissivity among others for platform EMC potential culprit units. In addition spacecraft-level EMC analyses and tests on the avionics and flight models will be performed in order to cover potential resonance effects and demonstrate appropriate system-level margins.

5.3.3.4 Contamination

Particulate and molecular contamination of the payload sensitive optical chain, i.e. from entrance window to CCD, must be avoided in order to limit optical transmission loss and scattered straylight. Particulate and molecular residuals shall be less than respectively 5000 parts per million and 1×10^{-6} g/cm² at end of life on the entrance window. This requires regular contamination monitoring, careful material selection, efficient camera covers, clean integration rooms (typically ISO 8 or 5) and potentially dedicated tents, cleaning procedures, including outgassing mitigation measures such as vacuum cleaning, wiping or bake-out, to limit the contaminant deposits throughout all stages of the assembly, integration and verification (AIV) process. A large part of the budget is allocated to the prime-level AIV activities, but also to the launch itself where particulates fall-outs from the fairing will inevitably contaminate the spacecraft parts. Also during launch, appropriate venting must be implemented to avoid trapping of contaminants. During flight icing, moisture release and outgassing of organic material (e.g. Carbon Fibre Reinforced Plastic) must be mitigated. Appropriate heating capability must be implemented in order to bake-out the critical surfaces which may still induce in-orbit contamination, and the thrusters must be oriented so as not to impinge on the payload sensitive elements.

5.3.4 Cameras static co-alignment

The maximum static misalignment of the cameras' line of sights between the integration room and the flight conditions must be limited. Such an absolute misalignment results in a decreased overlapping of the field of views between camera groups and among cameras of the same group leading to the loss of stars in the edge regions. The current specification is ~ 3.4 arcmin for the overall line of sight alignment error of each camera and guarantees that less than 1% of the stars in the field of view are lost.

5.3.5 Spacecraft and cameras' pointing stability

5.3.5.1 Relative Pointing Error

During science observations, the maximum Relative Pointing Error (RPE) of the spacecraft must be limited to 3 arcsec (95% confidence level) over the integration time of the normal cameras, i.e. 25 seconds. With this effect, the star image is blurred which should be limited to avoid confusion with contaminant stars, but does not have affect its centroid position in a significant way. The RPE is driven by AOCS high-frequency noise and in particular reaction wheel friction jumps and by microvibrations.

5.3.5.2 High-frequency Amplitude Spectral Density of the cameras' Mean Pointing Error

The pointing stability requirement is particularly stringent and is the subject of many challenges for the spacecraft design. The key parameter is the Mean Pointing Error (MPE) stability of each camera. Its specification is illustrated in Figure 5.7.

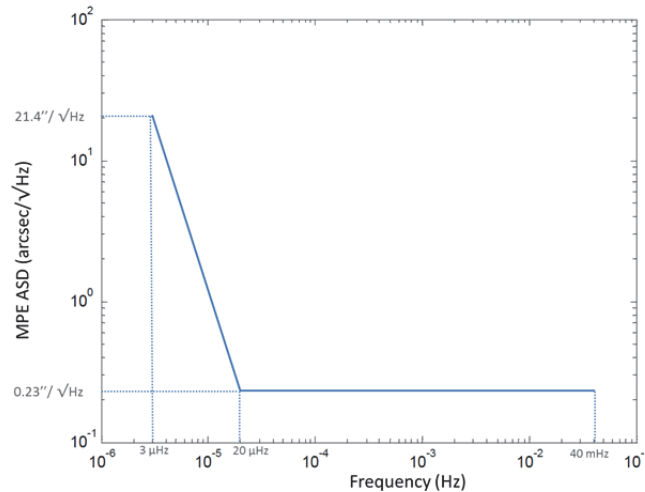


Figure 5.7: Amplitude Spectral Density of the Mean Pointing Error.

It is currently specified in the frequency domain (as opposed to a simple rms value for instance) as per the science requirement on the systematic residual error from which it is derived, in order to limit peaks at specific frequencies that would obscure star oscillations. Its equivalent in rms terms is ~ 46 milliarcsec. These levels impose the use of a fine guidance sensor. The payload fast cameras are used for this purpose as no currently available star tracker can fulfil the corresponding specification. Due to the frequency regime in which it is applied, it affects mostly the AOCS design and short or medium-term disturbances induced for instance by thermo-elastic effects, especially if they are of periodic nature. The AOCS-related contributors are e.g. the fine guidance sensor noise and drift and the AOCS controller and actuation errors in the relevant frequency domain. The other contributors are e.g. optical bench thermo-elastic deformations due to slow variations of the Sun Aspect Angle during quarterly observation periods, power/thermal periodic dissipations occurring on the service module and transferred to the payload module. Despite that both spacecraft concepts described below are compliant with this pointing requirement, it should be noted that it is currently being reviewed with the goal to relax the specification. This follows the recommendation by the Mission Adoption Review to define it in the time domain rather than frequency, which will be beneficial especially for its lower-frequency part driven by the thermo-elastic effects, as well as to allow structural deformation levels measurable with off-the-shelf verification methods, such as photogrammetry.

5.4 Spacecraft design

Following the definition phase (B1), two spacecraft competitive concepts, respectively led by Airbus DS Ltd and OHB System AG, are currently proposed and are presented hereafter.

5.4.1 Airbus – Spacecraft design – Prismatic configuration

The spacecraft is based on a prism-shaped structure with equilateral triangle basis (see Figure 5.8), which is inherently stiff. Three main vertical panels of $5\text{ m} \times 2\text{ m}$ constitute the all-CFRP main structure, together with closing panels and stiffening struts. The 26 cameras that constitute PLATO's payload are installed horizontally on one of the 3 vertical panels.

This vertical accommodation offers an optimised area for the payload, while the load of the significant payload mass is directly carried by the main structure. In consequence, the central main structure functions as the optical bench, and together with cameras and payload electronics, they constitute what can be defined as the Payload Module (PLM), thus acting as the main spacecraft bus. The 26 cameras are attached through

an individual Camera Support Structure (CSS) on one of the vertical panels, and are installed through holes on that panel in a way that minimises the payload harness mass while preserving the camera “subgroup” arrangement, here spread over 4 rows.

This design isolates the Front-End Electronics (FEE) from the main panel of the optical bench, offering a natural filtering of FEE dissipation noise onto Optical Bench thermo-elastic performances, as their heat is further evacuated via a radiator located on the inner opposite (electronics) panel (see Figure 5.9).

In order to minimise thermal disturbances towards the optical bench, and thus thermo-elastic distortions, the Service Module (SVM) equipment as well as the payload electronics units are accommodated in individual suspended backpacks on a second vertical panel, which heat is radiated away from the optical bench into space.

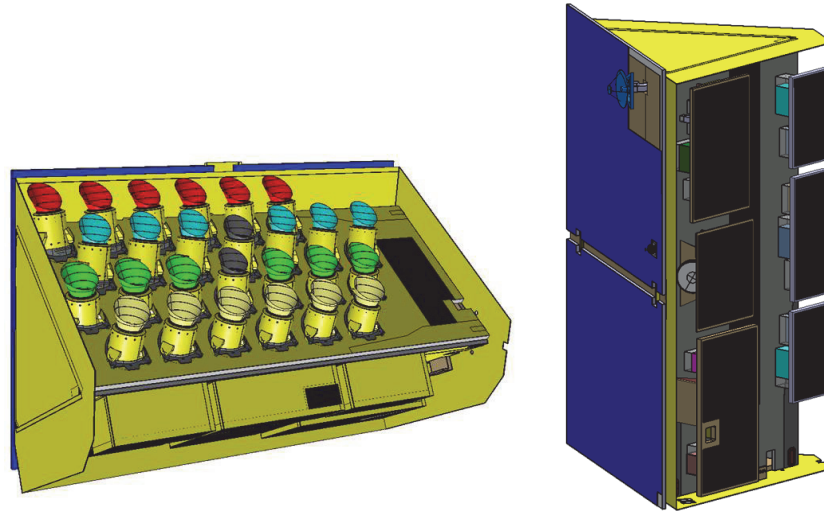


Figure 5.8: Airbus concept: general views showing the optical bench supporting all the cameras (left), and the backpacks supporting all SVM equipment and payload electronics (right).

Up to 9 backpacks are defined, each carrying a consistent set of equipment corresponding to each main functional chain of the spacecraft (3 panels for PLM electronics, 1 panel for DHS, 1 panel for TT&C, 1 panel for the reaction wheels, and one for each of the power, AOCS and propulsion). Each of them is simple in its design, with a simple plate, mounted off the main structure with interfaces that minimise the distortions that they can induce on the primary structure.

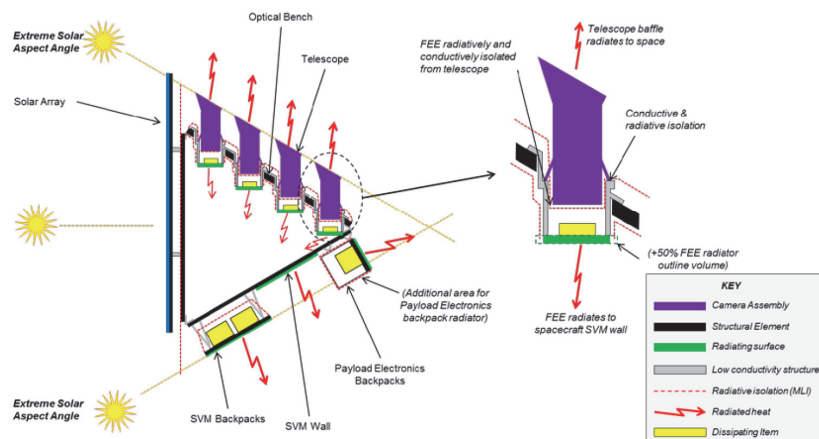


Figure 5.9: Airbus system thermal design concept to limit thermo-elastic distortions.

Finally, the sunshield is enveloping the optical bench to protect the cameras from Sun illumination, down to 60 degree ecliptic latitude and accommodates the flat solar arrays on one of the primary structural panels, which benefit from a large area, leading to comfortable power margins and growth potential. The top and bottom sides of the spacecraft are covered with MLI to complete the payload sunshielding function. The triangular shape of the spacecraft allows both the payload side and the SVM side to be permanently in the shade.

The design is based on an inversion of the classical separation of SVM and PLM. While the PLM constitutes the main satellite bus the SVM is mounted on it. Despite this, this configuration allows parallel integration of the SVM and PLM.

The heavily camera-loaded side panel however leads to a large offset of the centre of mass, which requires a specific launch vehicle adapter geometrically compensating for it that has been studied jointly with Arianespace. The mass of the PLATO Airbus spacecraft is about 2134 kg at launch for a 30 cameras payload complement, heavier than the 26 cameras baseline, including launch adapter and 103 kg of propellant, and it generates about 1950 W of power, all margins included.

5.4.2 OHB – Spacecraft design – PLM and SVM separation

The spacecraft is based on a separation between SVM and PLM as illustrated in Figure 5.10 to isolate the PLM as much as possible from the SVM thermal dissipations and mechanical distortions, which is a rather classical scheme for science missions as it was used for Herschel and is foreseen for Euclid. This modular scheme allows parallel integration of the SVM and PLM.

The PLM functionally consists of the set of 26 cameras, the optical bench assembly, the payload harness and the payload electronics, even though the latter are physically located on the SVM to limit their adverse impact on the cameras stability.

The SVM, which base shape is quasi-hexagonal, accommodates all the platform equipment necessary to support the functions of the payload module, that is, DHS, TT&C, sunshield/solar arrays and power subsystem, AOCS and propulsion. This equipment is mostly mounted on the SVM side panels with a few exceptions such as the star trackers (on the SVM top panel), the thrusters, the HGA (on the SVM bottom panel) and the 2 propellant tanks of 96 L each equatorially mounted within the central tube. This 1666 mm central tube made of CFRP provides the main load bearing path and interfaces on one side to the 1666 mm standard launch adapter and on the top side with the optical bench module. One of the side panels is dedicated to the payload electronic units and most side panels act as radiators to evacuate the heat towards deep space.

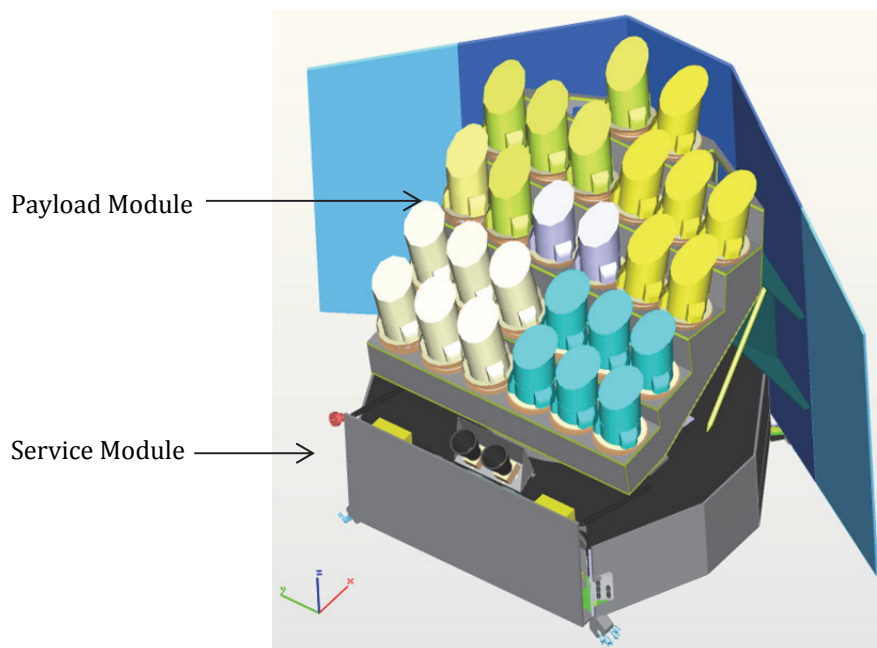


Figure 5.10: OHB spacecraft: separated PLM and SVM configuration.

The spacecraft height is about 4 m and its width 5.3 m from solar array tip to tip when fully deployed. This deployed configuration allows the payload to be fully protected from the Sun at any allowed observing attitude, while providing power to all units as shown in Figure 5.11.

The mass of the PLATO OHB spacecraft is about 2120 kg at launch for the baseline payload complement of 26 cameras, including launch adapter and 121 kg of propellant, and it produces about 2145 W of power, all margins included.

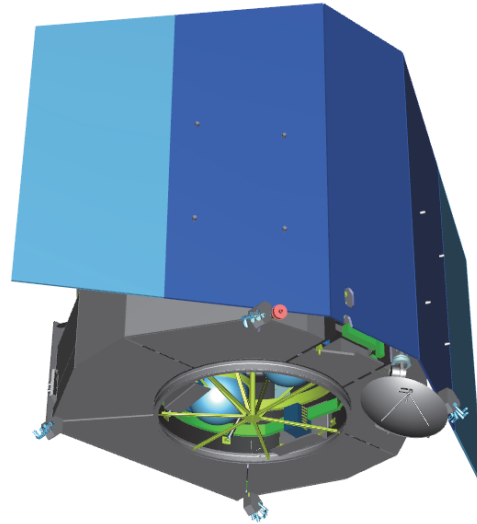


Figure 5.11: OHB spacecraft concept, illustrating the full protection of the payload by the sunshield in an extreme Sun Aspect Angle configuration.

The 26 cameras that constitute the PLATO's payload are installed on an optical bench which is the core of the payload module, with the two fast cameras centrally located to minimise inter-camera pointing errors. The 30-degree slanted optical bench is a closed box, with a stepped structure providing a high inherent stiffness. The top floor of the optical bench acts as a radiator for the FEEs towards deep space leaving the MLI-wrapped cameras isolated from it. The cameras interface with the optical bench via camera support structures mounted onto the optical bench steps with the FEE enclosed through holes in a cavity below.

This optical bench is entirely wrapped in MLI and further mounted on the SVM via bi-pods designed as to provide a quasi iso-static mounting, further decreasing the influence of the SVM onto the PLM. This is one of the key design features of this configuration in order to limit the thermo-elastic distortions of the optical bench and therefore the cameras. The harness interfacing with the cameras is routed along the optical bench and connects to the service module via a waterfall concept falling directly over the side panel accommodating the payload electronics units which ease integration of the PLM.

The entire PLM weights ~ 1023 kg including the 26 cameras and an overall 30% system margin.

5.5 Technology readiness

The platform design of the proposed PLATO spacecraft are heavily based on current technology and heritage from other missions. The AOCS and propulsion subsystems can use off-the-shelf equipment with no development required, except for the fine guidance sensor under responsibility of the PLATO Payload Mission Consortium. Data handling and communications equipment can be performed with current technology, and proposals from industrial contractors are based on modifications of units used in current missions.

The structure will be built using qualified materials and processes that have been selected to provide a stable, low-mass platform while featuring the strength and stiffness necessary to resist the launch loads. There is one mechanism on the spacecraft (2-DOF high-gain antenna pointing mechanism), which at most will require a minor modification to accommodate the large azimuth and elevation range of the Earth as seen by the Spacecraft. All platform units TRL is 5 and above.

Page intentionally left blank

6 Preparatory work and ground-based observations

6.1 PLATO target and field selection

Chapter 3 defines the samples of stellar targets (P1-P5), each with a specified requirement or goal about the number of cool dwarfs to be monitored within a given magnitude/noise range and surveyed fields. Sample P1 is the most important one, with at least 15,000 (goal: 20,000) dwarfs and subgiants later than spectral type F5V, brighter than $V=11$ and with a noise level better than 34 ppm, to be imaged within two long-duration fields combined. Telemetry limitations impose the pre-selection of PLATO targets for the detection of planets. The optimal field selection is closely related to the target selection. The success of the mission is related to our ability to select fields that maximise the number of F5 or later spectral type dwarfs and subgiants for which we can have photometry with the required SNR, i.e., fields in which P1 to P5 targets are maximised. We need to prepare a *PLATO Input Catalogue* (PIC) which includes P1-P5 targets, and provides their main parameters. Finally, the PIC will help us to assess the nature of the detected transiting bodies: a good knowledge of the host star parameters and its surroundings (for contaminant inspection) will help us to exclude false alarms and will optimise the follow up strategy. It will also allow us to get a first estimate of the size of the planet, e.g. to allow to rank planet candidates before starting follow-up observations.

The PIC will serve to: i) select the optimal PLATO fields; ii) select all appropriate $>F5$ dwarf and subgiants (samples P1-2 and P5), and M dwarfs (sample P4) within them; iii) characterise as much as possible the selected targets, i.e., estimate their temperature, gravity, variability, metallicity, binarity, chromospheric activity etc.; iv) provide a list of neighbours that contaminate the target star flux; v) give a first estimate of the transit object radius; vi) optimise the follow-up strategy. Pre-launch characterisation of PLATO targets will provide us with the basis for an initial statistical analysis of planetary system properties on a large scale.

The building of the PIC will require the assembly of information from very different input catalogues on a wide range of targets (from mid-F to M-dwarfs and subgiants). The main source for the PIC will be *Gaia* early, intermediate, and final release catalogues. A parallel survey of available photometric, spectroscopic catalogues and other databases for the assessment of target activity and neighbour star properties will complement the *Gaia* data. The analysis of additional catalogues, which has already started, can also be used as a backup for the PIC target selection and characterisations in the case of delays in the publication of the *Gaia* catalogues. We have demonstrated that available and forthcoming catalogues are sufficient to select all the PLATO samples (P1-P5), and to provide us with their very basic parameters, assuring the success of PLATO mission, independently from the *Gaia* performances. Surveys like LSST, PanSTARRS, SkyMapper, VISTA, LAMOST, are in any case of fundamental importance for complete target characterisation, and for the exploration of neighbour star properties.

6.1.1 Statistical analysis of available stellar catalogues

A first approach to the target/field selection is the statistical analysis of the existing catalogues. For each star down to the PLATO limiting magnitude (that is $V < 13$ for the P5 sample, and even fainter for the P4 sample), we must assign at least a luminosity class and spectral type as a minimal task. No suitable all-sky catalogs of stellar parameters exist for this task. We reviewed all main available photometric and astrometric catalogs for their potential of the minimal task of telling field dwarfs from giants, and the related stellar classification techniques. We assessed the completeness and contamination level of some published databases of FGK dwarfs (Ammons et al. 2006; Ofek 2008; Belikov & Röser 2008; Pickles & Depagne 2010), mostly based on 2MASS and Tycho-2 and therefore limited at the faint end by the photometric and astrometric errors of Tycho-2. As both the completeness and the classification accuracy of those databases fade rapidly in the magnitude range $10 < V < 11$, we constructed a new all-sky database (Nascimbeni et al. 2016) of FGKM dwarfs (UCAC4-RPM) by applying the reduced proper-motion technique to the UCAC4 catalog and using the RAVE spectroscopic catalog as a calibrator. We found that a merge of the Tycho-2 catalog at the bright end ($V < 10$) and our UCAC4-RPM at the faint end ($10 < V < 13$) is suitable to our purposes. The fraction of false positives (mostly field red giants) at $V \leq 11$ is about 18%, measured by cross-matching the UCAC4-RPM catalog with RAVE. The fraction of true negatives missed by UCAC4-RPM is

very similar (15%), thus the UCAC4-RPM estimate of the number of PLATO targets is expected to be a good approximation of reality. UCAC4-RPM counts are also consistent with Galactic model predictions.

UCAC4-RPM gives an all-sky average of 0.28, 9.4, 72 stars per deg^2 at $V < 8.2$, $V < 11$, $V < 13$ respectively, with a gradient along Galactic latitude which is negligible at the bright end (isotropic sample) and of a factor of at most $\sim 2-3$ at $V = 13$ (Figure 6.1).

As for the P4 sample (M dwarfs down to $V \sim 15-16$), the Besancon model provides us with a reliable estimate of the number of M0-M9 dwarfs per deg^2 as a function of the V limiting magnitude: $\log(N) = 0.504 \cdot V - 7.173$. Such a sample is limited within a very small volume of the Galaxy, so it is essentially isotropic (no particular reddening problems). This translates into a reliable estimate of the number of M dwarf stars expected per Plato FOV (2232 deg^2) of $\sim 5,200$ for $V < 15$ and $\sim 16,500$ for $V < 16$. Taking into account the analysis in Nascimbeni et al. (2016), there is an uncertainty of $\sim 20\%$ to be associated to the above numbers.

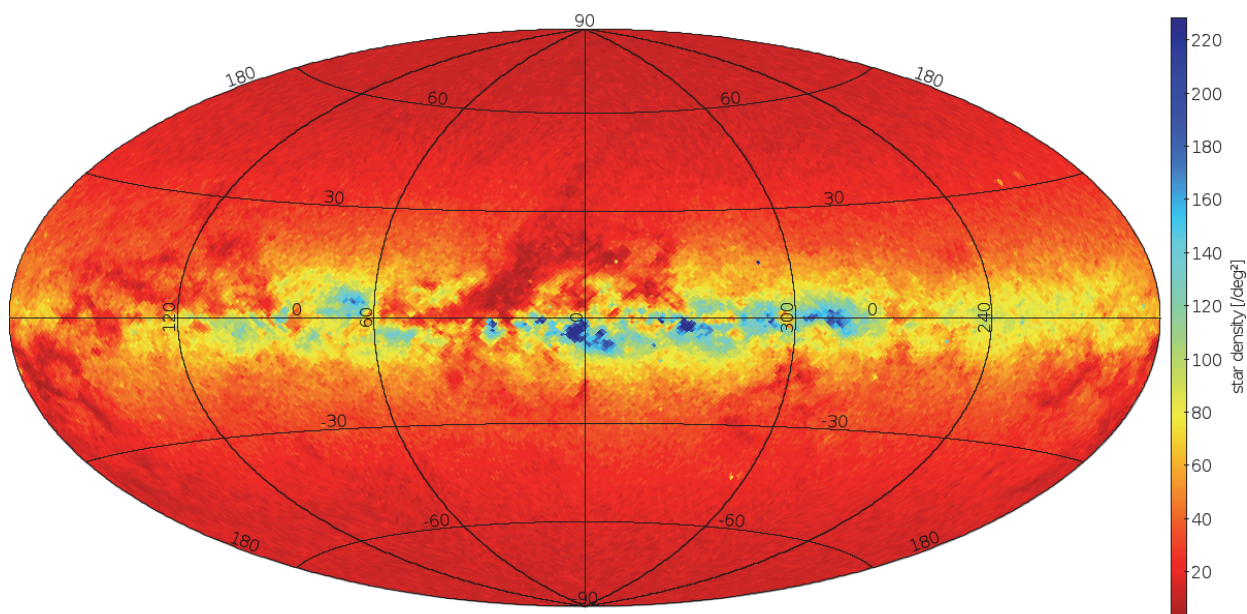


Figure 6.1: All-sky chart of $V < 13$ dwarf and sub-giants later than F5, from the UCAC4-RPM catalogue (Nascimbeni et al. 2016). Areal density is linearly color-coded from 30 deg^{-2} (pure red) to 80 deg^{-2} (pure yellow) and 220 deg^{-2} (deep blue). Star density varies within a factor of 2-3 as a function of Galactic latitude, as predicted by Galactic models, except for a few regions at $|b| < 5$ with extreme amounts of crowding and/or interstellar extinction.

6.1.2 Reddening analysis

PLATO targets are located close to the Sun. At the limiting magnitude of sample P1 ($V = 11$), the brightest (F5) stars can be observed out to ~ 300 pc (~ 200 pc for the G0 stars). For a magnitude limit at $V = 13$ the limiting distances increase by a factor 2.5. It is very well known that the Sun is located in a local bubble, with a radius of about 150-200 pc (Lallement et al. 2003; Vergely et al. 2010) where the reddening is negligible. At increasing distances the reddening increases, depending on the specific directions. An estimate of the reddening from all sky survey of the Holmberg Geneva-Copenhagen Catalogue (2009) shows that it remains very low [$E(B-V) < 0.02$] out to 300–400 pc from the Sun. This distance includes basically all targets limited to $V=11$ and the influence of the distance from the Galactic plane is marginal. This guarantees that, even independently from *Gaia*, samples P1 and P2 can be selected from available catalogues with a reasonable completeness and low contamination level.

The reddening between 400 and 800 pc (corresponding to the deeper P5 samples) can be determined from other distance-limited reddening maps, typically obtained measuring individual bright stars, such as those published by Neckle and Klare (1980). These maps show that, in general, the reddening rapidly increases just before 1 kpc, in agreement with the average values obtained by infrared measurements of Marshall et al. (2006). A consequence of this analysis is that the rapid increase of the reddening beyond about 1 kpc can be used for a colour separation of much more distant, contaminating sources, such as bright giants, enabling us

to select P1, P4, and P5 samples from available catalogues (UCAC4 and 2MASS) minimising the contamination by bright giants.

6.1.3 Field selection and field content

The two long-duration PLATO fields will represent the core of the mission. Observational constraints require that the centres of both long-duration fields lie within two “allowed regions” defined by an ecliptic latitude $|\beta| > 63^\circ$ (R-SCI-050). Both these two regions, one in the northern and one in the southern hemisphere, are symmetrically located at high declinations ($|\delta| \gtrsim 40^\circ$), include the celestial poles, and are tangent to the Galactic plane in two points at $l \sim 276^\circ$ and $l \sim 96^\circ$, respectively. The allowed regions are only slightly larger ($\sim 2,750 \text{ deg}^2$) than the PLATO FOV, but the R-SCI-050 constraint holds only for the centre of the field. It is easy to verify that the sky area covered by the envelope of every possible long-duration field is huge: about 40% of the whole sky.

The choice of the long-duration fields should be driven by i) the fulfilment of the requirements concerning the number of observable targets for all five P1-P5 samples, with emphasis on the maximisation of the P1-P2 samples; ii) the minimisation of the rate of expected astrophysical false positives due to crowding, above all from blended eclipsing binaries. The scientific requirements on stellar counts are met within the estimated uncertainties for every PLATO field choice centred at $b < 45^\circ$. On the other hand, both the number of expected false positives and the number of nearby dust clouds rise steeply for $|b| < 30^\circ$. The best trade-off strategy is then to select fields centred at about $|b| \sim 30^\circ$. As for the Galactic longitude, we note that the regions at low declination ($|\delta| < 60^\circ$) are, on average, less affected by interstellar extinction (as shown by the dust maps). Also, low-declination regions have the advantage of more efficient observations for the ground-based follow-up phase. A proposed conservative choice (to minimise contaminants, still satisfying the scientific requirements in terms of target numbers) for the long-duration fields is:

- 1) ($l = 253^\circ$, $b = -30^\circ$) for a Southern Plato Field (SPF) and
- 2) ($l = 65^\circ$, $b = 30^\circ$) for a Northern Plato Field (NPF; see Figure 6.2).

These fields are approximately centred on Pictor (South) and Lyra/Hercules (North) constellations. The northern field includes the *Kepler* field on a corner. An additional, thorough study of the contaminant problem will allow us to verify whether the field centre can be moved to lower Galactic latitudes ($|b| \sim 25^\circ$), thus potentially increasing the number of targets. We also provisionally defined ten additional step & stare fields (SS), all centred at $b = +30$ and -30 and equi-spaced along the Galactic longitudes. They are named STEP01 to STEP10, and plotted on an Aitoff projections on Figure 6.2.

A detailed geometrical model of the PLATO field, combined with full implementation of the PSSR noise model with 24 N-CAM telescopes at end of life and with UCAC4-RPM as input catalogue, provides us with a reliable estimate of the stellar counts for the P1 and P5 samples (listed in Table 6.1). As for the P4 sample, the estimate comes from the statistical analysis mentioned in Section 6.1.1. We note that the target fields proposed here serve for purposes during the design phase of the mission and demonstrate that field exists which allow us to fulfil PLATO’s science goals.

6.1.4 Target selection and characterisation from *Gaia* catalogue

The *Gaia* all-sky survey, launched in 2013, will monitor astrometrically, photometrically, and, in part, spectroscopically, during its 5-yr nominal mission lifetime, all point sources with $6 < V < 20$, and will generate a huge database encompassing $\sim 10^9$ objects. Using the continuous scanning principle first adopted by *Hipparcos*, *Gaia* will determine the five basic astrometric parameters: two positional coordinates α and δ , two proper motion components μ_α and μ_δ , and the parallax π for all objects, with end-of-mission astrometric precision between $7 \mu\text{as}$ (at $V = 6$) and $200 \mu\text{as}$ (at $V = 20$). The precise determination of fundamental stellar parameters by *Gaia* will be instrumental to identify bright, nearby cool F-, G-, K-, M-dwarfs and sub-giants across the huge sky region covered by the PLATO fields.

During the implementation phase, the first objective will be to coordinate the analysis of all available information (astrometric, photometric, and spectroscopic) from *Gaia* early, intermediate and possibly final release catalogues. This will provide well-classified nearby dwarf/sub-giant stars from which to choose, in order to populate the PIC, ahead of launch. To this end, a collaboration agreement has been established between the PLATO Mission Consortium and the Data Processing & Analysis Consortium (DPAC) of the *Gaia* mission (www.rssd.esa.int/gaia/dpac), responsible for the preparation of the data analysis algorithms to

reduce the astrometric, photometric, and spectroscopic data. The analysis of the first simulations, provided by DPAC’s Coordination Unit 2 (CU2), indicates that a “clean” sample of main-sequence dwarfs later than F5, with only $\sim 1\%$ “contamination” from cool giants, can be selected with simple cut-offs in distance and reddening-corrected absolute magnitude in the *Gaia* main photometric pass-band MG. This was the result of the exquisite precision estimates of *Gaia* parallaxes ($\ll 1\%$ uncertainty for all potential PLATO PIC targets), based on detailed error models, taking into account the selection of specific gate schemes in order to avoid saturation on bright ($V < 13$) stars. The contaminants can be reduced to a negligible fraction ($\sim 0.1\%$), using the information on effective temperature T_{eff} and surface gravity $\log(g)$ from *Gaia* spectro-photometry, which will be accurate to $\sim 200\text{--}300$ K and $0.2\text{--}0.3$ dex, respectively, for bright stars ($V < 14$).

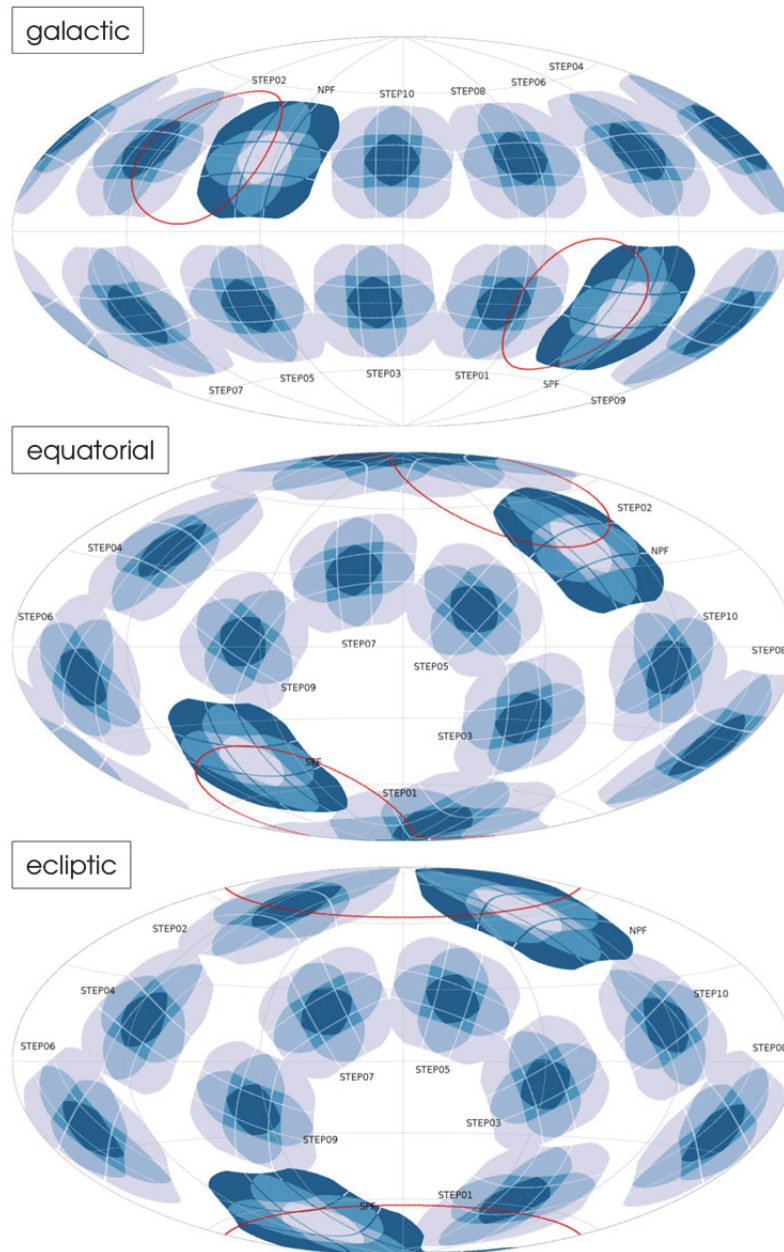


Figure 6.2: Aitoff projections of the two preliminary LD fields (SPF, NPF) and ten step-and-stare fields (STEP01–STEP10), all centred at $|\beta| = 30^\circ$, in the Galactic (upper plot), equatorial (middle), and ecliptic (lower) reference frame. The red line is the LD pointing requirement limit at $|\beta| = 63^\circ$. The LD fields are color-coded on an inverted scale.

Table 6.1: Estimated P1-P5 stellar counts from the UCAC4-RPM catalogue.

nominal EOL 24t, current design, updated FOV

	P1	P5	P5 V<11, 34<s<80	P5 V<13, s<80	P1+5 V<11 s<80
SPF	6,896	173,543	14,622	40,283	21,518
NPF	6,191	148,908	14,152	39,039	20,343
STEP1	6,242	178,112	14,651	39,447	20,893
STEP2	6,446	127,063	12,913	35,719	19,359
STEP3	5,769	153,505	13,220	35,969	18,989
STEP4	5,908	146,181	12,743	35,248	18,651
STEP5	6,219	160,394	13,699	38,564	19,918
STEP6	6,339	153,900	12,961	35,923	19,300

At fainter magnitudes, and especially for the analysis of contaminants, ground-based surveys will be highly complementary to *Gaia*. *Gaia* is going to deliver exquisite astrometry and monochromatic fluxes down to $V \sim 21$, but its two-channel spectro-photometer BP/RP is limited by blending to $V \sim 15$, where, instead, forthcoming surveys like LSST will deliver reliable multi-color photometry with a single-visit limiting magnitude of $r < 24$. Upon release of the *Gaia* early and intermediate release catalogues, in-depth investigations of the quality of *Gaia* astro-spectrophotometric measurements will be carried out for both “primary” stars included in the core data analysis (processed by CU3) as well as for stars showing hints of variability (processed by other CUs). The reassessment of *Gaia* performance in astrometry, photometry, and spectroscopy on bright stars of interest for the PIC until the publication of the final *Gaia* catalogue (ca. 2022).

6.1.5 PIC target characterisation

After field selection and the identification of the targets to be observed with PLATO, we will focus our attention on the determination of the target properties. A thorough astrophysical characterisation of the PIC target stars will help, for example, minimising false positives, and the optimisation of expensive, time-consuming follow-up work. The target characterisation will normally involve the determination of a complete set of stellar parameters (e.g. distance, proper motion, magnitudes, T_{eff} , surface gravity $\log(g)$, metallicity [M/H], extinction, stellar activity, age indicators) for each PIC entry. This, combined with information on binarity/multiplicity and/or the presence of planetary-mass companions (likely available at the level of *Gaia* intermediate data releases), will also allow for detailed prioritisation of the PIC targets.

The principal source of target parameters will be the *Gaia* catalogues. Cross-matching of other catalogues will help to complete target characterisation. The level of magnetic activity will be collected from available catalogues in the literature and archives (e.g. X- rays, UV emission lines, CaII H&K indices, H-alpha EWs) in order to define subsamples of stars with different activity levels. Recalling that high magnetic activity is an indicator of youth, choosing stars having different activity levels will allow us to investigate the properties of planetary systems in an evolutionary contest. The identification and analysis of photometric contaminants requires very deep limiting magnitudes (even very faint contaminants at $V > 21$, if variable, risk mimicking a planetary transit on a P1–P5 target). We will exploit existing wide-field catalogues such as the SDSS and forthcoming ground-based survey such as LSST, SkyMapper, PanSTARRS.

Archival spectra of PLATO targets will also be used for characterisation. Dedicated surveys for further characterisation will be considered. Small aperture telescopes equipped with suitable narrow-band filters might provide reliable temperature and gravity for PLATO targets in a limited amount of time, and will be used where appropriate.

6.2 PLATO ground-based follow-up observations

After identification of a planet candidate, ground-based follow up observations are needed to confirm and characterise the planetary nature of the companion. In fact, for most candidates accurate masses can only come from spectroscopic radial velocity observations since accurate masses from transit timing variations (TTVs) require co-planar planetary systems which will form only a small sub-set of PLATO detections. To ensure the determination of planetary masses for the most interesting PLATO planets (the core sample with

bright host stars), the mission includes an organised ground-based follow-up campaign (see Section 8.4.7). The team performing these observations (GOP Team) will be subject to an open call by ESA. The GOP Team will organise their respective telescope resources. For the purpose of a feasibility study in terms of available telescope resources to European astronomers, the PMC has made an estimate about the required resources during Phase B1 presented here. Later on, the GOP Team selected by ESA may be able to raise even larger resources, e.g. by including non-European resources which are not considered here, and/or by prolonging the follow-up over a time period longer than what is assumed here as part of the PLATO mission duration.

In general, the ground-based follow-up observations are divided into two kinds:

- 1) Observations designed to detect false positives (filtering observations).
- 2) Observations needed to characterise the planetary orbit (radial velocity observations).

The filtering observations will be mostly carried out on existing relatively small telescopes while the radial velocity (RV) observations will need the best and most stable instruments coupled to our premier telescopes. Hence, the importance of an efficient filtering campaign cannot be over stated. Intuitively we would also expect that the time required with our largest telescopes will be dominated by observations of the smallest (and presumably lightest) planets.

6.2.1 Filtering observations: the elimination of astrophysical mimics

Astrophysical false alarms, mainly due to eclipsing binaries, were shown to outnumber true transiting planets in ground-based and space-based photometric surveys for planets. In the case of PLATO, this problem is minimised by the brightness of the targets (i.e. Santerne et al. 2013). Complementary techniques are also foreseen in the PLATO project to identify astrophysical false alarms from the detailed analysis of light curves, the analysis of centroids to identify blended eclipsing binaries, the comparison of transits at different colors from the fast cameras, as well as the photometric, high resolution imaging, and spectroscopic ground-based follow-up observations. Experience gained by *Kepler*, K2, CoRoT and TESS missions will be extremely valuable for the removal of false positives (e.g. Torres et al. 2011; Díaz et al. 2014; Santerne et al. 2015).

False-positive rates depend on the set-up of the transit survey considered (PSF size, sampling, etc), on the characteristics of the host stars (e.g. magnitude, position with respect to the galactic plane, activity level, etc), and probably on the type of planets considered (radii, period). For *Kepler* the number of false positives remaining after a careful analysis of the precise light curves has been estimated by Fressin et al. (2013) to be about 10%. It's worth noting that the false alarm rate from *Kepler* candidates is still somewhat controversial (Santerne et al. 2016). Understanding the PLATO false-alarm rate is not straightforward as, while the availability of detailed preparatory data from *Gaia* and TESS would certainly act to improve the initial target selection, the large PLATO PSF would work in the opposite way. Given this uncertainty, we chose an extreme value of a factor ~ 2 for our estimate (i.e., there are as many false positive cases as planetary systems). For the P1 and P5 samples we estimate some ~ 1200 planets with host star brightness $V \leq 11$ – sufficient for RV follow up – considering the baseline observing scenario with two long-duration pointings. Of these some ~ 770 have radii $< 2 R_E$ and could be rocky in nature and maybe ~ 120 are in the habitable zone of their host stars – the main targets for PLATO. This estimate increases to ~ 2700 (~ 1800 small planets) for an alternative observing scenario with 1 long-duration pointing and 6 step-and-stare pointings. Hence, being conservative, we may expect to filter some 5000 candidate transits over the nominal mission.

A typical set of filtering observations on stars of this brightness could be:

1. Low-precision spectroscopy (1–2m telescopes), 3×20 min (including overheads).
2. High-resolution imaging (e.g. lucky imaging on 2m telescopes), taking 30 min per target (including overheads).
3. On and off transit photometry (1–2m telescopes), 2×20 min (including overheads)
4. High-resolution spectroscopy (HARPS like instrument, 4m telescopes), 3×20 min (including overheads).

5. Rossiter-McLaughlin (RM) observations (ESPRESSO like instrument, 8m telescopes) for the smallest objects in the HZ: 10h per target (including overheads). In special cases, for the faintest targets, the E-ELT + a HIRES-type instrument would be needed.

This is a maximum set of observations per target and is illustrated in Figure 6.3.

During the process, false-alarms are identified and the number of targets for the respective next filtering steps reduces. The process should lead at the end at losing half of the candidates, according to our initial hypothesis. As a first “working” guess, we conservatively chose that (see also Figure 6.3)

- 20% of the candidates will turn out to still be binaries undetected by the light curve vetting when doing moderate precision RV observations (Step 1), i.e. 80% of the candidates will still be going down the list,
- 50% of the candidates will have a companion within the PSF with magnitude difference smaller than 4 in the PLATO PSF (Step 2), requiring then on-off photometry (Step 3), and that in 50% of the cases, the transit will be a diluted one (deeper transit on the companion),
- 25% of the small planets on long period orbits will have an activity level (Step 4) allowing for credible RM effect to be observed (see below).

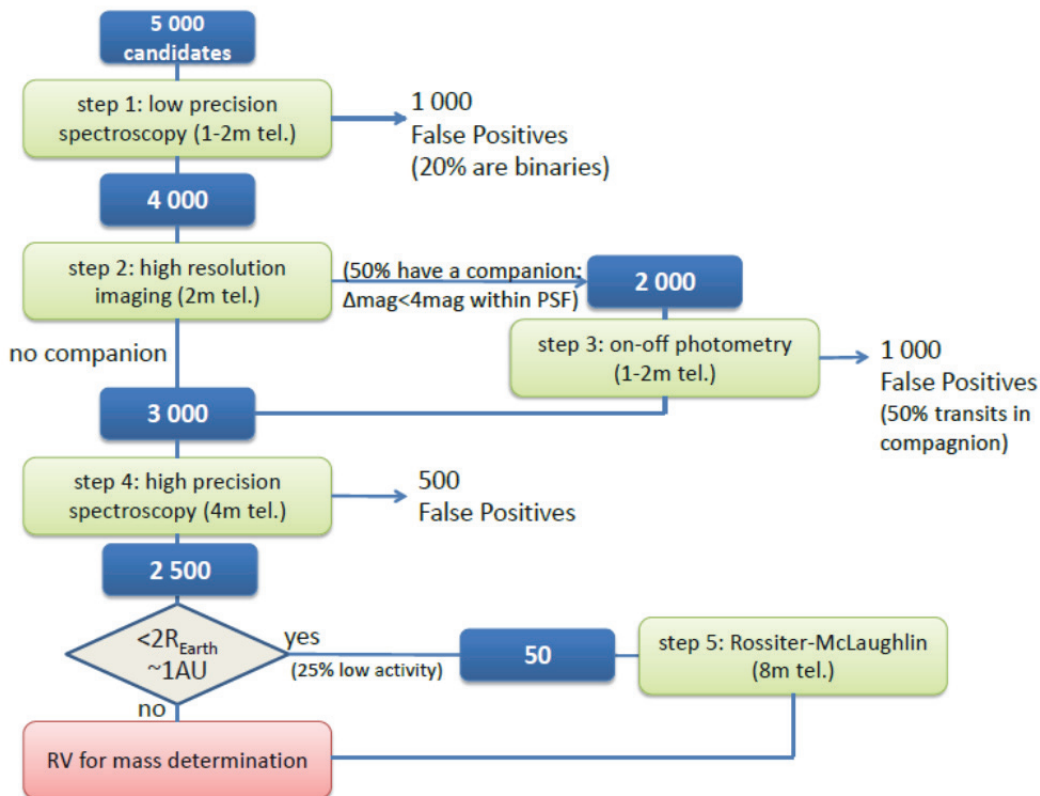


Figure 6.3: An example filtering strategy for PLATO targets with expected success rates for each type of observation. Starting from ~5000 candidates we would expect to recover ~2500 candidates.

We note that additional filtering methods (e.g. PLATO centroids), are not considered here. Furthermore, many of the contaminating targets will be known from *Gaia* allowing further optimisation of the filtering process.

Overall this would require some 835 nights spread over several years on 1–2m telescopes and a further 300 nights with 4m telescopes. Nominally an additional 50 nights of 8m telescope time would be needed for the RM observations but we expect few transits of these longer period systems will be accessible to our 8m telescopes as the likelihood of transits being well placed for observation from a specific location are slim. For the baseline observing scenario of two long-duration pointings, the required number of nights for filtering observations is half of the above values, as given in Table 6.2.

6.2.2 Optimisation of the radial velocity follow-up

The mass of the planet candidates is determined through a Keplerian modelling of the observed radial-velocity variation of the central star. The number of observations required for the mass determination, at a given precision, depends on the precision of the measurements, on characteristics of the star, and on planet parameters. In order to make the description “uniform” with regard to the mentioned parameters, a convenient approach is to suppose that the planet mass will be characterised when we have gathered 20 “phase points” along the orbit. Such “phase points” can be individual or binned measurements. Their “cost” (integrated telescope time to obtain them) and “efficiency” (actual equivalent precision of the binned radial velocities) will then depend on:

- the planet orbital period: possible size of the bin cannot be bigger than $P/20$ if we want 20 points in phase to describe the orbit;
- the planet mass;
- the precision of individual radial-velocity observations. This includes instrumental precision, photon noise and intrinsic stellar effects (granulation, activity, etc). Note here that below a few tens of cm/s this is completely dominated by stellar effects and thus the instrumental intrinsic precision is of secondary importance.

6.2.2.1 “Equivalent-precision” radial velocity measurements: beat the noise by “brute force”

Instrumental stability of new-generation, high-resolution spectrographs is at the level of cm/s (ESPRESSO: <10 cm/s) to tens of cm/s (HARPS: 50 cm/s). In order to fully take advantage of these instrumental capabilities the photon noise level has to be achieved, i.e. more stable instruments are installed on larger telescopes. For example, typical photon-noise benchmarks for the ESPRESSO on the VLT are 10 cm/s in 15 min for a $V=8$ star, or 20 cm/s in 1 hour for a $V=11$ star.

The same level of precision cannot be reached for all stars due to various sources of stellar intrinsic limitations: brightness, spectral type, luminosity class, and especially activity level. Usually, the stellar contribution to radial-velocity uncertainties is dominated by activity-related effects. Stellar oscillations and granulation are expected to contribute at the level of a few tens of cm/s, even for quiet stars. This is a serious concern for mass determination of low-mass planets on longer-period orbits, but, although stellar noise is the major limitation on very high precision Doppler measurements, adequate observing strategies help mitigate its effect down to the required “equivalent precision” necessary to detect Earth-mass planets in the habitable zone of G dwarfs (Dumusque et al. 2011a,b). Note that slightly more massive planets or similar-mass planets around later type stars will much easier to characterise.

For low activity level (most suited for Earth-type planets), the observed combined effect of the different stellar “noises” has been estimated through simulations drawn from real HARPS asteroseismology data (for oscillations and granulation, i.e. for timescales up to ~ 1 day) and from the modelling of families of spots on the star surface for different spectral types and various level of stellar activities⁶. These results are discussed in detail in the Definition study documentation, but demonstrate that even for the lowest mass planets the required accuracy can be achieved by averaging sufficient radial velocity measurement (“equivalent RV precision”) and still maintaining sufficient orbital phase resolution.

For the quietest stars an “equivalent precision” as low as 7 cm/s can be obtained. It however degrades when the activity level goes up. We do not currently know which stars PLATO will actually observe, but we assume their activities levels follow those in the solar neighbourhood drawn from the HARPS GTO volume-limited sub-sample. The distribution shows that 24% of the stars have $\log(R'_{\text{HK}}) < -5.0$ (non-active Sun) and 50% are less active than the average Sun ($\log(R'_{\text{HK}}) = -4.9$).

⁶ We implicitly suppose here that there is no significant stellar noise with timescale between the rotational period of the star and 1 year.

6.2.3 Organisation of the ground-based follow-up

6.2.3.1 Required telescope time for planet mass determinations

From the information on the planet yield, the cost of “equivalent precision” radial velocities, and the distribution of stellar activity in the sample, we can estimate the amount of telescope time required to measure the mass of PLATO candidates (Table 6.2). These estimates are based on a detailed study assuming:

- A distribution in planet masses and orbital separations based on *Kepler* results (Fressin et al. 2013). We however do not consider hot and warm Jupiters, since they are expected to be already well studied in ground-based surveys and with TESS.
- An ad-hoc number of required “phase points” for each considered planet mass to reach a given precision. This number is based on a very conservative experience gathered over the years in the framework of planet-search programmes at high precision.
- An adequate match of the binning used and the period of the planet.

A realistic spread between different telescope sizes for a given planet category has been used. Observing facilities and observing strategy are selected in order to match required precision and photon-noise limits.

Table 6.2: Estimates of ground-based telescope resources needed for follow up of planet candidates discovered during the PLATO Long-duration Observation Phase in both hemispheres.

Telescope Class	Filtering/Candidate Confirmation		Radial Velocity Measurements		Total Nights
	(nights/year)	(Total nights in 7 years)	(nights/year)	(Total nights in 9 years)	
1-2m low-resolution spectroscopy	~35	~245	-	-	~245
1-2m high-resolution imaging	~15	~105	-	-	~105
1-2m on-off photometry	~10	~70	-	-	~70
1-2m high-resolution spectroscopy			~3	~30	~30
4m high-resolution spectroscopy	~20	~140	~100	~900	~1040
8m high-resolution spectroscopy	~5	~35	~80	~720	~755

Note 1: The time spans of 7 years for the filtering observations and of 9 years for the radial velocity observations are assumptions based on estimates of available telescope resources.

Note 2: The numbers reported in the Table are global for northern and southern sky visibility.

It is worth noting that while we have been conservative in our analysis, there is much on-going theoretical and observational effort to understand the effects of activity signals on photometric and radial velocity measurements. There have already been some successes in correcting for activity albeit only in the case of the most massive planets (e.g. Hébrard et al. 2014; Bruno et al. 2016). The situation by 2025 is likely to be much improved.

6.2.3.2 Strategy for ground-based follow-up observations in view of available telescope resources

The PLATO mission is an effective planet survey, detecting hundreds of small planets and thousands of larger planets. Measuring planet masses for the full sample of expected PLATO planets around bright stars requires a significant amount of telescope time. A complete census of the sample will need a world-wide-

effort. Here we discuss the strategy by which this goal can be achieved, taking into account a realistic estimate of available telescope resources.

To characterise all planets for their masses is a huge effort limited by several factors:

a) Magnitude of the host star

Based on experience of existing RV spectroscopy instruments, determining planet masses for small planets is limited to bright host stars ($V \leq 11$).

b) Activity of the host star

In recent years, RV spectroscopy data have shown that stellar activity is a limiting factor for planet mass measurements. In particular for the smallest planets only the quietest stars will allow us to determine accurate masses.

c) Available telescope resources

The required telescope resources require 1 – 8m class telescopes.

d) Time period for which RV follow-up can be performed

This is not a strict limit, because in principle scientifically interesting targets can and will be followed by the community over the time it needs to answer the science question investigated. For the sake of dimensioning the resources for the PLATO space mission, however, the RV follow-up is limited to 9 years (up to 5 years after end of observations). Targets not completed in that time interval will become part of the PLATO legacy.

The smallest planets will benefit from ground-based follow-up observations starting after one transit (this will be challenging). Obtaining spectroscopy while the spacecraft is obtaining photometry seems one of the best methods to mitigate stellar activity.

We assume that filtering observations are spread over 7 years. For the long-period planets (up to 1 year), additional telescope time is required to determine their masses. Mass determination therefore continues in years 8 and 9 after launch.

The number of nights given in Table 6.2 are total estimates and need to be distributed among different observatories. The distribution of PLATO fields in the northern and southern hemisphere naturally leads to a differentiation on the required time.

In view of the large total telescope resources needed to determine planet masses for all host stars with $V \leq 11$, a strategy is needed which keeps the effort within reasonable limits for existing and future observatories/instruments but still delivers the PLATO science. We suggest proceeding in steps:

1. Focus on a sample of PLATO's unique planet parameter space, guaranteeing the maximum scientific return, taking into account the limiting factors a) and b) above.

We point out that PLATO addresses a very broad range of science areas and “maximum science return” therefore cannot be obtained by considering a certain sample of planets defined by simple criteria such as host star brightness, orbital distance, planet size, etc. This means we expect that individual objects of high scientific interest will be investigated for all kinds of star/planet combinations. Here we simplify to a discussion of “samples” for the sake of dimensioning the follow-up resources.

2. For a sub-sample of planets obtain PLATO telescope resources from major European observatories, namely ESO and La Palma.

This sample shall be large enough to ensure the main science objectives can be reached at a minimum level.

3. Enlarge the sample of planets with determined masses by obtaining time at smaller European observatories and with teams with guaranteed telescope time available.
4. Enlarge the RV follow-up effort beyond Europe by including international observatories/teams.
5. Remaining planets, not cleared in the 9 years PLATO observation+RV period, become part of the PLATO legacy and can continue to be studied by the international community in the years to come.

This strategy leads to essentially 80% of the best targets down to Super-Earths (~200 planets) being characterised. Earth mass planets are by far the most difficult case (even a 2–3 M_E planet would be much easier to obtain radial velocity information on) and our observations are limited by the availability of an ESPRESSO like instrument on 8m class telescopes. None the less our success rate is already about 50% for longer period planets from ESO (keeping in mind that max ~60% can be reached from one hemisphere only). This improves to about 80% if a similar facility becomes available in the northern hemisphere. *This should be seen against the backdrop that we do not expect to have any radial velocity information for any similar systems before the launch of PLATO.*

If planets in the step-and-stare phases are also be considered, then additional resources need to be added. We note, however, that after NASA's TESS mission and respective follow-up program a large fraction of short-period, hot, planets will already have RV data available at the time of PLATO launch. Adding the full sample may therefore significantly overestimate the needs for PLATO.

Note: We do not yet consider the P4 stellar sample of M dwarfs here but note that optimised facilities are available specifically for these objects (e.g. CARMENES), and should be continued until after PLATO launch.

Page intentionally left blank

7 Mission performance

The main scientific goals of PLATO concern the detection and characterisation of extrasolar planets for their radius, mass, and age. PLATO’s ‘Rosetta stone targets’ will be the small planets, in particular those which orbit in the habitable zone of solar-like stars. They need to be characterised with high accuracy (3% in radius, 10% in mass and age). The total sample shall, however, also include a large number of characterised planets of all sizes at all orbital distances to provide substantial constraints to planet formation and evolution theories and place our solar system into a general context of planet evolution. To achieve these mission goals, the following parameters of science mission performance are important:

- The total number of **bright stars** which will be observed. This sample splits into three sub-samples:
 - P1 sample, which includes the ‘Rosetta stone targets’ of highly accurately characterised long-period small planets in the habitable zone of solar-like stars (see Section 3.4.2.1).

The required high accuracies for the P1 sample are:

- Radius: < 3% for an Earth-sized planet orbiting a G0V star with $V \leq 10$
- Mass: < 10% for suitably bright RV follow-up targets (assumed as $V \leq 11$)
- Age: 10% for a G0V star with $V \leq 10$
- P2 sample (see Section 3.4.2) which provides planets orbiting very bright stars ($V < 8.2$), whose atmospheres could be characterised by ground-based or space-borne facilities. It will allow for dedicated asteroseismologic studies of a wide sample of well characterised stars, needed to better calibrate stellar models.
- P5-bright sample, with lower SNR (P5 sample, see Section 3.4.2.1) observed in long pointings. This sample provides planet detections similar to what we know from NASA’s *Kepler* mission sample, but for stars brighter than magnitude 11, therefore allowing mass measurements from ground. Most of them will have lower accuracy in planet parameters than the P1 sample, but provide significant input into statistical analysis of exoplanet properties.
- The **statistical P5 sample** will be, as an added benefit, complemented by the faint ($V \leq 13$) targets in the long and short pointings. These targets provide additional light curves for exoplanet search. Planetary masses will be delivered with TTVs and RV for larger planets.

Our benchmark test for accuracies is therefore an Earth-sized planet around a Sun ($V=10$) orbiting with 1 year orbital period in the P1 sample. Obviously, accuracies will be better for planets with smaller orbital periods (more transits observed), brighter host stars (better SNR) and larger planets (larger transit signal). Here, we focus on the benchmark test to demonstrate the performance in the “most difficult case” scenario.

Furthermore, the final number of stars observed and resulting planet yield will depend on the observing scenario chosen within the 4 years science observation baseline (see Section 6.1.3). Our baseline observing scenario is a division into two long pointings of 2 years each. This scenario maximises PLATO’s unique science return, that is, small planets in the habitable zone of solar like stars. The PLATO mission is flexible enough to, e.g., stay one year longer on the first long pointing field if decided. In this case, the 4th year will be dedicated to a step-and-stare phase, maximising the statistics of well characterised short-period planets with PLATO (see Figure 2.3). The final baseline observing scenario concerning the share between long- and short-pointings will be decided two years before launch, but can also be adapted during mission operation to optimise the science return. In case an additional extended mission phase of 2–4 years can be granted, it is obvious that the planet yield will be extended enormously and it will be possible to maximise both, long and short periods, at the same time. However, the baseline of 4 years is sufficient to make PLATO a unique mission providing scientific results that no other exoplanet mission will be able to achieve before.

7.1 Instrument performance

PLATO aims at obtaining high precision, continuous time series of photometric measurements of a large sample of stars. The drivers for performance are the high **photometric efficiency** of the instrument (optics

transmission and vignetting, CCD quantum efficiency, CCD charge transfer efficiency, low particulate and molecular contamination) and the high **photometric stability** of the instrument (pointing performance, thermal stability).

PLATO’s noise requirements have been set to allow for the detection and characterisation of planets and stars with high accuracy (see Section 7.2). Figure 7.1 shows as example the simulated signal averaging three transits for our benchmark study case, an Earth around a Sun. It can be seen that an Earth can be detected already with a noise level of 80 ppm in 1 hour, whereas highly accurate characterisation requires 34 ppm in 1 hour as discussed below.

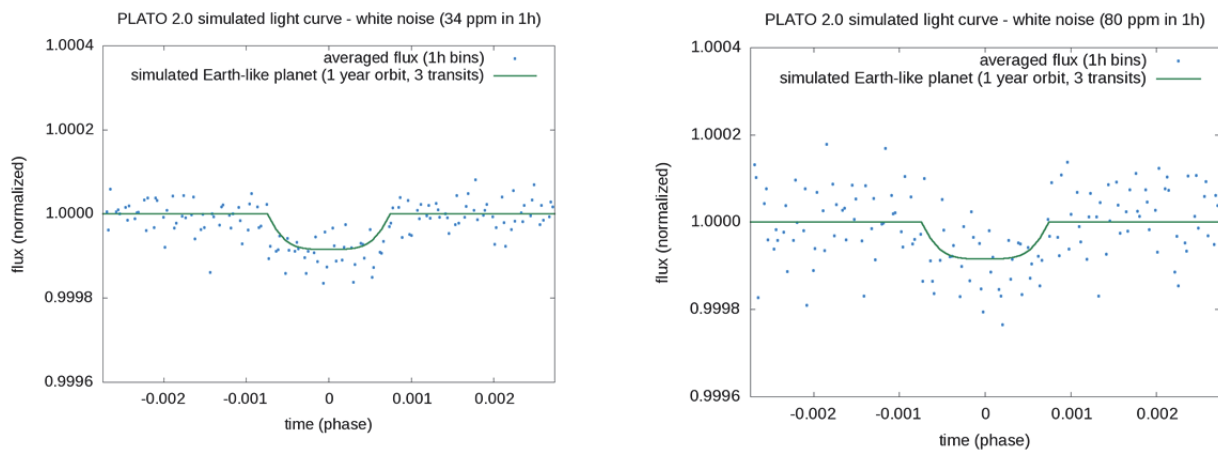


Figure 7.1: Benchmark light curves for planet detection with PLATO. The figures show data corresponding to 3 simulated transits of a planet with the size of the Earth orbiting a star with the size of the Sun in an orbit of 1 year period. Left, the noise level in the light curve is 34 ppm in 1h. Right, same with a noise level of 80 ppm in 1h.

The Noise-to-signal ratio (NSR) is therefore one of the key performance parameters of the PLATO instrument. It depends on a large number of optical and electronic instrument parameters, on the spacecraft, the mission operation and the stars themselves. Several complex software simulation tools were developed so far (and will be developed further) in order to understand and quantify the complete signal chain from the signal source to the data products.

NSR is mostly driven by instrument efficiency and various noise sources. Instrument efficiency reflects the ratio between incoming photons and resulting photoelectrons. It is mainly restricted by the transmissivity of the optics, the quantum efficiency and the charge transfer efficiency of the CCD. Some of these are impacted by aging effects, e.g. due to radiation in space, and therefore instrument and science performance studies have been quantified for efficiencies at different radiation levels.

The noise sources are dominated by the random noise whose largest contributor is photon noise from the target since PLATO points at bright stars. The systematic noise is dominated by changes of shape and position of the PSF in the focal plane. At the high frequency end the largest contributor is pointing jitter of the spacecraft. At the low frequency end the largest contributors are kinematic differential aberration and thermo-elastic deformations of the spacecraft. During Phase B1, it has been successfully demonstrated that these effects can be corrected efficiently by data processing.

7.2 Science performance

The anticipated high accuracy of planet parameters for PLATO demands a correspondingly high accuracy of stellar parameters. Planetary radii are measured as ratio to stellar radii, planet masses require knowledge of stellar mass and finally the age of a planetary system is deduced from the age of the host star. We therefore first demonstrate that PLATO can achieve the required stellar parameter accuracy and then discuss the corresponding planet parameters below.

7.2.1 Stellar parameters

The accuracy which can be obtained for the seismic determination of the ages, masses, and radii of solar-like stars has been assessed in Phase B1 taking into account the instrument noise budget. Involving a team of asteroseismologists, theoretical calculations, numerical simulations and a blind test ('hare-and-hounds exercise') have been performed to estimate the accuracy of stellar parameters that can be achieved today.

Figure 7.2 shows the relative age uncertainty for a solar-like star ($V=10$) at 6 Gyrs with end of life (EOL) instrument performance for 28 N-cameras (previous design) and 24 N-cameras (nominal design). At $V=10$, the age uncertainty for the reference star amounts to $<10\%$. These estimations consider only statistical uncertainties. There are systematic uncertainties that need to be evaluated on a case by case basis. However, available information from *Gaia*, PLATO lessons learned on stellar models, and ground-based facilities will certainly lead to a reduction of those systematic uncertainties. We have not considered systematic uncertainties for the theoretical calculations presented in Figure 7.2 but we do have considered them in the hare-and-hounds exercise (see Figure 7.3).

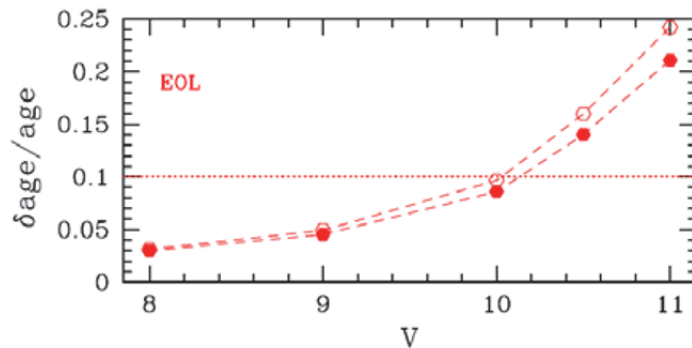


Figure 7.2 Relative random error (equivalent 1σ precision) for the age of the reference stars as a function of the apparent magnitude for 28 telescopes (filled dots) and 24 telescopes (open dots) for 2 years continuous observations.

Figure 7.3 shows the results of the hare-and-hounds exercise by five modellers for 2 years of PLATO observations for the instrument baseline of 28 N-cameras. The age uncertainties, including systematic uncertainties at the status of our knowledge today, are between 12% and 13% for stars of V magnitude between 9.8 and 10.2 for a stellar age of 6 Gyr. The results show that after correcting for systematic errors the PLATO age specification can be reached. The specification for the stellar mass and radius will be even more easily recovered. We do not expect a significant change of these results going to 24 N-cameras.

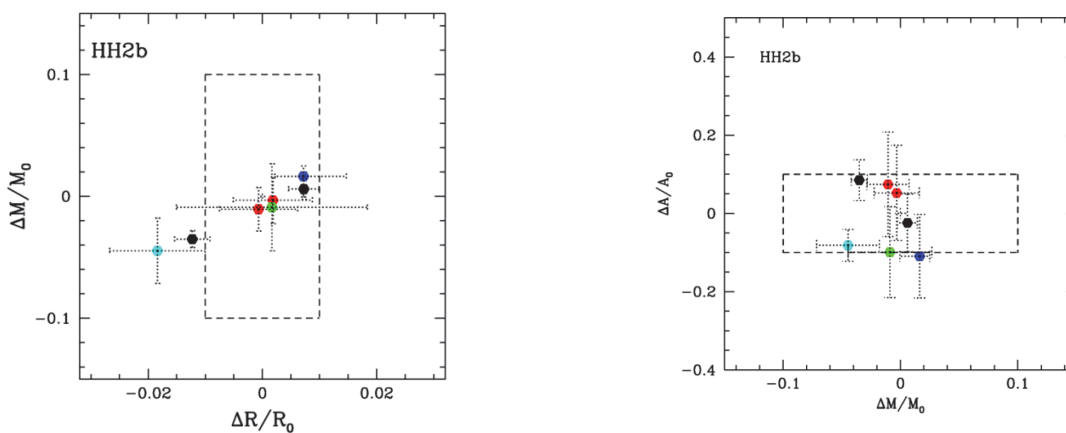


Figure 7.3. Results of seismic modelling for Hare-and-Hound exercise: relative differences for the stellar masses against radii on the left and stellar ages against masses on the right. The dashed box corresponds to the requirements specified for PLATO: 10% in stellar mass and 1% in stellar radius for a 'Sun' with $V=10$. Each colour corresponds to the results of one modeller.

7.2.2 Planet parameters

The transit depth provides the planet-to-stellar radius ratio. The scientific requirement for PLATO is to provide a radius accuracy of 3% for a G0V star of $V=10$, which means that the radius ratio needs to be obtained with 2% uncertainty. Whether this accuracy can be achieved has been studied with simulations of realistic noise-to signal ratios with 24 N-cameras EOL, including random and systematic noise sources. It is necessary to take the transit duration and number of observed transits into account, because the transit depth is measured from averaging several points, and multiple transits can be averaged to increase the SNR. We do not include the impact of stellar activity as we are testing instrument performance.

Figure 7.4 shows the expected uncertainty in the absolute planetary radius of an Earth-sized planet orbiting a G0V star as a function of the visual magnitude of the host star and the number of transits observed. For the calculation of the uncertainties, we assumed that a central (i.e. zero impact parameter) transit of an Earth-sized planet occurs around a quiet G0V star whose limb darkening law is known. The stellar density is assumed to be derived by asteroseismology, so the scaled semi-major axis (a/R_{star}) is known to 2% accuracy, while the stellar radius is known to 1%. It can be seen that, for the benchmark case of an Earth around the Sun, two transits are enough to achieve the required planetary radius accuracy for a $V=10$ mag star. For planets with shorter orbital periods more transits can be observed, improving the final accuracy. Larger planets will produce a larger signal for the same amount of transits, hence improving the final accuracy in the planetary radius.

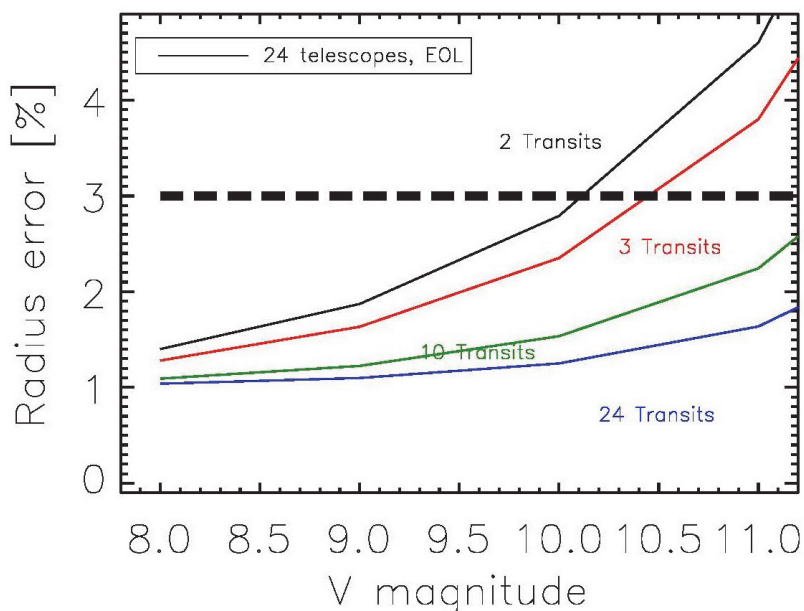


Figure 7.4. Uncertainty in the absolute planet radius as a function of the V magnitude of the reference star with 24 N-Cameras, EOL. The benchmark performance of 3% uncertainty is shown with a horizontal dashed line. See details about the simulations in the text.

The second important planet parameter relevant to characterise the planet mean density and hence constrain bulk compositions is the planetary mass. The mass is derived from ground-based follow-up observations obtained by high-resolution spectroscopy. We consider here only planets orbiting stars brighter than $V=11$, since for fainter objects such ground-based observations get too time consuming to be obtained on a larger sample.

The possible mass accuracy depends critically on instrumental and astrophysical noise. For an instrument like ESPRESSO at the VLT (ESO) the estimated performances are in the range of 1–10 cm/s, with 7 cm/s being the most frequently given estimate. Figure 7.5 shows the estimated mass precision for a range of stellar types with planets orbiting at the inner edge of the HZ. With the assumed ESPRESSO performance of 7 cm/s the required mass precision can be reached for (super-)Earths orbiting quiet solar-like stars. The final mass precision will of course be dependent on the actual performance of the ESPRESSO instrument. Intuitively, one may expect the radial velocity semi-amplitude to scale with stellar and planet mass, and orbital period,

so that the lowest mass planets around the highest mass stars in the longest period orbits are the most difficult to detect.

A planet with $1 M_E$ orbiting in the HZ of a solar type star represents one of the most difficult configurations to be encountered by PLATO. For this we have assumed a realistic observation strategy with yearly gaps in observation due to visibility and poor weather conditions. Other configurations (higher planet mass and/or shorter orbital periods) will be easier to solve. The final modelling strategy employed will be dictated by the actual performance of ESPRESSO, which will be known more than 5 years in advance of the PLATO launch in 2025.

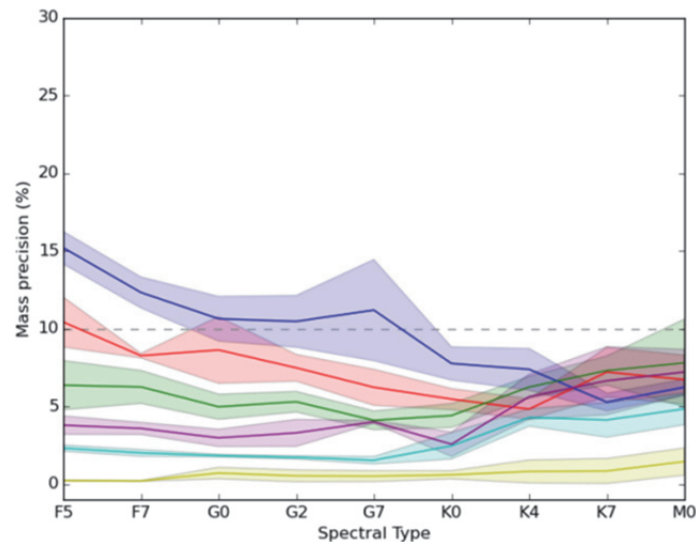


Figure 7.5. Planetary mass precision achievable for the inner edge of the optimistic HZ, as a function of the host star’s spectral type. The solid lines denote the median precision, while the shaded bands encompass the 1-sigma regions. Colours correspond to different input planet masses: $2M_E$ (blue); $3M_E$ (red); $5M_E$ (green); $10M_E$ (purple); M_{Nep} (turquoise), and M_J (yellow). The horizontal, dashed line denotes the PLATO science requirement of 10% for a G0V star.

7.2.3 Planet yield

To estimate the overall science performance of PLATO, the final yield of characterised planets needs to be known. We have estimated the yield based on the stellar sample sizes shown in Section 6.1.3, the baseline observing strategy and the current knowledge of the instrument performance. We first discuss the yield of planets in terms of detection and radius characterisation, and their suitability for asteroseismology studies (hence accurate age determinations). Then we discuss the yield when taking into account realistic estimates for ground-based follow-up observations to derive planetary masses.

7.2.3.1 PLATO Detections & Characterisation

One of the mission design drivers for PLATO is assuring the detectability of planets with the size of the Earth around stars with the size of the Sun in 1-year period orbits. For the P1 sample (< 34 ppm in 1 hour), the SNR of a single transit for an Earth-Sun analogue is 9 and 13 when integrating 2 transits. It is generally considered that a $SNR > 10$ guarantees the detectability of 100% of the transit signals (see Fressin et al. 2013, based on studies by Jenkins et al. 1996, 2010). A third transit event is beneficial to confirm the consistency of previous observations.

With a nominal mission duration of 4 years there are two possibilities for the observing strategy (see above):

- to observe 2 consecutive fields in a Long-Duration Observation Phase of 2 year duration each towards different directions on the sky, guaranteeing typically 2, and only in some favourable cases 3, transit events for planets in the HZ of Sun-like stars. This scenario is labelled (2+2) and is our baseline.
- to observe 1 field in a Long-Duration Observation Phase of 3 years duration, guaranteeing 3 transit events for planets in the HZ of Sun-like stars, followed by a step-and-stare phase with several

pointings of few months each. The step-and-stare phase allows us to obtain large statistics of short period planets in different regions of the Galaxy. We have considered 6 pointings of 2 months duration. This scenario is labelled (3+1).

The mission is being designed for an in-orbit lifetime of 6.5 years and a mission duration of up to 8 years is possible. If a mission extension is granted beyond the nominal science operations of 4 years, the additional time could be used, e.g., for the following scenario: 2 long-pointings with durations between 2 and 3 years plus a step-and-stare phase with a total duration of 1 year. This scenario is labelled (3+2+1).

The expected planet yields resulting from these 3 scenarios is given in Table 7.1.

Table 7.1. Expected planet yield for detection with PLATO. It includes planets around bright ($V \leq 11$) P1 stars which can potentially be fully characterised (asteroseismology and mass from ground) and fainter ($V \leq 13$) P5 stars, where the characterisation is limited. We show the planet yield for different observing scenarios.

	stellar sample	24 N-cam (2+2)	24 N-cam (3+1)	24 N-cam (3+2+1)
all planets, all orbital periods, $V \leq 13$	P1+P5	~4 600	~11 000	~13 000
all planets, all orbital periods, $V \leq 11$	P1+P5 bright	~1 200	~2 700	~3 300
small planets ($R < 2 R_E$), all orbital periods, $V \leq 11$	P1+P5 bright	~770	~1 800	~2 200
small planets ($R < 2 R_E$), in HZ, $V \leq 11$	P1+P5 bright	6 - 280	3 - 140	6 - 280

The planet yield is the result of the stellar population observed, the planet occurrence rate, the geometric transit probability, the observing strategy, and the detection efficiency:

- We consider here only the P1 and P5 samples, dwarf and sub-giant stars of spectral types between F5 and K7. PLATO can also detect transiting planets around giant stars, as *Kepler* did and TESS will do (see, for example, Lillo-Box et al. 2016; Campante et al. 2016), but here we concentrate on the planet yield for the solar-like samples.
- The planet occurrence rate and the geometric transit probability are imposed by nature and do not depend on instrument performance. The planet occurrence rates are taken from Fressin et al. (2013), except in the habitable zone. The planet occurrence rate in the habitable zone is still highly debated in the literature. Values found today range from 2% to 100% of solar-like stars hosting planets with the size of the Earth (up to super-Earths) in the HZ (see Winn & Fabrycky 2015 and references therein; Batalha 2014; Burke et al. 2015; Traub 2016, etc.). We consider a representative average value of 40% occurrence for Earth and super-Earth sized planets in the habitable zone for the P1 and P5 samples, but we also provide in Table 7.1 the values considering the expected range (2% to 100%) for the yield of small planets in the HZ around $V \leq 11$ stars. It must be understood that there are large uncertainties in these estimations. On the one side the statistical uncertainties in the planet occurrence rates, and on the other side systematic uncertainties related to our limited knowledge on the actual stellar parameters of the populations observed. These have a strong influence on the stellar insolation on top of the atmosphere and hence on the planetary energy balance. It is realistic to consider that the different biases will contribute to a typical uncertainty in the planet yield of transit surveys up to 50% (see Sullivan et al. 2015), if not larger. It will take observations by PLATO to constrain this value significantly better.
- The observing strategies considered have been discussed above.

- The detection efficiency depends on the transit depth, hence the radius ratio between planet and star, and the noise level in the light curve. It is different for the P1 sample, which is both magnitude and noise limited ($V \leq 11$, $\text{NSR} < 34$ ppm in 1h), and for the P5 sample, only magnitude limited ($V \leq 13$):
 - For the LOP fields, we will take as benchmark the detection of an Earth-sized planet around a solar-like star in 1 year period orbit, which is about 80 ppm depth and 13h duration.
 - For P1 sample (< 34 ppm in 1h) the detection efficiency is assumed to be 100%.
 - For P5 sample the detection efficiency of Neptune-sized and giant planets is assumed to be 100%. For planets smaller than 2 Earth radii we set a stricter limit. The detectability of small planets is 50% for the light curves with less than 80 ppm noise in 1h and 0% elsewhere, which is conservative.
 - For the step-and-stare phases we consider detection of planets up to 30 days orbital period. Single transit events of planetary objects will also be detected (see Osborn et al. 2016 and references therein), but we will not consider them further here. For the P1 sample the detection efficiency is assumed to be 100%. For the P5 sample, Neptune-sized and giant planets have 100% detection efficiency and small planets 50% efficiency if the $\text{NSR} < 80$ ppm in 1h and 0% elsewhere.

7.2.3.2 Planets with RV follow-up

In Section 7.2.3.1 we estimated the detection capabilities of the PLATO satellite for transiting planets, including stars sufficiently bright for asteroseismology. The full characterisation of planets, however, requires the additional determination of their mass via ground-based follow-up spectroscopy. This yield for fully characterised planets is therefore dependent on the availability of telescope resources and time spent to perform the follow-up observations.

We have done an exercise to dimension the telescope resources required to confirm and characterise planets detected by the PLATO mission through ground-based follow-up observations. For our benchmark case of the Earth around the Sun we take as a starting point the subsample of planets detected during the long-pointing phases orbiting stars brighter than $V = 11$, because for fainter targets follow-up is not feasible on a large scale.

We also account for the impact of stellar activity further reducing the considered subsample to those planets orbiting quiet stars. First, we mitigate the impact of stellar activity on the RV signal by adopting a strategy reducing the impact of granulation and stellar oscillations (see Dumusque et al. 2011a, b). In this way, we also estimate the amount of resources devoted to each target depending on the planet mass, the orbital period, and the level of stellar activity. Secondly, for the most difficult cases, we devote resources only to the planets orbiting quiet stars. We estimate the fraction of quiet stars from simulations drawn from real HARPS asteroseismology data (for oscillations and granulation, i.e. for timescales up to ~ 1 day) and from the modelling of families of spots on the star surface for different spectral types and various level of stellar activities. We implicitly suppose here that there is no significant stellar noise with timescale between the rotational period of the star and 1 year. The distribution for stars in the solar neighbourhood drawn from the HARPS GTO volume-limited sub-sample shows that 24% of the stars have $\log(R'_{\text{HK}}) < -5.0$ (non-active Sun) and 50% are less active than the average Sun ($\log(R'_{\text{HK}}) = -4.9$). Therefore, we reduce the sample of detections as follows:

- Super Earths:
 - In short periods (< 85 days): 50% of the planets detected orbit quiet stars suitable for RV,
 - In long periods (> 85 days): 25% of the planets detected orbit quiet stars suitable for RV,
- Earths:
 - For all periods: 25% of the planets detected orbit quiet stars suitable for RV.

In our approach we devote follow up resources in small class telescopes (1–2m) to culling of false positives with low precision spectroscopy and high resolution imaging and on-off photometry. Mid-class telescopes (4m) are devoted to high precision spectroscopy and only the most difficult cases (small planets at long orbital periods) will go to 8m class telescopes for Rossiter-McLaughlin (confirmation of planetary nature) and RV follow-up (see Section 6.2).

Using resources comparable to a large ESO program (55 nights per year at 8m class telescopes, 65 nights per year at 4m class telescopes), we have enough resources to obtain masses for 100 super Earths (9 of them with semi-major axis comparable to 1 au) and 22 Earth-sized planets (7 of them with semi-major axis comparable to 1 au) and some tens of Neptunes. We have not allocated resources to Jupiter-sized planets as we do not consider them the main science goal for this exercise. Using facilities in La Palma (32 nights per year) we could follow-up additional 52 super-Earths (including 5 with semi-major axis comparable to 1 au). For comparison, CoRoT has published RV values for 31 giant planets and for one small planet, the short period super-Earth CoRoT-7b. *Kepler* has published RV values for about 70 planets, 60 of them being giants and most in short period orbits. K2 has published additional RV measurements for about a dozen planets in short period orbits.

PLATO is therefore expected to provide a unique sample of fully characterised (radius, mass, age) sample of small planets.

8 Ground Segment

8.1 PLATO data products

The baseline telemetry budget yields a daily data volume of 435 Gb. The data products will be reformatted into a standard self-describing format in common use by the astronomical community (e.g. FITS).

PLATO data products are divided into the following categories:

Level-0 (L0):

- The imagerettes of selected targets for all individual telescopes.
- The validated light curves and centroid curves of selected targets for all individual telescopes. These are all the downloaded light curves (one each from each star and from each telescope) as well as the centroid curves, validated by assessing the quality and integrity of the data. They do not include instrument corrections other than those already applied on-board.
- Housekeeping data.
- Ancillary data, e.g. pointing information.
- Quality control data.

Level-1 (L1):

- The calibrated light curves and centroid curves for each target, corrected for instrumental effects such as those related to temperature sensitivity, some specific CCD corrections, and a posteriori jitter correction. Level-1 treatment includes the derivation from the imagerettes, when available, of the light curves and centroid curves. Moreover, for the normal telescopes and for each star, the Level-1 light curves and centroid curves are (suitably) averaged, and an associated uncertainty is provided.
- Processed imagerettes of selected targets and images of sky regions.
- Ancillary data, e.g. pointing information.
- Associated calibration data.
- Quality control data.

Level-2 (L2):

- The planetary transit candidates and their parameters, as a minimum target identifier, planetary ephemeris of the system, depth and duration of the transit, estimated radius, and their corresponding uncertainties.
- The results of the asteroseismic analysis, and their corresponding uncertainties.
- The stellar rotation periods and stellar activity properties inferred from activity-related periodicities in the light curves.
- The seismically-determined stellar masses, radii and ages of stars, (and their formal uncertainties), obtained from stellar model fits to the frequencies of oscillation.
- The list of planetary systems confirmed through the detection of Transit Time Variations (TTVs), which will be characterised by combining information from the planetary transits and the seismology of the planet-hosting stars.

Level-3 (L3):

- The list of confirmed planetary systems, which will be fully characterised by combining information from the planetary transits, the seismology of the planet-hosting stars, and the results of ground-based observations.

Ground-based observations data (Lg):

- Ground-based observations for filtering false planet transit detections include:
 - Low-precision spectroscopy (1–2m telescopes);
 - High-resolution imaging (2m telescopes);
 - On and off transit photometry (1–2m telescopes);
 - High-resolution spectroscopy (4–8m telescopes);
 - Rossiter-McLaughlin (RM) observations (8 m telescopes).

From these ground-based observations, false-detections will be identified and the number of targets for the next steps reduced.

- Ground-based observations for the characterisation of planets include:
 - High-resolution spectroscopy (1-2 m, 4 m and 8 m telescopes);
 - Rossiter-McLaughlin (RM) observations (8 m telescopes).

For these ground-based observations raw, calibration and processed data will be available. From these observations, high precision measurement of radial velocity variations of the central star will be obtained. Cross-correlation function results will be available together with the spectra and derived radial velocities.

Within the PMC, these four data processing levels are thus organised according to specific PLATO Data Products, from DP0 to DP6, with DP0 and DP1 corresponding to Level 0 and Level 1 data respectively. The Level 2 data comprise DP2 to DP6, listed in Table 8.1 below.

Table 8.1: PLATO Science Data Products

Validated imagettes, light curves and centroid curves	DP0	L0
Calibrated imagettes, light curves and centroid curves	DP1	L1
Planetary candidate transits and their parameters	DP2	L2
Asteroseismic mode parameters	DP3	L2
Stellar rotation and activity	DP4	L2
Stellar radii, masses, and ages	DP5	L2
Living catalogue of confirmed planetary systems and their characteristics using light curves and transit time variations	DP6	L2
Follow-up ground-based observations		Lg
Living catalogue of confirmed planetary systems and their characteristics using new ground-based follow-up observations (Lg)	DP6+Lg	L3

8.2 Ground Segment overview

The Ground Segment consists of six main elements:

- An ESA provided Mission Operations Centre (MOC);
- an ESA provided Science Operations Centre (SOC);
- a PLATO Data Centre (PDC), provided by the PLATO Mission Consortium (PMC);
- a PMC Science Management (PSM) Group;
- a PMC Calibration/Operation Team (PCOT);

- a Ground-Based Observations Program (GOP) Team.

The roles and responsibilities of each Ground Segment element are described in the following sections.

8.3 Mission operations

ESA will establish a PLATO Mission Operations Centre (MOC) located at ESOC and provide a ground station network and ground communications between MOC and stations to ensure the necessary telecommanding, telemetry and science data return capabilities of the mission. The MOC is responsible for the operation of the spacecraft and operations ground segment, and in particular for the following tasks:

- Performing uplink of the satellite and payload telecommands and receiving telemetry.
- Managing the science data file transfer from space to ground.
- Monitoring and managing the spacecraft health and safety in line with the spacecraft autonomy capabilities.
- Monitoring the payload safety and reacting to contingencies and anomalies according to pre-defined procedures provided by the PMC.
- Performing mission planning of all spacecraft and ground segment activities.
- Informing the SOC of all significant anomalies or deviations from nominal behaviour of the satellite for onward transmission to PMC as relevant.
- Executing predetermined procedures to safeguard the spacecraft and payload, and preserve data integrity.
- Performing maintenance of the satellite's on-board software.
- Performing uplinks of payload on-board software as generated, validated, and delivered by the PMC.
- Providing commanding for attitude and orbit control and other on-board subsystems providing flight dynamics support, including orbit determination and control, etc., as required by the mission.
- Handling provision of the telemetry and science data files to the SOC.
- Producing and providing ancillary data to the SOC (e.g. orbit files, on-board to UTC time correlation, etc).

8.4 Science operations

8.4.1 Overall concept

For each spacecraft pointing, the list of targets to be observed will be identified and compiled in the PLATO Input Catalogue (PIC). A first version of the PIC with the targets in the first LOP sky field will be delivered by the PMC two years before launch. Updates of the PIC are planned nine months before launch and six months before the start of each sky field observation in the LOP and SOP. Other fine tunings on the PIC are possible at any time during mission operations following the mission planning cycle.

A “prime sample” will be defined by the PMC consisting of PIC targets to be observed with high PLATO accuracy. The “prime sample” with the targets in the first LOP sky field will be defined nine months before launch and updated six months before every satellite sky field pointing. Ground-based observations will be performed for planetary candidates within this sample during the course of the mission. The best estimate of the ground-based observation time needed for these candidates is given in Section 6.2. For this task, a GOP Team to be responsible of the actual observations will be selected through an ESA AO.

Before launch, the final observing scenario, the PIC and the definition of the “prime sample” will be prepared under the supervision of the Science Working Team (SWT) and reviewed under the responsibility of the ESA Advisory Structure. Further reviews will be done in the course of operations as needed, following updates of the PIC and of the “prime sample” and/or based on the findings of PLATO.

The planning of science operations will be performed at the SOC based upon the inputs from the PDC, endorsed by the PLATO Science Working Team, and from the approved Guest Observer (GO) programmes.

The observing schedules will be checked at the SOC and then forwarded to the MOC where they are to be uplinked and executed on board.

During the telecommunication period that will be scheduled several times per week, the data will be acquired via the ground station and delivered to the MOC. The SOC shall retrieve this Level 0 data and perform a quick look assessment and validate this data through the running of quality control. The data will be placed in the SOC archive after which the standard pipeline generation process will be executed, whereby the Level 0 data will pass through a pipeline thus generating Level 1 products, again being placed into the archive. Further quality control checks will be performed by the SOC of this data set to confirm correct integrity and scientific merit before it is made public in the archive.

The SOC will be the main interface point between the PDC and the MOC as regards payload operations in particular relating to safeguarding the payload and optimising the quality of the data set. Such interactions will also include the fine tuning of on-board software, parameters and payload configuration as a result of the quick look data checks of the L0 products.

The PDC data base will access the archive and retrieve L0, L1 and other data sets at which point it will make it available to the centres within the PLATO Mission Consortium to produce the L2 and L3 data. Upon generation of the L2 and L3 product data set with the input from the GOP Team, the PMC will provide those back to the SOC for their ingestion into the archive.

8.4.2 Calibration activities

8.4.2.1 On-ground calibration operations (Payload)

The PMC shall support the SOC in the production of the L1 data by performing the task of calibration of scientific data. This includes the definition of a calibration plan, the specification of observations or payload configurations required to gather calibration data, the derivation of the calibration parameters and their delivery to the SOC for implementation into the L1 processing pipeline.

Specific calibration data will be collected during the development phase on sub-system to instrument levels, either as initial estimates for the commissioning and operational phases or to aid calibration model development.

All calibration data collected on-ground as well as in-orbit shall be stored in the Mission Archive for use in the L1 processing.

8.4.2.2 In-Orbit calibration operations

In-orbit calibrations will be carried out i) during in-flight commissioning and performance verification; ii) during normal operations, using the science & HK data; iii) by observing specific calibration fields, generally combined with the on-going long observation campaign.

The in-orbit calibration procedures will be performed throughout the mission, with certain activities specifically tailored to the performance verification phase, and also carried out on normal science data throughout the operations phase, with SGS tasks oriented to identifying calibration sources and extracting the calibration parameters. Note that most of the procedures permit several calibrations to be carried out.

During the Development & Operation phases, the PDC will deliver to the SOC the calibration data and instrument parameter data sets to support quick look assessment and real time analysis of data. In addition, calibration data to support processing of Level 0 and Level 1 data sets shall also be provided for importing into the Archive. Finally, calibration algorithms and procedures shall be delivered to SOC.

8.4.3 Science Operations Centre

ESA will establish a Science Operations Centre (SOC) located at ESAC. The SOC is the only interface to the MOC during routine operations and is responsible for the following tasks:

- Planning scientific, calibration and engineering observations and the construction of optimised schedules.
- Supporting the issuing of GO calls for proposals.

- Providing quick-look analysis development, implementation and operation, performed in partnership with the PMC.
- Issuing payload configuration change requests to the MOC as appropriate to optimise the quality of the PLATO data.
- Developing, implementing and operating the data processing pipelines to produce validated L0 and L1 data products. This includes the necessary calibration information. This task is performed in partnership with the PMC.
- Generating, validating, archiving and distributing L0 and L1 products.
- Performing quality control of the L0 and L1 products.
- Supporting the AO for the selection of the GOP Team.
- Supporting the PMC and GOP Team activities for the generation and archival of the L3 data.
- Providing support to the scientific user community and to the Time Allocation Committee.
- Providing low-level, ancillary and housekeeping data to the PMC.
- Developing and operating the PLATO Archive to make the data products and scientific results of the mission available to the community.
- Making data processing tools available to the community, with the support of the PMC.

8.4.4 PLATO Data Centre

8.4.4.1 PDC responsibilities

The PDC is under the responsibility of the PLATO Mission Consortium. The PDC supports the SOC in the production of the L1 data by carrying out the following tasks:

- Based on the calibration procedure and calibration data provided by the instrument team, and together with the PMC Calibration/Operation Team (PCOT), the derivation of the calibration parameters and their delivery to the SOC for implementation into the L1 processing pipeline.
- Definition of algorithms and support to the implementation of modules to monitor the scientific integrity and health of the observations.
- Definition of algorithms and support to the implementation of modules in the data analysis system for the removal of instrumental effects and generation of L1 data.
- Provision of the PLATO Input Catalogue to the SOC for the scientific mission planning.
- Provision of input to the scientific quality control software and procedures.
- Provision of the necessary algorithms and tools for the optimisation of the onboard processing.
- Provision of tools and support to simulate, test and validate the L0 to L1 processing pipeline.

The PDC implements, tests and maintains the data analysis tools needed to generate the Level 2 data and Level 2 scientific data products, which include catalogues, list of planets, their parameters and additional characterisation information.

The PDC is responsible for the development and maintenance of all systems required to process the final PLATO mission products and for the computing infrastructure required to deliver the PLATO Level 2 scientific data products. Specifically:

- The PDC technically designs, implements, tests and maintains the data analysis tools needed to generate the (exoplanet and stellar) Level 2 data and higher level scientific products, which include catalogues, list of planets, their parameters and additional characterisation information. The scientific validation of the data analysis tools will occur within the PDC based upon PSM specifications and with PSM involvement.

- The PDC shall develop and maintain a main PDC Data Base (PDC-DB) which will acquire, from the SOC, the L0 and L1 data, and other data. The PDC-DB shall make the data available to the PDC Data Processing Centres (PDPCs) to produce the L2 and L3 data products. The validated L2/L3 data products, will then be provided back to the SOC. The PDC-DB shall be a central hub for the exchange and maintenance of data within the PDC.
- The PDC is responsible for the management of the database that assembles all ground-based follow-up observations on PLATO targets, plus ancillary data extracted from various existing catalogues and databases, and places them in the PDC Data Base at the disposal of the PLATO Mission Consortium.
- Provision of data analysis support tools to assist the science team to inspect and to scientifically validate the PLATO data products within the PDC. In particular, these tools will assist the PS & the PSM to update the ranking of planetary candidates and to confirm planetary systems.

8.4.4.2 PDC development

The software and hardware technologies available today would suffice to build a successful PDC. The complexity of the PDC lies mostly in the management, integration, and validation of its many hardware and software components.

The PDC will adopt a well defined cyclical development schedule (6 month cycles). Software developed in the PDC will be released at the end of each cycle, with this being integrated into an end-of-cycle system. Over the development lifetime, there will always be a working system, with this working system increasing in functionality over time, such that by the system readiness review prior to launch, the processing system has fully met the requirements.

This approach ensures that work developed over many sites is integrated on a frequent timescale – ensuring that any interface issues are resolved at an early stage. It enables end-to-end testing to commence at an early stage – thus facilitating the 'smooth transition' of a system handling test data to one handling real instrument data (from the lab during development) to one handling real data from the S/C during flight operations.

A key part of the development process will be access to simulation data, required to test all software components. This data will simulate the PLATO telemetry stream, PLATO pixel level data and PLATO catalogue level data. Simulation data will be released ahead of each cycle to allow for testing of the following cycle release. The simulation data is provided to the PDC-DB and is then available through the PDC-DB interface to all PDPCs.

The PDC shall remain operational for at least three years after the end of the PLATO space operations phase to enable the confirmation of planets with periods of up to three years.

8.4.4.3 PDC facilities

The PDC will encompass several facilities in Europe. The PDC-DB at MPSSR (Germany) will hold the PLATO scientific data products, the input catalogue, and all relevant preparatory and follow-up data on the PLATO targets that are required for the processing of the L2 data products, in particular specifically acquired ground-based follow-up observations. Computing resources will be distributed among five Data Processing Centres: PDPC-C at IoA-Cambridge (UK) for the Exoplanet Analysis System, PDPC-I at IAS (France) for the Stellar Analysis System, PDPC-A at ASI (Italy) for the Input Catalogue, PDPC-L at LAM (France) for the Preparatory and Follow-Up Database Management, and PDPC-M at MPSSR (Germany) for the running of the data analysis support tools. The PDC activities through all phases of the mission will be funded through institutional and national agencies.

8.4.5 PLATO Mission Consortium Science Management

8.4.5.1 PSM responsibilities

The PMC Science Management group (PSM) is responsible for the activities related to scientific preparation of the mission within the PMC. During the post-launch phases, the PSM takes an active role in the definition and validation of the final L2 and L3 data products. The PSM also supports the SWT and the PS, and provides specifications and inputs to the PDC. The main duties are:

- Organization and overall management of the teams and staff assigned to the PSM.
- Overall project planning of the PSM.
- Responsibility for carrying out preparatory activities ensuring the scientific results of the mission. Special emphasis is given to the preparation of scientific specifications (algorithms of tools for exoplanet and stellar science) to the PDC to implement optimized methods and tools for PLATO data exploitation as well as to provide inputs for the PIC, provide the basis for the target field selection and to prepare the ground-based follow-up activities.
- Updates of algorithm specifications implemented by the PDC and updates of the fields and targets used in the PIC for both the long duration observation fields but especially for the stop and stare fields.
- Scientific validation of L2 and L3 data products in the operation and post-operation phases, including organisation of follow-up observations (and hence the prioritisation of candidates).

8.4.5.2 PSM facilities and resources

The PSM consists of sub-groups totalling more than 100, mainly European, experts who provide the needed state-of-the art scientific know-how, including in particular expertise from previous space missions like CoRoT and *Kepler* and expertise in ground-based follow-up observations for planet confirmation. This expertise is specially required to set-up an efficient scheme for planet detection, ranking and definition of the requirements for the ground-based follow-up observations. This is a lessons-learned from the on-going transit search space missions. The PSM also provides the expertise for target field selection and characterisation and the specification of the PLATO Input Catalogue. Experts in the PSM will provide updated stellar models to optimise the determination of stellar parameters. The complementary science task in the PSM includes experts from various scientific fields, not only on different aspects of stellar science not covered in the core program, but as well on extragalactic science and transient phenomena in the Universe. These experts will help maximising the scientific return of the mission by expanding its science exploitation. The PSM will fund its activities through all phases of the mission by institutional and agency funding, depending on the national and institutional environments of the participants.

8.4.6 PMC Calibration/Operation Team

The PMC Calibration/Operation Team is responsible for the activities related to the operation and calibration of the PLATO payload, in particular:

- Providing the PLATO Instrument TM/TC Database.
- Providing the PLATO Instrument User's Manuals.
- Providing payload operational procedures and command sequences.
- Providing payload operational constraints.
- Providing updated payload performance parameters.
- Analysing payload operation/telemetry, manage non-conformances and provide inputs for on-board software change management.
- Maintaining and validate the on-board software including inflight parameter configurations.
- Maintaining and validate the instrument data base, e.g. by updating of parameters derived by on-ground data processing.
- Providing all information relevant to scientific data calibration (including calibration plans and calibration results, and calibration algorithms and data for archiving).
- Providing input for the definition of the procedures, algorithms, and software tools for removal of instrumental artifacts and the extraction of physical parameters.

8.4.7 Ground based Observations Programme (GOP) Team

The GOP Team will have to adhere to the following requirements:

- The GOP Team will organise and execute the ground-based observations dedicated to filtering and necessary for the generation of the L3 products, for the candidates from the prime sample, and following the requirements issued by the PMC.
- Ground-based data products (Lg) produced under responsibility of the GOP Team will be provided to the PMC for filtering and production of L3 products. The ground-based data products will be made accessible to ESA for their release after the publication of the planetary parameters, or no later than six months after the completion of the ground-based observations.

Using the deliveries from the GOP Team, the PMC will be responsible to routinely update the L2 products and generate and deliver the Level-3 products of the prime sample to SOC for their inclusion in the PLATO Archive.

8.4.8 Level 2 and Level 3 data processing

The PDC will retrieve the L0 and L1 data products existing in the PLATO Archive. The transfer mechanism will be running at the PDC on an automatic basis and will retrieve products from the archive that have been updated or changed since its last retrieval.

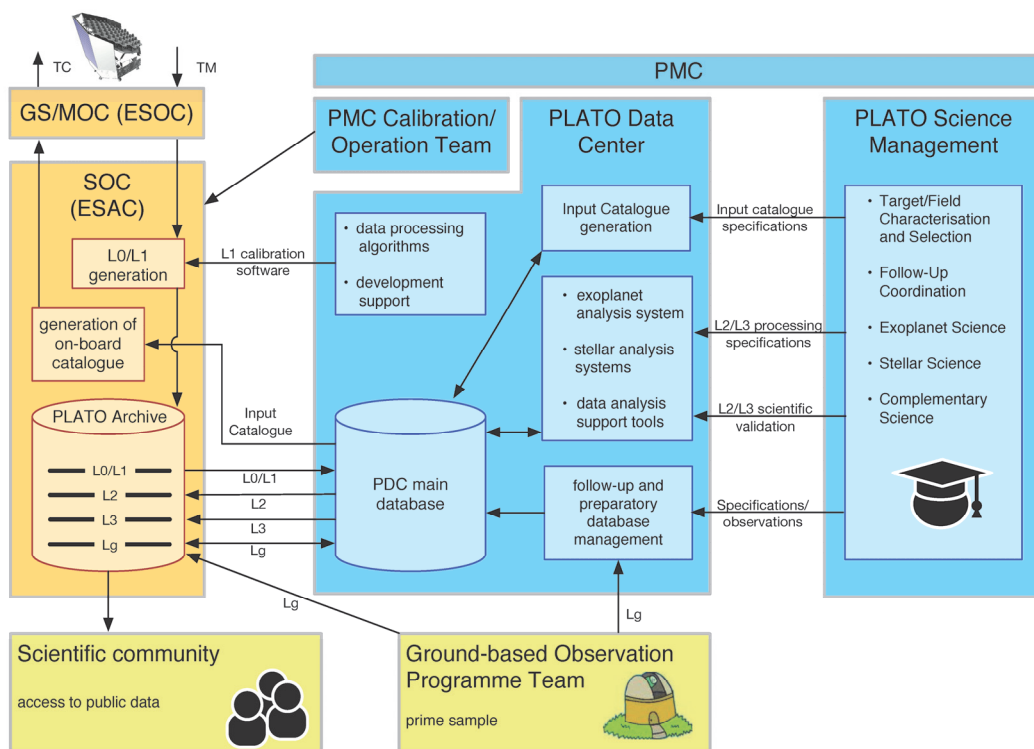


Figure 8.1: Organisation of the Science ground segment for L2/L3 generation during operations. The PDC includes the PDC Main Data Base (PDC-DB) and five PLATO Data Processing Centres (PDPCs).

The products (including associated auxiliary products) will be placed into the PDC main database (PDC-DB), as can be seen in Figure 8.1. Access to the PDC-DB is possible by all the sub-centres of the PDC to allow the L2 generation process to be started. After acquisition of the L1 data from the PDC-DB by the stellar PDPC, the PLATO light curves are Fourier transformed and power spectra are analysed to provide the oscillation mode parameters DP3. In parallel, analyses of the light curves provide the stellar rotation and activity information DP4. Finally, DP3 and DP4 are used together with the science ancillary and catalogue data, which are stored and managed in the PDC, for producing DP5. The exoplanet PDPC processing of the L1 data, for the production of the L2 products, is based on a ca. two week cycle. This cycle will allow an update of DP2 providing a ranked list of candidate planet systems. False positive modelling is undertaken to

refine the estimate of probable planet systems, using follow up information when available. The ca. two weekly cycle allows for triggering of the ground based follow-up of objects which pass a certain threshold of interest and enables triggering of imagerettes of planet candidates. Successive updates are applied over a three-month main processing cycle, corresponding to the period between PLATO satellite field rotations. At the close of the three month period, a full update of the L2/L3 parameters for the objects observed by PLATO will be made to the PDC-DB.

The PSM group will access the L2/L3 pipeline products, and L0 and L1 data as needed, via the data analysis support tools in the PDC. The PSM will in particular evaluate and update the planet ranking and specify the requirements for ground-based follow-up to the GOP. The GOP Team then executes the ground-based observations. The PSM will scientifically validate L2/L3 data, using software tools available at the PDC. The PSM group will furthermore evaluate the scientific performance of the L2 pipeline on real data in the operation phase and provide updated scientific specifications to the PDC data processing as needed.

Upon delivery to the SOC, the L2 (DP6) and L3 data products will be placed into the archive and shall then be made public to the scientific community.

External datasets (including preparatory and ground-based follow up data) will be generated around each of the target L2/3 data-sets and a selection of these will also be fed into the SOC and the PLATO Archive.

Page intentionally left blank

9 Management

9.1 Project management

The overarching responsibility for all aspects of the PLATO mission rests with ESA's Directorate of Science. ESA is responsible for:

- the overall PLATO mission definition and space segment development;
- the development, procurement, manufacturing, assembly, integration, test, verification and timely delivery of a fully integrated spacecraft capable of accommodating the PLATO scientific instrument, fulfilling the mission requirements and achieving the mission objectives;
- the procurement of the CCD chips for the Focal Plan Arrays of the PLATO cameras, as an Agency Furnished Item and their delivery to the PLATO Mission Consortium (PMC);
- the development, procurement, integration and verification of the Mission Operation Centre (MOC) and of the Science Operation Centre (SOC), part of the Science Ground Segment (SGS);
- the launch, early operations, commissioning and operations of the spacecraft.

During the development and commissioning phases, an ESA-appointed Project Manager will be responsible for implementing and managing ESA's activities. After a successful In-Orbit Commissioning Review, a Mission Manager will take over the responsibility for the mission throughout its routine and any extended phases.

Funded by national Funding Agencies, within the remit of a Multi-Lateral Agreement (MLA) including ESA and the national Funding Agencies, the PMC, under the leadership of a PMC Lead (PCL) or Principal Investigator (PI), is responsible for:

- providing the instrument according to the agreed interfaces and schedule;
- contributing to the integration and tests of the instrument at system level, under the control of ESA;
- supporting the instrument maintenance and operations throughout the mission lifetime;
- providing contributions to the Science Ground Segment (SGS).

In preparation for and during the operation of the mission, the PMC will be also responsible for generating, the PLATO Input Catalogue (PIC), containing the list of targets to be observed for each spacecraft pointing, and of defining a "prime sample", consisting of PIC targets to be observed with high PLATO accuracy.

In order to fulfil the PLATO scientific objectives, the Ground-based Observation Programme (GOP) will play an important role, as it is necessary for the confirmation and characterisation of planets. For this ESA will issue an Announcement of Opportunity (AO) for the community to participate in the ground-based observations of the candidates in the "prime sample". The selected GOP Team will be responsible of the ground-based observation campaign.

9.2 PLATO Mission Consortium (PMC) structure

The overall structure of the PMC is shown in the diagram in Figure 9.1 and briefly described in the following text.

The PMC is placed under the overall responsibility of the PMC Lead (PCL or PI). The PCL constitutes the formal interface of the consortium to ESA. The PCL ensures that the performances of the mission meet the science requirements set by the PLATO Science Working Team (PLATO SWT). The PCL also constitutes the main scientific interface of all consortium sub-structures with ESA and the PS. The PCL is one of the members of the SWT nominated by the PMC and appointed by ESA.

All consortium activities will be monitored by the PMC Board, which will serve as interface between the consortium on one hand, and the national agencies and institutes involved in the consortium on the other hand. The PMC Board addresses problems concerning the procurement of the PMC elements of the mission,

either payload, ground segment or science activities, before they eventually reach the Steering Committee level. The PMC Board is chaired by the PCL, and is constituted by members of the Consortium.

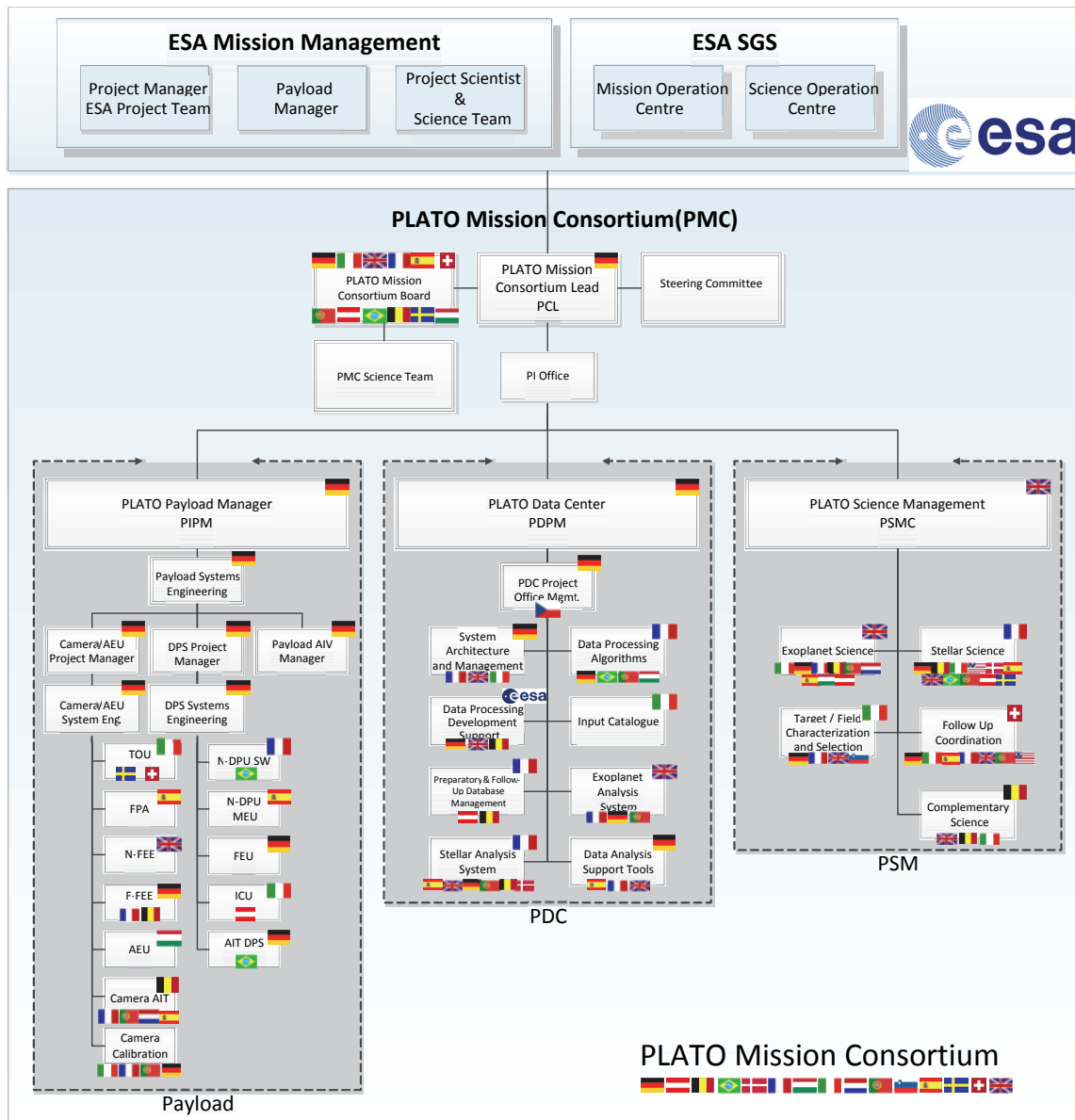


Figure 9.1: Organisation of the mission and structure of the PLATO Mission Consortium (PMC) with key elements and proposed national responsibilities of main work packages.

The PMC Board includes two representatives of each one of the main countries involved in the mission (France, Italy, Germany, Spain, UK and Switzerland) and one representative of all other contributors (Belgium, Portugal, Brazil, Austria, Sweden, Denmark, Hungary, and The Netherlands). The PIPM (see below) is invited to all Board meetings. The PMC Board meets at least once a year. The chair is responsible for the organisation of these meetings. The PCL may decide to hold additional meetings, as needed.

The PCL is supported by the PI Office, which has several tasks including the overall PMC management, the organisation of working groups involving expertise across the PMC (e.g. Performance Team, CCD WG), the coordination of PLATOSim development, the definition of PMC requirements, PMC system engineering, the coordination of support for calibration and operation activities (PCOT) and the coordination of PMC EPO activities.

The PLATO Instrument Project Manager (PIPM) acts as a support to the PCL on all technical and managerial aspects of the payload development. The hierarchical structure is shown in Figure 9.1. The PLATO Consortium Payload Management is commissioned to a German industrial partner, who appoints the

PIPM. The PIPM takes responsibility for the overall management of the payload development, including all schedule and quality aspects. The PLATO Data Centre (PDC) is the PMC contribution to the Science Ground Segment (SGS), which also includes the Science Operation Centre (SOC) under ESA responsibility. The PDC is led by the PLATO Data Processing Manager (PDPM). Science Activities will be carried out under responsibility of a specific substructure of the Consortium, called PMC Science Management (PSM). The PSM will define the algorithms for an optimised exploitation of the PLATO data, which will be implemented at the PDC. The PSM is also responsible for providing the PLATO Input Catalogue and the scientific validation of L2 and L3 data products.

9.3 Procurement philosophy

9.3.1 Procurement of spacecraft, industrial contractors and organisation

After selection of the PLATO mission in February 2014, parallel definition studies (Phase B1) of the PLATO mission were conducted by Industry under ESA contracts. These studies consolidated the design of the spacecraft, the definition of the interfaces with the payload, and the mission development plans and schedule in preparation for the industrialization. They were completed by a Mission Adoption Review (MAR) held in February-April 2016.

The MAR Board concluded that a payload module with 26 cameras provides a stable configuration for PLATO development with adequate mass margins, and secures the payload development schedule for a realistic launch by 2025. As a consequence, the MAR recommended that the scientific minimum requirements should be made compatible with the 26 cameras configuration (24 normal cameras +2 fast cameras).

Following the MAR, a bridging phase was initiated by ESA with the candidate prime contractors for addressing the MAR review findings and recommendations and preparing for PLATO implementation.

Subject to adoption of the PLATO mission by the ESA Science Program Committee (SPC), an Invitation to Tender (ITT) for the Implementation Phase (B2/C/D/E1) will be released in 2017. The scope of this contract would be to implement all industrial activities leading to a launch and commissioning of PLATO in the requested timeframe. The successful bidder will be appointed as Prime Contractor in charge, amongst other items, of system engineering and management of the sub-contractors.

9.3.2 Payload procurement

The PLATO Payload Module (PLM) is provided by the PLATO Mission Consortium which is financed by the national agencies. A detailed procurement plan can be found in the Instrument Procurement Plan.

9.4 Schedule

A PLATO reference schedule was conceived by the MAR management and programmatic panel on the basis of discussions with the candidate prime contractors. This schedule splits into two phases:

- kick-off to Critical Design Review (CDR) with the performance of the mechanical, thermal and early avionics tests prior to the CDR;
- CDR to Flight Acceptance Review (FAR) covering the integration and the final functional and environmental tests of the flight models of the spacecraft service and payload modules.

With this approach and considering a kick-off of the phase B2CDE1 by end-September 2017, the PLATO development schedule could support a launch date end-2025.

9.5 Science management

9.5.1 PLATO Science Working Team

A Science Working Team (SWT) will be appointed by ESA after the PLATO mission adoption. The SWT will be asked to review and endorse top-level requirements (in all areas of the project) that impact science return. In particular, the SWT will supervise the preparation and periodic update of the PIC and “prime sample” list. The SWT will consist of PMC members and external scientists selected by ESA through AOs.

9.5.2 Guest Observers programme

Members of the scientific community may participate in the PLATO mission by becoming Guest Observers (GOs) selected by ESA through calls for proposals. The calls will ask for complementary science programmes not covered by Sections 2.1 and 2.2. The aim is that all PLATO complementary science will be carried out through programmes proposed by the general scientific community. The high relevance of these additional scientific objectives is illustrated in Section 2.3, which highlights some of the many areas in which PLATO can make fundamental contributions.

A percentage of up to 8% of the science data rate (excluding calibration data) will be allocated to targets from the Guest Observer's programme. The total number of objects that may be observed with this allocation will range from thousands to tens of thousands, depending on the type of observations (e.g. imagerettes or light curves) and sampling times requested. The proposals may only target objects within the PLATO sky fields defined by the SWT, that is, without requiring dedicated repointing of the spacecraft. The duration of the proposed observations cannot exceed the observation durations of the corresponding fields.

9.5.3 Data policy

After the first quarter of observations and delivery of L0 and L1 products by the SOC to the PMC, 6 months will be required for Level-1 data validation (and updating of the pipeline), while for the following quarters, 3 months will be needed. The public release of L0, L1 and L2 products for each observation quarter will be made as soon as possible, but no later than one year after the end of each L1 product validation period. A fraction of the prime sample will remain proprietary of the PMC, as defined in the Science Management Plan.

L3 data of the prime sample (delivered by the PMC) and their ground-based associated observations (provided by the GOP Team) will be publicly released immediately after the publication of the planetary parameters, or as soon as possible but no later than six months after the completion of the ground-based observations.

The proprietary time of the targets selected through the Guest Observer programme call will be one year, starting counting at the time of the SOC delivery to the observer of the last portion of the observation L1 data. During the execution of the observations, the SOC will deliver L0 and L1 products to the observer every three months.

10 Communication and outreach

The existence of planets around other stars, and their potential as habitats for life, fascinates people. PLATO addresses a fundamental question of human existence: Are we alone in the Universe? It is vital that we capitalise on this unique opportunity to promote public scientific literacy and reinvigorate astronomy education.

ESA will have overall responsibility for the science communications, educational and outreach activities related to PLATO. ESA will have the right to use any data acquired by PLATO for outreach purposes, in coordination with the holders of the data rights as applicable, as covered by the ESA Rules on Information, Data and intellectual Property (ESA/REG/008).

An active public outreach activity will be established in close collaboration between ESA, the relevant bodies funding the provision of the scientific payload in the Member States and other institutions involved in the mission. Such outreach activity will be based on a regular flow of science results from the mission presented in a manner suitable for communication and public outreach purposes. Such an outreach activity necessitates the timely availability of suitably processed data and the full involvement of the various scientific teams engaged.

10.1 Education and public outreach strategy

The PMC has assembled an international team comprised of professional astronomers with extensive experience and communication skills. This team will produce engaging, attractive, concise and accurate materials prepared for media professionals, members of the public, and educators.

A primary task is to ensure high visibility, acceptance and identification with PLATO and its goals in the general public with a focus on young people. The consortium will deliver resources to enable effective media feeding via ESA's outreach and communication teams.

An ambitious and creative web portal: The PMC already maintains a web portal, which is used to document the progress of the mission project. Our aim is to maintain a state-of-the-art portal which includes technical information in concise, easy-to-digest text and graphics, and entertaining interactive content designed for interested members of the public, including resources targeted specifically at young people. The web portal will host an archive of mission press releases and associated image data, graphics and video content [1].

Visuals: We will commission professionally produced space-art, and still still-graphics and animations to inspire and communicate key mission findings.

Interactive and video assets: We will deliver audio podcasts and video sequences for the education tool iTunes U and YouTube on exoplanets, their detection via transits, and the scientific impact of the PLATO mission. We will develop interactive learning objects, which will be delivered by the PLATO Mission Consortium via the web portal and will be freely available for educators in schools, universities, museums and science organisations to disseminate.

Printed Materials: We will produce resource packs for school teachers in the languages of ESA member countries. Three sets will be made, aimed at kids of younger, and intermediate age, and older children teenagers, respectively. We will consult with school teachers to ensure we meet their needs. We will prepare brochures, stickers, posters and T-shirts promoting the mission.

Social Media: We will communicate key milestones via social media, amplifying the reach of ESA press releases and refreshing awareness of the assets held on the web portal. The precise tools are likely to evolve on the timescale of the mission, and we will adapt to changing public usage patterns. We already tweet under @PLATOMissionCon and will use blogs, social network pages, smart-phone apps and emerging tools as appropriate.

Exhibitions: We will develop a modular multi-lingual mobile exhibition system in ESA's corporate design to promote PLATO's science at appropriate high footfall public events held at science festivals, conferences, musea, etc. We have experience in designing, building and running a similar exhibit: "Is there anybody out

there? Looking for New Worlds”, which was show-cased at the 2008 Royal Society Summer Exhibition in London and subsequently at several other locations in Europe and Asia.

10.2 EPO team and credentials

EPO activities are an essential part of the PLATO Mission Consortium. An “Education and Public Outreach (EPO) Coordination Office (EPOCO)” is established. This office reports to the PCL.

The proposed structure of EPOCO has three sub-units:

1. Web-page maintenance

Coordinator: I. Pagano, INAF – Catania Astrophysical Observatory

Dr. Pagano oversees the team which maintains the PLATO website and develops content for these websites. We will provide top-nudge web content that underlines that ESA is at the leading edge of space-based astronomy.

2. Editorial Office

Coordinator: U. Köhler, DLR

Mr. Köhler, a planetary scientist, has a long experience in EPO from his involvement in the ESA solar-system missions (Mars Express, Venus Express, Rosetta), coordinating media contents with DLR’s and ESA’s communication department. He is also coordinating press and image releases between DLR, NASA and JAXA for the DLR science participations in deep-space missions. Through DLR’s participation in the CNES/ESA space telescope CoRoT, he became involved in EPO activities with exoplanet astronomy for German media. He is a fluent writer in German and English and an author of popular science books dealing with the Moon and Mars, as well as school text-books on planetary science and astronomy.

3. Visuals, writing and learning object design

Coordinators: C.A. Haswell & A.J. Norton, The Open University

The Open University (OU) is a world-leader in open-access, supported distance learning, and has public engagement at the heart of its mission. Its high profile TV offering often features astronomy, exemplified by “Stargazing Live” [2] and “Bang Goes the Theory” [3], typically reaching 300 million programme-views per year. This is complemented by our presence on iTunesU [4] comprising >3500 tracks with >64 million downloads by 9 million unique visitors to date, including >1 million subscriptions via the iTunes app; and four YouTube channels [5] containing >1600 videos, with >18 million views and >84,000 subscribers (more than any other European educational institution). Recently we made 14 episodes of “60 Second Adventures in Astronomy” [6] which might serve as a model for PLATO science communication videos. We also produced the first undergraduate textbook dealing with PLATO’s science: “Transiting Exoplanets”, Haswell, CUP, ISBN-10: 0521139384, and an exoplanet storybook for children: “Oogle Flip and the Planet Adventure”, Norton, Magic World Media, ISBN-10: 0982114168.

10.3 Wider context

The PLATO mission has an unrivalled opportunity to inspire and educate future scientists and citizens. The most significant problems of the 21st century, climate change and overpopulation, can only be solved with scientific and technological innovation. The mission and its EPO strategy thus have an importance that reaches far beyond the immediate science goals, despite the enormous intrinsic value of those goals.

URLs of our existing web resources:

[1] <http://www.oact.inaf.it/plato/PPLC/Home.html>

[2] <http://www.bbc.co.uk/programmes/b019h4g8>

[3] <http://www.bbc.co.uk/programmes/b00lwxj1>

[4] <http://open.edu/itunes/>

[5] <http://www.youtube.com/user/TheOpenUniversity>

[6] http://www.youtube.com/playlist?list=PLhQpDGfX5e7CSp3rm5SDv7D_idfkRzje-

11 References

- Abe, Y., et al., *AsBio*, 11, 443, (2011)
- Aerts, C., et al., *A&A*, 399, 639 (2003)
- Aerts, C., et al., *Asteroseismology, Astronomy and Astrophysics Library*.~ISBN 978-1-4020-5178-4. Springer Science+Business Media B.V. (2010)
- Agol, E., *ApJ*, 731, 31 (2011)
- Albrecht, S., et al., *ApJ*, 771, 11 (2014)
- Alibert, Y., et al., *A&A* 417, 25 (2004)
- Alibert, Y., et al., *A&A*, 434, 343 (2005)
- Almenara, J.M., et al., SF2A-2012, Proceedings of the Annual meeting of the French Society of Astronomy and Astrophysics (2012)
- Almenara, J.M., et al., *MNRAS*, 453, 2644 (2015)
- Alonso, R. et al., *A&A*, 506, 353 (2009a)
- Alonso, R. et al., *A&A*, 501, L23 (2009b)
- Alvan, L., et al., *A&A*, 581, 112 (2015)
- Anders F., et al., *A&A*, 597, 30 (2017)
- Angerhausen, D., et al., *PASP*, 127, 1113 (2015)
- Anglada-Escudé, G., et al., *Nature*, 536, 7617 (2016)
- Angus, R., et al., *MNRAS*, 450, 1787 (2015)
- Apai, D., et al., *ApJ*, 820, 40 (2016)
- Appourchaux, T., et al., *A&A* 543,54 (2012)
- Armstrong, D.J., et al., *MNRAS*, 444, 1873 (2014)
- Auclair-Desrotour, P., Le Poncin-Lafitte, C. & Mathis, S., *A&A*, 561, 7 (2014)
- Augustson, K., Brun, A.S., Miesch, M., Toomre, J., *ApJ*, 809, 149 (2015)
- Baglin, A. and the CoRoT team, 2 "The CoRoT legacy book", *Edp Sciences*, ISBN 978-2-7598-1876-1 (2016)
- Baglin, A. et al., 36th COSPAR Scientific Assembly, 36, 3749 (2006)
- Baglin, A., et al., 2013, *ASPC*, 479, 461 (2013)
- Ball, W.H. & Gizon, L., *A&A*, 568, 123 (2014)
- Ballard, S., & Johnson, J.A., *ApJ*, 816, 66 (2016)
- Ballard, S., et al., *ApJ*, 790, 12 (2014)
- Ballot, J., et al., *MNRAS*, 369, 1281 (2006)
- Ballot, J., et al., *A&A*, 486, 867 (2008)
- Ballot, J., et al., *A&A*, 530, A97 (2011)
- Barclay, T., et al., *ApJ*, 761, 53 (2012)
- Barclay, T., et al., *Nature*, 494, 452 (2013)
- Barnes, R., et al., eprint arXiv:1608.06919 (2016)
- Barnes, J.W. & Fortney, J. J., *ApJ*, 616, 1193 (2004)
- Barnes, S.A., *ApJ*, 669, 1167 (2007)
- Barnes, S.A., *IAUS*, 273, 465 (2011)
- Barstow, J.K., et al., *MNRAS*, 440, 1607 (2014)
- Basu, S., et al., *ApJ*, 758, 43 (2011)
- Batalha, N. M., et al., *ApJ*, 729, 27 (2011)
- Batalha, N., *PNAS*, 111, 35 (2014)
- Batygin, K., et al., *ApJ*, 738, 1 (2011)
- Bean, J. L., et al., *Nature*, 468, 669 (2010)
- Beck, P.G., et al., *Science*, 332, 205 (2011)
- Beck, P.G., et al., *AN*, 333, 976 (2012a)
- Beck, P.G., et al., *Nature*, 481, 55 (2012b)
- Becker, J.C., et al., *ApJ*, 812, 18 (2015)
- Bedding, T., et al., *ApJ*, 713, 176 (2010)
- Bedding, T., et al., *Nature*, 471, 608 (2011)
- Belkacem, K. & Samadi, R., *LNP*, 865, 179 (2013)
- Ben-Jaffel, L. & Ballester, G. E., *A&A*, 553, 52 (2013)
- Ben-Jaffel, L., *ApJ*, 671, L61 (2007)
- Ben-Jaffel, L. & Hosseini, S., *ApJ*, 709, 1284 (2010)
- Benneke, B. & Seager, S., *ApJ*, 753, 100 (2012)
- Benomar, O., et al., *A&A* 506, 15 (2009)
- Benomar, O., et al., *PASJ*, 66, 94 (2014)
- Benomar, O., et al., *MNRAS*, 452, 2654 (2015)
- Bergemann, M., et al., *MNRAS*, 427, 27 (2012)
- Berta, Z.K., et al., *ApJ*, 747, 35 (2012)
- Berta-Thompson, Z., et al., *Nature*, 527, 204 (2015)
- Bodenheimer, P., et al., *ApJ*, 592, 555 (2003)
- Bodman, E.H.L., & Quillen, A.C., *ApJ*, 819, L34 (2016)
- Boley, A.C. et al., *Icarus*, 207, 509 (2010)
- Bolmont, E., et al., *MNRAS*, 464, 3728 (2017)
- Bonfils, X., et al., *A&A*, 549, A109 (2013)
- Bonomo, A.S. & Lanza, A.F., *A&A*, 547,37 (2012)
- Borucki, W.J., *Icarus*, 58, 121B (1984)
- Borucki, W.J., et al., *Science*, 325, 709 (2009)
- Borucki, W.J., et al., *Science*, 327, 977 (2010)
- Borucki, W.J., et al., *Science*, 340, 587 (2013)
- Borucki, W.J., *RPPH*, vol.79, 03690 (2016)
- Boss, A.P., *Science*, 276, 1836 (1997)
- Boyajian, T.S., et al., *MNRAS*, 457, 3988 (2016)
- Brassard, P., et al., *ApJ*, 563, 1013 (2001)
- Breger, M., et al., *MNRAS*, 414, 1721 (2011)
- Breger, M., et al., *ApJ*, 759, 62 (2012)
- Bressan, A., et al., *MNRAS*, 427, 127 (2012)
- Broeg, C., et al., *EPJWC*, 47, 3005 (2013)
- Brun, A.S., et al., *Space Science Rev.*, 196, 303 (2015)
- Bruno, G., et al., *A&A*, 595, 89 (2016)
- Buchhave, L.A., et al., *AJ*, 152, 160 (2016)
- Budaj, J., et al., *A&A*, 557, A72 (2013)
- Buldgen, G., et al., *A&A*, 574, 42 (2015a)
- Buldgen, G., et al., *A&A*, 583, 62 (2015b)
- Burke et al., *ApJ*, 809, 8 (2015)
- Cabrera, J., *EAS Pub. Series*, 42, 2010, 109 (2008)
- Cabrera, J., et al., *A&A*, 522, A110, 10 (2010)
- Cabrera, J., et al., *ApJ*, 781, 18 (2014)
- Campante, T.L., et al., *A&A*, 534, 6 (2011)
- Campante, T.L., et al., *ApJ*, 819, 85 (2016)
- Carter, J.A., et al., *Science*, 337, 556 (2012)
- Casewell, S., et al., *ApJ*, 759, L34 (2012)
- Cassan, A., et al., *Nature*, 481, 167 (2012)
- Ceillier, T., et al., *A&A*, 555, 54 (2013)
- Chambers. J., et al., *M&PS*, 37, 1523 (2002)
- Chaplin, W.J., et al., *Science*, 332, 213 (2011a)
- Chaplin, W.J., et al., *ApJ*, 732, 5 (2011b)
- Chaplin, W.J. & Miglio, A., *ARA&A*, 51, 353 (2013)
- Chaplin, W.J., et al., *ApJ*, 766 (2013)
- Chaplin, W.J., et al., *ApJS*, 210, 1 (2014)
- Charbonneau, D., et al., *Protostars and Planets V*, 701, (2007)
- Charbonneau, D., et al., *Nature*, 462, 7275, 891 (2009)
- Charpinet, A., et al., *A&A*, 516, 6 (2010)
- Charpinet, S., et al., *Nature*, 461, 501 (2011)

- Chiappini, C., et al., *A&A*, 449, 591 (2006)
- Chiosi, C., *IAUS*, 239, 235 (2007)
- Christensen-Dalsgaard, J., et al., *MNRAS*, 414, 1158 (2011)
- Christensen-Dalsgaard, J. *Lecture Notes in Physics*, Springer, arXiv160206838C (2016)
- Ciardi, D.R., et al., *ApJ*, 763, 41 (2013)
- Cieplak, A.M. & Griest, K., *ApJ*, 767, 145 (2013)
- Cody, A.M., et al., *AJ*, 147, 82 (2014)
- Coelho, H.R., et al., *MNRAS*, 451, 3011 (2015)
- Corsaro, E., et al., *ApJ*, 757, 190 (2012)
- Cooper, C. S. & Showman, A. P., *ApJL*, 629, L45 (2005)
- Cowan, N.B. & Agol, E., *ApJL*, 678, L129 (2008)
- Cowan, N.B. & Agol, E., *ApJ*, 726, 82 (2011)
- Cranmer, S.R., et al., *ApJ*, 781, 124 (2014)
- Crossfield, I.J.M., et al., *ApJ*, 804, 10 (2015)
- Crossfield, I.J.M., *A&A*, 545, A97 (2012)
- Csizmadia, Sz., et al., *A&A*, 426, 1001 (2004)
- Cunha, M.S. & Metcalfe, T.S., *ApJ*, 666, 413 (2007)
- Czesla, S., et al., *A&A*, 505, 1277 (2009)
- Davies, G.R., et al., *MNRAS*, 446, 2959 (2015)
- Dawson, R.I., et al., *ApJ*, 791, 89 (2014)
- De Mooij, E.J.W., et al., *A&A*, 538, 46 (2012)
- De Ridder, J., et al., *Nature*, 459, 398 (2009)
- De Wit, J., et al., *Nature*, 537, 69 (2016)
- Deeg, H.J., et al., *A&A*, 338, 479 (1998)
- Deeg, H.J. & Doyle, L.R., *EPJWC*, 11, id.05005 (2011)
- Degroote, P., et al., *AN*, 331, 1065 (2010a)
- Degroote, P., et al., *Nature*, 464, 259 (2010b)
- Degroote, P., et al., *A&A*, 536, 82 (2011)
- Degroote, P., et al., *A&A*, 542, 88 (2012)
- Deheuvels, S., et al., *A&A*, 514, 31 (2010)
- Deheuvels, S., et al., *ApJ*, 756, 19 (2012)
- Deheuvels, S., et al., *A&A*, 564, 27 (2014)
- Deheuvels, S., et al., *A&A*, 589, 93 (2016)
- Deheuvels, S. & Michel, E., *A&A* 535, 91 (2011)
- Demory, B.-O., et al., *ApJL*, 735, L12 (2011a)
- Demory, B.-O., et al., *ApJS*, 197, 12 (2011b)
- Demory, B.-O., et al., *ApJL*, 751, L28 (2012)
- Demory, B.-O., *ApJL*, 789, L20 (2014)
- Demory, B.-O., et al., *Nature*, 532, 207 (2016)
- Díaz, R.F., et al., *MNRAS*, 441, 983 (2014)
- Derekas, A., et al., *MNRAS*, 425, 1312 (2012)
- DeVore, J., et al., *MNRAS*, 461, 2453 (2016)
- Dodson-Robinson S. E. & Bodenheimer, P., *Icarus*, 207, 491 (2010)
- Dong, S. & Zhu, Z., *ApJ*, 778, 53 (2013)
- Doyle, L. R., et al., *Science*, 333, 1602 (2011)
- Dressing, C.D., et al., *ApJ*, 800, 135 (2015)
- Duez, V. & Mathis, S., *A&A*, 517, 58 (2010)
- Dumusque, X., et al., *A&A*, 525, 140 (2011a)
- Dumusque, X., et al., *A&A*, 527, 82 (2011b)
- Dumusque, X., et al., *ApJ*, 789, 143 (2014)
- Dvorak, R., et al., *A&A*, 226, 335 (1989)
- Dziembowski, W.A., & Pamyatnykh, A.A., *MNRAS*, 385, 2061 (2008)
- Dzigan, Y., Zucker, S., *ApJL*, 753:L1 (2012)
- Edson, A.R., et al., *Icarus*, 212, 1 (2011)
- Edson, A.R., et al., *Astrobiology*, 12, issue 6 (2012)
- Eggenberger, P., et al., *A&A* 519, 116 (2010)
- Eggenberger, P., et al., *A&A*, 539, 70 (2012)
- Eggleton, P.P., *JASS*, 29, 145 (2012)
- Ehrenreich, D., et al., *A&A*, 547, 18 (2012)
- Ehrenreich, D., et al., *Nature*, 522, 459 (2015)
- Ekenbäck, A., et al., *ApJ*, 709, 670 (2010)
- Elkins-Tanton, L. & Seager, S., *ApJ*, 685, 1237 (2008)
- Erkaev, N.V., et al., *Astrobiology*, 13, 1011 (2013)
- Espinoza, N., et al., *ApJ*, in press (2016)
- Esteves, L.J., et al., *ApJ*, 772, 51 (2013)
- Esteves, L.J., et al., *ApJ*, 804, 150 (2015)
- Evans, T.M., et al., *ApJ*, 722, L16 (2013)
- Fabrycky, D.C., et al., *ApJ*, 750, 114 (2012)
- Fabrycky, D.C., et al., *ApJ*, 790, 146 (2014)
- Faedi, F., et al., *MNRAS*, 410, 899 (2011)
- Faigler, S., et al., *ApJ*, 771, 26 (2013)
- Figueira, P., et al., *A&A*, 493, 671 (2009)
- Figueira, P., et al., *A&A*, 541, 139 (2012)
- Fogtmann-Schulz, A., et al., *ApJ*, 781, 67 (2014)
- Fontaine, G., et al., *PASP*, 113, 409 (2001)
- Fontaine, G. & Brassard, P., *PASP*, 120, 1043 (2008)
- Fontaine, G., et al., *A&A*, 539, 12 (2012)
- Ford, E.B., *PNAS*, 111, 12616 (2014)
- Ford, E.B., & Holman, M.J., *ApJL*, 664, 51 (2007)
- Ford, E.B., et al., *ApJS*, 197, 9 (2011)
- Ford, E. B., et al., *ApJ*, 750, 113 (2012)
- Fortier, A., et al., *A&A*, 473, 311 (2007)
- Fortier, A., et al., *A&A*, 549, 44 (2013)
- Fortney, J. J., et al., *ApJ*, 659, 1661 (2007)
- Fortney, J. J. & Nettelmann, N., *SSRv*, 152, 423 (2010)
- Fossati, L., et al., *ApJ*, 714, L222 (2010)
- Fressin, F., et al., *ApJ*, 766, 81 (2013)
- García-Hernández, A., et al., *A&A*, 506, 79 (2009)
- García Muñoz, A. & Isaak, K.G., *PNAS*, 112, 13461 (2015)
- García Muñoz, A., et al., *ApJ*, 755, 103 (2012)
- García, R.A., et al., *Science*, 329, 1032 (2010)
- Gaulme, P., et al., *A&A*, 524, 47 (2010)
- Giammichele, N., et al., *ApJS*, 199, 29 (2012)
- Gibson, N.P., et al., *MNRAS*, 428, 4380 (2013)
- Gillet, D., et al., *A&A*, 553, 59 (2013)
- Gilliland, R.L., et al., *PASP*, 122, 131 (2010)
- Gilliland, R.L., et al., *ApJS*, 197, 6 (2011)
- Gilliland, R.L., et al., *ApJ*, 766, 40 (2013)
- Gillon, M., et al., *A&A*, 520, A97 (2010)
- Gillon, M., et al., *Nature*, 533, 221 (2016)
- Gizon, L., et al., *Proc. of the National Academy of Science*, 110, 13267 (2013)
- Gizon, L. & Solanki, S.K., *ApJ*, 589, 1009 (2003)
- Godolt, M., et al., *PSS*, 111 (2015)
- Gómez de Castro, A. I., et al., *Ap&SS*, 335, 283 (2011)
- Gough, D., *LNP*, 367, 283 (1990)
- Goupil, M.J., et al., *JPhCS*, 271, 012031 (2011)
- Grasset, O., et al., *ApJ*, 693, 722 (2009)
- Grenfell, J.L., et al., *P&SS*, 98, 66 (2014)
- Grigahcène, A., et al., *MNRAS*, 422, L43 (2012)
- Guilera, O. M., et al., *A&A*, 532, 142 (2011)
- Guillot, T., & Havel, M., *A&A*, 527, 20 (2011)
- Guillot, T., et al., *ApJL*, 459, L35 (1996)
- Guillot, T., et al., *A&A*, 453, L21 (2006)
- Haswell, C., et al., *ApJ*, 760, 79 (2012)

- Heber, U., *ARA&A*, 47, 211 (2009)
- Hébrard, É.M., et al., *MNRAS* 443, 2599 (2014)
- Hekker, S., et al., *MNRAS*, 418, 119 (2011)
- Hekker, S., et al., *A&A*, 544, 90 (2012)
- Helled, R. & Bodenheimer, P., *Icarus*, 211, 939 (2011)
- Helled, R., et al., *ApJ*, 726, 15 (2011)
- Helled, R. & Guillot, T., *ApJ*, 767, 113 (2013)
- Helled, R. & Schubert, G., *Icarus*, 198, 156 (2008)
- Heller, R., & Barnes, R., *Astrobiology*, 13, 18 (2012)
- Heller, R., *ApJ*, 787, 14 (2014)
- Heller, R., et al., *ApJ*, 820, 88 (2016)
- Heng, K., et al., *MNRAS*, 413, 2380 (2011)
- Hippke, M., et al., *ApJ*, 825, 73 (2016)
- Hippke, M., *ApJ*, 806 51 (2015)
- Hirano, T., et al., *ApJ*, 783, 9 (2014)
- Hogan, E., et al., *MNRAS*, 396, 2074 (2009)
- Holmström, M., et al., *Nature*, 451, 970 (2008)
- Hori, Y. & Ikoma, M., *MNRAS*, 416, 1419 (2011)
- Houdek, G., *Ap&SS*, 328, 237 (2010)
- Houdek, G. & Dupret, M.A., *LRSP*, 12,8 (2015)
- Howard, A.W., et al., *ApJS*, 201, 15 (2012)
- Howell, S., et al., *PASP*, 126, 398 (2014)
- Hu, R., et al., *ApJ*, 802, 51 (2015)
- Huber, D., et al., *ApJ*, 760, 32 (2012)
- Huber, D., et al., *ApJ*, 767, 127 (2013)
- Huber, D., *arXiv151107441* (2015)
- Huber, D., *arXiv160407442H* (2016)
- Hubickyj, O., et al., *Icarus*, 179, 415 (2005)
- Ida, S. & Lin, D.N.C., *ApJ*, 604, 388 (2004)
- Ikoma, M., et al., *ApJ*, 537, 1013 (2000)
- Jenkins, J., et al., *Icarus*, 119, 224 (1996)
- Jenkins, J., et al., *ApJ*, 713, L87 (2010)
- Johnson, J.A., et al., *PASP*, 122, 701 (2010a)
- Johnson, J.A., et al., *ApJL*, 721, L153 (2010b)
- Joshi, M.M., et al., *Icarus*, 129, Issue 2 (2011)
- Joshi, M.M. & Haberle, R.M., *Astrobiology*. 12, 1 (2012)
- Jura, M., *A.J.*, 130, 1261 (2005)
- Kallinger, T., et al., *A&A*, 570, 41 (2014)
- Kasting, J. F., et al., *Icarus*, 101, 108 (1993)
- Kennedy, G.M., & Kenyon, S.J., *ApJ*, 673, 502 (2008)
- Kiang, N. Y. et al., *MNRAS*, 452, 4 (2015)
- Kipping, D.M., *MNRAS*, 396, 1797 (2009)
- Kipping, D.M., et al., *MNRAS*, 400, 398 (2009)
- Kipping, D.M., et al., *ApJ*, 750, 115 (2012)
- Kipping, D.M., et al., *MNRAS*, 434, 1883 (2013)
- Kipping, D.M., et al., *MNRAS* 435, 2152 (2013b)
- Kipping, D.M., et al., *ApJ*, 795, 25 (2014)
- Kipping, D.M., et al., *ApJ*, 813, 14 (2015)
- Kitzmann, D., et al., *MNRAS*, 452, 3752 (2015)
- Kislyakova, K.G., et al., *Astrobiology*, 13, 1030 (2013)
- Kjeldsen, H., et al., *ApJ*, 683, L 175 (2008)
- Knutson, H.A., et al., *Nature*, 447, 183 (2007)
- Knutson, H.A., et al., *ApJ*, 690, 822 (2009)
- Knutson, H.A., et al., *ApJ*, 735, 27 (2011)
- Koch, D.G., et al., *ApJL*, 713, L79 (2010)
- Kolenberg, K., et al., *MNRAS*, 411, 878 (2011)
- Kollath, Z., et al., *MNRAS*, 414, 1111 (2011)
- Kopparapu, R.K., et al., *ApJ*, 765, 2 (2013)
- Kopparapu, R.K., et al., *ApJ*, 787, 29 (2014)
- Koskinen, T. T., et al., *Icarus*, 226, 1678 (2012)
- Kovacs, B., et al., *ApJ*, 724, 866 (2010)
- Kunder, A., et al., *AJ*, 141, 15 (2011)
- Lammer, H., et al., *Ap&SS*, 335, 9 (2011a)
- Lammer, H., et al., *Ap&SS*, 335, 39 (2011b)
- Lammer, H., et al., *EP&S*, 64, 179 (2012)
- Lammer, H., et al., *MNRAS*, 461, L62 (2016)
- Lanza, A.F., *LNP*, 914, 43 (2016)
- Laughlin, G., et al., *ApJ*, 729, 7 (2011)
- Le Borgne, J.-F., et al., *AJ*, 144, 39 (2012)
- Lebreton, Y. & Goupil, M.J., *A&A*, 544, 13 (2012)
- Lebreton, Y. & Goupil, M.J., *A&A*, 569, 21 (2014)
- Lebreton, Y., et al., *EAS Pub. Series*, 65, 9 (2014a)
- Lebreton, Y., et al., *EAS Pub. Series* 65, 177 (2014b)
- Lecavelier des Etangs, A., et al., *A&AS*, 140, 15 (1999)
- Lecavelier des Etangs, A., et al., *A&A*, 543, 4 (2012)
- Lecoute, J. & Charbier, G., *A&A*, 540, 20 (2012)
- Leconte, J., et al., *A&A*, 554, 69 (2013)
- Lefever, K., et al., *A&A*, 463, 1093 (2007)
- Léger, A., et al., *Icarus*, 169, 499L (2004)
- Liebert, J., et al., *ApJ*, 769, 7 (2013)
- Lillo-Box, J., et al., *A&A*, 589, 124 (2016)
- Linsky, J. L., et al., *ApJ*, 717, 1291 (2010)
- Lissauer, J.J., *ApJ*, 660, 149L (2007)
- Lissauer, J. J., et al., *Nature*, 470, 53 (2011)
- Lissauer, J. J., et al., *ApJ*, 770, 131 (2013)
- Lissauer, J.J., et al., *ApJ*, 784, 44 (2014)
- Llama, J., et al., *MNRAS*, 416, L41 (2011)
- Loeb, E.D., & Maoz, D., *MNRAS*, 432, 11 (2013)
- Ludwig, H.-G., et al., *A&A*, 506, 167 (2009)
- Lund, M.N., et al., *A&A*, 570, 54 (2014)
- Lundkvist, M.S., et al., *Nature Coms*, 7, 11201 (2016)
- MacDonald, M.G., et al., *AJ*, 152, 105 (2016)
- Madhusudhan, N. & Seager, S., *ApJ*, 707, 24 (2009)
- Maeder, A., *A&A*, 26, 215 (1973)
- Maeder, A., "Physics, Formation and Evolution of Rotating Stars", *Astronomy and Astrophysics Library*. ISBN 978-3-540-76948-4. Springer Berlin Heidelberg (2009)
- Maeder, A. & Zahn, J.-P., *A&A*, 265, 115Z (1992)
- Maeder, A. & Zahn, J.-P., *A&A*, 334, 1000 (1998)
- Magic, Z., et al., *A&A*, 560, 8 (2013)
- Magic, Z., et al., *A&A*, 573, 90 (2015a)
- Magic, Z., et al., *A&A*, 573, 89 (2015b)
- Mantegazza, L., et al., *A&A*, 542, 24 (2012)
- Marley, M.S., et al., *JGR*, 100, 23349 (1995)
- Marques, J.P., et al., *A&A*, 549, 74 (2013)
- Marsden, S.C., et al., *MNRAS* 444, 3517 (2014)
- Martins, F., *EAS*, 65, 75 (2014)
- Masuda, K., *ApJ*, 783, 53 (2014)
- Mathis, S., *LNP*, 865, 23 (2013)
- Mathis, S., *A&A*, 580, 3 (2015)
- Mathur, S., *ASPC*, 479 425 (2013)
- Mathur, S., *sf2a conf.*, p. 257 (2014)
- Mathur, S., et al., *ApJ*, 741, 119 (2011)
- Mathur, S., et al., *A&A*, 550, 32 (2013)
- Matijevic, G., et al., *AJ*, 143, 123 (2012)
- Mayer, L., et al., *MNRAS*, 363, 641 (2005)
- Mayor, M. & Queloz, D., *Nature*, 378, 355 (1995)
- Mazeh, T., et al., *A&A*, 521, 59 (2010)
- Mazumdar, A., *A&A*, 441, 1079 (2005)

- Mazumdar, A., et al, ApJ, 782, 18 (2014)
McArthur, B.E., et al., ApJ, 715, 1203 (2010)
McLaughlin, D.B., ApJ, 60, 22 (1924)
Meadows, V.S., et al., arXiv : 1698.08620 (2016)
Metcalfé, T.S., et al., ApJS, 214, 27 (2014)
Metcalfé, T.S., et al., ApJ, 811, 37 (2015)
Michel, E., et al., Science, 322, 558 (2008)
Miglio, A., et al., A&A, 520, 6 (2010)
Miglio, A., et al., MNRAS, 419, 2077 (2012a)
Miglio, A., et al., EPJWC, 1905012M (2012b)
Miglio, A., et al., MNRAS, 429, 423 (2013)
Militzer, B., et al., ApJL, 688, L45 (2008)
Miller, N. & Fortney, J.J., ApJL, 736, L29 (2011)
Mills, S.M., & Fabrycky, D., AJ, 153, 45 (2017)
Mills, S.M., et al., Nature, 533, 509 (2016)
Molnár, L., et al., MNRAS, 424, 31 (2012)
Montalban, J., et al., ApJ, 766, 118 (2013)
Monteiro, M.J.P.F.G., et al., ESASP, 485, 291 (2002)
Montet, B.T. & Simon, J.D., ApJ, 830, 39 (2016)
Moravveji, E., et al., ApJ, 747, 108 (2012a)
Moravveji, E., et al., ApJ, 749, 74 (2012b)
Mordasini, C., et al., A&A, 501, 1161 (2009)
Mordasini, C., et al., A&A, 541, 97 (2012a)
Mordasini, C., et al., A&A, 547, 111 (2012b)
Mortier, A., et al., A&A, 557, 70 (2013)
Mosser, B., et al., A&A, 532, 86 (2011)
Mosser, B., et al., A&A, 540, 143 (2012a)
Mosser, B., et al., A&A, 548, 10 (2012b)
Mosser, B., et al., A&A, 550, 126 (2013)
Moutou, C., et al., MNRAS, 459, 1993 (2016)
Muirhead, P.S., et al., ApJ, 767, 111 (2012)
Murphy, S.J., MNRAS, 453, 2569 (2015)
Nascimbeni, V., et al., MNRAS, 463, 4210 (2016)
Namouni, F., ApJL, 719, 145 (2010)
Nettelmann, N., et al., ApJ, 683, 1217 (2008)
Niedzielski, A., et al., ApJ, 803, 1 (2015)
Nielsen, M.B., et al., A&A, 568, 12 (2014)
Nielsen, M.B., et al., A&A, 582, 10 (2015)
Nikolov, N., et al., MNRAS, 447, 463 (2015)
Noack, L., & Breuer, D., P&SS, 98 41 (2013)
Nordhaus, J., & Spiegel, D.S., MNRAS, 432, 500 (2013)
Ofir, A., & Dreizler, S., A&A, 555, 58 (2013)
Ogilvie, G.I., MNRAS, 429, 613 (2013)
Ohta, Y., et al., ApJ, 690, 1 (2009)
Ollivier, M., et al., in the "CoRoT Legacy Book",
coordinator A. Baglin, ISBN: 978-2-7598-1876-
1 (2016)
Osborn, H.P., et al., MNRAS, 457, 2273 (2016)
Oshagh, M., et al., A&A, 556, 190 (2013)
Østensen, R., et al., MNRAS, 408, 51 (2010)
Pápics, P.I., et al., A&A, 528, 123 (2011)
Pápics, P.I., et al., A&A, 542, 55(2012)
Pápics, P.I., et al., A&A, 553, 127 (2013)
Parmentier, V., et al., ApJ, 828, 22 (2016)
Pasquini, L., et al., A&A, 473, 979 (2007)
Pepe, F., et al., AN, 335, 8 (2014)
Petigura, E.A., et al., PNAS, 110, 19273 (2013)
Petit, P., et al., MNRAS, 388, 80 (2008)
Pierens, A. & Nelson, R.P., A&A, 483, 633 (2007)
Pinheiro, F.J.G., et al., MNRAS, 445, 2223 (2014)
Podolak, M., et al., P&SS, 43, 1517 (1995)
Pont, F., et al., MNRAS, 432, 2917 (2013)
Poretti, E., et al., A&A, 506, 85 (2009)
Poretti, E., et al., A&A, 520, 108 (2010)
Poretti, E., et al., A&A, 528, 147 (2011)
Prsa, A., et al., AJ, 141, 83 (2011)
Queloz, D., et al., A&A, 359, L13 (2000)
Quintana, E.V., et al., ApJ, 767, 137 (2013)
Rafert, J.B. & Twigg, L.W., MNRAS, 193, 79 (1980)
Rappaport, S., et al., ApJ, 752, 1 (2012)
Rauer, H., et al., A&A, 529, 8 (2011)
Rauer, H., et al., in: 'Habitability of Other Planets and
Satellites ', ed: deVera (2013)
Rauer, H., et al., ExA, 38, 249 (2014)
Reese, D.R., et al., A&A, 539, 63 (2012)
Reese, D.R., et al., A&A, 592, 14 (2016)
Remus, M., et al., A&A, 541, 165 (2012)
Réville, V., et al., ApJ, 814, 99 (2015)
Ribas, I., et al., A&A, 596, 111 (2016)
Ricker, G., et al., JATIS, 1, 4003 (2015)
Rogers, T.M., et al., ApJ, 772, 21 (2013)
Roxburgh, I.W., A&A, 506, 435 (2009)
Rossiter, R.A., ApJ, 60, 15 (1924)
Rowe, J.F., et al., ApJ, 784, 45 (2014)
Saio, H., et al., ApJ, 650, 1111 (2006)
Samadi, R., et al., in Proc. of "The CoRoT Mission Pre-
Launch Status – Stellar Seismology and Planet
Finding" ESA SP-1306 (2006)
Samadi, R., et al., A&A, 559, 40 (2013)
Samus, N.N., et al., A&AT, 27, 73 (2012)
Sanchís-Ojeda, R., et al., Nature, 487, 449 (2012)
Sanchís-Ojeda, R., et al., AN 334, 180 (2013)
Santerne, A., et al., Proceedings SF2A-2013, Eds.: L.
Cambresy, F. Martins, E. Nuss, A. Palacios
(2013)
Santerne, A., et al., MNRAS, 451, 2337 (2015)
Santerne, A., et al., A&A, 587, 43 (2016)
Sartoretti, P. & Schneider, J., A&AS, 134, 553 (1999)
Saumon, D. & Guillot, T., ApJ, 609, 1170 (2004)
Scalo, J., et al., Astrobiology, 7, Issue 1 (2007)
Scaringi, S., et al., MNRAS, 431, 2535 (2013)
Scaringi, S., et al., MNRAS, 463, 2265 (2016)
Seager, S., et al., ApJ, 669, 1279 (2007)
Schneider, J., et al., Conf. Ser 134 (Ed Rebolo, Martin,
Zapatero Osirio) (1998)
Schneider, J., et al., A&A, 532, 79 (2011)
Shabram, M., et al., ApJ, 820, 93 (2016)
Shiode, J.H., et al., MNRAS, 430 1736 (2013)
Showman, A.P. & Guillot, T., A&A, 385, 166 (2002)
Showman, A.P. & Polvani, L.M., ApJ, 738, 71 (2011)
Showman, A.P., et al., ApJ, 699, 564 (2009)
Shporer, A. & Hu, R., AJ, 150, 112 (2015)
Shustov, B., et al., Ap&SS, 320, 187 (2009)
Shustov, B., et al., Ap&SS, 335, 273 (2011)
Silva Aguirre, V., et al., ApJ, 757, 99 (2012)
Silva Aguirre, V., et al., ApJ, 769, 141 (2013)
Silva Aguirre, V., et al., MNRAS, 452, 2127 (2015)
Silva-Valio, A., ApJ 683, 179 (2008)
Silva-Valio, A. & Lanza, A.F., A&A 529, 36 (2011)
Silvotti, R., et al., Nature, 449, 189 (2007)

- Silvotti, R., et al., *A&A*, 570, 130 (2014)
- Simon, A.E., et al., *MNRAS*, 419, 164 (2012)
- Simon, A.E., et al., *PASP*, 127, 1084 (2015)
- Sing, D.K., et al., *MNRAS*, 446, 2428 (2015)
- Sing, D.K., et al., *Nature*, 529, 59 (2016)
- Skemer, A.J., et al., *ApJ*, 817, 166 (2016)
- Slawson, R.W., et al., *AJ*, 142, 160 (2011)
- Sohl, F. & Schubert, G., In: *Treatise on Geophysics* (Editor-in-Chief G. Schubert), Volume 10, Planets and Moons, Ed. T. Spohn, p. 27-68, Elsevier (2007)
- Snellen, I.A.G., et al., *Nature*, 459, 543 (2009)
- Snellen, I.A.G., et al., *A&A*, 513, 76 (2010)
- Sonoi, T., et al., *A&A*, 583, A112 (2015)
- Sotin, C., et al., *Icarus*, 191, 337 (2007)
- Southworth, J., *ASPS*, 496, 164 (2015)
- Sozzetti, A., et al., *MNRAS*, 437, 497 (2014)
- Steffen, J.H. & Hwang, J.A., *MNRAS*, 448, 1956 (2015)
- Steffen, J.H., et al., *MNRAS*, 428, 1077 (2012)
- Stello, D., et al., *ApJ*, 739, 13 (2011)
- Stevenson, K.B., et al., *Science*, 346, 838 (2014)
- Straniero, O., et al., *PASA*, 20, 398 (2003)
- Strugarek, A., et al., *ApJ*, 815, 111 (2015)
- Suárez, J.C., et al., *A&A*, 449, 673 (2006)
- Suárez, J.C., et al., *ApJ*, 690, 1401 (2009)
- Suárez, J.C., et al., *A&A*, 563, 7 (2014)
- Sullivan, P.W., et al., *ApJ*, 809, 77 (2015)
- Swift, D.C., et al., *ApJ*, 744, 595 (2012)
- Szabó, R., et al., *MNRAS*, 409, 1244 (2010)
- Szabó, R., et al., *MNRAS*, 413, 2709 (2011)
- Thompson, M.A., et al., *MNRAS*, 458, 39 (2016)
- Thoul, A., et al., *A&A*, 551, 12 (2013)
- Tkachenko, A., et al., *A&A*, 556, 52 (2013)
- Tran, K., et al., *ApJ*, 774, 81 (2013)
- Traub, W.E., *ApJ*, arXiv:1605.02255 (2016)
- Tremblay, P.E., et al., *A&A*, 557, 7 (2013)
- Turbet, M., et al., *A&A*, 596, 112 (2016)
- Udry, S. & Santos, N. C., *ARA&A*, 45, 397 (2007)
- Uytterhoeven, K., et al., *A&A*, 534, 125 (2011)
- Valencia, D., et al., *Icarus*, 181, 545 (2006)
- Valencia, D., et al., *ApJ*, 665, 1413 (2007)
- Valle, G., et al., *A&A*, 575, 12 (2015a)
- Valle, G., et al., *A&A*, 579, 59 (2015b)
- Vanderburg, A., et al., *Nature*, 526, 546 (2015)
- Van Grootel, V., et al., *A&A*, 553, 97 (2013)
- Van Saders, J.L., et al., *Nature*, 529, 181 (2016)
- Van Eylen, V., et al., *ApJ*, 782, 14 (2014)
- Vazan, A. & Helled, R., *ApJ*, 756, 90 (2012)
- Verma, K., et al., *ApJ* 790, 138 (2014a)
- Verma, K., et al., *ApJ*, 794, 114 (2014b)
- Vidal-Madjar, A., et al., *Nature*, 422, 143 (2003)
- Vidal-Madjar, A., et al., *ApJ*, 604, 69 (2004)
- Vigan, A., et al., *A&A*, 544, 9 (2012)
- Wagner, F.W., et al., *Icarus*, 214, 366 (2011)
- Wagner, F.W., et al., *A&A*, 541, 103 (2012)
- Webber, M.W., et al., *ApJ*, 804, 94 (2015)
- Weiss, W.W., et al., *ApJ*, 819 (2016)
- Welsh, W.F., et al., *ApJL*, 713, L145 (2010)
- Welsh, W.F., et al., *Nature*, 481, 475 (2012)
- Winn, J.N. & Fabrycky, D.C., *ARA&A*, 53, 409 (2015)
- Winn, J.N., et al., *ApJ*, 631, 1215 (2005)
- Winn, J.N., et al., *ApJ*, 741, 1 (2011)
- Winn, J.N., *Exoplanets*, ed. S. Seager (Tucson, AZ: University of Arizona Press), 55 (2011)
- White, T.R., et al., *EPJWC*, 101, p.06068 (2015)
- Xue, Y., et al., *ApJ*, 784, 66 (2014)
- Yang, J., et al., *ApJ*, 787, Issue 1 (2014)
- Zahn, J.P., *A&A*, 265, 115 (1992)
- Zeng, L., et al., *ApJ*, 819, 127 (2016)
- Zhang, C.G., et al., *ApJ*, 759, 14 (2012)
- Zhang, C.G., et al., *RAA*, 13, 1127 (2013)
- Zhang, Q.S. & Li, Y., *ApJ*, 750, 11 (2012a)
- Zhang, Q.S. & Li, Y., *ApJ*, 746, 50 (2012b)
- Zsom, A., et al., *ApJ*, 778, 109 (2013)
- Zucker, S., et al., *ASPC*, 371, 447 (2007)
- Zwintz, K., et al., *A&A*, 550, 121 (2013)
- Zwintz, K., et al., *Nature*, 345, 550 (2014)

12 List of Acronyms

1D	one dimensional	DC	Direct Current
3D	three dimensional	DHS	Data Handling System
AEU	Ancillary Electronics Units	DLR	Deutsches Zentrum für Luft- und Raumfahrt
AFE	Analogue Front End	DOF	Degree Of Freedom
AGB	Asymptotic Giant Branch	DP	Data Product (DP1-DP6)
AGN	Active Galactic Nuclei	DPAC	<i>Gaia</i> Data Processing & Analysis Consortium
AIT	Assembly, Integration and Testing	DPS	Data Processing System
AIV	Assembly, Integration and Verification	DPU	Data Processing Unit
AO	Announcement of Opportunity	DTCP	Daily TeleCommunication Period
AOCS	Attitude and Orbit Control System	EB	Eclipsing Binary
APOGEE	APO Galactic Evolution Experiment	E-ELT	European Extremely Large Telescope
ASI	Agenzia Spaziale Italiana	EKF	Extended Kalman Filter
au	Astronomical Unit	EMC	ElectroMagnetic Compatibility
BP/RP	Gaia Blue Photometer/Red Photometer	EOS	Equation of State
CARMENES	Calar Alto high-Resolution search for M dwarfs with Exoearths with Near-infrared and optical Échelle Spectrographs	EPO	Education and Public Outreach
CBP	CircumBinary Planet	EPOCO	Education and Public Outreach Coordination Office
CCD	Charge Coupled Device	ESA	European Space Agency
CCSDS	Consultative Committee for Space Data Systems	ESAC	European Space Astronomy Centre
CDMS	Command and Data Management System	ESO	European Southern Observatory
CDR	Critical Design Review	ESOC	European Space Operations Centre
CFE/CFI	Customer Furnished Equipment/Item	ESPRESSO	Echelle SPECTrograph for Rocky Exoplanet and Stable Spectroscopic Observations
CFRP	Carbon-Fibre Reinforced Plastic	EUV	Extreme UltraViolet
CHEOPS	CHaracterising ExoPlanet Satellite	EW	Equivalent Width
CME	Coronal Mass Ejection	F-	Fast camera
CNES	Centre National d'Études Spatiales	FAR	Flight Acceptance Review
CoRoT	COncvection ROTation and planetary Transits	FDIR	Failure Detection Isolation and Recovery
CPU	Control Processing Unit	FEE	Front End Electronics
CSIC	Centro Superior de Investigaciones Científicas	FEU	Fast Electronics Unit
CSS	Camera Support Structure	FF	Full Frame
CTI	Charge Transfer Inefficiency	FGS	Fine Guidance Sensor
CTR	Central Time Reference	FIES	Fibre-fed Echelle Spectrograph
CU	Coordination Unit	FITS	Flexible Image Transport System
CV	Cataclysmic Variables	FoV	Field of View
DAC	Digital to Analogue Converter	FPA	Focal Plane Assembly
DB	DataBase	FPGA	Field-Programmable Gate Array
		FPM	Fine Pointing Mode

FSS	FEE Support Structure	MHD	MagnetoHydroDynamics
FT	Full Transfer	MLA	MultiLateral Agreement
GAM	Guided Attitude Mode	MLI	Multi-Layer Isolation
GCVS	General Catalogue of Variable Stars	MLT	Mixing Length Theory
GO	Guest Observer	MMU	Mass Memory Unit
GOP	Ground Based Observations Program	MOC	Mission operations Centre
GRB	Gamma-Ray Burst	MPE	Mean Pointing Error
GSE	Ground Support Equipment	MPI	Max Planck Institute
GTO	Guaranteed Time Observation	MPSRR	Max Planck Institute for Solar System Research
HARPS	High Accuracy Radial Velocity Planet Searcher	MS	Main Sequence
HAT	Hungarian-made Automated Telescope	MSM	Master Synchronisation Module
HGA	High Gain Antenna	MW	Milky Way
HIRES	High REsolution Spectrometer	N-	Normal camera
HK	House Keeping data	NASA	National Aeronautics and Space Administration
HR	Hertzprung–Russell	NGTS	Next Generation Transit Survey
HST	Hubble Space Telescope	NNO	New NORcia
HZ	Habitable Zone	NOT	Nordic Optical Telescope
IAS	Institut d'Astrophysique Spatiale	NPF	Northern PLATO Field
ICU	Instrument Control Unit	NSR	Noise to Signal Ratio
IGW	Internal Gravity Wave	OBC	On-Board Computer
INAF	Instituto Nazionale di Astrofisica	OCM	Orbit Control Manoeuvre
INM	Inertial Pointing Mode	OHP	Haute-Provence Observatory
INTA	Instituto Nacional de Tecnología Aeroespacial	OLM	OffLoading Mode
IR	InfraRed	OSE	Optical Sampling Effect
ISO	International Organization for Standardization	OU	Open University
ITT	Invitation To Tender	PanSTARRS	Panoramic Survey Telescope and Rapid Response System
JAXA	Japan Aerospace Exploration Agency	PCDU	Power Conditioning & Distribution Unit
JWST	James Webb Space Telescope	PCOT	PMC Calibration and Operations Team
KOI	Kepler Object of Interest	PCL	Payload Consortium Lead
LAM	Laboratoire d'Astrophysique de Marseille	PDC	PLATO Data Centre
LAMOST	Large Sky Area Multi-Object Fibre Spectroscopic Telescope	PDPC	PLATO Data Processing Centre
LEOP	Launch and Early Orbit Phase	PDPM	PLATO Data Processing Manager
LGA	Low Gain Antenna	PDS	Payload Data Storage
LOFAR	Low-Frequency Array	PI	Principal Investigator
LOP	Long-duration Observation Phase	PIC	PLATO Input Catalogue
LSST	Large Synoptic Survey Telescope	PIPM	PLATO Instrument Project Manager
LTE	Local Thermodynamic Equilibrium	PLATO	PLAnetary Transits and Oscillations of stars
MAR	Mission Adoption Review	PLM	Payload Module
MEU	Main Electronics Unit	PMC	PLATO Mission Consortium
MG	<i>Gaia</i> Magnitude	PMS	Pre Main Sequence
		ppm	part per million

PS	Project Scientist	SPB	Slow Pulsating B-star
PSF	Point Spread Function	SPC	Science Programme Committee
PSM	PLATO Mission Consortium Science Management	SPF	Southern PLATO Field
PSRR	PLATO Payload, Science Ground-segment and Science Performance System Requirement Review	SpW	Space Wire
PSU	Power Supply Unit	SS	Step&Stare
RAVE	RAdial Velocity Experiment	SVM	Service Module
RC	Red Clump	SW	SoftWare
RCS	Reaction Control System	SWT	Science Working Team
RF	Radio-Frequency	TAC	Time Allocation Committee
RFDA	RF Distribution Assembly	TBC	To Be Confirmed
RGB	Red Giant Branch	TC	Telecommand
RIU/RTU	Remote Interface/Terminal Unit	TCM	Trajectory Correction Manoeuvre
RM	Rossiter–McLaughlin effect	TDV	Transit Duration Variations
RMAP	Remote Memory Access Protocol	TESS	Transiting Exoplanet Survey Satellite
rms	Root mean square	TLS	Thüringer Landessternwarte Tautenburg
RPE	Relative Pointing Error	TM	Telemetry
RPM	Reduced Proper Motion	TNG	Telescopio Nazionale Galileo
RV	Radial Velocity	TOU	Telescope Optical Unit
RW	Reaction Wheels	TRL	Technology Readiness Level
S/C	Spacecraft	TRP	Temperature Reference Point
S/S	Sub-System	TT&C	Telemetry, Tracking and Command
SAM	Sun Acquisition Mode	TTV	Transit Time Variations
sdB	subdwarf B	TWTA	Travelling Wave Tube Amplifier
SDRAM	Synchronous Dynamic Random Access Memory	UCAC	USNO CCD Astrograph Catalog
SDSS	Sloan Digital Sky Survey	URL	Uniform Resource Locator
SEGUE	Sloan Extension for Galactic Understanding and Exploration	UV	UltraViolet
SFM	SaFe Mode	VIRGO	Variability of solar IRradiance and Gravity Oscillations
SGS	Science Ground Segment	VISTA	Visible and Infrared Survey Telescope for Astronomy
SKA	Square Kilometre Array	VLT	Very Large Telescope
SLM	SLew Mode	WD	White Dwarf
SMU	Satellite Management Unit	WDE	Wheel Drive Electronics
SNM	Science Normal Mode	WMM	Wheel Management Mode
SNR	Signal-to-Noise Ratio	WSO-UV	World Space Observatory - Ultraviolet
SOC	Science Operations Centre	XRB	X-Ray Binaries
SOHO	Solar & Heliospheric Observatory	XUV	Extreme UltraViolet
SOP	Step-and-stare Observation Phase	YSO	Young Stellar Object

Annex: Definition Study Contributors

Austria

Manuel Guedel (U Vienna), Franz Kerschbaum (U Vienna), Friedrich Kupka (U Vienna), Helmut Lammer (AAS), Armin Luntzer (U Vienna), Roland Ottensamer (U Vienna), Manfred Steller (ÖAW), Eduard Vorobiev (U Vienna), Konstanze Zwintz (Innsbruck)

Belgium

Conny Aerts (KUL), Ann Baeke (U Liege), Joris De Ridder (KUL), Jonas Debosscher (KUL), Marc-Antoine Dupret (U Liege), Michael Gillon (U Liege), Rik Huygen (KUL), Ehsan Moravveji (KUL), Thierry Morel (U Liege), Peter Papics (KUL), Sara Regibo (KUL), Etienne Renotte (U Liege), Pierre Royer (KUL), Hugues Sana (KUL), Andrew Tkachenko (KUL), Bart Vandenbussche (KUL)

Brazil

Fabio de Oliveira Fialho (USP), Eduardo Janot Pacheco (USP), Victor Atilio Marchiori (USP), Vanderlei Parro (IMT), Sérgio Ribeiro (IMT), Adriana Valio (CRAAM)

Czech Republic

Michal Svanda (AUUK)

Denmark

Victor Silva Aguirre (U Aarhus), Lars Buchhave (Copenhagen), Jorgen Christensen-Dalsgaard (U Aarhus), Oliver Gressel (Niels Bohr Inst.), Günter Houdek (U Aarhus), Christoffer Karoff (U Aarhus), Hans Kjeldsen (U Aarhus)

ESA

David Agolon (ESTEC), Tobias Boenke (ESTEC), Lionel Bonora (ESTEC), Ludovic Duvet (ESTEC), César García Marirrodriaga (ESTEC), Philippe Gondoin (ESTEC), Ana M. Heras (ESTEC), Astrid Heske (ESTEC), Bengt Johlander (ESTEC), Ralf Kohley (ESAC), Tim Oosterbroek (ESTEC), Laurence O'Rourke (ESAC), Göran Pilbratt (ESTEC), Thibaut Prodhomme (ESTEC), Anamarija Stankov (ESTEC), Peter Verhoeve (ESTEC)

France

Jose-Manuel Almenara (LAM), Thierry Appourchaux (IAS), Herve Ballans (IAS), Jerome Ballot (IRAP), Caroline Barban (OBSPM), Clément Baruteau (IRAP), Frederic Baudin (IAS), Paul Beck (CEA), Kevin Belkacem (LESIA), Isabelle Boisse (LAM), Xavier Bonfils (IPAG), Francois Bouchy (LAM), Gwenael Boué (IMCCE), Patrick Boumier (IAS), Allan-Sacha Brun (IRFU/Sap), Tristan Buey (LESIA), Christophe Cara (CEA), Claude Catala (OBSPM), Pierre-Yves Chabaud (LAM), Andre Chardin (IAS), Sébastien Charnoz (CEA), Enrico Corsaro (CEA), Orlagh L. Creevey (OCA), Aurélian Crida (OCA), Cilia Damiani (OBSPM), Sebastien Deheuvels (IRAP), Magali Deleuil (LAM), Alexis Deru (LESIA), Rodrigo Diaz (LAM), Thomas Fenouillet (LAM), Agnes Fienga (OCA), Mario Flock (CEA), Thierry Forveille (IPAG), Sebastien Fromang (CEA), Rafael A. Garcia (CEA), Marie Jo Goupil (OBSPM), Emmanuel Grolleau (LESIA), Tristan Guillot (OCA / CNRS), Guillaume Hébrard (IAP / OHP), Jacques Laskar (IMCCE), Yveline Lebreton (OBSPM), Alain Lecavelier (IAP), Geoffroy Lesur (IPAG), Patrick Levacher (LAM), Marco Mancini (LESIA), Joao Pedro Marques (Paris-Sud), Douglas Marshall (Paris Diderot), Stéphane Mathis (CEA/DSM/LESIA), Héloïse Meheut (CEA), Jean-Charles Meunier (LAM), Eric Michel (LESIA), Alessandro Morbidelli (OCA), Chrystel Moreau (LAM), Benoit Mosser (Meudon), Claire Moutou (LAM), Ana Palacios (Montpellier), Pascal Petit (OMP), Arnaud Pierens (Bordeaux), Philippe Plasson (LESIA), Bertrand Plez (Montpellier), Alejandra Recio-Blanco (OCA), Daniel Reese (LESIA), Françoise Remus (OBSPM), Michel Rieutord (IRAP), Fabrice Roy (LUTH), Réza Samadi (LESIA), Christian Surace (LAM), Didier Tiphène (OBSPM), Arthur Vigan (LAM)

Germany

Matthias Ammler-von Eiff (MPSSR), Bernhard Bandow (MPSSR), Peter Becker (DLR), Rainer Berlin (DLR), Aaron Birch (MPSSR), Stefanie Bogner (OHB), Anko Börner (DLR), Steve Boudreault (MPSSR), Michael Bruns (MPSSR), Raymond Burston (MPSSR), Juan Cabrera (DLR), Robert Cameron (MPSSR), Ludmila Carone (MPIA), Stefania Carpano (MPE), Valerian Chifu (MPSSR), Szilard Csizmadia (DLR), Johanna dall'Amico (OHB), Stefan Dreizler (IAG), Claudia Dreyer (DLR), Cornelis Dullemond (U Heidelberg), Philipp Eigmüller (DLR), Jochen Eisloffel ((TLS), Anders Erikson (DLR), Ines Ernst (DLR), Ignasi Forcada (OHB), Stefanie Gebauer (DLR), Laurent Gizon (MPSSR), Mareike Godolt (DLR), Stefanie Grabmüller (OHB), John Lee Grenfell (DLR), Denis Grießbach (DLR), Eike W. Guenther (TLS), Pablo Gutierrez-Marques (MPSSR), Artie P. Hatzes (TLS), Saskia Hekker (MPSSR), Rene Heller (MPSSR), Thomas Henning (MPIA), Frederic Hessmann (IAG), Rafal Iciek (OHB), Maximilian Klebor (OHB), Wilhelm Kley (U Tuebingen), Joerg Knoche (MPSSR), Alexander Koncz (DLR), Ahmad Mecsaci (OHB), Harald

Michaelis (DLR), Helmut Michels (MPSSR), Esa-Pekka Miettinen (MPSSR), Valery Mogulsky (OHB), Lutz Morgenroth (OHB), Antonio Garcia Munoz (TU Berlin), Nadine Nettelmann (U Rostock), Alessandro Orlandi (OHB), Carsten Paproth (DLR), Iancu Pardowitz (MPS), Martin Pätzold (U Cologne), Frank Pellowski (OHB), Gisbert Peter (DLR), Giovanni Picogna (LMU), Anthony Price (OHB), Andreas Quirrenbach (U Heidelberg), Heike Rauer (DLR), Klaus Raum (OHB), Ronald Redmer (U Rostock), Steve Rockstein (OHB), Eilke Santjer (DLR), Roland Schoeggel (OHB), Jesper Schou (MPSSR), Sonja Schuh (MPSSR), Hannah Schunker (MPSSR), Mario Schweitzer (OHB), Frank Sohl (DLR), Armin Stettner (OHB), Barbara Stracke (DLR), Klaus G. Strassmeier (AIP), Saskia Stude (MPSSR), Giovanni Tropea (OHB), Bernd Ulmer (DLR/IBU), Anja Veith (OHB), Karsten Westerdorff (DLR), Matthias Wieser (OHB), Tomasz Wocjan (OHB), Juergen Wohlfeil (DLR), Guenther Wuchterl (TLS), Jörg Würker (OHB)

Hungary

Tamas Barczy (Admatis), Gyula Horvath (C3S), Katalin Incze (C3S), Gabor Marosy (C3S), Attila Simon (Konkoly Obs.), Agoston Srp (C3S), Robert Szabo (Budapest), Gyula Szabo (Konkoly Obs.)

Israel

Aviv Ofir (Weizmann), Helled Ravit (U Telaviv)

Italy

Laura Affer (INAF-Palermo), Elio Antonello (INAF-Brera), Stefano Basso (INAF-Brera), Serena Benatti (INAF-Padova), Milena Benedettini (INAF-IAPS), Maria Bergomi (INAF-Padova), Katia Biazzo (INAF-Catania), David Biondi (INAF-IAPS), Federico Biondi (INAF-Padova), Alfio Bonanno (INAF-Torino), Aldo Stefano Bonomo (INAF-Torino), Francesco Borsa (INAF-Brera), Luca Borsato (INAF-Padova), Alessandro Bressan (INAF-Padova), Enzo Brocato (INAF-Roma), Roberto Buonanno (INAF-Roma), Santino Cassisi (INAF-Teramo), Marco Castellani (INAF-Roma), Riccardo Claudi (INAF-Padova), Rosario Cosentino (INAF-FGG), Giuseppe Cutispoto (INAF-Catania), Valentina D'Orazi (INAF-Padova), Mario Damasso (INAF-Torino), Domitilla de Martino (INAF-Napoli), Silvano Desidera (INAF-Padova), Salvatore Di Franco (INAF-Firenze), Anna Maria Di Giorgio (INAF-IAPS), Maria Pia Di Mauro (INAF-IAPS), Marco Dima (INAF-Padova), Jacopo Farinato (INAF-Padova), Ettore Flaccomio (INAF-Palermo), Mauro Focardi (INAF-Firenze), Antonio Frasca (INAF-Catania), Mauro Ghigo (INAF-Brera), Paolo Giommi (ASI), Leo Girardi (INAF-Padova), Giovanni Giusi (INAF-IAPS), Valentina Granata (UNIPD), Davide Greggio (INAF-Padova), Marco Gullieuszik (INAF-Padova), Antonino. F. Lanza (INAF-Catania), Alessandro C. Lanzafame (UNICT), Mario G. Lattanzi (INAF-Torino), Giuseppe Leto (INAF-Catania), Gianluca Li Causi (INAF-Roma), Mattia Libralato (UNIPD), John Scige Liu (INAF-IAPS), Giuseppe Lodato (UNIML), Demetrio Magrin (INAF-Padova), Luca Malavolta (UNIPD), Luca Marafatto (INAF-Padova), Marcella Marconi (INAF-Napoli), Paola Marigo (UNIPD), Silvia Marinoni (ASDC), Paola Maria Marrese (ASDC), Francesco Marzari (UNIPD), Dino Mesa (INAF-Padova), Sergio Messina (INAF-Catania), Giusi Micela (INAF-Palermo), Josephina Montalban (UNIPD), Roberto Morbidelli (INAF-Torino), Matteo Munari (INAF-Catania), Ulisse Munari (INAF-Padova), Iliaria Musella (INAF-Napoli), Domenico Nardiello (UNIPD), Valerio Nascimbeni (UNIPD), Renato Orfei (INAF-IAPS), Sergio Ortolani (UNIPD), Emanuele Pace (UNIFI), Isabella Pagano (INAF-Catania), Stefano Pezzuto (INAF-IAPS), Adriano Pietrinferni (INAF-Teramo), Giampaolo Piotto (UNIPD), Ennio Poretti (INAF-Brera), Loredana Prisinzano (INAF-Palermo), Roberto Ragazzoni (INAF-Padova), Gabriella Raimondo (INAF-Teramo), Monica Rainer (INAF-Brera), Vincenzo Ripepi (INAF-Napoli), Thaise Rodrigez (UNIPD), Marco Santoro (INAF), Gaetano Scandariato (INAF-Catania), Roberto Silvotti (INAF-Torino), Richard Smart (INAF-Torino), Alessandro Sozzetti (INAF-Torino), Daniele Spiga (INAF-Brera), Michele Trabucchi (UNIPD), Paolo Ventura (INAF-Roma), Rita Ventura (INAF-Catania), Francesco Verrecchia (ASDC), Valentina Viotto (INAF-Padova), Ricardo Zanmar Sanchez (INAF-Catania)

The Netherlands

Gert de Lange (SRON), Pieter Dieleman (SRON), Malcolm Fridlund (U Leiden), Michiel Min (SRON), Ignas Snellen (U Leiden)

Poland

Cezary Migaszewski (NCU), Ewa Szuszkiewicz (Szczecin)

Portugal

Manuel Abreu (CAAUL), Isa Brandao (CAUP), Joao Coelho (U Lisbon), Alexandre Correia (Aveiro), Margarida Cunha (CAUP), Elena Duarte (FCUL), Pedro Figueira (Porto), Antonio Gutierrez (DEIMOS), Marco Montalto (CAUP), Jose Manuel de Nunes Vincente Rebordao (U Lisbon), Alexandre Santerne (Porto), Nuno C. Santos (CAUP), Sergio Sousa (CAUP)

Spain

M. Angeles Alcacera (INTA), Carlos Allende Prieto (IAC), Roi Alonso (IAC), Ana Balado (INTA), David Barrado (INTA-CSIC), Tom Belenguier (INTA), Antonio Claret (IAA), Josep Colomé (ICE), Hans Deeg (IAC), Jose Javier Dias

(IAC), Julio Rodríguez Gomez (IAA), Nuria Huélamo (INTA-CSIC), Jorge Lillo-Box (INTA-CSIC), J. Miguel Mas Hesse (CAB-INTA), Maria Morales-Calderón (INTA-CSIC), Miriam Pajas (INTA), Enric Pallé (IAC), Clara Regulo (IAC), Ignasi Ribas (ICE), Rosario Sanz (IAA), L. Sarro (UNED), Enrique Solano (CAB-INTA), Juan-Carlos Suarez (IAA), Roser Urqui (CAB-INTA), J. Antonio Viceira (INTA), Francesc Vilardell (ICE), Holger Voss (Barcelona), Gonzalo Ramos Zapata (INTA)

Sweden

Bertram Bitsch (U Lund), Alexis Brandeker (U Stockholm), Melvyn B. Davies (U Lund), Sofia Feltzing (U Lund), Markus Janson (U Stockholm), Anders Johansen (U Lund)

Switzerland

Yann Alibert (U Bern), Timothy Bandy (U Bern), Willy Benz (U Bern), Giordano Bruno (U Bern), David Ehrenreich (U Geneva), Kevin Heng (U Bern), Christophe Lovis (U Geneva), Rosemary Mardling (U Geneva), Lucio Mayer (Zurich), Christoph Mordasini (U Bern), Francesco Pepe (U Geneva), Daniele Piazza (U Bern), Martin Rieder (U Bern), Damien Ségransan (U Geneva), Clement Surville (Zurich), Stephane Udry (U Geneva)

UK

Suzanne Aigrain (U Oxford), Richard Alexander (Leicester), Matthew Bate (Exeter), Mariangela Bonavita (Edinburgh), David Brown (U Warwick), Patrick Burgess (IoA-Cam), Matt Burleigh (Leicester), Giorgia Busso (IoA-Cam), Tiago Campante (U Birmingham), William J. Chaplin (U Birmingham), Cathie Clarke (IoA-Cam), Andrew Collier Cameron (St Andrews), Sue Cowell (IoA-Cam), Guy R. Davies (U Birmingham), Francesca De Angeli (IoA-Cam), Yvonne Elsworth (U Birmingham), D. Wyn Evans (IoA-Cam), Francesca Faedi (U Warwick), Duncan Forgan (St Andrews), Eduardo Gonzalez-Solares (IoA-Cam), Carole Haswell (Open Univ.), Simon Hodgkin (IoA-Cam), Greg Holland (IoA-Cam), Mike Irwin (IoA-Cam), Thomas Kennedy (MSSL), Ulrich Kolb (Open Univ.), Henrik Latter (DAMTP), James R. Lewis (IoA-Cam), Pablo-Aguilar Loren (Exeter), Nikku Madhusudhan (IoA-Cam), Farzana Meru (IoA-Cam), Andrea Miglio (U Birmingham), Richard Nelson (QMUL), Gordon Ogilvie (DAMTP), Sijme-Jan Paardekooper (QMUL), John Papaloizou (DAMTP), Don Pollacco (U Warwick), Ken Rice (Edinburgh), Marco Riello (IoA-Cam), Guy Rixon (IoA-Cam), Ian Roxburgh (QMUL), Alan Smith (MSSL), Caroline Terquem (U Oxford), Amaury Triaud (IoA-Cam), Floor van Leeuwen (IoA-Cam), Sergey V. Vorontsov (QMUL), Nicholas Walton (IoA-Cam), David Walton (MSSL), Chris Watson (QUB), Richard West (U Warwick), Peter Wheatley (U Warwick), Mark Wyatt (IoA-Cam)

USA

Sarbani Basu (Yale Univ.), Mathieu Havel (Columbia), Savita Mathur (SSI), Marc Pinsonneault (Ohio State)